CR 160898
C.1

(NASA-CR-160898) SHUTTLE ORBITER KU-BAND RADAR/COMMUNICATIONS SYSTEM DESIGN EVALUATION Final Report (Axiomatix, Los Angeles, Calif.) 372 p HC A16/MF A01 CSCL 17B G3/32

N81-26327

Unclas 41132

Axiomatix

SHUTTLE ORBITER KU-BAND RADAR/COMMUNICATIONS SYSTEM DESIGN EVALUATION

FINAL REPORT

Contract No. NAS 9-15795A/B

Prepared for

NASA Lyndon B. Johnson Space Center
Houston, Texas 77058

Prepared by

J. Dodds
J. Holmes
G. Huth
R. Iwasaki
R. Maronde
A. Polydoros
C. Weber
P. Broad

Axiomatix

9841 Airport Blvd., Suite 912
Los Angeles, California 90045

Axiomatix Report N. R8012-3
December 22, 1980

TABLE OF CONTENTS

LIST OF TABLES

LIST OF FIGURES

Page

Page

Page

1.0 EXECUTIVE SUMMARY

1.1 Purpose of Effort

The primary objective of this effort has been to examine and critique the design of the Hughes Aircraft Company (HAC) manufactured Ku-band radar/communications system for the Orbiter. The current contract is composed of two exhibits, A and B, with four subtasks in Exhibit A and three in Exhibit B. The emphasis of the subtasks has evolved during the course of the contract in response to changing requirements, and the term of the contract has been extended in parallel with HAC's delays in delivering hardware and documentation. For example, the radar range test evaluation task was deleted since this test is to be conducted well after the expiration of the contract. A system test evaluation task was added in its stead.

This final report covers the following tasks from Exhibits A and B:

- A1 - Ku-Band High-Gain Antenna/Widebeam Horn Design Evaluation
- A2 - Evaluation of Ku-band SPA and EA-1 LRU software
- A3 - System Test Evaluation
- A4 - Critical Design Review and Development Test Evaluation
- B1 - Ku-Band Bent-Pipe Channel Performance Evaluation
- B2 - Ku-Band LRU Interchangeability Analysis
- B3 - Deliverable Test Equipment Evaluation.

The effort expended on tasks A1, A2, A3, B1 and B3 has been documented in interim reports [1-5] and in monthly reports. The completion of tasks A4 and B2 was predicated on the availability of CDR data package and HAC LRU development specifications This documentation has only recently been made available; hence, these two tasks are not covered in separate interim reports but, rather, are included as Sections 5, 9 and 10 of this final report.

In those areas where deficiencies have been found, Axiomatix has suggested modifications and improvements to the Ku-band system and the associated test procedures.

1.2 General Approach

Axiomatix personnel have worked with NASA, HAC and Rockwell personnel while carrying out this contractual effort. By mutual consent of Axiomatix and the cognizant NASA personnel, effort within each subtask was directed to those problem areas of most concern and in which improvements could realistically be made within the present scope of the HAC hardware contract.

Axiomatix personnel have attended all regularly scheduled program reviews, design reviews, and special meetings concerning aspects of the Ku-band system relevant to the Axiomatix effort. Monthly reports have been submitted detailing the monthly activity and, in some cases, detailing technical results. Interim reports have been submitted at the completion of each subtask.

1.3 Contents of the Final Report

Section 2.0 is an introduction to the final report which ties together past Axiomatix efforts with the current effort, describes the contents of this report in greater detail, and summarizes Axiomatix conclusions and recommendations.

The relationship between each Ku-band subsystem and its relevant sections in this report is depicted in Figure 1.

Section 3.0 documents Axiomatix efforts under task A1, High-Gain Antenna/Widebeam Horn Evaluation. In the course of this effort, the existing antenna design was evaluated with the goal of understanding the causes of deficient performance, particularly in terms of excessive sidelobe levels. Several recommendations have been made and one has been incorporated--that of fences on the high-gain feed to reduce mutual-coupling effects between the main feed and the monopulse elements.

Section 4.0 covers task B1, Bent-Pipe Channel Performance Evaluation. Emphasis was placed on the mode 1, channel 3 performance. HAC has gone through several design iterations for a mid-bit data sampler at the high data rate digital port, and Axiomatix has reviewed those designs and made suggestions for improvement. Included in this effort is an analysis of the effects of long cable lengths at this input port in terms of data-dependent voltage variations and rise time effects. Axiomatix has provided results of this analysis to Rockwell for incorporation in the SPA specification.

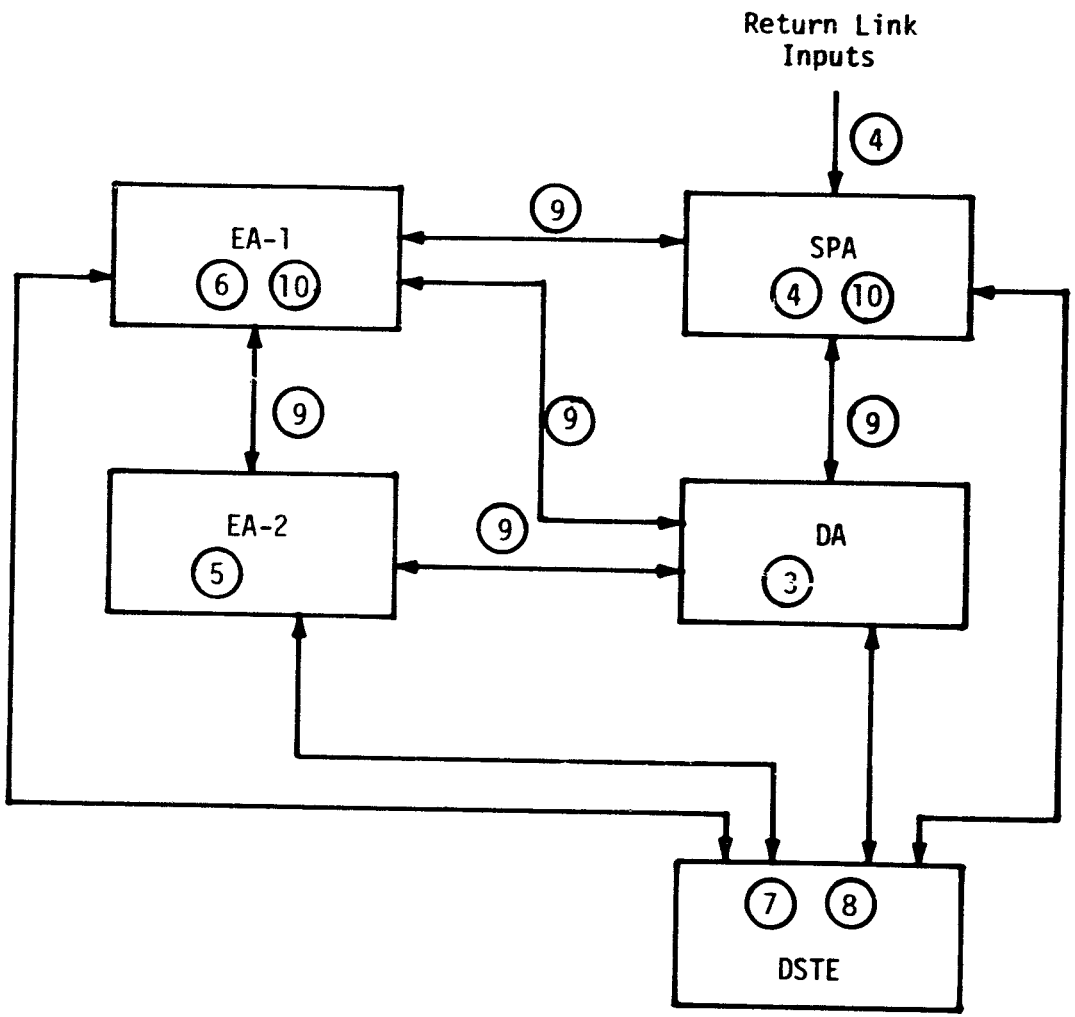

Figure 1. Relationship Between Ku-Band Equipment and Final Report Section.

Section 5.0 covers the analytical portion of task A4, Critical Design Review and Development Test Evaluation. Emphasis was placed on analysis of radar parameters difficult to measure in development tests: constant false alarm rate (CFAR) threshold and radar performance as a function of scan overlap.

Section 6.0 details the Axiomatix effort for task A2, SPA and EA-1 Software Evaluation. Only EA-1 software considered as documentation of the SPA software was not available. This effort consisted of examining in detail the inner workings and structure of the EA-1 software. Some of the more subtle aspects of the software are discussed in detail in this section, with the intent of providing additional clarity. A minor bug was found and has been corrected in a subsequent release. Included are recommendations for a more efficient use of processor memory and time.

Section 7.0 covers task B3, Deliverable System Test Equipment (DSTE) Evaluation. This section presents a concise description of the DSTE test modules and a series of matrices relating the Rockwell specification to the test modules. Recommendations are made concerning improved documentation and DSTE sell-off procedures.

Section 8.0 covers task A3, System Test Evaluation, and is closely related to the DSTE described in Section 7.0. The modified versions of the DSTE/Rockwell specification cross-reference matrices are presented in this section. These modified matrices show which of the test modules were actually used in ADL system test. Axiomatix concludes that more test modules should be used to make system test more meaningful

Section 9.0 covers task B2, LRU Interchangeability Analysis. This section is devoted to an analysis of inter-LRU signal parameters and the sensitivity of the LRU's to parameter variations.

Finally, Section 10.0 covers the remainder of task A4, Critical Design Review and Development Test Evaluation. This section presents a detailed analysis of the development test data from the SPA and EA-1 CDR.

1.4 Summary, Conclusions and Recommendations

1.4.1 High-Gain Antenna/Widebeam Horn

Electrical and physical characteristics of the antenna system have been evaluated. Test data shows higher-than-anticipated sidelobe levels. Axiomatix has found several design factors which can contribute to these sidelobe levels. The structure, shape and composition of the feed support bipods have been evaluated. Axiomatix suggests pod relocation as a means of suppressing the sidelobes in the azimuth plane. Alternate feed designs are suggested, including shaping of the teflon plug in the sum feed to promote spherical wavefronts, and the addition of "fences" to decouple the main feed and monopulse elements.

The design was also evaluated for deleterious temperature effects. Because no sensitive resonant cavities or tuned elements which might be detuned by thermal dimensional changes are incorporated in the design, Axiomatix concludes that the antenna performance should not be temperature dependent.

1.4.2 Bent-Pipe Channel Performance

HAC has experienced difficulty with the mid-bit data sampler at the high data rate digital input port of the SPA. Initial designs were not stable over the wide range of data rates (2 - 50 Mbps), input voltages, clock/data phase offset and rise times. In fact, the input signal voltage and rise time variances due to data-dependent cable effects had not been adequately characterized to permit an effective design. Axiomatix undertook an investigation of the effects of RG142 cable on various data patterns. The result is that a worst-case peak-to-peak voltage loss of 13% exists at the higher frequencies. Rise time effects were found to exhibit a complementary error function behavior, with a rapid initial rise followed by a slow rise (or fall) to steady state. These results have been presented to Rockwell for incorporation into the Ku-band specification.

Various HAC mid-bit detector designs have been evaluated by Axiomatix. The design selected incorporates a variable threshold for clock and data to accommodate the variability in input levels, a phase-frequency detector to track the input clock, and an out-of-lock detector to prevent anomolous lock. A complex bit timing error detector is used

which relies on the leading edges of data transitions to perform phase synchronization between data and clock. Axiomatix concludes that this version of the mid-bit detector will successfully track with a 25% data asymmetry and up to 90° phase shift between data and clock.

1.4.3 Radar Threshold Analysis

The statistics of the CFAR threshold for the Ku-band radar are derived. Exact analytical results are developed for both the mean and standard deviations in the designated search mode. The results are presented graphically as a function of signal-to-noise ratio (SNR) and range gate noise correlation.

The standard deviation is shown to be very sensitive to SNR and very insensitive to the noise correlation present in the range gates of the designated search mode.

1.4.4 Radar Performance as a Function of Scan Overlap

Stability of the deployed assembly may cause the antenna scan overlap to fall below the recommended value for off-zenith-centered scans. This will cause a degradation in the probability of target detection. Axiomatix has derived the relationshiop between the antenna overlap, dwell time and antenna gain, and their effects on the received target SNR and the resulting probability of detection. The results are presented as probability of detection versus target range and scan overlap. Maximum target energy is received when the scan overlap is approximately 45%, and probability of detection decreases to zero as overlap is decreased to zero.

1.4.5 EA-1 Software

Release IV of the EA-1 software has been evaluated with the intent of providing increased understanding of the algorithms and an alternate verification of performance. This software is used to control the status of the Ku-band system via commands from the MDM and the Orbiter D&C console. In addition, software routines control antenna scans, perform radar self-test, and provide general housekeeping functions for the system.

The initial phase of this effort entailed a detailed study of HAC documentation. During this phase, a cross-reference listing of program status flags was generated to facilitate understanding of the relationship between the various routines. This listing is included in the final report.

After the familiarization phase, the software was examined for potential problem areas and possible suboptimal coding techniques. A minor bug was found in the procedure termination routine and has been reported to HAC. An example of reconfiguration, one of the more complex executive functions, is presented in detail. Self-test tasks are discussed in detail and tables of MDM and D&C outputs are given for various phases of the self-test routine.

It was found that HAC uses a fairly time-consuming method of storing status flags. Flags are stored eight bits per computer word, which means that each time a flag is accessed, the flag bit must be stripped from the word. Axiomatix recommends an alternate technique for storing flags should execution time become critical in the EA-1 processor.

In general, the HAC documentation of the EA-1 software is excellent, although inclusion of a cross-reference listing of all variables would be useful.

1.4.6 Deliverable System Test Equipment

Axiomatix has evaluated the Deliverable System Test Equipment (DSTE) which has been delivered to ADL and will be delivered to ESTL. The DSTE is capable of performing system level developmental testing of the Ku-band equipment and is functionally organized into LRU test panels.

The DSTE is semiautomated, and HAC has generated a number of computer programs to test the Ku-band system. Axiomatix discusses these program modules in this report. In addition, Axiomatix has generated a series of matrices which are used to compare the Rockwell specification to the HAC test modules. These matrices also serve to identify those modules used to sell off the DSTE to the customer.

Axiomatix concludes that the modules provide a good selection of tests to exercise the system; however, not all modules are used, which limits the verification of the Ku-band system conformance to the Rockwell specification. Utilization of additional test modules or the Manual Control Program (MCP) mode would greatly increase the present capabilities.

1.4.7 System Test Evaluation

Axiomatix has reviewed and evaluated HAC Ku-band system test data. The approach involved discussions with cognizant Rockwell and HAC personnel to determine which tests were used for system verification. The results are presented in matrix form, using a format similar to the matrices employed to describe the DSTE.

The test modules used by HAC were originally generated for developed tests and were not intended for system verification; however, it would have been too costly and time-consuming to develop modules specifically to verify conformance to the Rockwell specification. A total of eight communications mode test modules and six radar mode test modules, of a total of 31, were used in system test. An additional six tests were also used.

The result is that compliance to the Rockwell specification was not verified to a significant degree; however, the system tests did show functional performance. Axiomatix recommends that additional test modules be generated to show compliance with the specification.

1.4.8 LRU Interchangeability

The LRU interchangeability task examined the LRU-to-LRU and the LRU-to-Orbiter interfaces to determine electrical compatibility. The conclusion is that the LRU's are <u>not</u> interchangeable since there are a number of serious interface deficiencies.

1.4.9 Critical Design Review and Development Test Evaluation

Axiomatix has reviewed and evaluated the SPA and EA-1 test data presented at the respective design reviews. The results of the investigation are presented in block diagram form for the SPA and in matrix form for the EA-1. The rationale is that the SPA is data oriented, and the test results can best be depicted by tracking the signal flow through the LRU. The EA-1 is more control oriented, and the results can best be highlighted in matrix form since data flow, or processing, is not a critical function of the EA-1.

In general, the SPA ADL LRU tests were fairly thorough; however, Axiomatix has four concerns, as follows:

(1) Most of the return link failures are serious.

(2) Return link output signals have not been adequately measured.

(3) The effects of input signal tolerance variations on return link and forward link performance are unknown.

(4) The minimum mode 2 return link data rate, 16 kbps, was not tested.

Axiomatix recommends that these concerns, which are discussed in greater detail in the report, be resolved as soon as possible.

A number of test omissions were found in the EA-1 CDR test data; however, cognizant personnel at NASA, Rockwell and HAC are aware of these problems, hence they have not been restated in this report. The matrices presented in Section 10.0 relate for the first time the HAC LRU specification to the Rockwell requirements. Axiomatix concludes that the HAC EA-1 tests are well documented and adequately test the EA-1 performance.

1.5 Continuing Effort

Axiomatix will continue to support the Ku-band system development and performance evaluation and will work with NASA, Rockwell and HAC personnel to solve design and operational problems in a timely and efficient manner.

2.0 INTRODUCTION

This final report documents the Axiomatix effort under NASA/JSC contract NAS 9-15795A/B, "Shuttle Orbiter Ku-Band Radar/Communications System Design Evaluation." The effort is a critique and design evaluation of the Hughes Aircraft Company (HAC) Ku-band radar/communication system and its associated test equipment and documentation.

2.1 Statement of Work

2.1.1 Objectives

The overall objectives of the effort have been to evaluate the Ku-band system performance and provide recommendations for improvements when technically desirable and economically feasible. Axiomatix has maintained a flexible approach: within each contractual subtask, Axiomatix has concentrated on those areas of concern which are deemed most critical and worthy of investigation at any given time. As a result, Axiomatix has been able to respond to the needs of NASA/JSC in a timely manner to provide expertise and technical resources when and where they were needed.

The Axiomatix effort can be divided into three principal areas of endeavor, as follows:

(1) Critique and evaluate HAC hardware for conformance to specification, based on design evaluation, test results and analysis.

(2) Evaluate the capability of HAC test procedures and equipment to verify LRU and system performance.

(3) Provide rapid response to NASA for technical consultation in areas of concern under the aegis of this contract.

2.1.2 Task Statements

During the course of this contract, emphasis has evolved from Shuttle rendezvous radar to communications. As a consequence, the tasks in this contract have been modified to reflect this change. In addition, delivery of HAC hardware, test results and documentation has been delayed.

The current contract consists of two principal parts, Exhibit A and Exhibit B. Exhibit A consists of the follow tasks:

Task 1. Ku-Band High-Gain Antenna/Widebeam Horn Design Evaluation

The contractor shall analyze the Ku-band high-gain antenna and widebeam horn antenna performance and assess the design changes needed to meet NASA requirements for radar and communication modes. Also, assess the need for polarization switching from linear to circular for communications operation. The contractor shall make recommendations to NASA for specific hardware design changes and/or changes to the procurement technical specification that will assure satisfactory compliance with the NASA performance requirements for all modes of operation.

Task 2. Evaluation of Ku-Band SPA and EA-1 LRU Software

The contractor shall evaluate the Ku-band software (firmware) logic flow diagrams as to conformance with the intended functions required of the SPA and EA-1 LRU's. Implementation of the algorithms defined by the flow diagram in software code will be examined in detail for potential problems.

The contractor shall provide a narrative description of the software functions, algorithms and programming techniques in order to facilitate understanding the systems and ease software modification and maintenance. The contractor will make recommendations as to modifications, where applicable, to simplify the software and/or increase reliability.

Task 3. System Test Evaluation

The contractor shall evaluate and assess the data obtained by the Ku-band hardware vendor during system testing. The data shall be evaluated to assure that the Ku-band system as a whole is in compliance with the requirements of the technical specification. For those areas of the hardware design that do not lend themselves to verification by direct measurement during test, the contractor shall perform appropriate analysis, using the data available, to assure conformance with the requirements. The contractor shall identify any areas of nonconformance and provide an assessment of the impact to overall system performance.

Task 4. Critical Design Review and Development Test Evaluation

The contractor shall evaluate the data provided for the Critical Design Review (CDR) and evaluate and assess the data obtained by the Ku-band hardware vendor during LRU tests. The data shall be evaluated to assure compliance with the requirements of the technical specification for each LRU and the overall Ku-band system. For those areas of the hardware design that do not lend themselves to verification by direct measurement during test, the contractor shall perform appropriate analysis, using the data available, to assure conformance with the requirements. The contractor shall identify any areas of nonconformance and provide an assessment of the impact to overall system performance as a result of the CDR and LRU tests. The contractor shall provide recommendations to NASA for changes (if required) to the hardware design to meet the requirements of the technical specification.

Exhibit B consists of the following tasks:

Task 1. Ku-Band Bent-Pipe Channel Performance Evaluation

The contractor shall analyze implementation of the Ku-band Signal Processor Assembly (SPA) and the Electronic Assembly-1 (EA-1) to determine performance of the wideband bent-pipe channel and the narrowband bent-pipe channels. The contractor shall analyze the interfaces between the Payload Interrogator (PI) and the SPA and between Payload Station (SP) and the SPA to determine the effect of interface signal variations on communication channel crosstalk and signal distortion. From these analyses, the contractor shall recommend solutions to any performance problems identified. These recommendations may involve changes to the interface characteristics between the PI and SPA and between the PS and the SPA as well as optimizations of the SPA and EA-1 implementations.

Task 2. Ku-Band Line Replaceable Unit (LRU) Interchangeability Analysis

The contractor shall review the system specifications, the LRU specifications, the engineering model system test results, the acceptance test plan (ATP), and the qualification test plan (QTP) to determine the LRU interchangeability. The contractor shall investigate ways of simplifying ATP QTP and reducing the system test time by demonstrating that

to the degree of LRU interchangeability, LRU tests can be used to satisfy the requirements of the system test.

Task 3. Deliverable Test Equipment Evaluation

The contractor shall evaluate the Deliverable Test Equipment (DTE) design for use in the Avionic Development Laboratory (ADL) and the Electronic System Test Laboratory (ESTL). The Contractor shall evaluate the software (firmware) used to operate the DTE in terms of the ADL and ESTL test requirements. The contractor shall make recommendations to NASA as to software (firmware) or hardware changes to the DTE that will simplify ADL and ESTL tests and reduce the required test time.

2.2 General Approach

During the course of this contract, Axiomatix personnel have worked with cognizant NASA, Rockwell and HAC personnel to help solve on-going problems and provide expertise in areas of concern requiring fast response. Axiomatix personnel have attended all scheduled program reviews, design reviews and special meetings at Rockwell and HAC concerning problem areas which are relevant to the Axiomatix contract. Examples of the latter effort are SPA bit synchronizer reviews and EA-1 Block III servo meetings.

Monthly reports have been submitted which describe activities during the reporting period and which, in some cases, describe detailed technical results. Interim reports have been submitted for all tasks except Task A4 and B2.

Task A4, "Critical Design Review and Development Test Evaluation." was delayed due to slips in the Critical Design Review (CDR) schedule and a lack of test data. Task B2, "LRU Interchangeability Analysis," was delayed due to the lack of current LRU development specifications from HAC. As a result, both interim reports are included in this final report in lieu of submission under separate cover.

Where deficiencies have been found, modifications and improvements to the Ku-band system and test procedures have been suggested.

2.2.1 Relationship to Other Tasks

The effort described in this report represents an extension of past Axiomatix work on the Ku-band system, and Axiomatix will continue to provide NASA with expertise under ongoing contracts. The EA-2 and DA CDR test data will be evaluated under a separate contract, and Axiomatix will continue to monitor, critique and evaluate the Ku-band system as required by NASA/JSC.

2.3 Contents of the Final Report

The relationship between the sections in this final report and the Ku-band system units, including deliverable test equipment, is depicted in Figure 2. The circled numerals represent the sections in this report. The sections are ordered as follows: the first four sections cover efforts relevant to the four LRU's; the next two sections cover the Deliverable System Test Equipment (DSTE) and the results of system test; the next section covers interchangeability analysis; finally, the last section describes the test data presented at the EA-1 and SPA critical design reviews.

Section 3.0 presents results of the Axiomatix evaluation of the Ku-band high-gain antenna and widebeam horn, which is covered under Task A1. Axiomatix personnel reviewed the results of antenna tests conducted by HAC, investigated the detailed design of the antenna and consulted with Hughes personnel.

Section 3.1 is an introduction to the problems associated with the antenna system. The primary problem encountered is a high sidelobe level in the high-gain antenna. Section 3.3 is a general description of the high-gain antenna, including reflector, support structure and feed elements. Section 3.4 is a discussion of the measured RF performance of the high-gain antenna. In section 3.5, Axiomatix presents results of an investigation into possible thermal efforts on the antenna performance since these effects are difficult to measure experimentally. Section 3.6 presents the results of the Axiomatix study, including recommendations for performance improvement. Section 3.7 covers aspects of the widebeam horn in a manner parallel to the sections covering the high-gain antenna and, in section 3.8, Axiomatix presents conclusions reached as a result of the study.

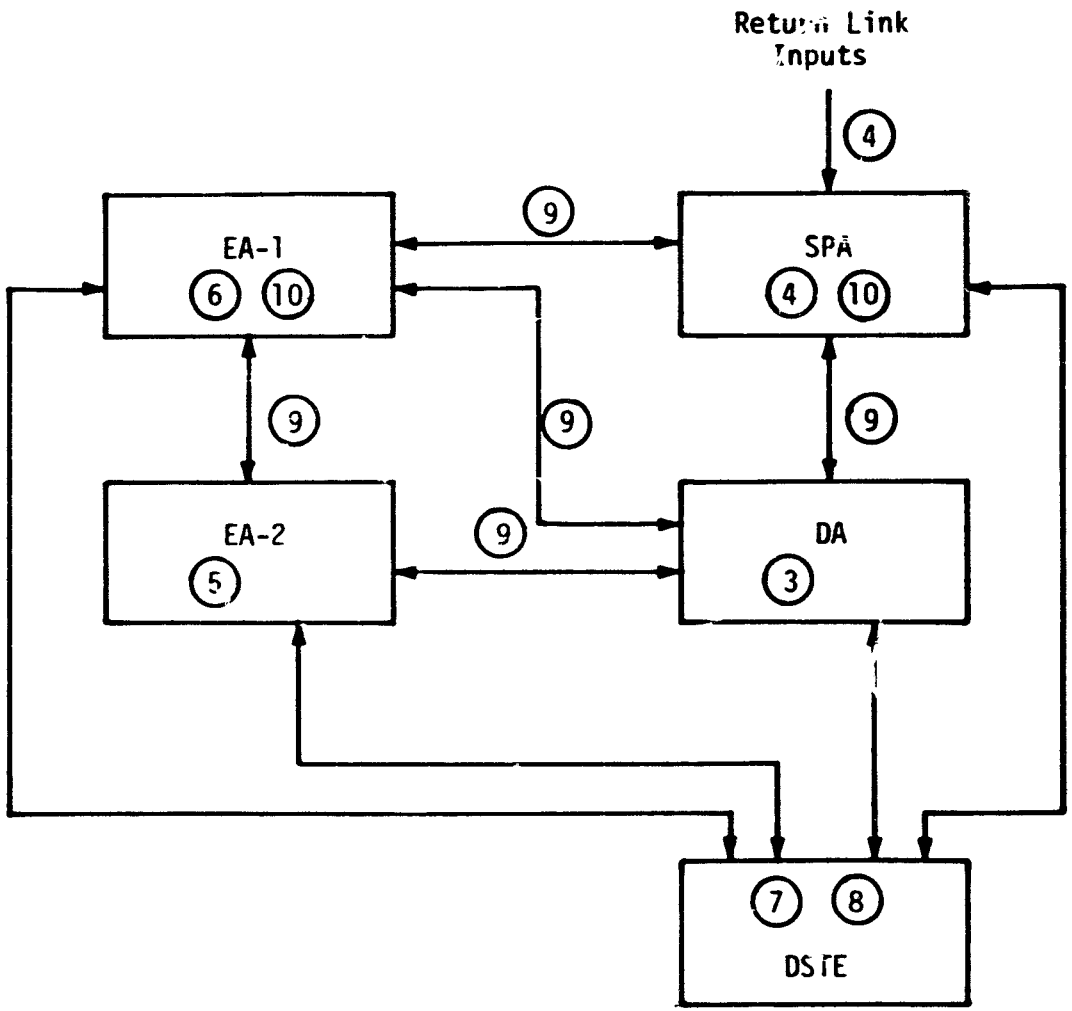

Figure 2. Relationship Between Ku-Band Equipment and Final Report Section.

Section 4.0 describes Axiomatix's evaluation of the wideband bent-pipe channel performance, including aspects of the signal input parameters relevant to the channel performance. Since HAC has experienced difficulty with the SPA bit synchronizer at the mode 1, channel 3 input, effort has been concentrated on this item. This effort is covered by Task B1 of the contract.

This section is divided into three primary areas of investigation. The first covers input parameter characteristics critical to the channel performance. Included is a discussion of the cable and connector effects on the parameters. This port is connected to the data source via a 92' cable and up to seven connector pairs. This cable has a severe effect on pulse rise time and voltage levels. NASA had noticed data-dependent voltage effects at the cable output and, in this section, Axiomatix presents analytical results confirming this observation and permitting an accurate prediction of the expected variations. Results of this analysis have been incorporated into the Rockwell specification.

The next two major areas of investigation cover detailed critiques of the HAC-proposed bit synchronizer. These devices are intended to sample input data as close as possible to the center of the data bit at a rate determined by the source clock. The effects of all relevant data/clock parameters are examined and performance margins are presented. Timing diagrams are used extensively to describe the bit synchronizer performance and an analysis of a linearized model of the phase/frequency detector is included to supplement the results from the timing diagrams.

Section 5.0 covers the analytical portion of Task A4, "Critical Design Review and Development Test Evaluation." Emphasis was placed on an analysis of radar parameters difficult to measure in development test: constant false alarm rate (CFAR) threshold and detection performance as a function of scan overlap. The HAC radar computes a detection threshold based on prior samples of noise and signal-plus-noise. The threshold is scaled to produce an average false alarm rate predicated on assumptions concerning the noise characteristics. Axiomatix has derived an exact formulation for the threshold statistics, mean and standard deviation, based on the HAC radar signal processing and Gaussian noise statistics.

The resultant values are plotted as a function of signal-to-noise ratio (SNR) and noise correlation from range gate to range gate, and compared with simulation results.

Radar detection performance is a function of scan overlap. Stability considerations of the deployed assembly have forced HAC to modify the antenna servo, resulting in degraded scan performance due to less than optimum scan overlap. In section 5.2, Axiomatix derives the relationship between antenna dwell time, scan overlap, antenna gain and received target SNR, and the resultant probabilities of detection.

The EA-1 is the primary control element in the Ku-band system, and the EA-1 software is the "brains" of the EA-1. Axiomatix has evaluated the EA-1 software under Task A2 of the contract, and results of this effort are given in Section 6.0 of the report. This software performs various control functions and mathematical transformations, including generation of the radar and communications scans, mode control of the Ku-band system in response to MDM and D&C inputs, and radar self-test.

The Axiomatix effort had two objectives. The first was to better understand the inner workings of the software and to document these findings; the second was to evaluate the ability of the software to perform the desired functions. Several examples of software functions are discussed in detail to aid comprehension, and a cross-reference listing of status flags is given. The latter is an aid to understanding the interaction of the various software routines. Self-test is discussed and the status of the MDM and D&C outputs is presented as a function of the current self-test task being executed.

The Deliverable System Test Equipment (DSTE) is evaluated in Section 7.0 under Task A3 of the contract. Under a separate contract, Axiomatix personnel have attended the DSTE seminar presented at Hughes. This experience, and the evaluation of available documentation, have enabled Axiomatix to report on the ability of the DSTE to perform as intended. The DSTE consists of LRU test panels, a minicomputer system for test control, a Ku-band signal conditioner, a power control panel and some general-purpose test equipment, and is capable of performing system level development tests. Thirty-one (31) test modules (software) were written to exercise the Ku-band system.

The basic approach taken by Axiomatix was to generate a matrix to compare the Ku-band system requirements as detailed in the Rockwell specification to the 31 test modules. Ideally, the test modules should test a majority of the Rockwell System requirements. In this same matrix, the modules used to sell off the DSTE will also be identified.

Section 8.0 covers Task A3 of the contract, "System Test Evaluation", and is closely related to the DSTE task described in Section 7.0. Axiomatix has reviewed and evaluated data obtained by HAC during Ku-band system testing. Results are presented in matrix form similar to the format used in Section 7.0. Those modules actually used in system test have been flagged in the matrices. A brief description of additional tests is also included.

In Section 9.0, Axiomatix evaluates the Ku-band LRU interchangeability which is covered by Task B4 of the contract. The Ku-band communications and radar system consists of four LRU's: EA-1, EA-2, SPA and DA. Because of the sheer number and complexity of the interfaces and since the LRU is the basic building block of the Ku-band system, it must be assured that each LRU is interchangeable with another similar LRU.

The approach for completing the LRU interchangeability study (Task B2) was to examine each of the LRU-to-LRU and LRU-to-Orbiter interfaces using the Rockwell Ku-band specification and the four Hughes LRU specifications for baseline information to determine electrical compatibility by verifying that the document describing the signal output was consistent with the document specifying the signal input. Since electrical compatibility was the objective of this study, only interface parameters such as input/output impedances, rise/fall times, proper voltage levels and proper power levels were compared. Performance parameters such as SNR, BER, spurious products and phase noise were not included in this study since performance parameters are verified during development, acceptance and qualification testing. Therefore, this study centered on examining the electrical compatibility of all the interfaces.

The remainder of Task A4, "Development Test Evaluation," is discussed in Section 10.0. Section 10.1 covers the SPA and Section 10.2 covers the EA-1. The results of the evaluation are presented in block diagram form for the SPA, with each test highlighted in the appropriate signal flow path, and represent ADL test data presented at the CDR.

The EA-1 evaluation is based on both ADL and ESTL test results and is presented in matrix form. The HAC specification number is correlated with the HAC test number and the appropriate Rockwell specification.

2.3.1 Issues Not Covered in Major Sections

During this contract, Axiomatix was asked by NASA/JSC to provide expertise to help solve minor and, in some cases, major problems on a rapid-response basis. The results of these efforts sometimes did not warrant a formal report, and could usually be covered with a brief telephone call or informal memo. These issues are not covered in this report. One major issue not reviewed in a separate section is the question of the Block III servo. Axiomatix was privy to several meetings concerning this problem and has made suggestions to aid in the problem resolution. One suggestion, the addition of dither, will be incorporated into the system. However, Axiomatix did not issue an interim report; hence, no major section has been dedicated to the Block III servo.

2.4 Conclusions and Recommendations

2.4.1 High-Gain Antenna and Widebeam Horn

The high sidelobe levels of the high-gain Ku-band antenna are a primary influence on the antenna system performance. Several relatively easily verifiable improvements have been suggested to decrease the sidelobe levels of the high-gain antenna. If effective, these changes may negate the necessity of alternate, more expensive, changes to the Shuttle radar/communication system. In particular, specific recommendations have been made to correct the three areas which have been determined to be contributors to the high sidelobe problem. First, the concept of leakage radiation shorting elements on the ground plane was introduced to minimize the parasitic mutual-coupling effects between the sum feed and the monopulse elements. Second, the feed support pods have been identified as obstacles in the primary sum feed pattern and, therefore, pod relocation and shaping and material substitution were suggested as possible remedies to the illumination taper blockage on the reflector. Finally, some ideas on encouraging the launching of quasi-spherical waves from the sum feed were outlined to minimize phase aberrations for the parabolic system.

Thermal effects do not appear to be a problem for either the high-gain antenna or the widebeam horn.

2.4.2 Bent-Pipe Channel Performance Evaluation

Long runs of cable in the Orbiter from the data source to the SPA can cause severe frequency-dependent variations in data quality which inpact the design of the SPA high data rate digital input port. As a result of this investigation, the Rockwell specification has been modified to include more severe variations in input voltage variations and degraded pulse rise times, and HAC has been forces to include an adaptive threshold at the mode 1 channel 3 input. Axiomatix concludes that, with this modification and incorporation of the bit synchronizer/midbit detector analyzed in section 4.5, source data with parameters within specification presented at this port will be tracked and sampled correctly.

2.4.3 Radar Performance

In section 5.1, Axiomatix derives statistics of the CFAR threshold mean and standard deviation for the HAC radar. The analytical results are more optimistic than the simulation results, for which no explanation is offered.

The normalized standard deviation is shown to be very sensitive to SNR and very insensitive to the noise correlation present in the range gates of the designated search mode. The substantial variation in the CFAR threshold is dominant at large values of SNR where the normalized standard deviation is greater than 0.3. Whether or not this significantly affects the resulting probability of detection is a matter which deserves additional attention.

On the optimistic side, the threshold setting and target return are correlated; this leads us to conjecture that this variation may not appreciably affect the probability of detection. On the pessimistic side, there is a substantial variation of the CFAR threshold setting away from that developed from the noise-only condition.

In Section 5.2, the relationship between scan overlap and probability of detection is derived.

Maximum target energy is received when the antenna scan overlap is approximately 45% when measured with respect to the half-power beamwidth. This compares reasonably with the commonly accepted value of 30% when the approximate nature of the antenna mainlobe model is considered. Probability of detection decreases with lower values of scan overlap until zero detection is "achieved" with no overlap. These results should be considered when deciding which values of scan overlap are tolerable.

2.4.4 EA-1 Software

The EA-1 software is well documented and annotated, with the exception of the omission of a cross-reference listing in the documentation. In this report, Axiomatix has provided a cross-reference listing of status flags to partially fill this gap. A minor bug in the procedure termination routine has been found and the fix is discussed in section 1.1. Executive reconfiguration and self-test are examined and appear to perform as expected. Discussion of the MDM output during self-test is very brief in the HAC documentation; a more complete discussion of the MDM outputs is provided in this report. A change in the method of flag storage is recommended if processing time becomes a critical factor in future versions of the EA-1 software.

2.4.5 Deliverable System Test Equipment

The 31 test modules provide a good cross-section of tests with which to exercise the Ku-band system. However, based on the test modules currently available, the DSTE is very limited when being used to verify the Ku-band system performance as per the Rockwell specification. Additional test modules or utilization of the MCP mode would greatly increase the present capabilities.

2.4.6 System Test Evaluation

The 31 test modules can provide a good cross-section of tests to exercise the Ku-band system; however, only a limited number of tests were run. If compliance to the Rockwell Rev. B specification was to have been confirmed during system tests, then the tests were very superficial since only a small number of Rev. B paragraphs were verified, as shown in the section 8.5 matrices. If the purpose of the system tests was to gain additional confidence that the system was functioning, the tests served their purpose.

It is Axiomatix's opinion that, at some time, compliance to the Rockwell Rev. B specification must be demonstrated, and the longer it takes for this demonstration, the more potential exists for serious system problems. It is recommended that additional test modules be generated for the STE and DSTE's which are capable of specification compliance verification.

2.4.7 LRU Interchangeability

Tables 15-23 provide the results summary for the LRU interchangeability study. Even though some LRU's are presently functioning as a system, the conclusions from Tables 15-23 are that some serious interface deficiencies exist which must be corrected in order to assure LRU interchangeability. The conclusion of this study is therefore that the LRU's are not interchangeable at the present time.

In order to assure LRU interchangeability, Axiomatix makes the following recommendations:

(1) Each interface discrepancy listed in Tables 15-23 must be addressed by Rockwell and/or Hughes and resolved. Full resolution includes making the appropriate documentation changes to the Rockwell and/or Hughes LRU specifications.

(2) In this study, Axiomatix reviewed only the Rockwell systems specification and the four Hughes LRU specifications. Careful attention must be given to determine whether or not the LRU's are built per their respective specifications, and it is recommended that the development and acceptance tests be reviewed to assure hardware conformance.

(3) Most interfaces specify some input/output voltage tolerances and, to assure LRU interchangeability, the affected bus voltage variations must be tested. It is recommended that the acceptance tests and development test exercise the interfaces over the bus voltage range of +24 VDC to +32 VDC. The EA-1 ATP already performs some tests as a function of bus voltage. However, each ATP should be reviewed in detail to verify if such bus voltage tests are conducted and, if so, which interfaces or performance parameters are tested.

2.4.8 CDR Test Data Evaluation

In general, the SPA ADL LRU tests were fairly thorough. All the possible input signal combinations and the minimum and maximum data rates (except for one case) were tested and verified. The forward link digital output signal parameters were measured and found to meet the Rockwell requirements.

After evaluating the test data, Axiomatix has four concerns, listed as follows:

(1) Most of the return link failures are very serious in nature and must be resolved as rapidly as possible. Axiomatix recommends that Hughes respond to each of the failures listed in Tables 30 and 31, indicating the corrective action and submitting additional test data.

(2) The return link output signals (reference Table) have not been adequately measured. Axiomatix recommends that Rockwell update the Ku-band specification to eliminate all TBS's and that Hughes supply additional test data.

(3) The effects of input signal tolerance variations on return link and forward link performance are unknown. It is possible for tolerance variations to have a very serious impact on system performance. Axiomatix recommends that additional data be supplied, either in the form of previous SRU data or new test data, to verify the effects of signal variations (reference Tables and).

(4) The minimum mode 2 return link data rate, 16 kbps, was not tested. Axiomatix recommends that future tests include 16 kbps for mode 2 return link.

In reviewing the EA-1 CDR test data, a number of test omissions and failures were apparent. Since the Axiomatix evaluation revealed nothing that is not known to NASA, Rockwell or HAC, or has not been documented, Axiomatix feels it unnecessary to restate the omissions, failures and corrective action plans.

It is the opinion of Axiomatix that the Hughes tests were well documented and adequately tested the EA-1 performance. Finally, one benefit resulting from this CDR test data review by Axiomatix is that a document now exists in section 10.4 which, for the first time, relates the HAC EA-1 LRU specification to the Rockwell requirements.

3.0 HIGH-GAIN ANTENNA/WIDEBEAM HORN

3.1 Introduction/Background

Axiomatix has been tasked by NASA JSC to evaluate the design of the Shuttle Ku-band high-gain antenna and widebeam horn antenna. This is Task #1 of Contract NAS 9-15795. The high-gain antenna is used for both rendezvous radar and communications. In the radar mode, the antenna is linearly polarized and, in the communication mode, it is circularly polarized. The widebeam horn antenna is to be used for sidelobe discimination in the radar mode and as a TDRS acquisition aid in the communications mode.

In this section, we describe the antenna suit, with emphasis on the design aspects which produce performance degradation. Design changes are suggested to improve the antenna system performance. In addition to the electrical (RF) problems being encountered, mechanical resonances in the antenna structure as well as excessive drifts, possibly due to servo components and gyros, have seriously impaired the scan performance of the antenna, particularly in the radar mode. The resonance and drift problems are currently under active investigation by Rockwell, HAC and Axiomatix. Results and recommendations in this area will be covered in a subsequent report; however, in anticipation of continued scan difficulties, the radar detection performance as a function of scan overlap has been analyzed and is included in section 5.2.

A primary area of concern of the high-gain antenna performance is the higher-than-expected sidelobe levels. In the communications mode (circular polarization), a sidelobe level of -20.6 dB has been measured in the azimuth plane. This is close to the expected variation of the received TDRS forward link signal, and acquisition with a sidelobe cannot be precluded.

If the sidelobes cannot be reduced to acceptable levels, an alternate technique must be used to reduce the possibility of sidelobe acquisitions. Candidate schemes include tighter power control of TDRS, reduced receiver sensitivity or multiple-detection thresholds.

In the radar mode (linear polarization), a sidelobe level of -16.8 dB in the azimuth plane has been measured. The radar sidelobe avoidance technique uses the widebeam horn to discriminate a sidelobe from the peak of the high-gain antenna. It is anticipated that the horn will be circularly polarized to optimize communication performance; hence, a 3 dB degradation will be experienced in the radar mode. However, if the proper

technique is used for radar sidelobe avoidance, i.e., relative comparison of the received power in the high-gain antenna and the horn, there appears to be adequate margin.

In order to improve the sidelobe levels of the high-gain antenna, Hughes has experimented with several types of feeds. In this report, Axiomatix suggests other passive changes to improve the sidelobe levels.

The impact of maintaining linear polarization with the widebeam horn on TDRS acquisition is examined, as is the impact of circular polarization on radar sidelobe avoidance. With linear polarization, the Shuttle cannot meet EIRP specification in the communication mode, which means that TDRS must open-loop point the KSA antenna accurately enough to ensure that adequate power is received at the Shuttle for a successful scan.

3.2 Summary

In Section 3.3, we describe the physical characteristics of the high-gain antenna reflector and feed elements. Deficiencies in the sum feed are discussed, and lack of atmospheric venting is posed as a potential problem area. In section 3.4, we discuss the measured RF performance of the high-gain antenna and relate the high sidelobe levels measured to the physical characteristics of the antenna.

Concern has been expressed as to temperature effects on the high-gain antenna performance. In section 3.5, we discuss attributes of the feed which might be influenced by temperature extremes and conclude that the antenna should be insensitive to temperature variations.

In section 3.6, we give detailed suggestions for improvements to the high-gain antenna system. In particular, the feed support bipod structure is considered a significant contributor to the high sidelobe levels measured in the azimuth plane. Pod relocation, material changes and shaping are suggested as improvements. Alternate feed designs are presented to further improve system performance. The exact degree of improvement will be difficult to estimate analytically; it is suggested that these changes be implemented experimentally and the effects measured.

Section 3.7 contains a description of the widebeam horn, with a discussion of potential temperature effects due to the polarizer.

3.3 General Description, High-Gain Antenna

The Ku-band high gain antenna system is a prime focus paraboloid with linear polarization for the rendezvous radar function and right-hand circular polarization for the communications mode. A monopulse comparator subsystem is included to maintain tracking capabilities during operational use. The antenna system is stowed in the Orbiter payload bay during launch and reentry and is only deployed on orbit for rendezvous and communications in space.

Because of the tight stowage requirement, the focal length f(10 inch) of the paraboloid had to be substantially decreased to fit within the volume allotted. The diameter of the dish itself (36 inches) was maintained to be as large as deemed feasible to achieve the narrow 3 dB beamwidths (1.6°) desired. Therefore, the subsequent f/D ratio, a design parameter of reflector antenna systems, was extremely low (0.28), and this greatly affected the overall antenna performance from that predicted by Hughes during the Conceptual Design Review.

In order to reduce the weight of the deployed antenna system, a lightweight graphite epoxy paraboloid antenna was employed. This reflector is composed of layers of woven carbon fiber cloth impregnated with epoxy formed on a master mandrel to mold it to the appropriate contours. Stiffening structures, also made of graphite epoxy, are then bonded at the rear of the reflector to add strength and reduce inertial flexing of the surface. The reflector surface itself is not metallized, depending on both the anisotropic conductivity and the dielectric mismatch of the epoxy/free space interface for high reflectivity.

The feed for the antenna system is composed of a sum horn and monopulse-tracking elements, the combination of which create a parasitic mutual-coupling effect which appears to degrade the system performance. In order to describe the feed system, however, the two subsystems will be described separately.

3.3.1 Antenna Sum Feed

The sum feed is composed of a short section of square waveguide that gradually tapers into the circular waveguide feed aperture which is 0.5 inch in diameter. Since the physical dimensions of the aperture

were reduced to permit the placement of the surrounding monopulse elements, the sum feed aperture is filled with a shaped teflon plug to increase the effective circular waveguide diameter sufficient to sustain the proper propagating modes.

The placement of the orthogonal coaxial probe feeds which create the circular polarization capability was experimentally determined by actual measurements. Theoretically, the optimum placement of the probes is a quarter of the guide wavelength in front of the short, which is the position of maximum electric field. Due to the tight space restrictions, the orthogonal wire short of the probe closest to the aperture was placed closer than desirable to the second probe, which can adversely affect the cross-polarization isolation. Earlier, coplanar orthogonal probes were attempted but, due to mutual-coupling effects, this approach was discontinued.

The lengths of the center coaxial probes extending into the waveguide were also experimentally determined by adjusting the length of a variable center conductor probe into a matched load terminated waveguide and measuring the return loss. This design approach generally is valid, except that, for short waveguide sections with multiple discontinuities, the final overall matching must be accomplished after the total feed, including the monopulse elements, are assembled. Since the voltage standing wave ratio (VSWR), a measure of the impedance mismatch, was subsequently reduced from 1.5 to 1.2 or less during the latter phases of testing, it is assumed this latter procedure was performed.

The actual sum feed aperture extends 0.1 inch past the two-inch square ground plane. This circular "lip" provides some reduction in the mutual coupling effects between sum feed and the adjacent monopulse elements. The inserted teflon plug, which is physically captured within the circular waveguide when the back half of the feed section is attached, completely fills the waveguide. The tapered aperture end is about 0.3 inch long. The opposite end is counterbored to facilitate the transition to the square waveguide. Various dielectric rod antenna shapes were extended out from the radiating circular aperture but, because of the mutual coupling effects with the monopulse elements and the related high sidelobe levels, a tapered teflon plug that did not extend past the circular waveguide lip was finally chosen. It appears that this lip aids in the launching of the radiated wave; however, some diffraction effects are still obviously present. The height of this

lip was experimentally determined to minimize the sidelobe level, which increased substantially after incorporation of the monopulse elements around the sum feed. It appears that little more could be done to increase this isolation, such as corrugations or chokes, since the monopulse elements are located immediately adjacent (in fact are bent around) the sum feed. One possible modification to reduce this mutual coupling is included in section 3.6, which lists recommendations for improvement.

No impedance transition provisions (such as a tapered horn) into free space were included in the design. In fact the best description of the radiating aperture would be a rather abrupt dielectric/free-space interface at the end of a circular waveguide. Therefore, it is questionable whether a spherical wavefront is radiated from this open-ended waveguide sum feed. The concept of generating a plane wavefront from a paraboloid relies on a spherical wavefront emanating from the prime focus; therefore, some of the inherent degradation in expected low sidelobe levels can be attributed to the sum feed design. Another area of concern is the illumination at the edges of the reflector dish is partially blocked by the side support pods, which greatly distorts the illumination taper.

An earlier version of this antenna system used a four-inch square ground plane housing the monopulse phase comparator in conjunction with the feed. Obviously this constituted too much blockage of the antenna system and significant improvements in sidelobe levels were noted when the ground plane cross-section was reduced to a two-inch square feed and the large comparator was relocated along the feed support.

3.3.2 Antenna Monopulse Elements

The monopulse elements consists of four short waveguide sections terminated into receiving slots which detect comparative phase differences between opposite pairs of elements, thereby indicating the proper direction the antenna must be pointed to perform the tracking function. Again coaxial probes are used as transducers to transfer the signals in the waveguide to the semirigid coaxial cables which go to the comparator circuit located on the feed mount. The placement and lengths of the coaxial probes, as well as the dimensions of the slots, were experimentally derived by radiating into a matched load or free space and minimizing the VSWR. The length of the short waveguide sections was determined by the allotted feed envelope, and no resonance effects were utilized in the overall design. The basic

feed performance was determined to be essentially frequency independent within the frequency range of interest. Therefore, it is also relatively temperature independent. (A more detailed discussion of the thermal effects will be made in a later section which will delve into the large temperature extremes to be encountered).

A number of different types of monopulse elements were tested. A standard monopulse system successfully employed on other programs consisted of printed circuit dipoles and, therefore, these elements were initially used. Various geometric configurations such as "in-line" and "star" layouts were tried, but the final monopulse system utilizes slots in a ground plane forming a small planar array surrounding the sum feed. The reasons that this particular design was selected were that its performance was comparable to the other configurations, fabrication was simpler and dimensional reproducibility was better. The presence of the dipoles protruding above the ground plane also increased the amount of coupling of the sum feed to the monopulse elements.

The feed is machined out of a block of aluminum which is then gold-plated to reduce resistive losses and minimize the effects of corrosion. The feed consists of two halves which are bolted together. The front half consists of the circular sum feed and the slotted waveguides of the monopulse elements. The rear half contains the sum feed square waveguide and the coaxial probe connections. Since intricate machining is required, electron discharge machining (EDM) is extensively used to form precise corners.

A front and cross-sectional views of the sum feed and monopulse elements are sketched in Figure 3 to illustrate the design. Figure 4 shows the overall feed and support structure with the attached monopulse comparator circuitry. It can be seen that the feed does cause significant blockage in the crucial central portion of the dish, even after the reduction of the feed cross-section by relocating the phase comparator circuitry.

3.3.3 Additional Feed Design Considerations

One aspect of the design that has not been discussed but must not be overlooked is to incorporate adequate venting provisions to prevent damage to the protective 5 mil kapton windows over the monopulse

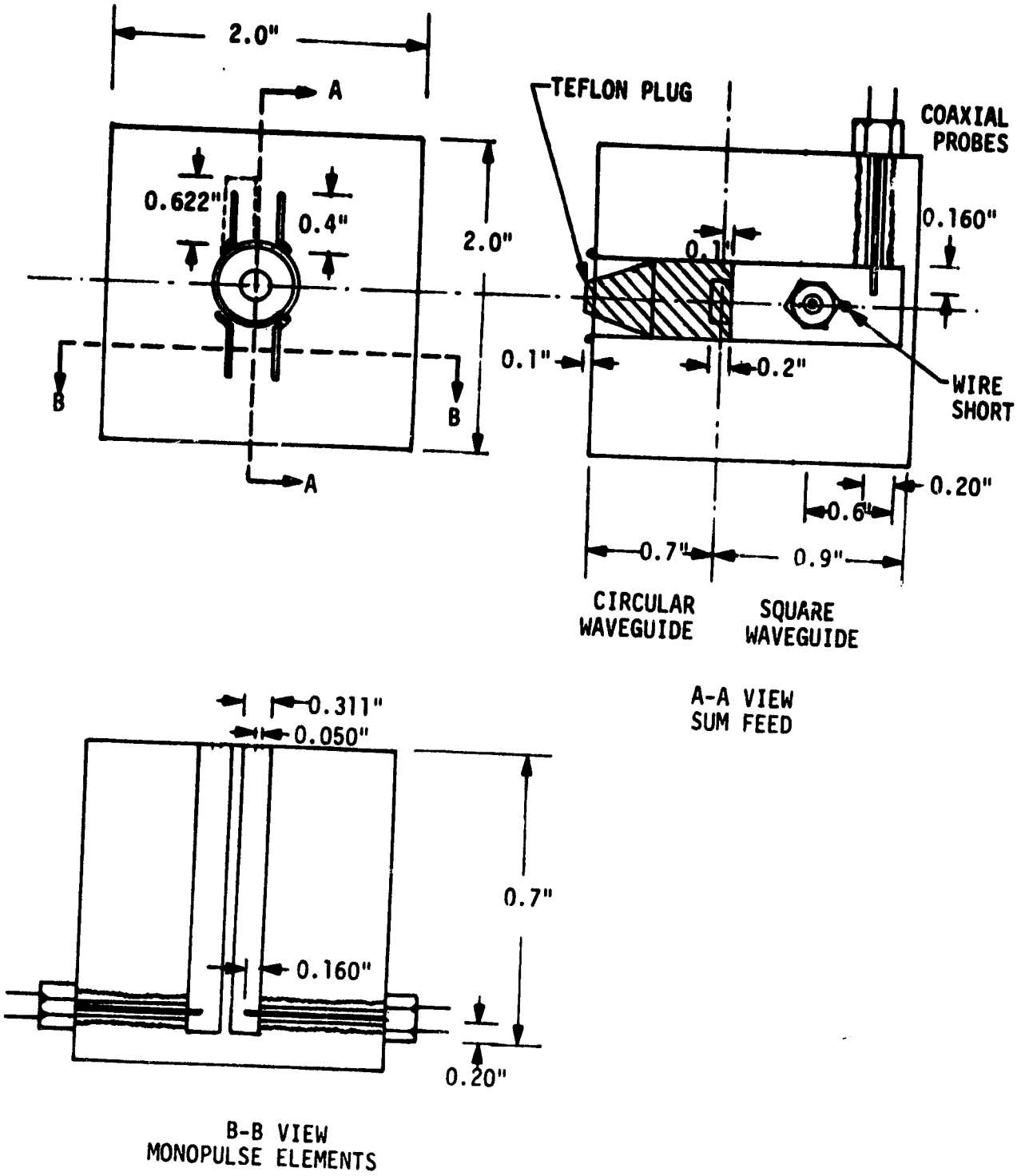

Figure 3. Ku-Band Feed Design Sketch
(not to scale)

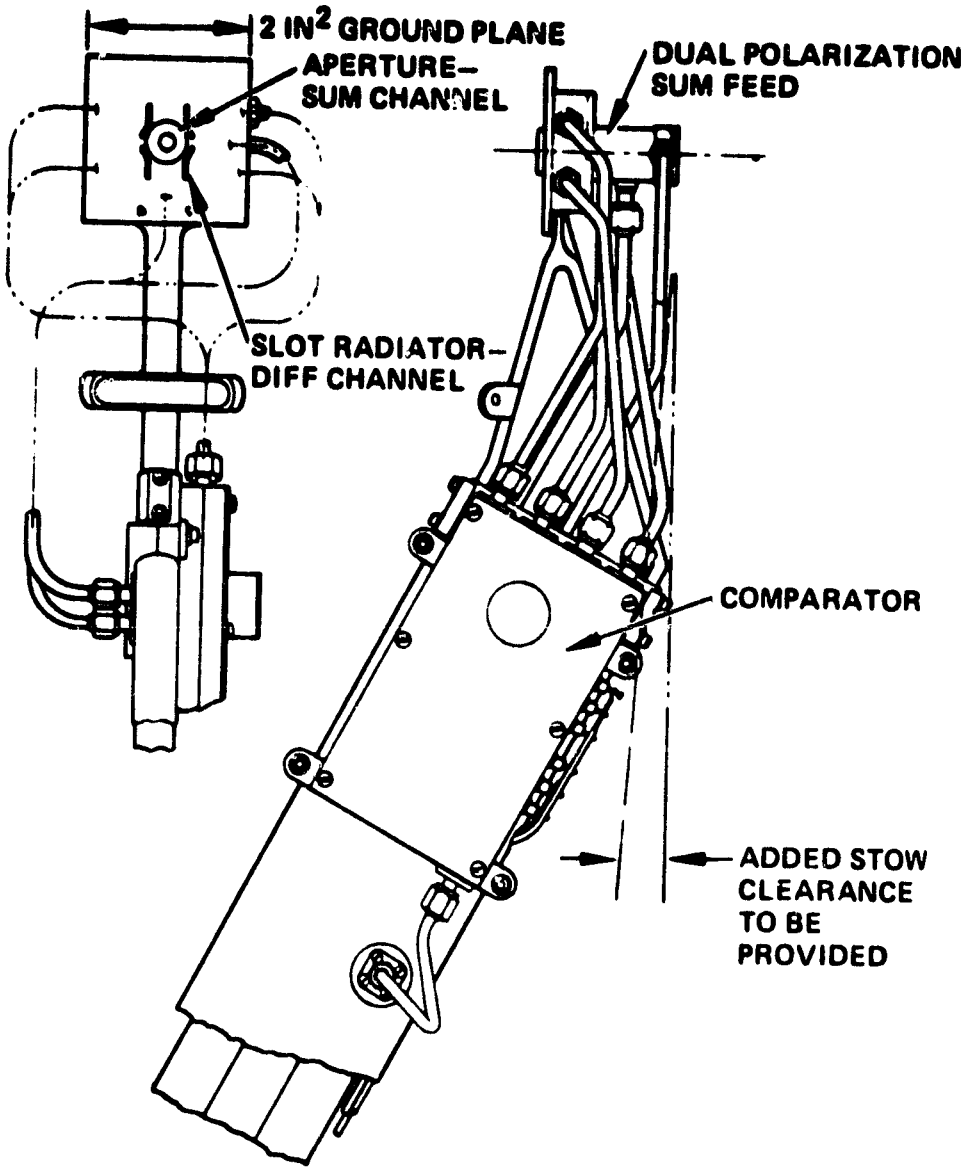

Figure 4. Feed and Feed Support Structure for the Ku-Band Antenna System

elements and the inserted teflon plug of the sum feed due to the abrupt pressure changes arising from launch. The large pressure differentials can cause separation of the windows or loss of the teflon plug, the latter effect being critical since the sum feed cannot propagate Ku-band microwave signals without the dielectric medium in the reduced diameter circular waveguide. Even if only partial ejection of the teflon plug occurred, the resultant protrusion would behave like a dielectric rod antenna with the earlier observed effect of parasitic coupling to the monopulse elements and therefore result in much higher sidelobe levels.

Vents can be introduced in a number of positions without greatly affecting the RF performance. For example, since the feed is a two-piece flanged section, small holes can be machined at the flange face in the corners of all five waveguides since the electric fields are negligible there. Similarly, small holes can be drilled at the corners of the rear walls of the waveguides at the plane of the short, but this is more difficult to align. Since the semirigid coaxial cable probe is usually filled with a dielectric (teflon) and the signal strength is greatest there by design, it is probably wise to avoid these areas for venting purposes.

Hughes has subjected a breadboard feed design to an abrupt vacuum test, with no adverse effects. It was felt that adequate venting was provided by the nonhermetic seal connector probes and loose-fitting flanges. The test involved decreasing the pressure from atmospheric to 10^{-3}mm (Hg) of vacuum in about 15 seconds. Although it appears adequate, more details of the exact launch profile depressurization should be known, and prudent design would incorporate venting provisions to accommodate multiple launches.

Another concern is the effect of ultraviolet light from the sun affecting the material properties of the teflon plug in the sum feed which is critical to the proper operation of the radar and communication modes. Although, in the low f/D ratio antenna system, the feed is blocked effectively from direct exposure to the sun, whatever energy that is reflected from the reflector is highly concentrated since it is focussed at the feed. A protective kapton window might also be considered to cover the sum feed aperture, similar to the kapton windows used for the monopulse elements.

3.4 RF Performance

The RF performance of the Ku-band antenna system reflects the fact that a low f/D ratio prime focus system was selected over a larger f/D ratio system such as a Cassegrain with a subreflector. The higher than expected sidelobe levels, which may result in inadvertent sidelobe acquisition, arise from two separate effects. First, the center-fed parabola has a large amount of blockage from the feed, feed support, and pods. Second, the sum feed system, composed of a dielectric loaded circular waveguide, is not noted for its illumination taper or its spherical wavefronts, and parasitic mutual coupling to the monopulse elements is evident. It is essential to characterize the apparent causes of these limitations so that future modifications, if required, will be straightforward.

The measured principal plane antenna patterns are shown in Figures 5 and 6 for two typical modes: linear polarization and circular polarization at 13.77 GHz. Examining these patterns reveals some basic characteristics which will generally suffice to describe the pattern at other frequencies, since it was designed to be a wideband system. As depicted in the circular polarization case pattern of Figure 5, the elevation plane (denoted by EL) possibly shows the blockage effects of the feed support by the lower than -30 dB sidelobe. Generally this obstructed energy is simply redistributed, and it is not uncommon to find sidelobes in another region greater than would be measured if the blockage did not exist due to the disturbance in the interference patterns. Although a raster scan was made of the immediate vicinity of the main beam, a more thorough program of antenna pattern measurements should be conducted for the final flight version to verify that no extraneous sidelobes of substantial magnitude exist.

The measured 3 dB beamwidth is broader than originally specified (1.5°-1.6°) but the increase does not appear to be significant. The measurement techniques used the expanded scale (6x magnification) to resolve the angular relationship to greater than tenths of a degree, and calibration curves of the pattern measurement system were taken at a later date to confirm that nonlinearities did not exist. In practice, especially when the flight model antenna patterns are measured, calibration verification curves using a series-connected precision attenuator might be recorded both before and after a series of patterns to conclusively demonstrate the validity of the beamwidth and sidelobe levels.

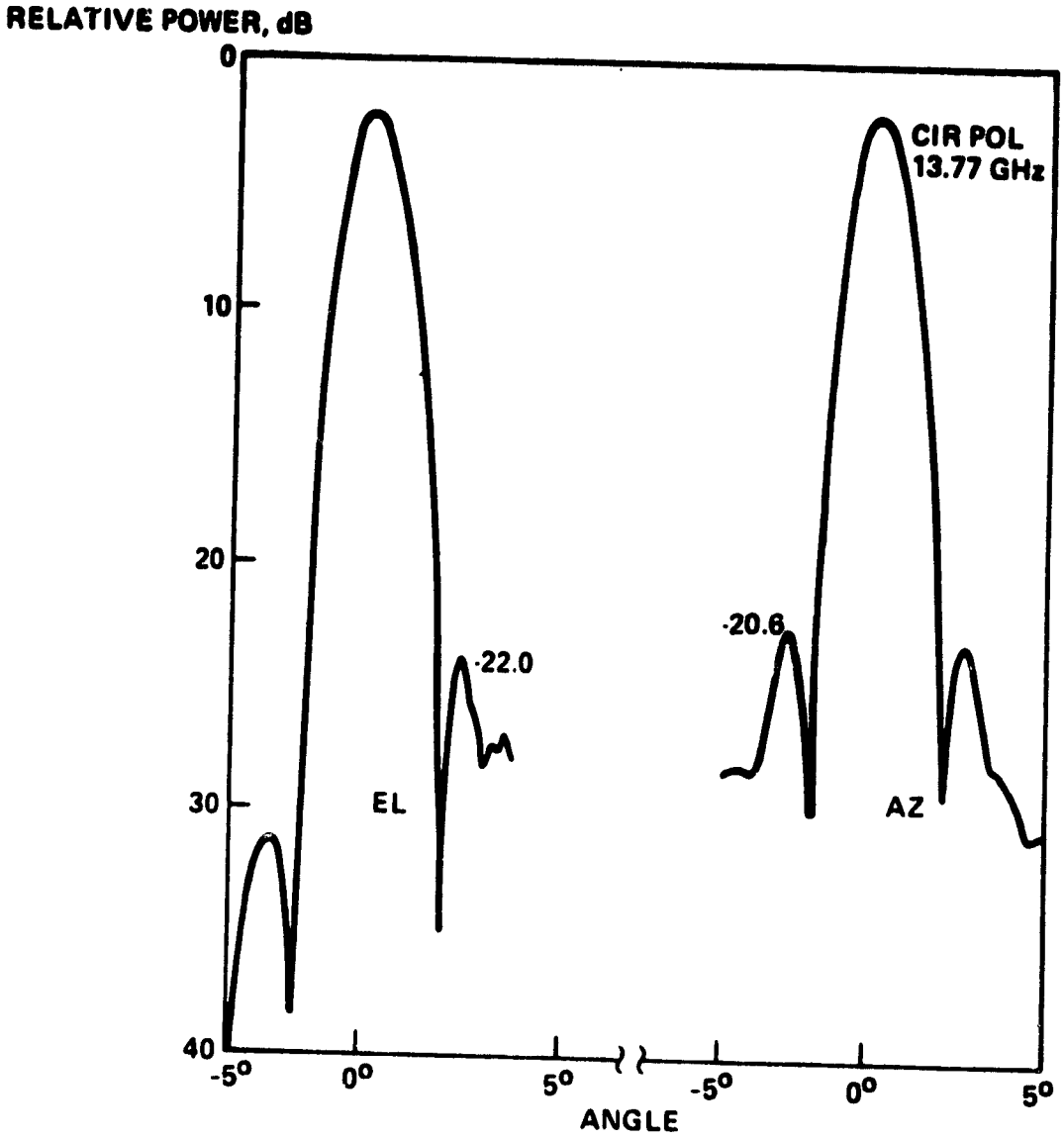

Figure 5. Principal Plane Ku-Band Pattern Measurements for the Circularly Polarized Communication Mode

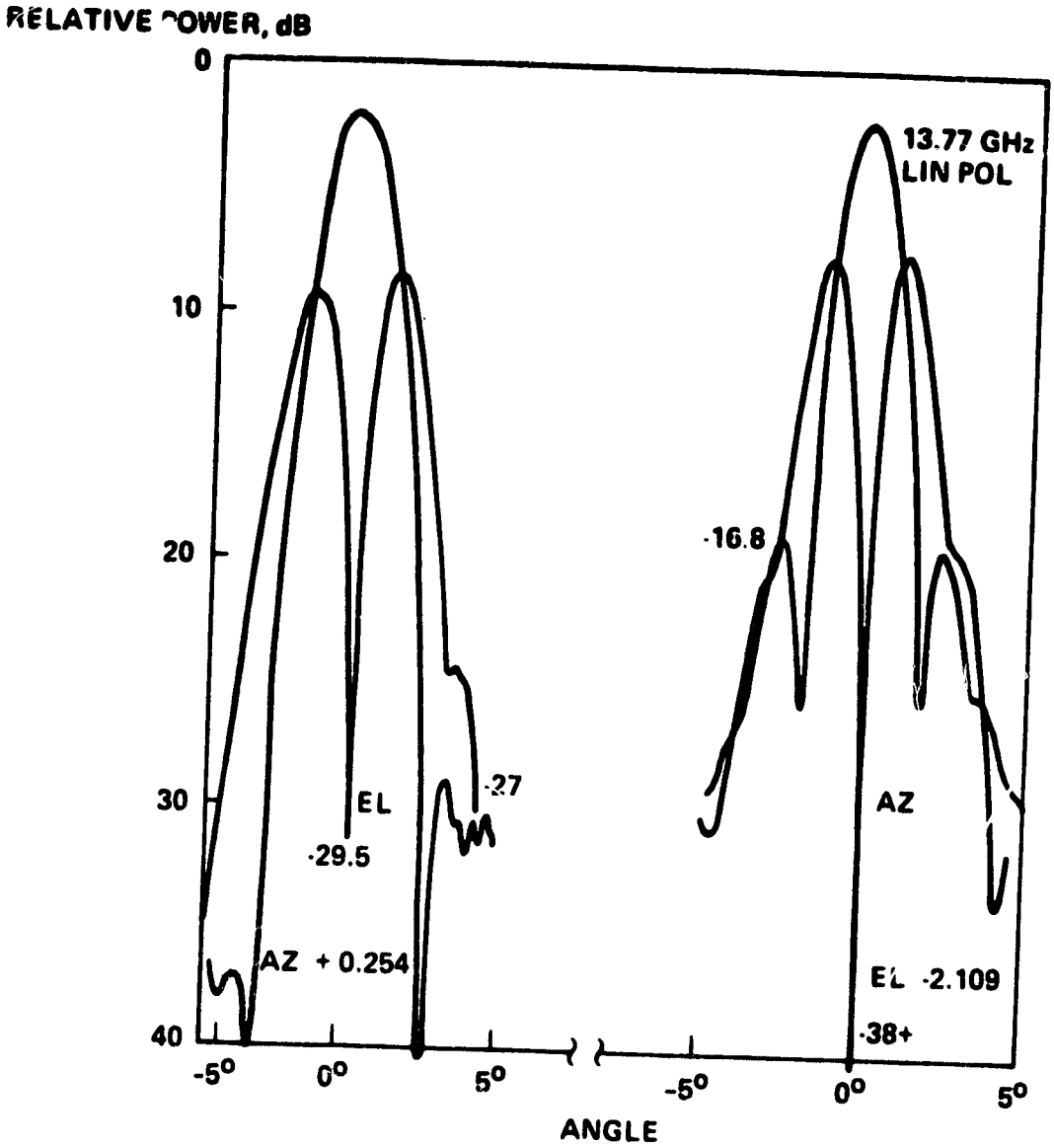

Figure 6. Principal Plane Pattern Measurements for the Sum and Difference Channels of the Ku-Band Antenna for the Linearly Polarized Radar Mode

The -16.8 dB sidelobes in the azimuth plane are unreasonable. Although this behavior is attributed to a nonideal ADL paraboloid reflector, there may be some other suitable explanations. One possibility, which will be discussed in the last section dealing with recommended improvements, addresses placement of the graphite epoxy feed supporting pods which are in the azimuth plane and block the illumination taper. Another is the existence of parasitic mutual coupling of the sum feed with the monopulse elements since the primary sum feed radiation pattern is greatly distorted when the monopulse elements are added.

3.5 Thermal Effects on the Ku-Band Feed

The calculated temperature extreme that the Ku-band feed will be subjected to is approximately -170°F (160°K). Therefore, some concern has been expressed as to the temperature dependence, if any, of the feed. Attempting to utilize the existing knowledge of the present design, especially the measured wideband frequency performance, it does not appear that there are any critical temperature-dependent effects which might adversely affect the feed performance, excluding possible mechanical stresses and material phase transitions. The design parameters were rather loose; many aspects of the design were experimentally determined and, therefore, not subject to precise dimensions. As a result, thermal expansion and contraction effects were, therefore, minimized for this wideband system. No sensitive resonant cavities or filters which might be detuned by thermal dimensional changes were incorporated into the design. The closest structures that resemble a resonant cavity are the short waveguide sections of the monopulse elements with the radiating slots. Experimentally, however, these elements have been measured to operate over the range 13.75 to 15.15 GHz and therefore do not seem temperature-sensitive since they are not frequency-sensitive.

Under standard laboratory conditions, it is very difficult and expensive to measure the performance of an antenna system over the anticipated operating temperatures of space since the feed would have to be cryogenically cooled below the dew point of the surroundings, necessitating enclosure within a vacuum chamber. Further, the essential antenna parameters, beamwidth and sidelobe level measurements require far field pattern measurements, so that a large transparent vacuum chamber window would be required. Thus, the temperature-dependence measurements of an antenna system would have to be considered impractical on the ground. The best one could realistically achieve is, possibly, to measure the return loss of a cooled and heated feed assembly in a vacuum chamber with the feed pointed at a matched load. Swept frequency measurement could then establish whether temperature-dependent effects exist.

In response to the concern shown over the temperature dependence, a simple heating test of the feed was made using a heat gun during antenna pattern measurements. As would be expected, no effects were noted. It is felt that such tests are not truly representative since the feed will

assume a very low temperature, and the temperature differential calculated will be much larger than can be achieved under these conditions.

Rather than speculate on the effects of the calculated cold temperatures, it might be more productive to examine potential solutions to the problem. The present thoughts involve adding a strip heater to the feed assembly similar to that used to warm the monopulse comparator circuitry. Rather than using active heating, however, if passive means are available for thermal control, then these methods should be looked at instead of wasting valuable electrical power. A thermal enclosure about the feed and feed support would greatly reduce the temperature extremes presently expected. This enclosure could be in the wedge shape described later to minimize RF blockage effects. It would also serve to protect the feed, comparator, and connecting cables from physical damage due to deployment and stowage.

3.6 Recommendations for Improvement

One of the goals of the Ku-band antenna study is to make recommendations, if possible, to improve the performance of the system. After describing the antenna in some detail, some areas of improvement became apparent, especially in regards to the higher-than-expected sidelobe levels. This section outlines some modifications which seem reasonable to investigate further.

One of the explanations for the poor sidelobe performance of the Ku-band antenna is the mutual-coupling effects between the sum feed and the monopulse elements. The primary sum feed antenna pattern is disturbed significantly when the monopulse elements are added. The original 20 dB taper on the reflector is reduced to a 10 dB taper. In order to reduce this mutual coupling, the addition of shorting elements on the ground plane to place the null from the VSWR on the monopulse slots is proposed. Earlier Hughes tests of a similar technique indicated substantial perturbations in pattern measurements by the placement of obstacles on the ground plane, but efforts were discontinued due to the poor results. In the next section, we describe a more systematic technique for the placement of shorting elements.

The other major contributor to high sidelobe levels appears to arise from the blockage of the primary sum feed illumination pattern by the adjacent feed support pods in the azimuth plane. Three modifications are suggested. The first is to relocate the pods out of the azimuth plane, preferably into positions 120° from the feed support to disrupt the cumulative blockage of both pods in one plane. If it is determined that little mechanical support of the feed is actually required, then possibly only one support pod parallel to the boresight of the sum feed might be studied. A better solution is to attach the pods at 120° angles to the edge of the reflector such that the pods block only the secondary pattern from the illuminated reflector. The amount of effective blockage for this configuration is much less, even though the pods are longer. Finally, a nonconductive material can be used to fabricate the pods instead of conductive graphite epoxy.

A more subtle design method might also be used to decrease the effective blockage cross-section. Shaping the pods and feed support into diamond and hexagonal wedges can greatly reduce the deleterious effects of the obstacles.

And finally, in order to control the launching of spherical wave fronts by using a dielectric lens concept, some possible design shapes for the dielectric plug are developed.

3.6.1 Reduction of Mutual-Coupling Effects

There was a noticeable degradation in the illumination taper of the primary pattern of the sum feed when the monopulse elements were incorporated. In order to attempt to alter this deleterious interaction, a slight modification of the ground plane is proposed to create an effective short for the leakage radiation diffracted around the lip of the sum feed. This short is positioned to take advantage of the directionality of the leakage radiation compared to the incident radiation from the reflector.

Basically, the idea is to position a null from the resultant standing wave from the short at the slot center. As Figure 7 indicates, the location of this annular ring sector is $3/4\lambda$ from the sum feed. The height of the short should be approximately that of the extension of the lip of the sum feed, but the exact dimension would probably be experimentally determined.

The incident radiation from the reflector should not be adversely affected by this annular ring sector short by geometrical considerations since the height is small compared to a wavelength and the separation between the annular rings is greater than $\lambda/2$, which avoids reactive termination conditions as in corrugations.

If improvement is noted, then it would be logical to add other annular ring sectors $\lambda/2$ beyond the first one to improve the effectiveness of the short.

3.6.2 Pod Relocation

The blockage effect of a center fed paraboloid is especially critical since the majority of the illumination taper of the feed is in the central area of the dish, and therefore any obstruction greatly alters the antenna pattern, usually by broadening the beamwidth and increasing the sidelobe levels.

The most logical explanation for the degraded sidelobe behavior for the linear polarization case (and therefore the circular polarization case) is the use of horizontal graphite-epoxy support pods for mechanical rigidity of the main feed support. Since graphite epoxy is considered conductive, these pods have a large effect blockage cross-section, similar to the reason for changing the orientation of linear polarization with respect to the feed support.

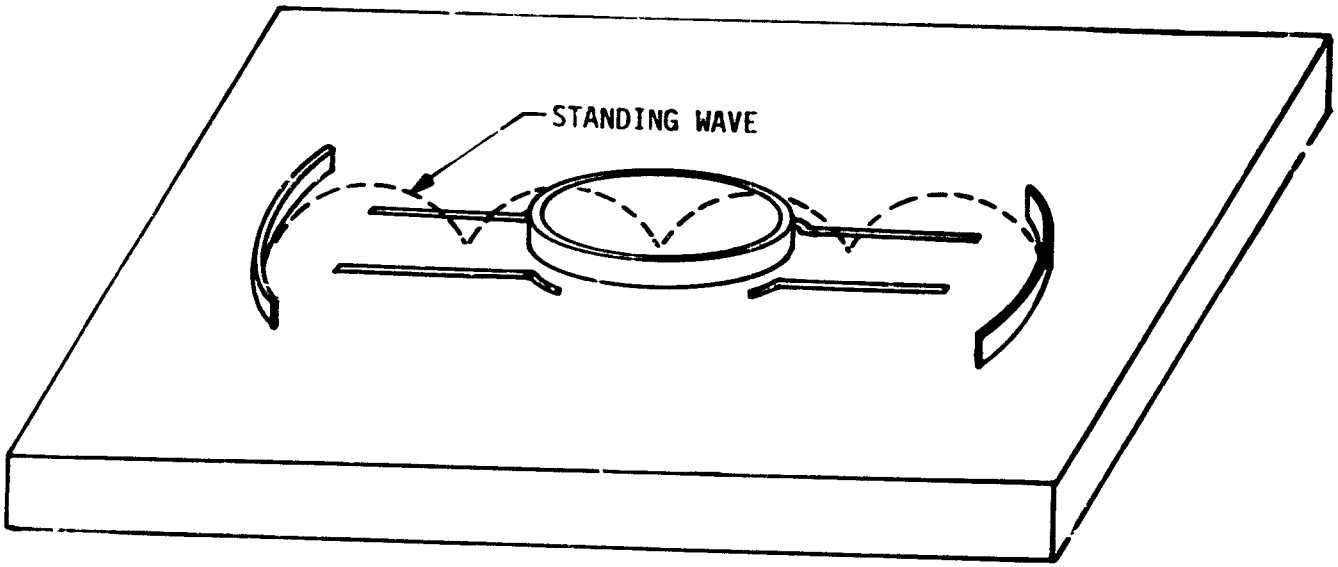

Figure 7. Annular Ring Sector Short to Reduce Mutual Coupling

A sketch of the physical relationship between the sum feed pods and reflector is shown in Figure 8a. Although the pods are relatively short, they would exert substantial influence on the patterns since they are positioned so that all radiation in that plane is blocked. Since the f/D ratio of the antenna is so low, the effective blockage cross-section is large because the angles subtended by the pods increase when the pods are located closer to the focus. In this particular case, the pods are so close to the center of the paraboloidal reflector that they intrinsically will obstruct the primary pattern of the sum feed even before illuminating the reflector, as depicted in Figure 8b. If the edge of the reflector is roughly ±70° from the sum feed, the pods are approximately ±30° from the center (more exact angular relationships should be obtained if further analysis is desired). Thus, the primary pattern of the sum feed is completely blocked in the azimuth plane beyond the 30° from boresight. Further, the central portion of the primary pattern after reflection is blocked by the feed, but this blockage cross-section has been greatly reduced by the relocation of the phase comparator and the reduction of the ground plane area to 4 square inches. Thus the presence of the support pods, being conductive, completely disrupts the primary and secondary patterns, resulting in poor sidelobe levels.

If the support pods were attached to the edge of the reflector instead of the central area, the effective blockage cross-section would be reduced and the sidelobes correspondingly reduced in magnitude, as sketched in Figure 8c.

3.6.3 Pod Orientation

Conductive support structures are known to affect patterns for the case when the electric field is parallel to the conductive member. The explanation, it appeared, was that the conductive member acted in a manner to electrically short the incident electric fields, creating a standing wave in the vicinity of the parallel member. Electric field vectors orthogonal to the conductive member, however, can propagate around the obstacle since electric fields can exist normal to a conductive surface. For the case of circular polarization, since the electric field vector rotates, the standing-wave phenomenon in similarly applicable for the parallel

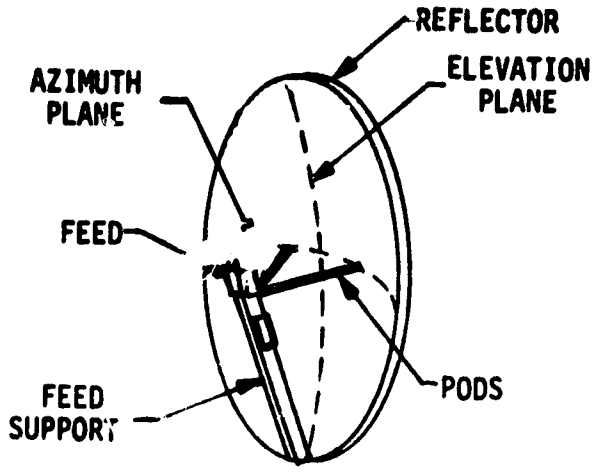

Figure 8a. Sketch of Support Pods on the Ku-Band Antenna

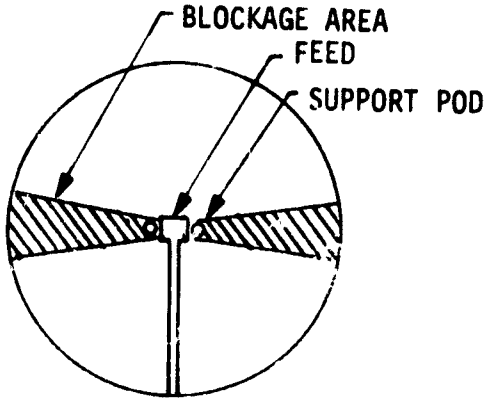

Figure 8b. Obstructed Primary Feed Pattern

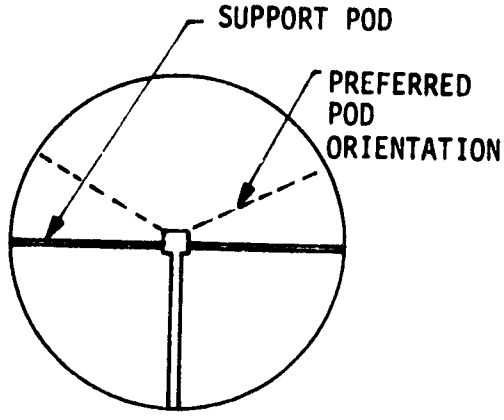

Figure 8c. Reflector Edge Pods

component of the electric field but not for the orthogonal component. Therefore, a polarizing mechanism exists similar to the wire grid structures used to filter out the orientation of linear polarization parallel to the wires.

This effect was noted early in the development of this Ku-band antenna. The sidelobe levels decreased when the orientation of linear polarization was rotated to the azimuth plane, which is perpendicular to the feed support. However, now the support pods became aligned parallel to the electric field and became predominant blocking mechanisms, although to a lesser extent.

If the support pods were located 129° from the feed support, the sidelobes would be further reduced since the blocked areas are not in the same plane. Therefore the magnitude of the perturbation is caused by only one pod, which is not the present situation where there are two pods in the azimuth plane, the plane which has the high sidelobe problem. By distributing the disturbances due to the pod placement about the antenna pattern, it is possible to reduce the sidelobe contributions in any single plane, thereby decreasing the sidelobe level.

3.6.4 Pod Material

The reason why the side support pods result in such large blockage is the fact that graphite-epoxy is quite conductive and, therefore, creates standing-wave patterns in the region of the pods.

One solution is to fabricate the pods from less conductive material such as fiberglass or kevlar. These materials, being dielectrics, would cause some phase shift problems for the rays incident upon the pods, but actual blockage would be minimized.

One potential problem area if material substitution is used is thermal expansion differentials since graphite epoxy is noted for its low coefficient of thermal expansion. For the relatively short pod lengths considered here, however, this should not deter the serious consideration of this approach.

3.6.5 Pod Shaping

Another approach might be considered to further improve the side-lobe levels. Earlier work by Ruze [1] and Kay [2] discussed the improvement in gain of antennas when blockage of the obstacle was tapered to allow incident radiation to propagate around the obstacle rather than be reflected away by flat surfaces. Their problem was to minimize the effects of metallic structures supporting a radome. On a comparative scale, that type of blockage was very small since, on a cross-sectional basis, the width of the structural members were quite small compared to the antenna reflector cross-section. However, for the case of this Ku-band antenna, the feed and feed support structure are quite large compared to the reflector and the microwave wavelengths. Therefore, the shaping of the obstacle should have a correspondingly larger improvement.

The specific shape to be considered is a pyramid over the feed and a hexagonal wedge or a variant thereof along the feed support which will permit some radiation, however distorted, to be collected by the reflector. Ideally, the hexagonal wedge has long tapers on both sides which behave as transitions and provide a grazing incidence angle to the incident radiation. Since the illumination taper is greatest at the center of the dish, the region where the feed is mounted, this area is intrinsically the most critical. An easy test to determine the feasibility of this approach consists of a simple substitution whereby a section of heavy-duty aluminum foil is folded into the appropriate shape and taped onto the breadboard or engineering model. The result should be readily apparent by the measurement of sidelobe levels. This shaped reflector along the feed/feed support can also serve as a thermal shield to reduce the large temperature extremes calculated to exist at the feed. A fiberglass shell bonded with heavy-duty aluminum foil which is painted with white thermal control paint will help to passively maintain the feed at a higher temperature than the presently calculated -170°F (nonoperational state) and reduce temperature fluctuations on the phase comparator circuitry which have temperature-sensitive varactor diodes subject to "carrier freeze-out" at low temperatures.

3.6.6 Dielectric Plug Design

One design requirement discovered during the early phases of the Hughes antenna feed development was the control of the illumination taper which was too uniform and, therefore, resulted in extremely poor sidelobe levels. After many trial tests, the present dielectric plug shape was evolved which resulted in a satisfactory primary feed pattern without the monopulse elements with a 20 dB taper. (The presence of the monopulse elements, and the mutual coupling, however, reduced it to a 10 dB taper.) This shape is sketched in Figure 9a, which shows a 0.5 inch diameter circular teflon plug tapered at the aperture end to simulate a dielectric rod antenna which concentrates the radiated energy in the dielectric as though it was a dielectric waveguide. The other end of the plug, facing into the coaxial probe transducer, is counterbored to form a transition from the square waveguide to the circular waveguide section. This "concave" surface is conducive to creating a nonplanar wavefront since the central portion of the propagating mode travels at a higher velocity than at the perimeter of the circular waveguide, thereby creating a "bulge" in the wavefront which might result in a quasi-spherical wave at the aperture end since the circular waveguide section is relatively short. However, on the aperture end, the tapered dielectric section used to concentrate the radiated energy acts to slow the central portion of the propagating mode, thereby compensating for the concave surface at the opposite end. A sketch of the probable phase fronts for the present design, which coincides with that actually measured, is shown in Figure 9b. Since the tapered rod was experimentally found to be essential in creating a satisfactory illumination or amplitude taper in the primary pattern, any suggested modifications to improve antenna performance must realistically use this baseline design.

3.6.7 Modifications to Promote Spherical Wavefronts

Since collimation from paraboloids rely on a spherical wave emanating from the focus, it would seem logical that an effort be made to alter the siutation to favor creating at least a semblance of such a spherical wave. This nonspherical wavefront effect would be accentuated for lower f/D antenna systems since a longer focal length geometrically reduces the

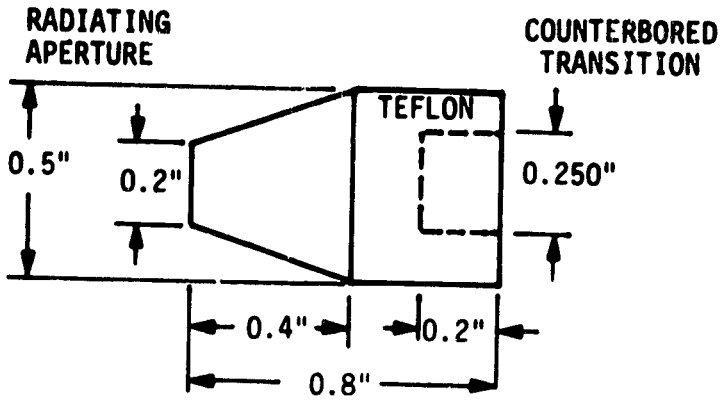

Figure 9a. Present Design of Teflon Plug

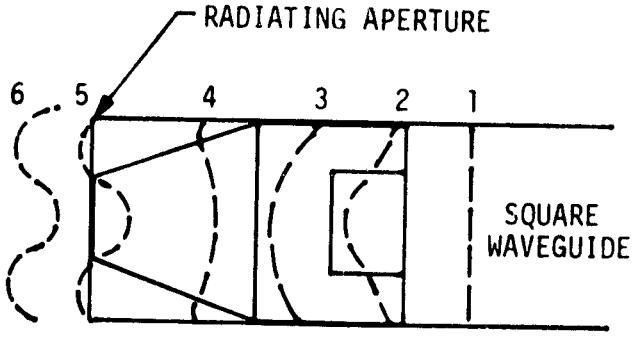

Figure 9b. Sketch of Approximate Phase Fronts for the Present Teflon Plug

magnitude of the deviation from a true spherical wave, measured in fractions of a wavelength. The optical equivalent of this situation is spherical aberration, where the degree of distortion corresponds to the sidelobe problem.

A spherical wavefront requires that the central portion of the radiated energy from the feed be launched into free space earlier than the planar wavefront within the dielectric-filled circular waveguide. A sketch of the proposed modifications to the existing teflon plug is illustrated in Figure . Note that the present design configuration is generally maintained since it has successfully evolved by extensive testing to a satisfactory performance level. Since few further modifications to decouple the sum feed from the monopulse elements are obvious, the spherical wavefronts concept, which has not been emphasized earlier, is pursued.

One method to create this desired effect is to drill a small hole in the center of the teflon plug, thereby creating a propagating mode which can have a longitudinal component of electric field, creating the "bulge" that generates the required curvature at the radiating aperture. Since this perturbation is distributed, the cumulative effect is to cause a high degree of distortion, with the faster central portion of the mode "dragging along" the slower edge portion which serves as a slow wave structure. The depth and diameter of the hole would have to be determined by analysis, but the concept does permit a degree of control over the shaping of the launched wavefront which has not been investigated previously. And, if this hole traverses the entire length of the dielectric plug, it can also serve as a convenient means of venting the square waveguide section of the sum feed to relieve the contained atmospheric pressure during the launch.

Another method of creating a quasi-spherical wave is to shape the dielectric aperture as a lens system. Since a planar propagating wavefront exists within the circular waveguide, the "bulge" can be encouraged by a concave surface, such that the aperture appears indented in the center of the plug. Since the central portion is launched earlier than the edges, a more exaggerated curved wavefront results. Again, further analysis would be required for determining the optimum curvature if the concept is pursued, but a simple experimental verification can be obtained by machining a test teflon plug and comparing the resulting sidelobe levels.

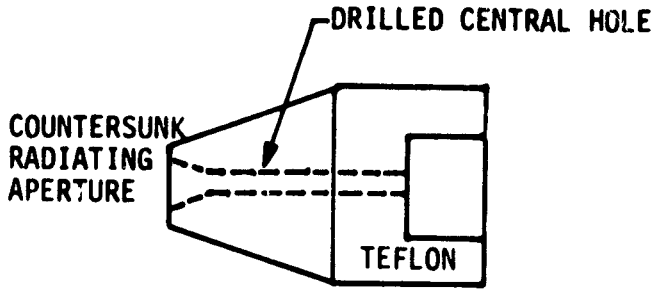

Figure 10a. Modified Design of Teflon Plug to Encourage Quasi-Spherical Wavefront

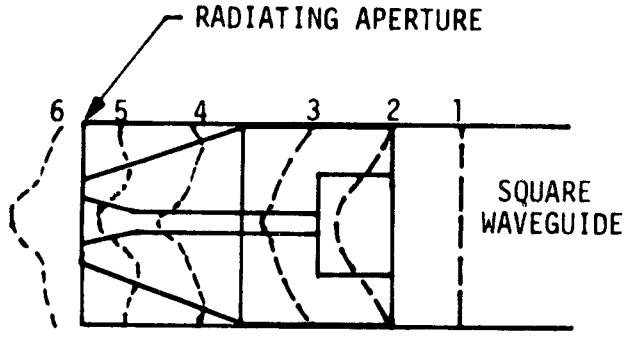

Figure 10b. Sketch of Approximate Phase Fronts for the Modified Teflon Plug

A sketch of the desired phase fronts resulting from these modifications is shown in Figure 10b. Note that, although perfect spherical waves are not produced, the general wavefront is not as distorted in terms of the magnitudes of the phase deviations as in Figure 9b .

3.6.8 Differential Monopulse Element Nulls

The explanation used in Axiomatix Report R7804-3 for the absence of a well-defined null in a particular plane difference channel was attributed to the geometrical relationship of the dipoles to the incoming phase front on which the monopulse tracking system is based. This phase front problem would be more apparent for lower f/D ratios of the antenna reflector systems. The orientation of linear polarization in the plane of incidence suffers from a lack of phase resolution since it approaches the dipole at the grazing angle. Because of this grazing angle of incidence, the phase itself cannot be well characterized by the dipole, which is of the order of half a wavelength long. An attempt to pictorially describe this phenomenon is shown in Figure 11a, which shows that the phase front from the edge of the reflector is incident on the monopulse dipole at close to a grazing angle. A more detailed description is shown in Figure 11b which shows the phase relationship of the incident wave on the dipole for the ray path designated by A. It is seen that the phase relationship cannot be well defined for this orientation of polarization and this particular dipole orientation. This is not true for the ray path designated B since the electric field vector would be oriented parallel to the dipole, and a prominent null would exist.

One corrective measure would be to use a curved dipole as shown in Figure 11c. This configuration would most closely resemble the focused spherical phase front and would thereby avoid the shallow null problem.

The present monopulse design uses slots in a ground plane, and the same explanation is valid except that now the shallow null is transferred to the orthogonal plane from the case of the dipole. But since the orientation of linear polarization has been rotated to the azimuthal plane, the shallow null is still in the elevation plane. The grazing angle for the slot configuration is shown in Figure 11d, where, due to the finite width of the slot, phase resolution can be degraded for a low f/D system unless a complex spheroidal ground plane is used.

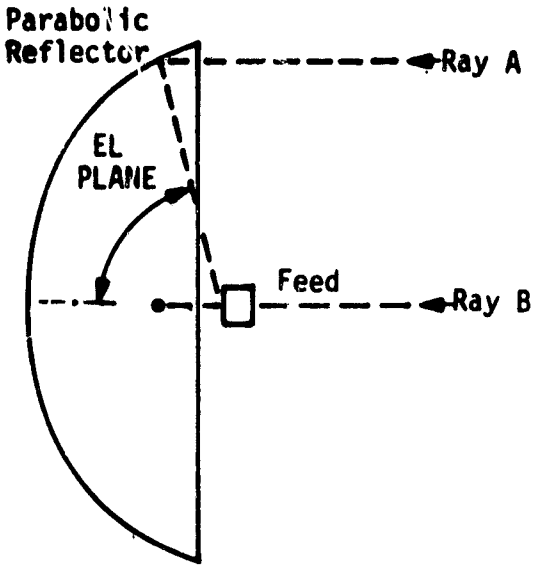

Figure 11a. Ray Paths for the Parabolic Antenna

Figure 11b. Incident Electric Field on the Dipole

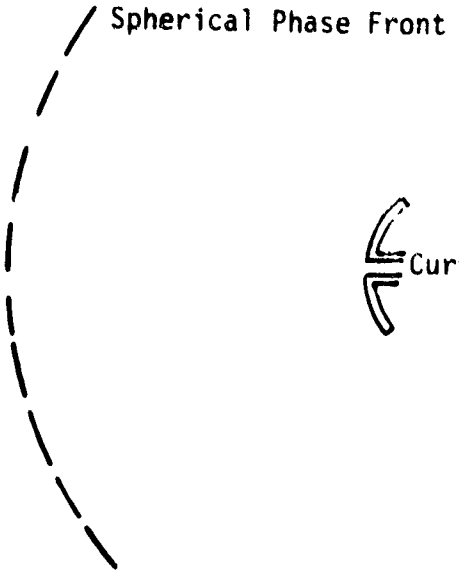

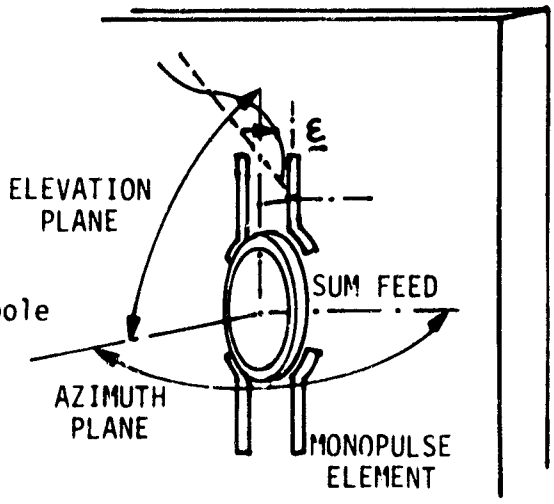

Figure 11d. Incident Electric Field on the Monopulse Element

Figure 11c. Curved Dipole Configuration

3.7. Ku-Band Wide-Beam Horn

The Ku-band wide-beam horn has two distinct functions. The first use is to determine main beam acquisition for the rendezvous radar by establishing a threshold level for comparison with the narrow beam antenna sidelobes. The second function is the wide area acquisition of the TDRS signal for communications.

Since the TDRS signal is right-hand circularly polarized (RHCP) and the radar is linearly polarized, there has been some compromise in the radar performance. There is an inherent 3 dB loss when linear polarization is received with a RHCP horn since the linear polarization is composed equally of right and left-hand circular polarization components.

The purpose of this section is to describe the wide-beam horn in some detail and determine the system trade-offs. Since the horn was initially designed for linear polarization as a result of a possible Skylab mission, the antenna pattern measurements with the circular polarization transducer are not available at this time. However, the earlier linear polarization measurements indicate reasonable performance parameters.

3.7.1 Physical Description

The basic conical horn design is a cone with a slope length of 7.7 inches, an aperture diameter of 3.2 inches and a double cone angle of 24°, as sketched in Figure 12. The circular polarization (RHCP) transducer is located immediately behind the horn and consists of a section of circular waveguide with four pairs of tuning screws 45° to the incident linear polarization which act as reactive elements to generate the differential phase shifts required to change the linear polarization to circular polarization.

Some of the general design graphs used to create the differential phase shifts are shown in Figure 13[3] to explain the multiple-lumped-element loading concept of this type of transducer. Instead of a square waveguide, the linear polarization is introduced into the circular waveguide at a 45° angle to simulate a power splitter since the equal orthogonal components parallel and perpendicular to the tuning screws then undergo the differential phase shifts which result in generating circular polarization.

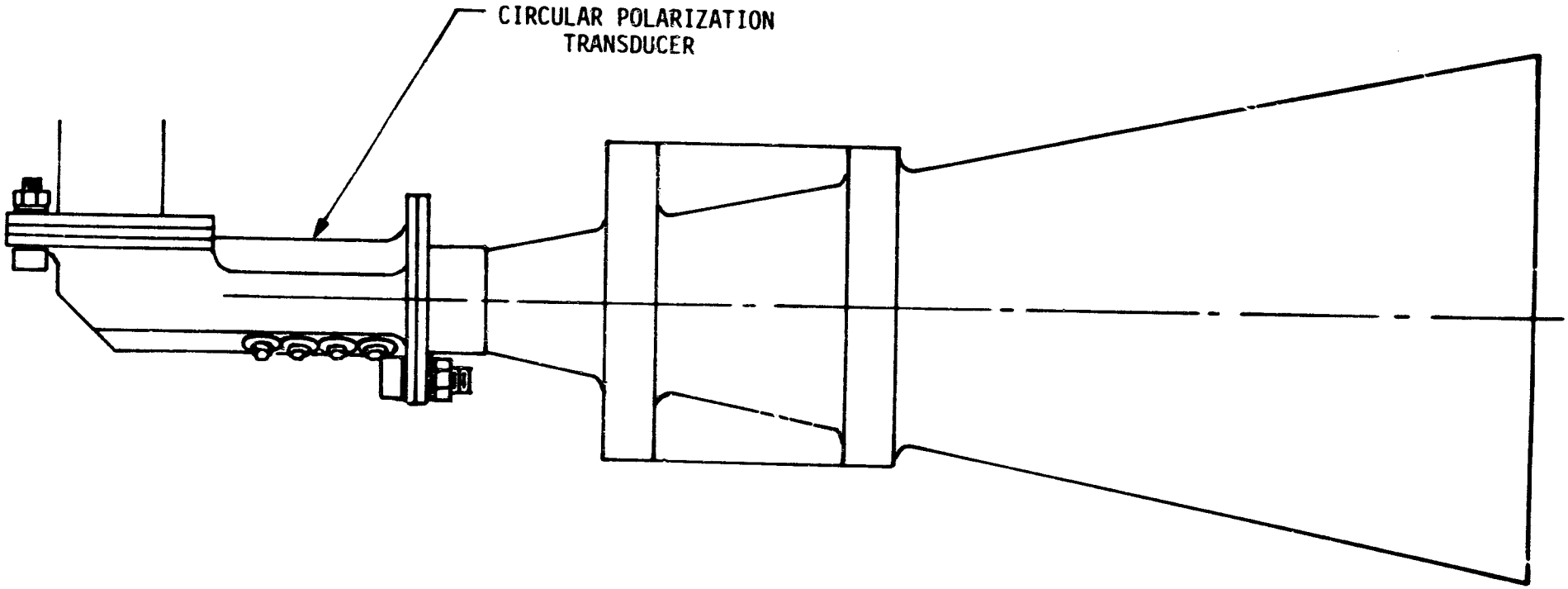

Figure 12. Sketch of Ku-Band Wide Beam Conical Horn with Circular Polarization Transducer

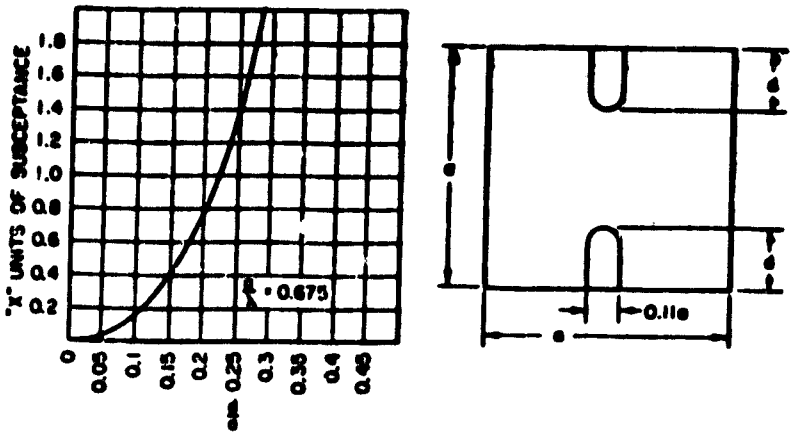

Figure 13a. Susceptance as a Function of Probe Penetration.

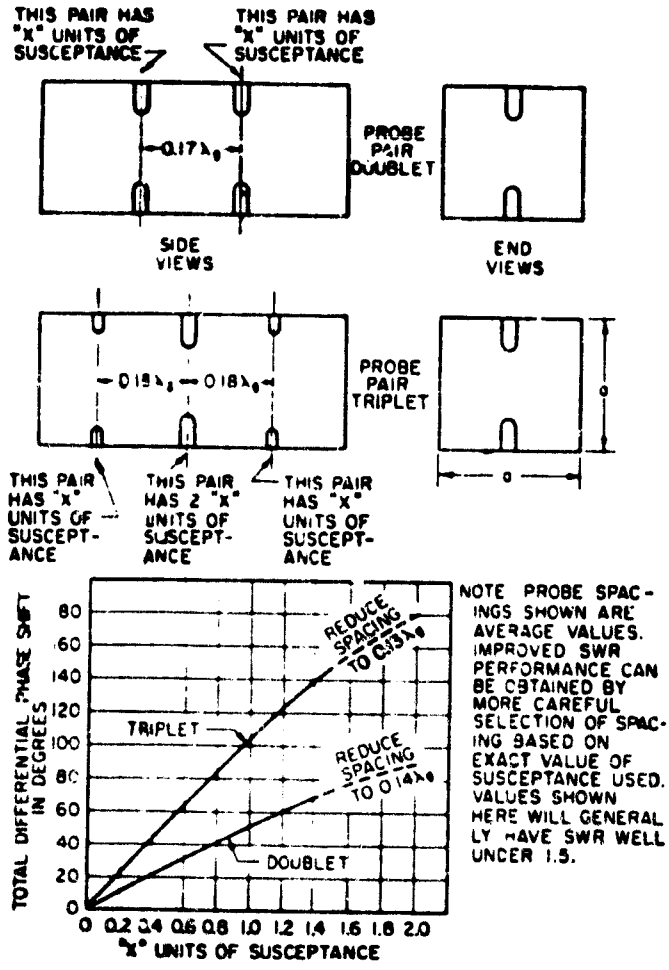

Figure 13b. Probe phase-shifter design.

3.7.2 Pattern Measurements

The only Ku-band wide-beam antenna pattern measurements released to date have been the linear polarization patterns taken for the proposed Skylab mission. Since the wide-beam antenna is being converted to right-hand circular polarization (RHCP), the patterns themselves can be used only as a representative sample of what might be expected for the RHCP case, although the efficiency of the circular polarization transducer over the broad frequency range will greatly affect the final patterns.

The most noticeable characteristic of this type of conical horn is the varying beamwidths in the E and H planes at the same frequency, as shown in Table 1.

Table 1. Ku-Band Wide Beam Horn-Linear Polarization

Freq. (GHz)	Gain (dB) [at rotary joint]	3 dB Beamwidth (°) - E and H Planes
13.77	18.4	16.6/18.8
13.90	19.0	16.4/19.9
14.00	18.8	16.7/19.0
15.15	19.7	14.4/17.3

This distortion from a "circular" beam causes ellipticity and, therefore, RHCP polarization loss off-boresight. If the gain magnitude is important, then another horn like the corrugated conical horn which has similar E and H plane beamwidths might be considered as a substitute.

As was mentioned previously for the narrow-beam antenna, the inclusion of calibration curves with an in-line precision attenuator both before and after a series of pattern measurements is essential to verify the validity of the beamwidths and gain.

3.7.3 Design Comments

The smooth conical horn has the disadvantage of greater ellipticity off axis due to the different beamwidths in the E and H planes. Corrugated conical feed horns, on the other hand, are noted for their more equal beamwidths in both planes, and some thoughts on considering other types of horns might be fruitful.

The use of the multiple-lumped-element loading technique by Hughes for creating circular polarization does optimize the wide bandwidth requirement since the frequencies are 13.775 GHz for the communications receive mode and 15 GHz for the communications transmit mode. It is also easy to design by using lockable tuning screws for final adjustments.

However, because of the existence of tuning screws, there is some frequency dependence for the circular polarizer and, therefore, certain precautions should be taken. For example, the operation of the circular polarizer should be measured outside the specified frequency range to determine the frequency sensitivity characteristic and thereby deduce the expected temperature sensitivity. Since the tuning screws are located fairly close together and the probe lengths are short, it is not expected that temperature effects would be significant. Again, as in the case of the narrow-beam Ku-band feed, it is recommended that passive means of thermal control be employed to protect it against temperature extremes and resulting thermal gradients from the abrupt operation of the transmitter.

3.8 Conclusions

The high sidelobe levels of the high-gain Ku-band antenna are a primary influence on the antenna system performance. Several relatively easily verifiable improvements have been suggested to decrease the sidelobe levels of the high-gain antenna. If effective, these changes may negate the necessity of alternate, more expensive changes to the Shuttle radar/communication system. In particular, specific recommendations have been made to correct the three areas which have been determined to be contributors to the high sidelobe problem. First, the concept of leakage radiation shorting elements on the ground plane was introduced to minimize the parasitic mutual-coupling effects between the sum feed and the monopulse elements. Second, the feed support pods have been identified as obstacles in the primary sum feed pattern and, therefore, pod relocation and shaping and material substitution were suggested as possible remedies to the illumination taper blockage on the reflector. And finally, some ideas on encouraging the launching of quasi-spherical waves from the sum feed were outlined to minimize phase aberrations for the parabolic system.

4.0 KU-BAND BENT-PIPE CHANNEL PERFORMANCE EVALUATION

4.1 Introduction

4.1.1 Background

This section describes results obtained under Task #1, Exhibit "B", "Ku-Band Bent-Pipe Channel Performance Evaluation." Since Hughes has been experiencing the greatest difficulty with the wideband bent-pipe channel, we have concentrated our efforts in this area. Specifically, the SPA mode 1 channel 3 input port has a bit detector which is the subject of considerable redesign effort by Hughes. This port accepts high data rate NRZ data (2 - 50 Mbps) and clock. The SPA input bit detector attempts to sample the data at mid-bit in order to preclude sampling during a transition. The inherent problem is the wide variability of data rate and input waveform parameters.

The original bit detector circuit consisted of a derived two-phase clock and a coincidence circuit. Proximity of data/clock transitions would trigger sampling on the alternate clock phase. This circuit proved to be unstable under worst-case conditions of data asymmetry and rise time. A relatively simple modification, that of providing a four-phase clock, also proved unsuitable at the higher data rates. As a result, Hughes has had to design a new bit synchronizer.

4.1.2 Summary

This section describes the two principal designs considered by Hughes as well as our analysis of these designs. During the progress of this work, it became evident that the input waveform parameters had not been adequately characterized and specified. In particular, distortion due to cable effects, in terms of frequency-dependent attenuation and rise time, had not been accounted for. In section 4.3, we discuss the model used to calculate the effects of cable attenuation and rise time degradation. Results of this analysis were subsequently incorporated in the Rockwell specification. Discussions of the two prime candidate designs for a bit synchronizer are contained in sections 4.4 and 4.5.

The first synchronizer, which was proposed by Pat Conway, is shown in Figure 15. Since a detailed description is given in section 4.4, we will summarize by stating that this loop utilizes a phase-frequency detector to frequency track the received data clock

frequency and a mid-bit and transition point sample detector to generate a bit timing error (phase error) signal to control the relative phase between the local clock and the local data stream.

It was determined that the basic design was adequate with symmetric bits but could lock up with a large timing error and be quasi-stable (timing will not change unless the clock or bit sequence drifts). This will result in incorrectly detecting some bits.

In particular, for the case of 25% asymmetry at 50 Mbps, the following is true:

(1) With timing errors up to ±2.5 ns (±12.5%), no timing change is performed by the loop and no bit errors will be made.

(2) With timing errors between ±2.5 ns and ±7.5 ns (±37.5%), the loop error control will reduce the timing error and no bit errors will occur.

(3) With timing errors between ±7.5 ns and ±10 ns (±50%), the loop will not adjust the timing error, but bit errors will occur.

A second bit synchronizer was analyzed and is treated in detail in section 4.5. This synchronizer also utilizes a phase-frequency detector as the first one did, but has a different and rather complex bit timing error detector to adjust the phase between the received and local bit epochs. Whereas the Conway synchronizer tracked transitions, this synchronizer tracks rising edges of the bit stream only. It was determined (section 4.5) that this new bit synchronizer will successfully track the rising edges of the received data bits with 25% asymmetry and up to a 90° phase shift between the received clock and the data bit timing. Furthermore, the data bits will be sampled correctly under these conditions. In both synchronizers, it is advisable to zero the digital-to-analog converter loop filter voltage in order to avoid the possibility of false lock.

4.2 Conclusions

Hughes has elected to implement the modified Pat Conway bit synchronizer as described in section 4.5. With input data and clock parameters within the specified limits, the bit synchronizer should track and bit detect correctly.

4.3 High Data Rate Channel Cable and Connector Loss Effects

4.3.1 Introduction

During the redesign effort of the mode 1 channel 3 bit synchronizer, it became obvious that the current input specifications were inadequate. The specifications did not account for data-dependent losses, e.g., losses incurred due to cable attenuation of the higher frequencies, whereas this effect had been noted in cable measurements. In addition, rise time effects had not been adequately modeled. Since the new bit synchronizer is going to incorporate a variable threshold to adaptively set decision levels, it has become mandatory to more accurately predict the input waveform parameters.

4.3.2 Data-Dependent Loss Effects

The concept of data-dependent loss is depicted in Figure 14. A long run of 1's or 0's will allow the cable output voltage to reach MAX "1" or MIN "0", respectively, whereas a single pulse preceded and followed by data of the opposite sense will attain only MIN "1" or MAX "0."

The analysis techniques involved modeling the frequency-dependent loss of the cable and connectors, calculating the Fourier transform of a single pulse, attenuating the Fourier coefficients, and taking the inverse transform to ascertain the loss. In actual fact, since the calculations were performed on a computer, the most simple approach was to approximate the single pulse with a very low duty cycle rectangular pulse train. Thus, the Fourier series was used.

Worst-case conditions assume 92 ft of cable with seven connector pairs. From [4], we find that the cable attenuation of RG142 can be modeled as $1.92 \times 10^{-4}\ f^{0.538}$ dB per 100 ft. This is derived from the table on page 194 of [4] by using a linear regression of the tabular data. The resultant correlation coefficient is 0.9997, indicating that the log of attenuation versus the log of frequency can be accurately approximated by a straight line in the range of interest. Assuming SMA connectors, the connector loss is given as $0.03\sqrt{f_{GHz}}$ dB per connector.

The resultant data-dependent loss is calculated to be 11.4%. That is, a single pulse will be 88.6% of the steady-state voltage difference. This can be written as:

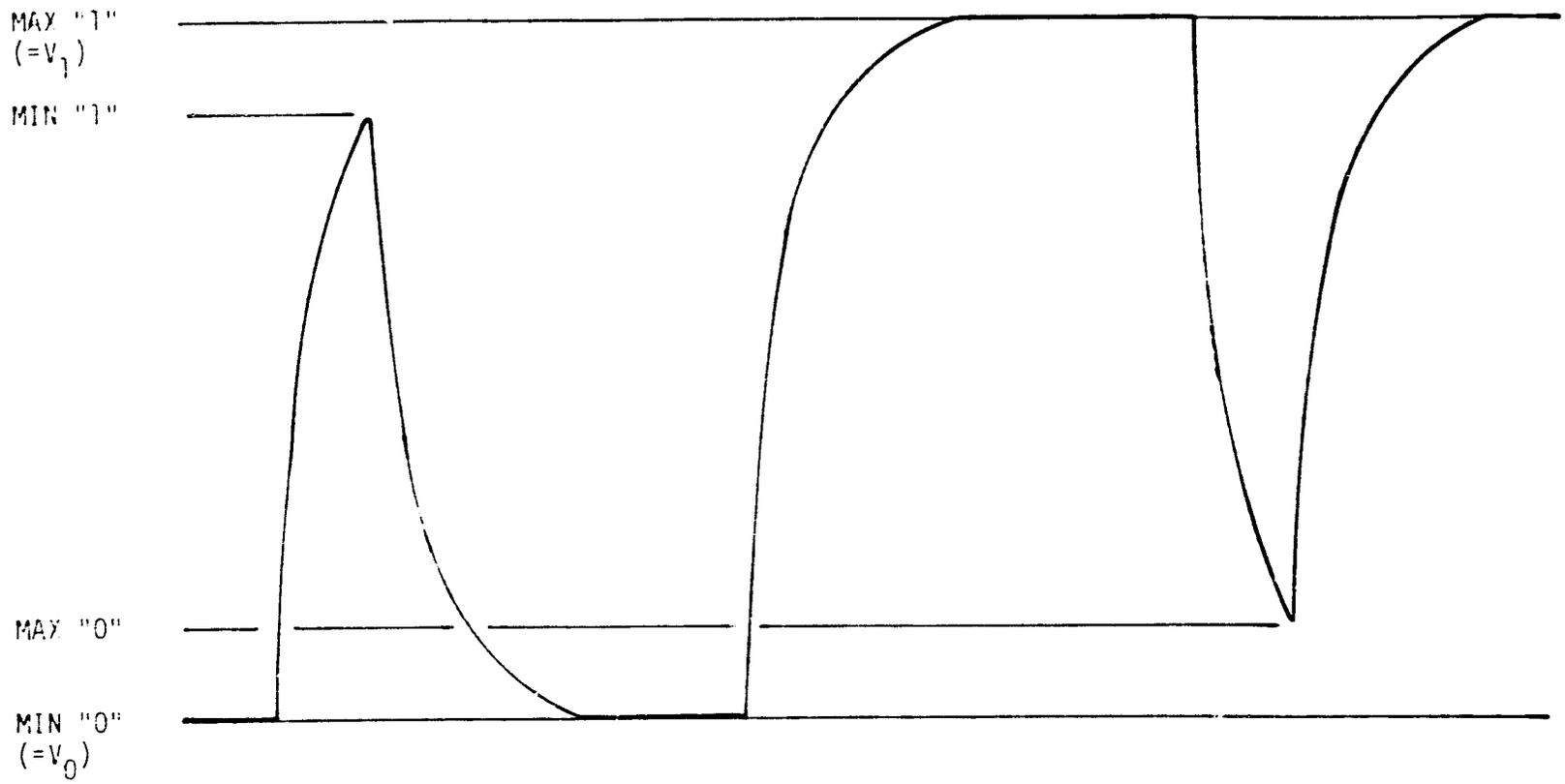

Figure 14. Worst-Case Short-Term Variation Single Pulse After Steady State

$$\text{MIN "1"} = V_0 + 0.886\,(V_1 - V_0)\ ,$$

$$\text{MAX "0"} = V_1 - 0.886\,(V_1 - V_0)\ .$$

4.3.3 Cable Rise Time Effects

The response of a cable to fast rise time inputs cannot be modeled as a simple filter. Cable measurements indicate a very rapid initial rise, followed by a slow tapering off to the final value. From [5] and [6], we find that the response to a unit step (1/S) input can be given as:

$$V[t] = 1 - \mathrm{erf}\left(\frac{\ell\, K}{4R_0\sqrt{t}}\right),$$

with ℓ the cable length, K the cable attenuation constant in ohms per unit length per square root hertz, and R_0 the characteristic impedance. This expression is obtained by multiplying the Laplace transform of the cable transfer function by 1/S, then taking the inverse transform.

The parameter K is not necessarily readily available for all cables. Cable specifications are normally supplied as dB attenuation per 100 ft at a specific frequency.

We can determine K/R_0 as a function of attenuation, as follows:

$$\frac{E_0}{E_i} = e^{-\left(\frac{K}{R_0}\right)\frac{\sqrt{S}}{2}\ell}\ , \text{ the cable transfer function.}$$

With $s = j\omega$ and $\sqrt{j} = \dfrac{1+j}{\sqrt{2}}$,

$$\frac{E_0}{E_i} = e^{-\frac{K}{R_0}\,\frac{\sqrt{f}\,\sqrt{2\pi}}{2}\,\frac{(1+j)\ell}{\sqrt{2}}}\ ,$$

A, attenuation per 100 ft, is

$$A = \left|\frac{E_0}{E_i}\right| = e^{-\left(\frac{K}{R_0}\right)\sqrt{f}\,\frac{100}{2}\,\sqrt{\pi}}$$

and

$$A\left(\frac{dB}{100\ ft}\right) = 20 \log \left[e^{\left(\frac{K}{R_0}\right)\sqrt{\pi}\ \sqrt{f}\ 50}\right]$$

$$= 10^3 \left(\frac{K}{R_0}\right) \sqrt{\pi f} \log e$$

Thus,

$$K/R_0 = \frac{A}{\sqrt{f}}\left(\frac{1}{\log e\ \sqrt{\pi} \times 10^3}\right),$$

which can be substituted into the step response to give

$$V(t) = \operatorname{erfc}\left(\frac{3.25 \times 10^{-4}}{\sqrt{t}} \frac{\ell A}{\sqrt{f}}\right).$$

4.4 Critique of a Hughes Shuttle Ku-Band Data Sampler/Bit Synchronizer

4.4.1 Summary and Conclusions

A bit synchronizer proposed by P. H. Conway of Hughes Aircraft is analyzed in a noise-free environment. This task is accomplished by considering the basic operation of the loop via timing diagrams and by linearizing the bit synchronizer as an equivalent, continuous, phased-lock loop (PLL).

It was determined that the basic approach was a good design which, with proper implementation of the accumulator, up/down counter and logic should provide accurate mid-bit sampling with symmetric bits.

However, when bit asymmetry occurs, the bit synchronizer can lock up with a large timing error, yet be quasi-stable (timing will not change unless the clock and bit sequence drift). This will result in incorrectly detecting some bits. The apriori probability of falling into this quasi-stable region is equal to the asymmetry (defined in 4.4.6) expressed as a fraction. This assumes a uniform distribution over T sec. Thus, except for the case of no asymmetry, there is always some possibility of remaining in lock but incorrectly detecting some bits.

As a final comment, if the timing difference between the bit stream and the clock can be held to less than $\pm \frac{1-ASY}{2}$ T sec (T is the undistorted bit duration), the bit synchronizer loop will never get into the third zone, where bit errors are made but the loop holds lock.

4.4.2 Introduction and Description of the New Bit Synchronizer

The purpose of this report is to discuss one "fix" to the operation of a Shuttle Ku-band bit synchronizer which utilizes both clock and data inputs. The present bit synchronizer has a jitter problem and, consequently, occasionally will sample the same bit twice and skip the following bit.

An alternative bit synchronizer suggested by P. H. Conway of Hughes Aircraft [7] is shown in Figure 15. The loop is composed of a Motorola high-frequency phase-frequency detector (ϕ-DET) [8-10] which is capable of detecting both phase and frequency errors and is used to track the clock, and a bit transition detector which attempts to track the transitions of the data bits.

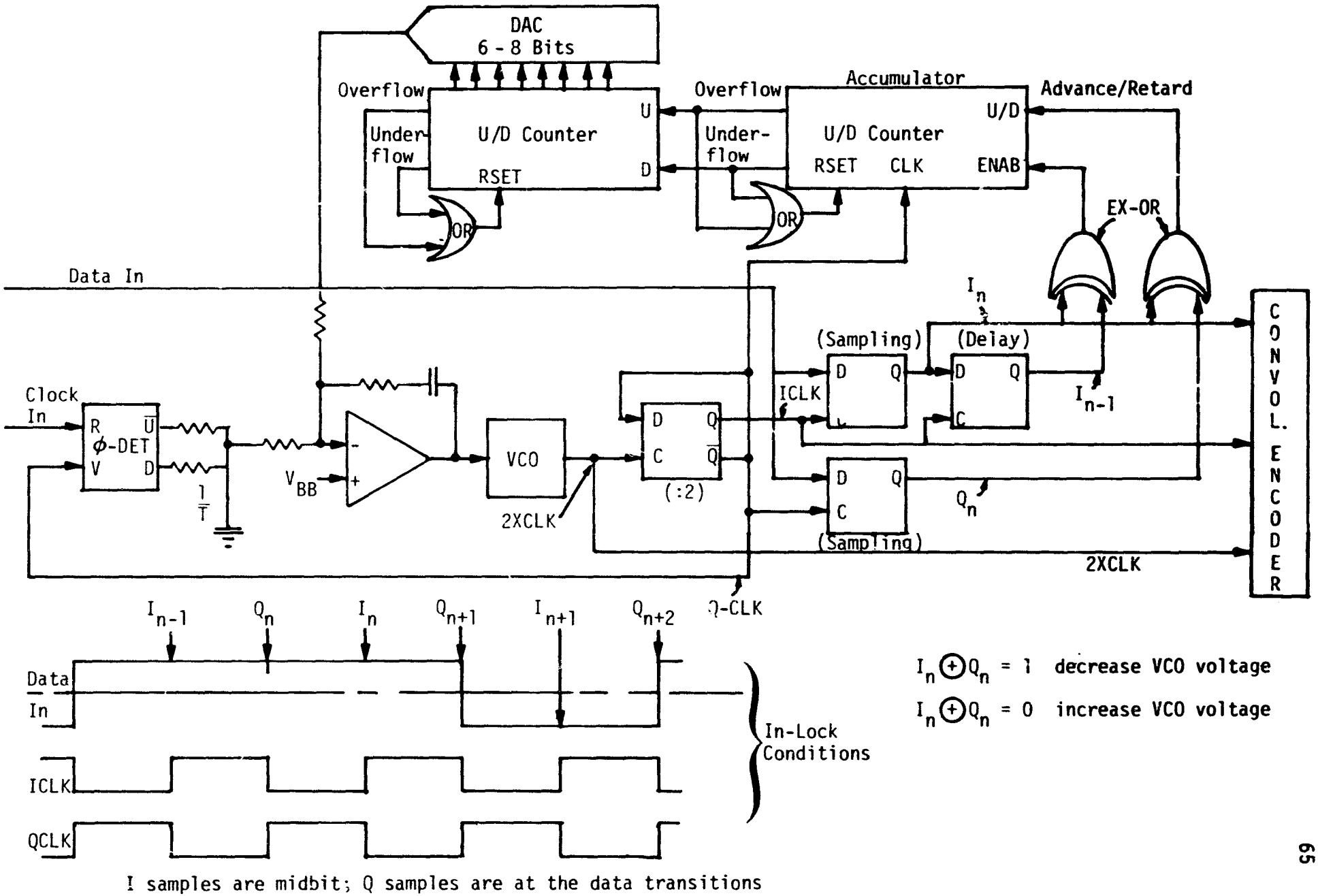

I samples are midbit; Q samples are at the data transitions

Figure 15. Ku-Band Data Sampler With PLL Clock Tracking

The Q clock signal shown in Figure 15 is compared with the received clock (clock in) which, by virtue of the phase/frequency detector, produces a signal which has a dc component proportional to the frequency error (if there is one). Then, when in frequency lock, it produces a signal which has a dc component proportional to the phase error between the input clock and the VCO output.

Now, if the digital-to-analog converter (DAC) output was not hooked up to the loop filter, the bit synchronizer would track the received clock with negigible phase error. However, since the received clock and data are at the same frequency but are not phase coherent, it is necessary to bump the clock phase so that data samples are taken at mid-bit. The function of the DAC is to provide samples of the data at the mid-bit point. The VCO clock runs at twice the rate of the received clock and is divided down to the clock rate by the D flip-flop following the VCO. Actually, this flip-flop provides both an I and a Q clock which are phased one-half a bit apart, as shown in the lower left corner of Figure .

The I and Q clocks are used to sample the data one-half of a bit apart, when synchronized. This sampling is effected by the two D flip-flops following the divide by 2 flip-flop. By using the "exclusive-OR" of two successive data samples, a transition detector is created, thereby producing a binary one with a transition and a binary zero when there is no transition. This control enables or disables the up/down counter to count either up or down. By comparing the I and Q data samples (I_n and Q_n in Figure 15), an estimate of the error in the actual transition sample (Q_n) and the data transition location is obtained. It is to be noted that the exclusive-OR output yields only the algebraic sign of the error, not the magnitude. This error, assuming a data transition, will be accumulated in the up/down (U/D) counter until it either underflows or overflows. The accumulator actually has two functions. The first is to reduce the speed to the DAC; the second is to control the quantization of the loop phase error control. The second up/down counter feeds into a DAC which converts the accumulated count into an analog voltage, which drives the bit synchronizer loop filter. In effect, the up/down counter acts upon the bit timing error signal the same way

an integrator would. This integration is precisely what is needed to force the mid-bit data sampler into the mid-bit position! This fact will be made clearer in subsection 4.4.5.

In conclusion, the bit synchronizer shown in Figure 15 is designed to track the clock and sample the data sequence at the mid-bit point. We now consider the phase/frequency detector and the bit detector in more detail in the following sections.

4.4.3 Description of the Motorola Phase/Frequency Detector

Both the MC4344/MC4044 [9] and MC12040 [10] Motorola phase/frequency detectors can be used in a broad range of phased-lock loop applications. Both sets of detectors are functionally equivalent, however, the MC12040 is capable of operating at higher clock speeds. Because of the functional equivalence, we shall confine our discussion to the MC4344/MC4044 unit.

The Motorola MC4344/MC4044 phase/frequency detector is composed of a phase/frequency detector, a quadrature phase detector, a charge pump and an amplifier. It is the function of the charge pump to convert the pulses out of the phase/frequency detector to a DC value which is essentially proportional to either the phase or frequency error.

In Figure 16, the phase/frequency flow table for the phase/frequency detector is given, along with the charge pump/amplifier frequency control.

In order to understand the usage of Figure 16, we shall consider an example. Assume that the received clock (R input to the ϕ-frequency detector) lags the local reference (V input to the ϕ-frequency detector) by one-twelfth of a square wave clock cycle, as shown in Case I of Figure 17. Starting at state 8 in Figure 17, which corresponds to the R,V pair being in state 1,0, we go to Figure 16a and note that state (8) (with the parentheses) produces an output U1 = 1 and D1 = 1. Now, in the time interval denoted by (7), we note that R,V = 1,1. Moving horizontally in the same row to the left, one column (under R-V = 1,1), we find a seven. Therefore, we look vertically in the column for (7) which we find one row higher, with a corresponding output of U1 = 1 and D1 = 1. The next input is R = 0, V = 1. Moving horizontally in the fifth row, we find a 2. Moving vertically to the second row, we find the (2), which has a

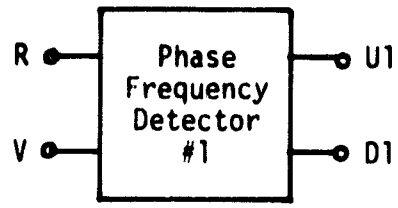

R-V	R-V	R-V	R-V	U1	D1
0-0	0-1	1-1	1-0		
(1)	2	3	(4)	0	1
5	(2)	(3)	8	0	1
(5)	6	7	8	1	1
9	(6)	7	12	1	1
5	2	(7)	12	1	1
1	2	7	(8)	1	1
(9)	(10)	11	12	1	0
5	6	(11)	(12)	1	0

(a) Phase Frequency Detector Flow Table

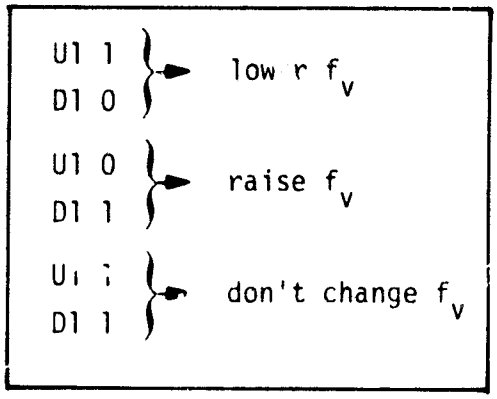

(b) Charge Pump-Amplifier Control

Figure 16. Phase/Frequency Detector Flow Table and the Charge Pump-Amplifier Frequency Control

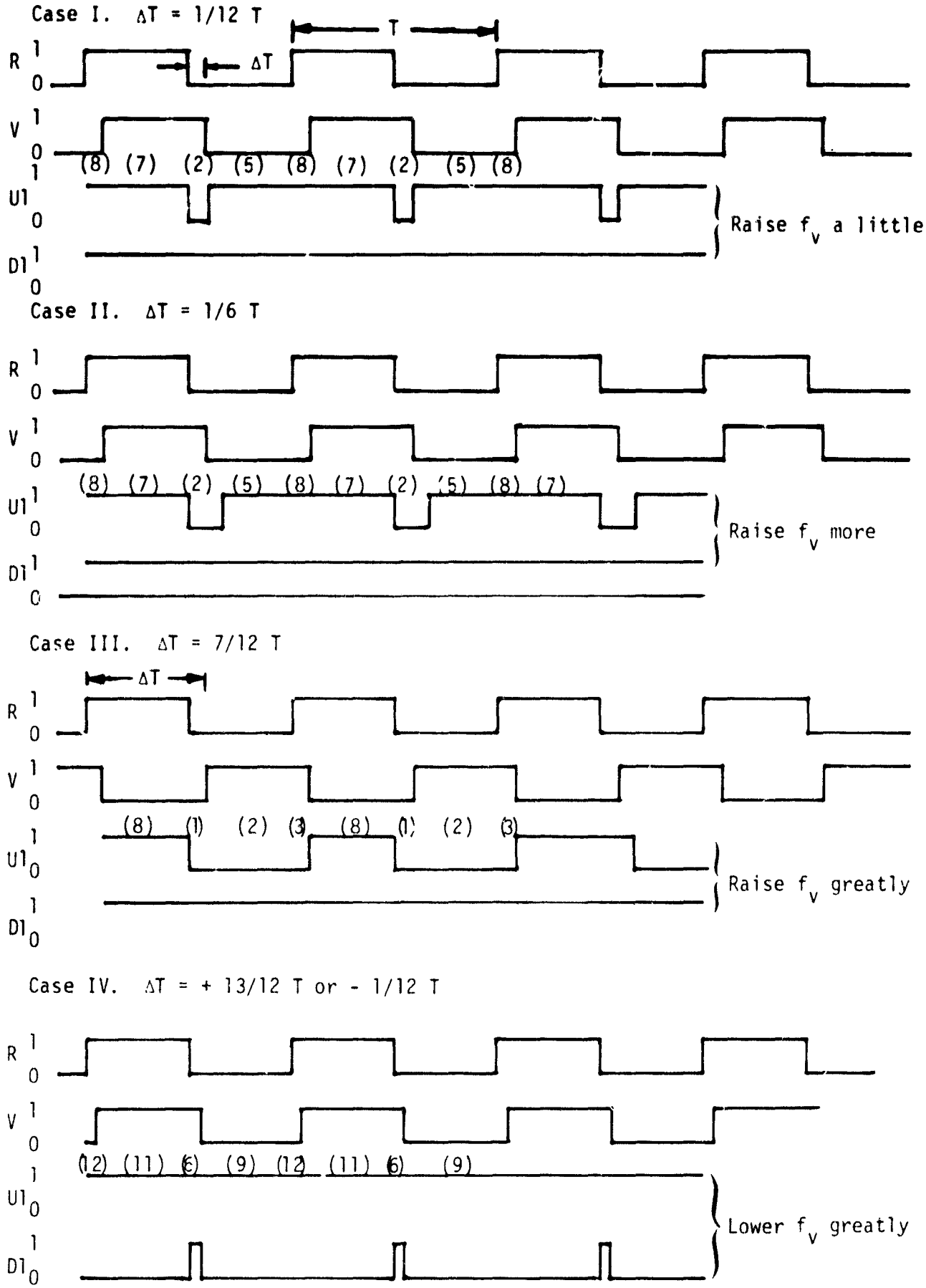

Figure 17. Performance of the Phase/Frequency Detector for Various Phase Errors

corresponding output of U1 = 0, D1 = 1. Hence, at this point, the U1 output drops to zero while the V1 remains at one, as shown in Figure 17. Continuing in this manner, we find that the phase/frequency detector goes through the states (5), (8), (7), (2), (5), (8), etc., generating the waveforms U1 and D1 shown in Case I, Figure 17. Now, by considering Figure 16b, we see that, when U1,D1 = 0,1, the DC voltage out of the charge pump/amplifier is increased and, when U1,D1 = 1,1, the DC voltage does not change. As a consequence, the DC voltage applied to the loop filter-amplifier increases to the VCO input, causing the local reference to catch up to the received clock.

By viewing Figure 17 cases II and III, it is seen that a large timing or phase error produces a larger DC voltage out of the charge pump. By virtue of the way the charge pump works, the error control signal, when properly smoothed, is proportional to the timing error over the region $\pm T$, where T is the clock or bit period. In viewing the error to be phase rather than timing, we find the error signal to be linear over $\pm 2\pi$.

In case IV of Figure 17, the situation when the timing error is increased to $\frac{13}{12}T \left(\text{or } -\frac{1}{12}T\right)$ is shown. Even though the error is equivalent to case I of Figure 17, the error signal derived from the flow table of Figure 16 yields a different error control voltage. The reason for this difference is obvious when one considers the S-curve of Figure 18.

Because of the memory in the phase/frequency detector, there are two error control signals for each error position, or phase error, ϕ. The arrows in Figure 18 indicate how the the loop behaves as the phase increases, first to 2π and then to 4π on a different branch, then returns to zero on the new branch. The original stable point was 0 rad on the first branch but the second branch is stable at 2π rad (T sec).

The above discussions were concerned with phase or timing errors. We now consider frequency errors. Using the flow table of Figure 16a, we can establish that, when $f_R/f_V = 10$ or when $f_V/f_R = 10$, error control amplitude is monotonically increasing with increasing frequency error (it is not linear). The results are plotted in Figure 19 for the case of 10:1 frequency error and Figure 20 for 3:1 errors.

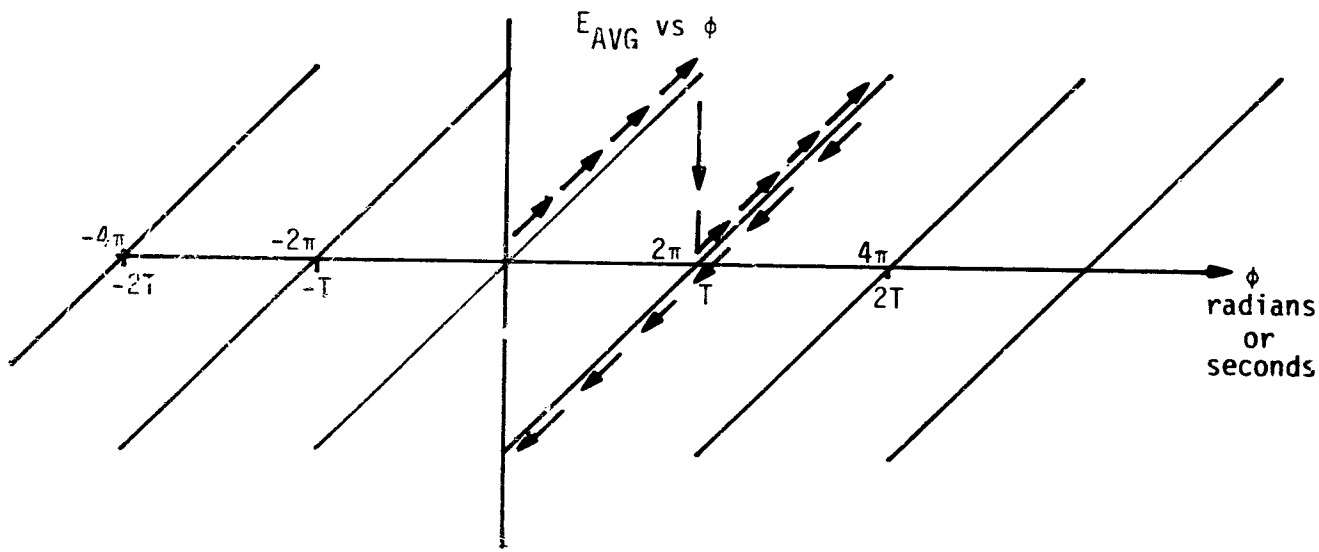

Figure 18. S-Curve of the Phase/Frequency Detector (Frequency Locked)

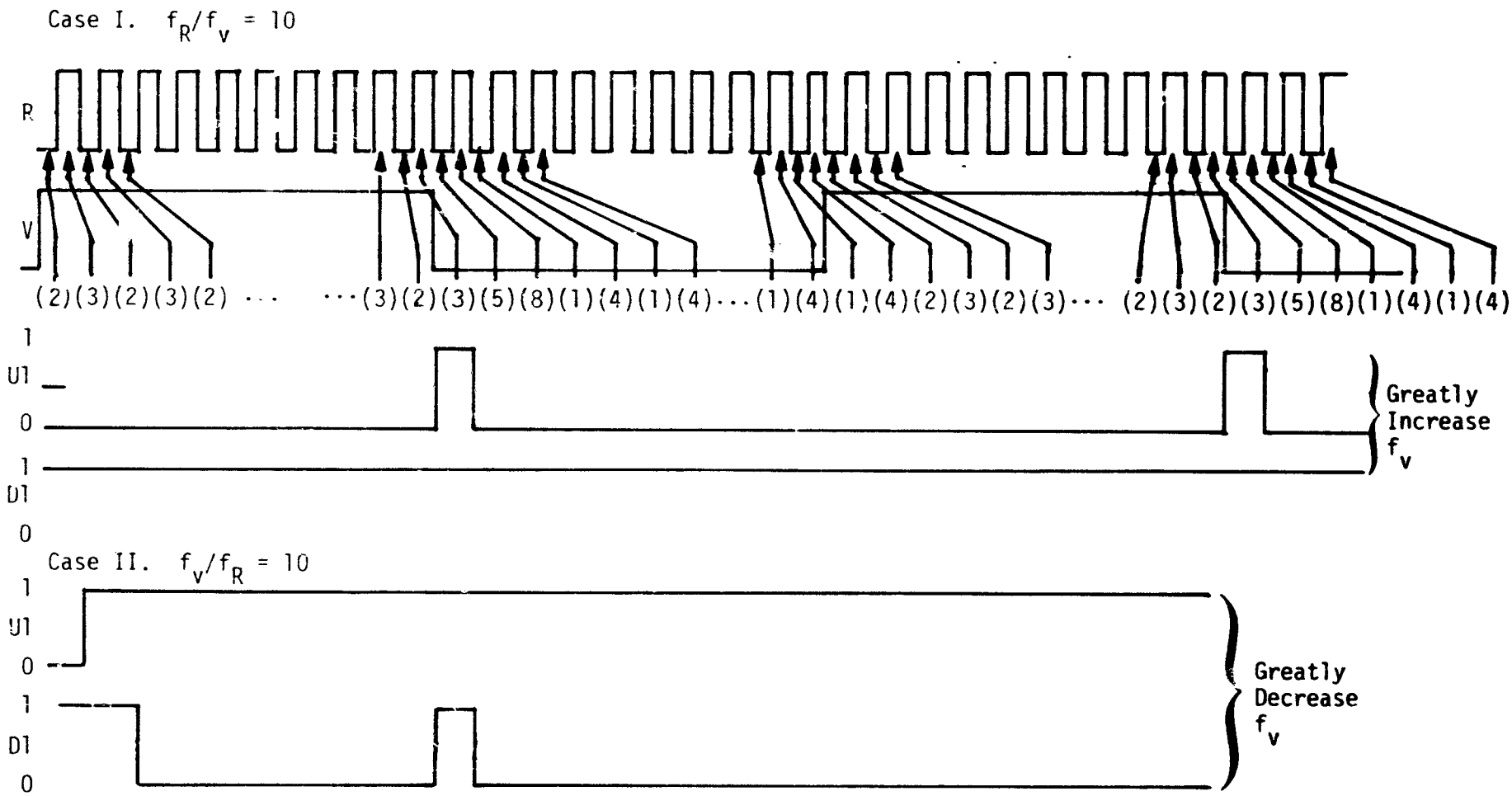

Figure 19. Phase/Frequency Detector When a Large Frequency Error Exists

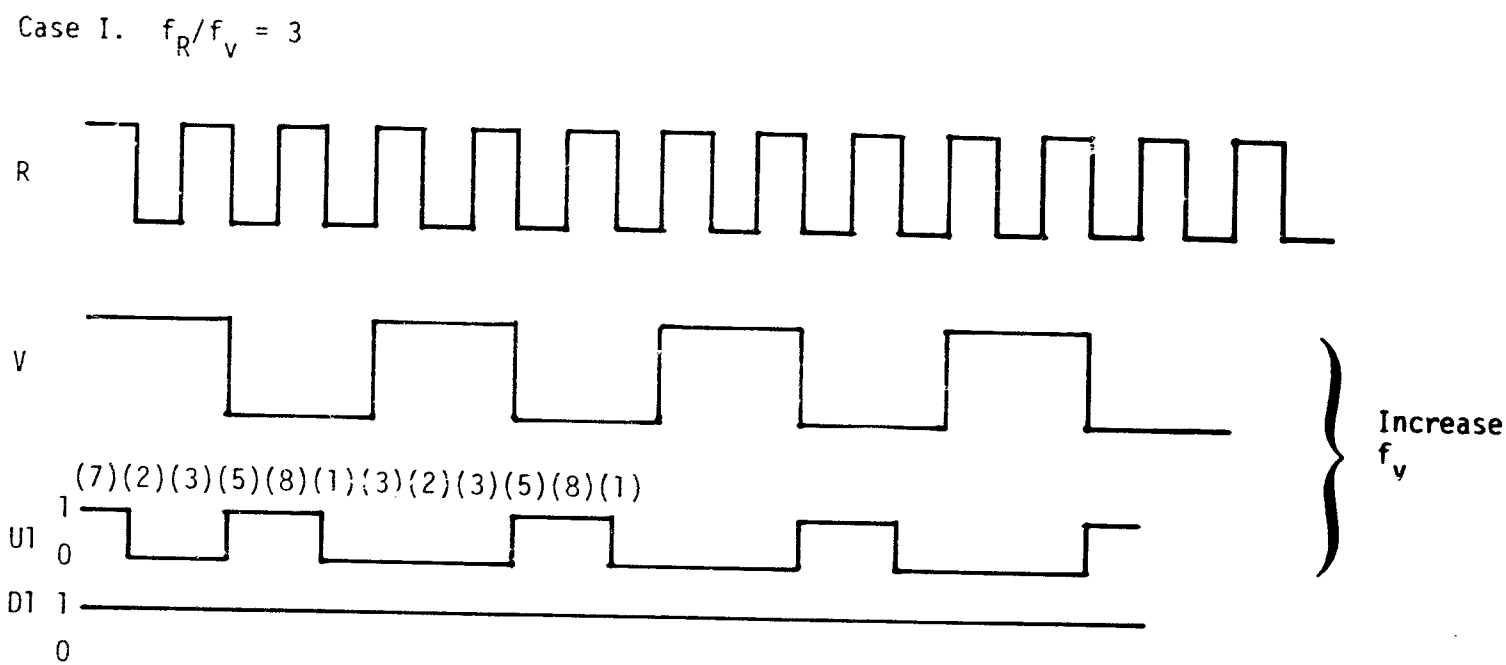

Figure 20. Phase/Frequency Detector for a 3.1 Frequency Error

4.4.4 Description of the Data Detector

As was mentioned previously, the phase/frequency detector provides an error signal to track the clock while the data detector provides a perturbation error signal to force the data sampling to be mid-bit. The divide-by-two D flip-flop of Figure 14 produces both the I and Q samples which are one-half a bit apart in time when the loop is in frequency lock. The in-phase samples are delayed one bit in the second D flip-flop, labeled "delay" in Figure 14. Using an exclusive-OR gate, the present data bit is modulo-two added with the previous data bit. When the past and present data bits are of the same algebraic sign, obviously no transition could have occurred; hence, sampling the transition point could yield no useful timing information so that the accumulator is not enabled. On the other hand, when a transition occurs, the previous and past data bits do not agree and useful information can be obtained from a transition sample. The exclusive-OR gate enables the accumulator only when a transition occurs.

Data bit timing error information is obtained by comparing the present I and Q samples via an exclusive-OR gate. As shown in Figure 21, when the clock timing samples are either late or early, the modulo-two sum of I_n and Q_n is either 0 or 1, respectively. Therefore, $I_n \oplus Q_n$, where $\oplus$ denotes modulo-two addition, determines in which direction the loop timing should be adjusted in order that the Q samples lie very near the transition of the bits. Therefore, the I samples will be in the mid-point of the data bits, which is the result desired to avoid missing bit samples.

By using an accumulator with overflow, an up/down counter can be used to reduce the speed of the up/down counter driving the DAC. Furthermore, the accumulator sets the quantization error in the bit time tracking accuracy. The DAC converts the up/down counter output to an analog voltage which, in turn, adds with the phase/frequency detector to produce the loop filter input signal.

When the bit synchronizer is not frequency locked, it produces no useful information. Although it is not necessary, inhibiting the bit detector DAC output during acquisition would improve acquisition time.

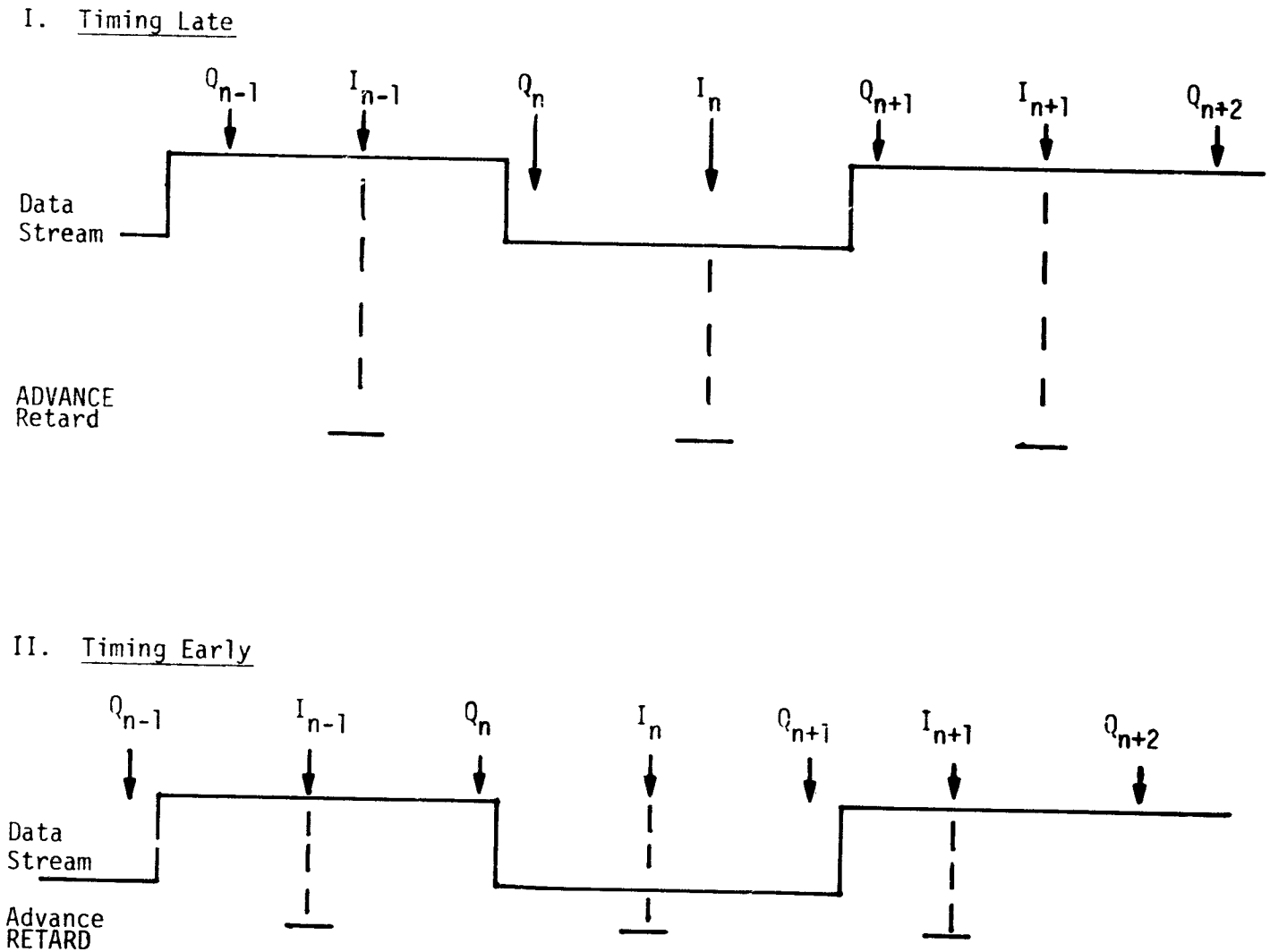

Figure 21. I-Q Relationship for Bit Sampling Showing Bit Timing Control

4.4.5 Linearized Analog Equivalent Loop Analysis

In this section, we model the loop of Figure 14 in a simplified, linearized, loop structure shown in Figure 22. First we replace the phase/frequency detector with a phase detector (multiplier). Next, we replace the data detector with a phase detector (multiplier). Finally, the accumulator and up/down counter are replaced with an integrator since, in effect, that is the function they perform.

In order to utilize this model, the clock and the data must be replaced with sinusoidal signals, as shown in Figure 22. We have assumed that the phase of the data is arbitrary with respect to the clock which is indicated by the phase angle ψ.

The phase error is defined to be the error between the data clock and the VCO reference, r(t). thus,

$$\phi(t) = \theta + \psi - \hat{\theta}(t) \tag{1}$$

We shall now show that, for any value of ψ, $\phi(t) \to 0$ as $t \to \infty$. Note that $\phi(t)$ is proportional to $\varepsilon_4(t)$. Now,

$$\varepsilon_1(t) = CLK(t)\cdot r(t) = \sqrt{2}A \sin\left(\omega_0 t+\theta\right) \sqrt{2}B \sin\left(\omega_0 t + \hat{\theta}\right) \tag{2}$$

or

$$\varepsilon_1(t) = AB \sin(\theta-\hat{\theta}) \tag{3}$$

where we have neglected the $2\omega_0$ term which will be filtered out by the loop filter and VCO. Now,

$$\varepsilon_2(t) = AB \sin(\theta-\hat{\theta}) + \frac{K_F}{S}\varepsilon_4(t) \tag{4}$$

where

$$\frac{1}{S}\varepsilon_4(t) = \int_{-\infty}^{t} \varepsilon_4(u)\, du \tag{5}$$

with S being the Heaviside operator. We use the Heaviside operator notation in what follows. Now we have

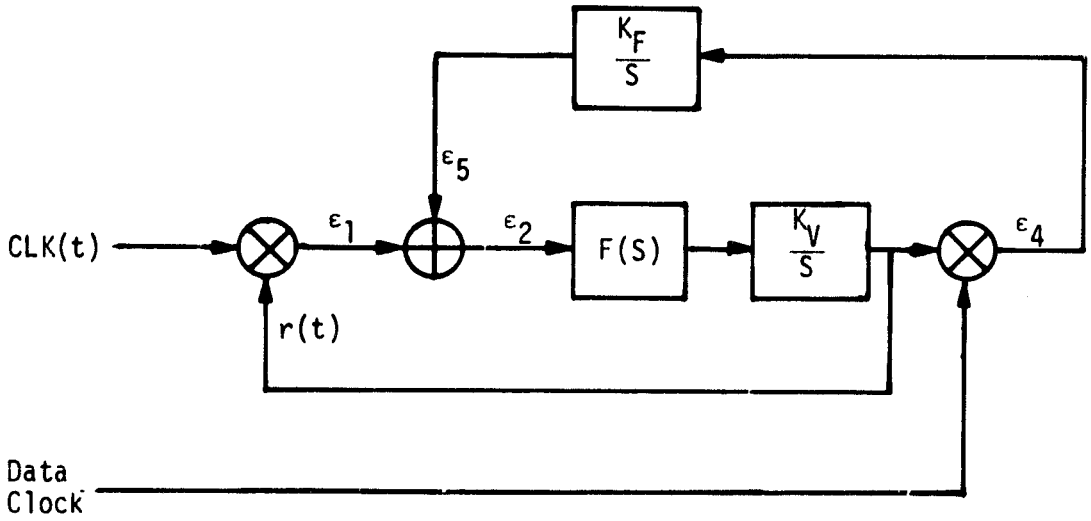

$$CLK(t) = \sqrt{2}\ A \sin(\omega_0 t + \theta)$$

$$r(t) = \sqrt{2}\ B \cos(\omega_0 t + \hat{\theta})$$

$$DCLK(t) = \sqrt{2}\ A \sin(\omega_0 t + \theta + \psi)$$

Figure 22. Simplified, Linearized Model of the Bit Synchronizer

$$\varepsilon_4(t) = r(t)\cdot DCLK(t) = \sqrt{2}B\cos(\omega_0 t+\hat{\theta})\ \sqrt{2}A\sin(\omega_0 t+\theta+\psi) \tag{6}$$

or

$$\varepsilon_4(t) = AB\sin(\theta+\psi-\hat{\theta}) = AB\sin\phi \tag{7}$$

If we linearize (3) and (7), we obtain

$$\varepsilon_1(t) = AB(\theta-\hat{\theta}) \tag{8}$$

$$\varepsilon_4(t) = AB(\theta-\hat{\theta}+\psi) = \varepsilon_1(t) + AB\psi \tag{9}$$

Now we can also linearize (4) to yield

$$\varepsilon_2(t) = AB(\theta-\hat{\theta}) + \frac{K_F}{S}AB\phi \tag{10}$$

The phase estimate out of the VCO, $\hat{\theta}(t)$, in Heaviside operator notation is given by

$$\hat{\theta} = F(S)\frac{K_V}{S}\varepsilon_2 = F(S)\frac{K_V}{S}\left\{AB(\theta-\hat{\theta}) + \frac{K_V}{S}AB\phi\right\} \tag{11}$$

where F(S) is the loop filter represented as a function of the LaPlace variable S. Now, $\hat{\theta}$ also satisfies, from (1),

$$\hat{\theta} = \theta + \psi - \phi \tag{12}$$

so that

$$\theta + \psi - \phi = F(S)\frac{K_V}{S}\left\{AB(\theta-\psi) + \frac{K_F}{S}AB\phi\right\} \tag{13}$$

Since θ is unimportant in our analysis, we can let it be zero, producing from (13)

$$\Phi(S) = \frac{\left(1 + \frac{ABK_V F(S)}{S}\right)\Psi(S)}{\left[\frac{ABK_V F(S)}{S} + \frac{ABK_V K_F F(S)}{S^2} + 1\right]} \tag{14}$$

where $\Psi(S)$ is the LaPlace transform of $\psi(t)$, i.e.,

$$\Psi(S) = \mathscr{L}\{\psi(t)\} \tag{15}$$

and $\Phi(S)$ is the LaPlace transform

$$\Phi(S) = \mathscr{L}\{\phi(t)\} \tag{16}$$

In order to evaluate how well the loop samples the midpoint of the bit, we must consider the phase error, $\phi(t)$, as time increases without bound. Letting the $\Psi(S)$ be modeled as a phase step in time so that

$$\Psi(S) = \frac{\psi_0}{S} \quad , \tag{17}$$

where ψ_0 is a uniform random variable taking on values in the range $(-\pi, \pi)$ and using the final value theorem of LaPlace transforms, we have

$$\lim_{t\to\infty} \phi(t) = \lim_{S\to 0} [S\Phi(S)] \tag{18}$$

Hence, using (17) and (18) produces

$$\lim_{t\to\infty} \phi(t) = \lim_{S\to 0} \left[\frac{\left(1 + \frac{ABK_V F(S)}{S}\right) \psi_0}{\frac{ABK_V F(S)}{S} + \frac{ABK_V K_F F(S)}{S^2} + 1} \right] \tag{19}$$

Assuming a second-order loop requires that the loop filter be of the form

$$F(S) = \frac{1 + \tau_2 S}{\tau_1 S} \tag{20}$$

so that (19) can be evaluated as

$$\lim_{t\to\infty} \phi(t) = 0 \quad , \quad |K_F| > 0 \tag{21}$$

which means that, in our simplified and unquantized model, the data samples are always taken midbit, as desired, irrespective of the phase relationship between the clock and the data. It should be noted that, if θ were not zero, the result of (21) would still hold. It is interesting to consider the tracking error, $\phi(t)$, when the feedback integrator is removed, corresponding to $K_F = 0$. In this case, we find that

$$\lim_{t\to\infty} \phi(t) = \lim_{S\to 0} \left[\frac{\psi_0 \left[S^2 + ABK \frac{(1+\tau_2 S)}{\tau_1} \right]}{\frac{ABK_V}{\tau_1} (1+\tau_2 S) + S^2} \right] = \psi_0 \tag{22}$$

Therefore, without the integrator (or accumulator up/down counter), the bit synchronizer is incapable of controlling the location of the data bit samples. This fact satifies one's intuition.

We now establish that, while $\varepsilon_2(t)\to 0$ as $t\to\infty$, neither $\varepsilon_5(t)$ nor $\varepsilon_1(t)$ approach zero as $t\to\infty$. From Figure 22, it is obvious that

$$\varepsilon_5(t) = \frac{K_F}{S} \varepsilon_4(t) \cong \frac{K_F}{S} AB(\theta+\psi-\hat{\theta}) \tag{23}$$

Also, the oscillator output phase estimate is given by [using (11) and (23)]

$$\hat{\theta} = F(S) \frac{K_V}{S} \left\{ AB(\theta-\hat{\theta}) + \varepsilon_5 \right\} \tag{24}$$

Rearranging, we obtain

$$\hat{\theta} + \frac{ABK_V F(S)}{S} \hat{\theta} = AB \frac{K_V}{S} F(S)\theta + \frac{K_V}{S} F(S) \varepsilon_5 \tag{25}$$

Solving (25) for $\hat{\theta}$, we obtain

$$\hat{\theta} = \frac{\frac{AK_V}{S} F(S)\, \theta(S) + \frac{K_V}{S} F(S)\, \epsilon_5(S)}{\left[1 + \frac{ABK_V F(S)}{S}\right]} \tag{26}$$

Rearranging (23) produces

$$\epsilon_5 = \frac{ABK_F}{S} \left(\theta(S) + \psi(S)\right) - \frac{ABK_F}{S} \hat{\theta} \tag{27}$$

Using (27) in (26) produces, after some algebra, the result (again letting $\theta = 0$)

$$\epsilon_5(S) = \frac{\frac{ABK_F}{S} \psi(S)}{\left[1 + \frac{ABK_F K_V F(S)/S^2}{1 + ABK_V F(S)/S}\right]} \tag{28}$$

Again using the final value theorem, we obtain

$$\lim_{t \to \infty} \epsilon_5(t) = \lim_{S \to 0} \left[S\epsilon_5(S)\right] \tag{29}$$

so that, assuming $\psi(t)$ is a step in phase of ψ_0 rad, we have, using (28) and the fact that $\psi(S) = \psi_0/S$, that

$$\lim_{t \to \infty} \epsilon_5(t) = AB\psi_0 \tag{30}$$

It can be shown that (30) also holds for a first-order loop (where $F(S)=1$) and it also holds for a step in phase of θ.

Now consider the steady-state value of $\epsilon_1(t)$. We use linearized equations in the following. From (8), we have

$$\epsilon_1 = AB(\theta - \hat{\theta}) \tag{31}$$

and from (10) we have

$$\varepsilon_2 = AB(\theta-\hat{\theta}) + \frac{K_F}{S}\varepsilon_4 \tag{32}$$

Also from (9), we have

$$\varepsilon_4 = \varepsilon_1 + AB\psi \tag{33}$$

Now, since

$$\hat{\theta} = \frac{K_V}{S}F(S)\,\varepsilon_2 = F(S)\,\frac{K_V}{S}\left[\varepsilon_1 + \frac{K_F}{S}\varepsilon_4\right] \tag{34}$$

we can use (33) in (34) to yield

$$\hat{\theta} = F(S)\,\frac{K_V}{S}\left[\varepsilon_1 + \frac{K_F}{S}\left(\varepsilon_1 + AB\psi\right)\right] \tag{35}$$

From (31), we have

$$\hat{\theta} = \theta - \frac{\varepsilon_1}{AB} \tag{36}$$

Now equating (36) and (35) produces (letting $\theta = 0$)

$$\varepsilon_1(S) = \frac{-\dfrac{ABK_VK_F}{S^2}\,\Psi(S)}{\left[\dfrac{K_VF(S)}{S} + \dfrac{K_VK_F}{S^2} + \dfrac{1}{AB}\right]} \tag{37}$$

Again assuming a step in the phase term $\psi(t)$ yields

$$\varepsilon_1(S) = \frac{-\dfrac{ABK_VK_F}{S^2}\dfrac{\psi_0}{S}}{\left[\dfrac{K_VF(S)}{S} + \dfrac{K_VK_F}{S^2} + \dfrac{1}{AB}\right]} \tag{38}$$

using

$$\lim_{t\to\infty} \varepsilon_1(t) = \lim_{S\to 0} S\varepsilon(S) \tag{39}$$

produces

$$\lim_{t\to\infty} \varepsilon_1(t) = -AB\psi_0 \tag{40}$$

From (30) and (40) and Figure 22, we deduce that $\varepsilon_2(t)\to 0$. Therefore, when tracking, the bit synchronizer operates in such a manner that $\varepsilon_2(t) \cong 0$ and $\varepsilon_1(t) \cong -\varepsilon_5(t)$. Without the feedback, of course, the loop would drive $\varepsilon_1(t) \cong 0$.

4.4.6 The Effects of Asymmetry on Bit Detection

In this section, we address the problem of bit asymmetry on both synchronization and bit demodulation. Bit asymmetry percentage is defined by

$$ASY = \frac{|T_1 - T_0|}{T_1 + T_0} \times 100\% \tag{41}$$

where T_1 is the bit duration of a "one" when preceded and followed by a zero, and T_0 is the bit duration of a "zero" when preceded and followed by a one. It is predicted that the total asymmetry due to rise time and transmitted asymmetry will be in the region of 25-35% when the bit rate is at 50 Mbps.

In Figures 23a-c, the case of 25% asymmetry is shown for an alternating one/zero sequence, running at 50 Mbps, with three distinct timing error regions. Since T_1 = 15 ns and T_0 = 25 ns, we see that, in

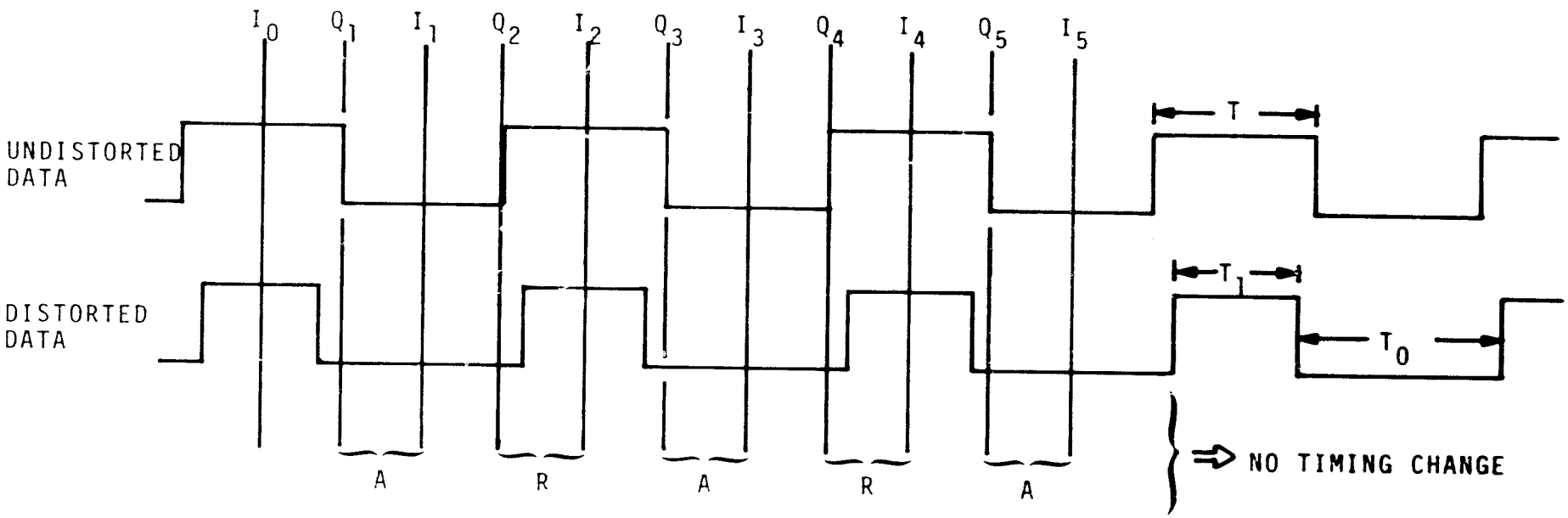

Bit Synchronizer Timing Error Circuit Legend:

A = advance timing (increase VCO frequency)

R = retard timing (lower VCO frequency)

INH = inhibit accumulator (don't change VCO frequency)

R_b = 50 Mbps

CONCLUSION: With timing errors up to ±2.5 ns, no timing change, and bits are correctly detected.

Figure 23a. One/Zero Bit Sequence with 25% Asymmetry and 0 to ±2.5 ns Timing Error

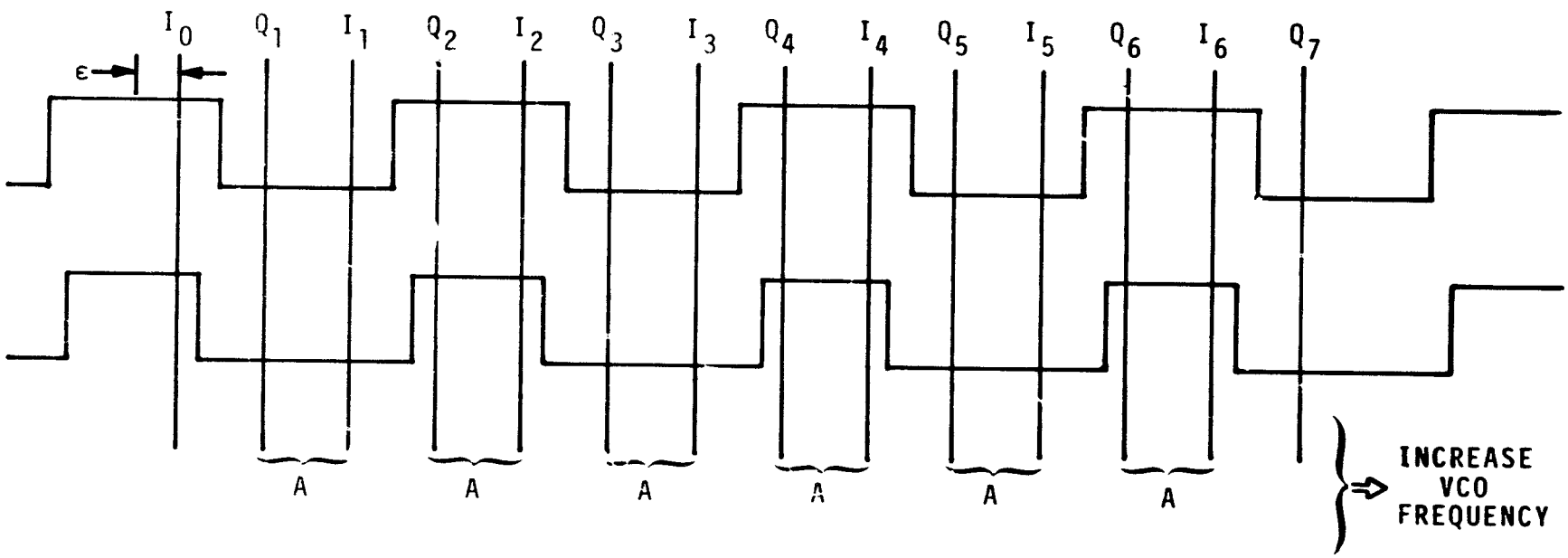

Bit Synchronizer Timing Error Circuit Legend:

A = advance timing (increase VCO frequency)

R = retard timing (lower VCO frequency)

INH = inhibit accumulator (don't change VCO frequency)

R_b = 50 Mbps

CONCLUSION: With timing errors in the region ±2.5 ns to ±7.5 ns, the loop reduces the timing error and correctly detects the bits.

Figure 23b. One/Zero Bit Sequence with 25% Asymmetry and ±2.5 to ±7.5 ns Timing Error

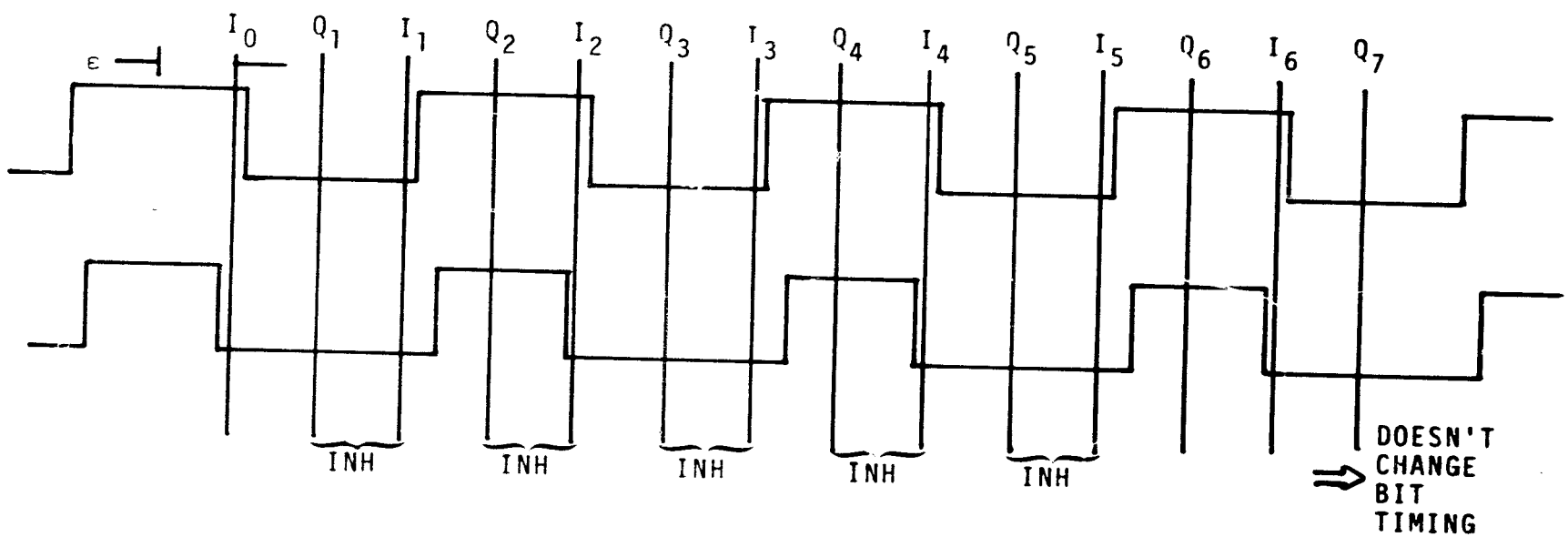

INH = INHIBIT

Bit Synchronizer Timing Error Circuit Legend:

A = advance timing (increase VCO frequency)

R = retard timing (lower VCO frequency)

INH = inhibit accumulator (don't change VCO frequency)

R_b = 50 Mbps

CONCLUSION: With timing errors in the region ±7.5 ns to ±10 ns, the loop does <u>not</u> change its timing but it does incorrectly detect some bits (50% error rate for the square-wave data sequence).

Figure 23c. One/Zero Bit Sequence with 25% Asymmetry and ±7.5 to ±10 ns Timing Error

fact, ASY=25%. For the vertical lines, the Q_i, I_i pairs determine which way to adjust the phase of the VCO according to $I_n + Q_n = 0 \rightarrow$ ADVANCE (INCREASE VCO VOLTAGE) and $I_n + Q_n = 1 \rightarrow$ RETARD (DECREASE VCO VOLTAGE) when $I_n + I_{n-1} = 1$, and no bit timing change when $I_n + I_{n1} = 0$. For example, in Figure 23a, region I errors are illustrated. For this timing relationship, the input to the accumulator up/down counter would be the sequence advance (A), retard (R), advance (A), etc. or, equivalently, ones and minus ones to the accumulator which would not change the sample points relative to the bit stream. In Figure 23b, the error is ±5 ns, which produces a sequence of advances. In this region (±2.5-±7.5 ns), the loop would pull in to the ±2.5 ns region and correctly decode the data bits. When a shift of 5 ns (7.5-10 ns) is considered in Figure 23c, we find that there would be a sequence of A's and R's which would not reduce the error but would cause bit errors to be made in the bit sampling process. For the case of alternating one/zero shown, the detected bits are all zeros, resulting in errors on every other bit. By carefully considering Figures 23a-c, it can be concluded that, with 25% asymmetry, the following is true (timing error is defined as timing difference between sampling at the center of the bits and the actual sampling point):

1. With timing errors up to ±2.5 ns, no timing change is effected by the loop and no bit errors are made.

2. With timing errors between ±2.5 ns and ±7.5 ns, loop error control will reduce timing error and no bit errors will occur.

3. With timing errors between ±7.5 ns and ±10 ns, the loop will not adjust the timing, <u>but bit errors will occur</u>.

The case of 35% bit asymmetry is illustrated in Figure 24 for an alternating one-zero sequence. After careful study, we conclude that the following is true:

1. With timing errors up to ±3.5 ns, no timing change is effected by the loop and no bit errors are made.

2. With timing errors between ±3.5 ns and ±6.5 ns, loop error control will reduce the timing error and no bit errors will occur.

3. With timing errors between ±6.5 ns and ±10 ns, the loop will not adjust timing, however, <u>bit errors will occur</u>.

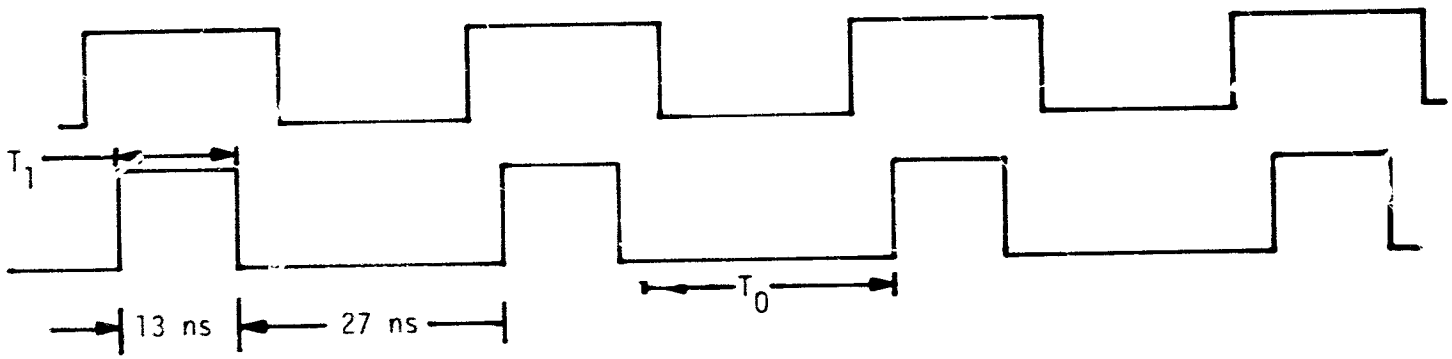

Figure 24. One/Zero Sequence With 35% Asymmetry

Sequences other than the one-zero alternating sequence were considered and the result was basically the same for any level of asymmetry.

In conclusion, we see that three "zones" or timing error regions will apply. The first region is a dead zone in the sense that the no-error control signal is generated in the accumulator because the error signals alternate back and forth in algebraic sign. This region extends in magnitude from zero timing error to $\frac{ASY \cdot T}{2}$ seconds, where T is the undistorted bit symbol duration. The bits are correctly detected in this region.

The second region extends from $\frac{ASY \cdot T}{2}$ seconds to $\left(\frac{1-ASY}{2}\right)T$ seconds. In this region, the loop provides an error control signal from the bit timing error detector which reduces the error to the outer edge of zone 1. The bits are correctly detected in this region.

In the third zone, the error ranges from $\left(\frac{1-ASY}{2}\right)T$ seconds to T/2 seconds. This region causes the bit timing error detector to produce a sequence of alternating ones and minus ones which will therefore not exceed the accumulator threshold and, consequently, not update the loop (i.e., a quasistable lock point). Bit errors will occur in this region. When the one-zero sequence is considered, only zeros or all ones will be detected depending on whether the one bits or the zero bits are of greater duration due to asymmetry. For arbitrary sequences of ones and zeros, errors will occur although not at a 50% rate.

As a final comment, if we assume that the a priori probability of the initial timing just after acquistion is uniformly distributed, the probability of locking in the third region, where bit errors occur, is given by

$$P_{FL} = \frac{\frac{T}{2} - \left(1 - ASY\right)\frac{T}{2}}{\frac{T}{2}} = ASY$$

and therefore, only with zero asymmetry does this problem disappear. If the timing error between clock and bit stream could be held to be less than $\left(\frac{1-ASY}{2}\right)T$ seconds in magnitude, it is possible to avoid the troublesome third region.

4.5 Critique of the HAC Shuttle Ku-Band Leading Edge Bit Synchronizer

4.5.1 Summary and Conclusions

A bit synchronizer proposed by Hughes Aircraft (Culver City) is analyzed via timing diagrams in a noise-free environment. This synchronizer is, in part, a substantial revision of the bit synchronizer proposed by P. H. Conway [11] of Hughes Aircraft Company (HAC).

Based on a review of a HAC note [12] and the timing diagrams of Figures 26 through 33, it is believed that this new bit synchronizer will track the rising edge of the data bits with 25% asymmetry and up to a 90° phase shift between the received clock and data bit timing. In addition, the data bits will be demodulated correctly.

It is not true that phase shifts larger than 90° will necessarily be corrected by this bit synchronizer, as evidenced by Figures 32 and 33. However, the specifications currently require the loop to operate over only a ±75° phase shift between the received data stream leading edges and the bit synchronizer leading edges; consequently, there should be no problem.

4.5.2 Introduction and Description of the Leading Edge Bit Synchronizer

The purpose of the bit synchronizer, shown in Figure 25, is to track the leading edge of the incoming bit stream with the aid of the received clock and, from this, to regenerate a symmetric bit stream to be processed by the convolutional encoder. In addition, the synchronizer provides a clock at the data rate as well as twice the data rate.

In Figure 25, two additional subsystems are shown; the first is an adaptive threshold device that attempts to restore symmetry to the bit stream, and the second is a false frequency lock detector. Since the asymmetry corrector will be the subject of another report, we will now discuss the false frequency lock detector.

The purpose of the false frequency lock detector is to ascertain whether the bit synchronizer is in true lock or false frequency lock. This is accomplished by counting both the received clock and the synchronizer-generated clock in two separate 8-bit counters. After either one counts to its maximum count of 256, the other counter is inhibited from further counting. At this point, the count of the unfilled counter is compared to 256. If the error is small enough, true lock is accepted;

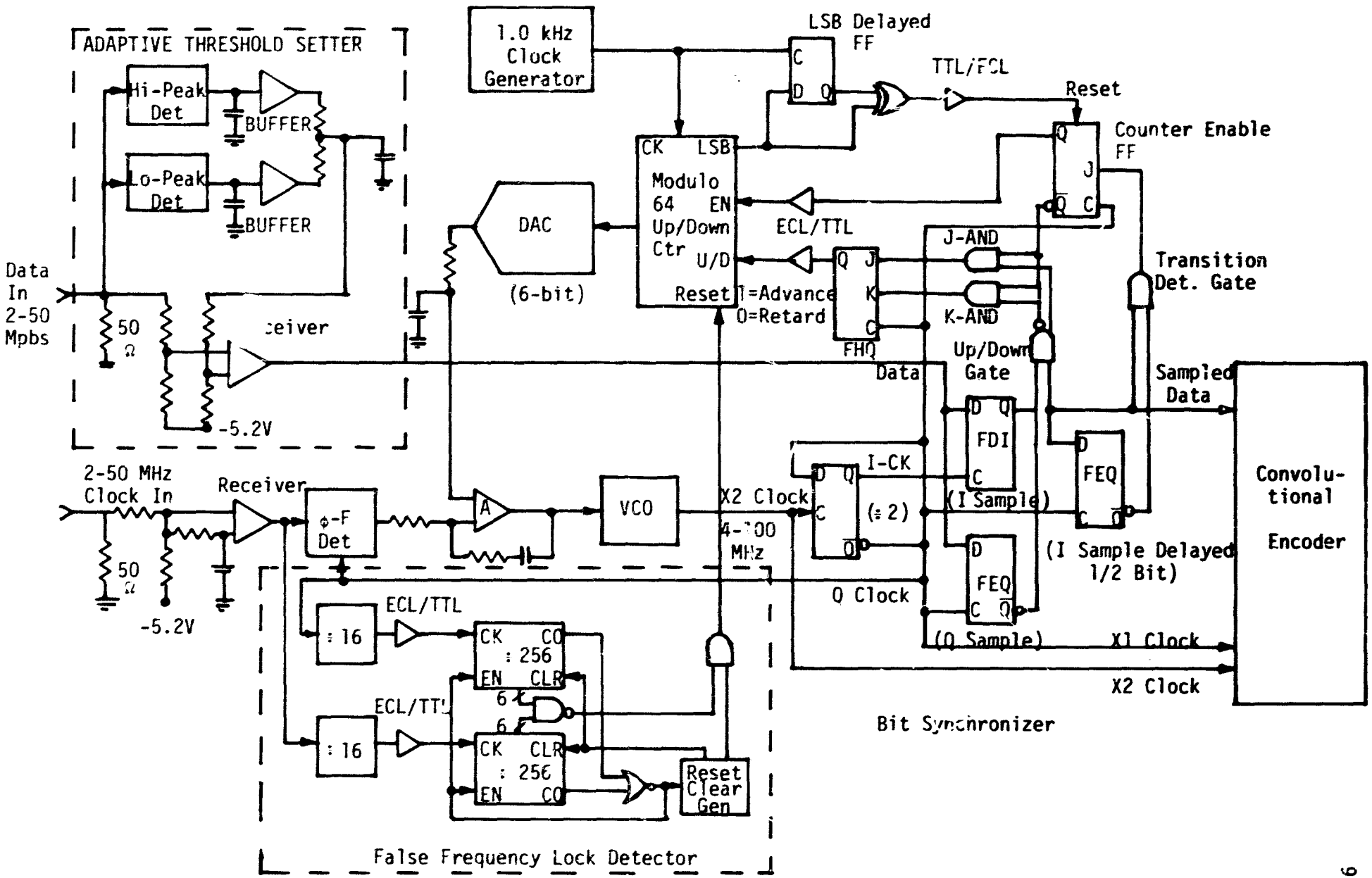

Figure 25. Hugnes Culver City Ku-Band Bit Synchronizer Block Diagram

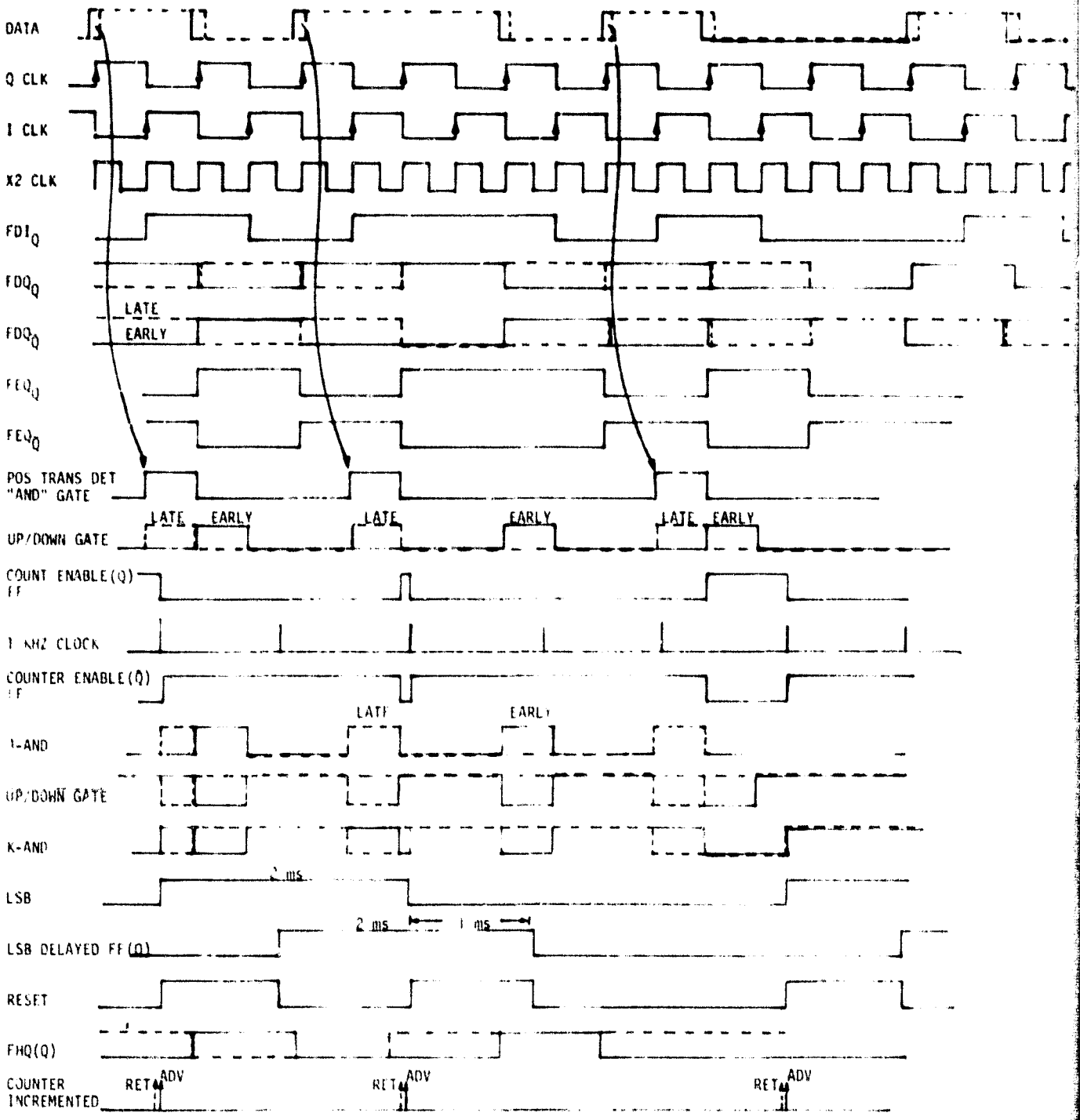

Figure 26. Timing Diagram of the Bit Synchronizer Illustrating An Early and Late Bit Sequence For the Culver City Ku-Band Bit Synchronizer

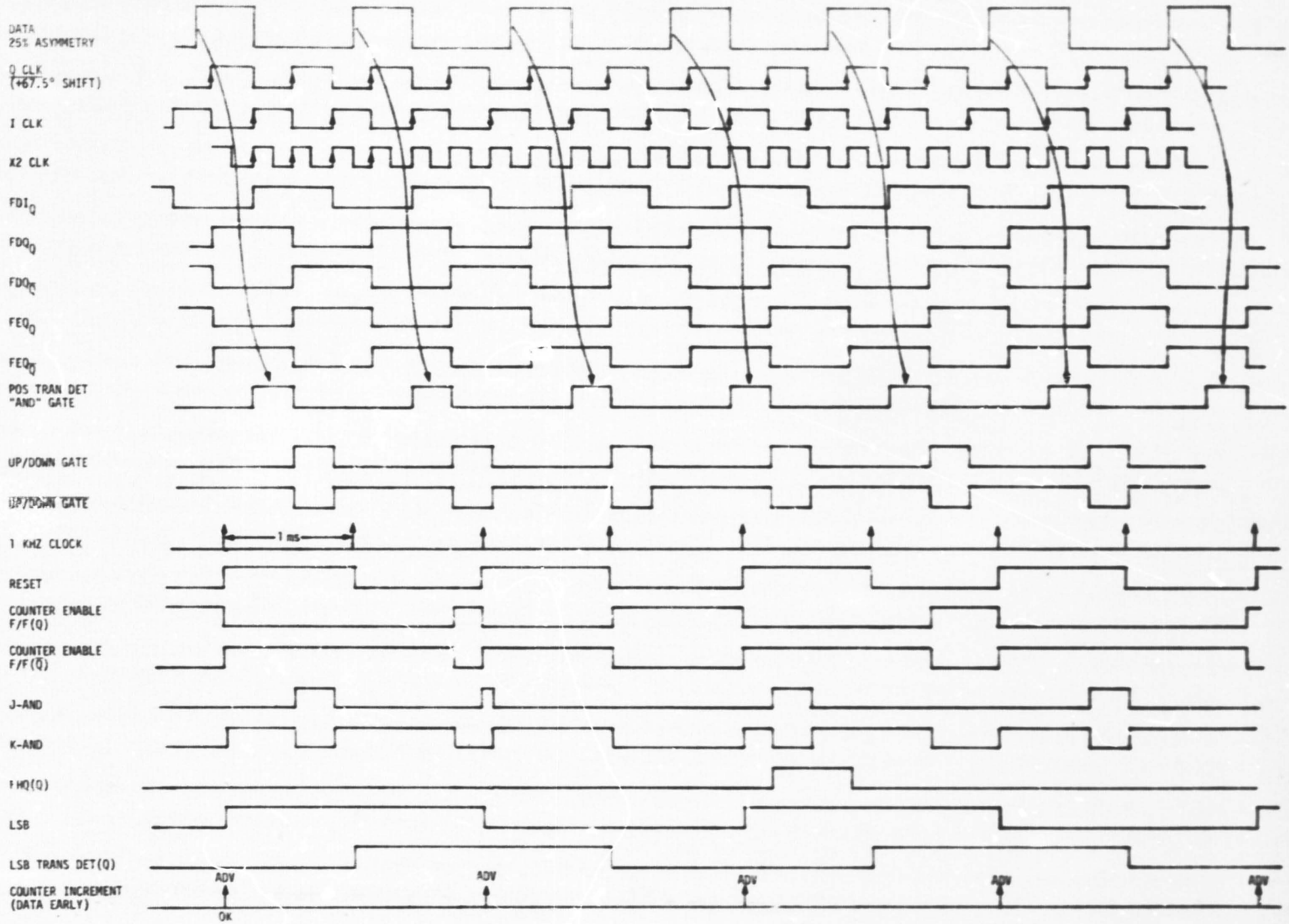

Figure 27 Timing Diagram of the Bit Synchronizer Illustrating the Case of 25% Asymmetry and the Data Leading the Q-Samples by 67.5° (Results Hold Up To 90°)

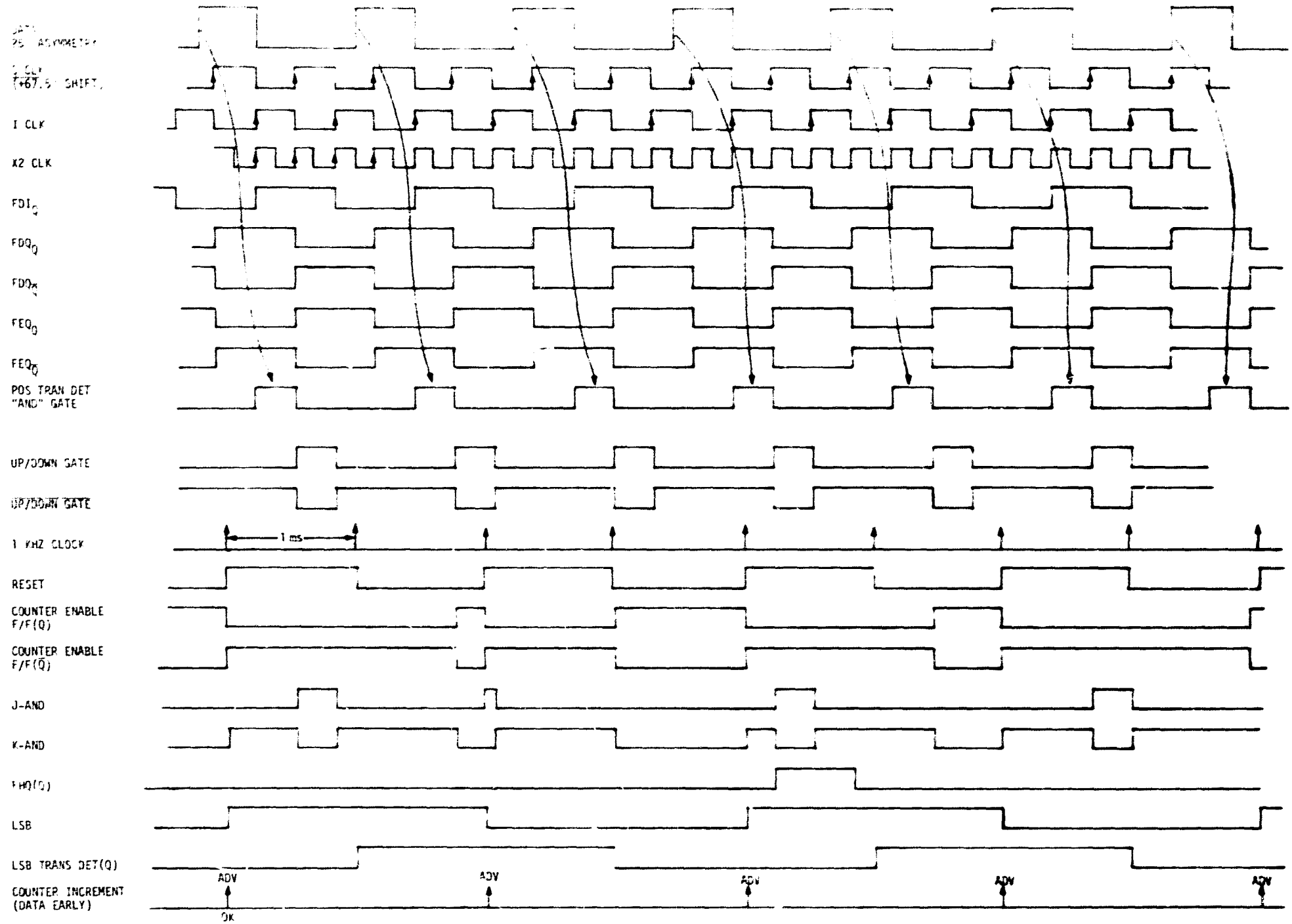

Figure 27 Timing Diagram of the Bit Synchronizer Illustrating the Case of 25° Asymmetry and the Data Leading the μ-Sampler by 67.5° (Results Hold Up To 90°)

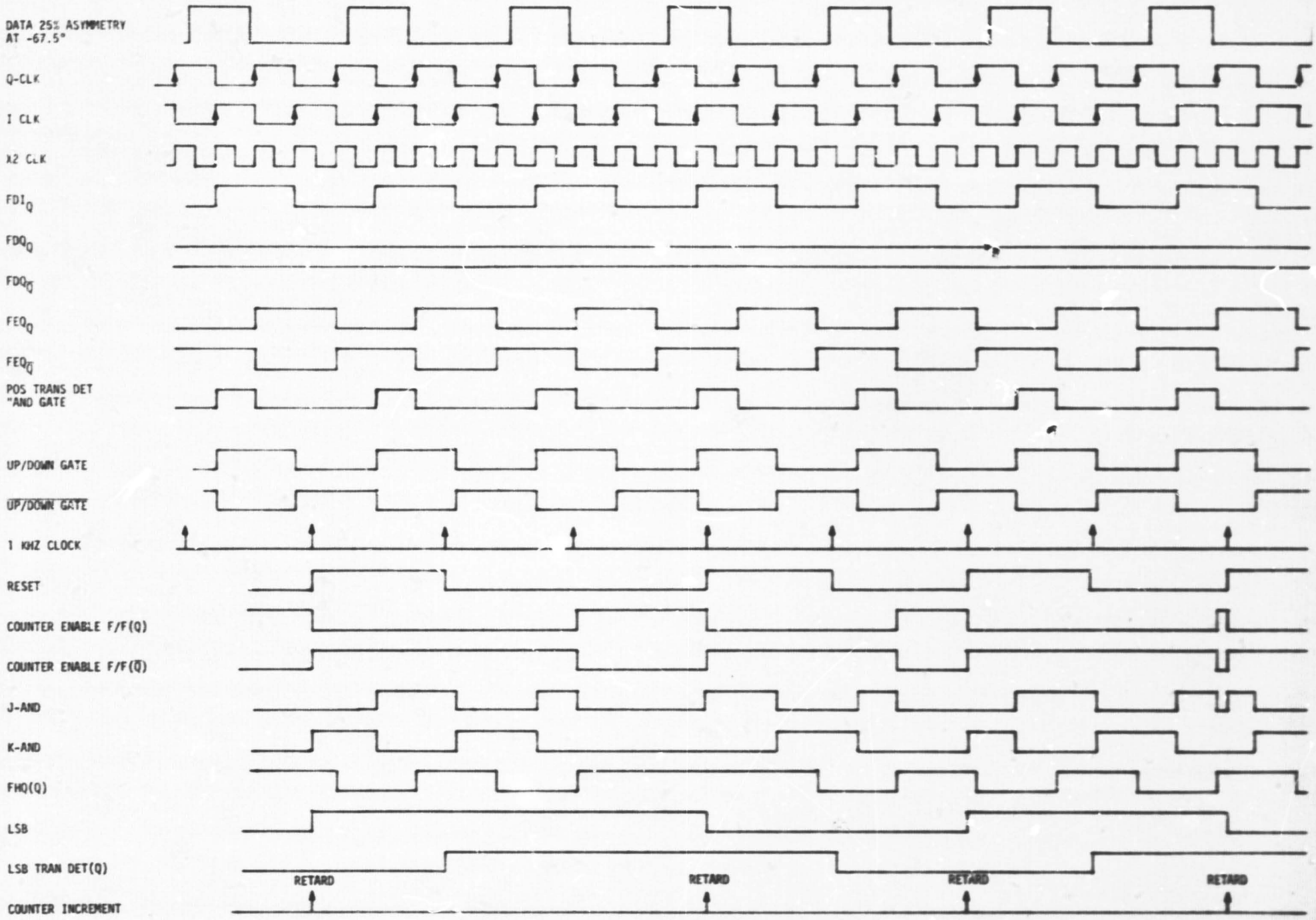

Figure 25. Timing Diagram of the Bit Synchronizer Illustrating the Case of 25% Asymmetry and the Data Lagging the Q-Samples by 67.5° (Results Hold Up to 90°)

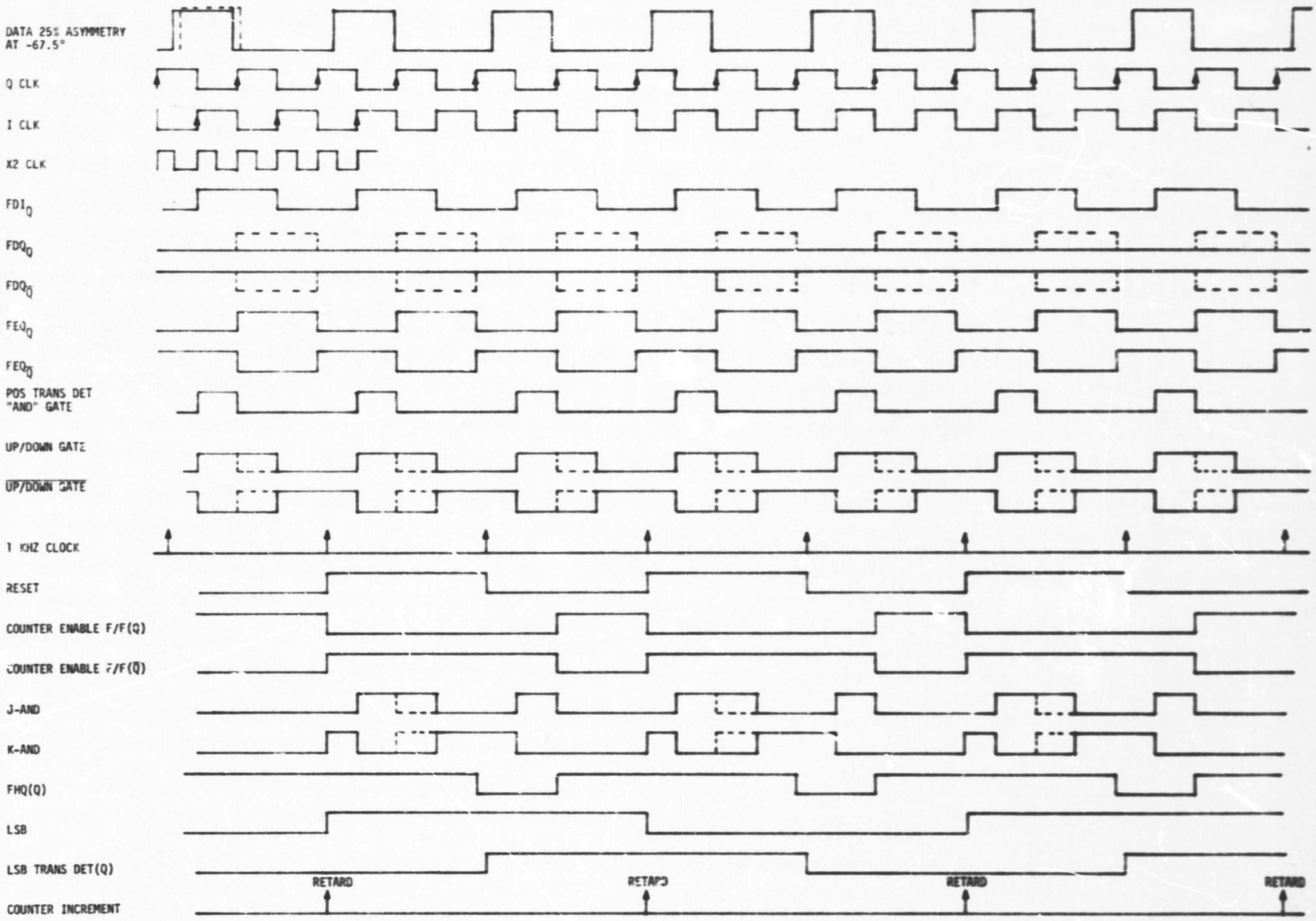

Figure 24. Timing Diagram of the Bit Synchronizer Illustrating the Case of 25% Asymmetry and the Data Lagging the Q-Samples by 67.5° (Different 1 kHz Clock Phase Than That of Figure 4)

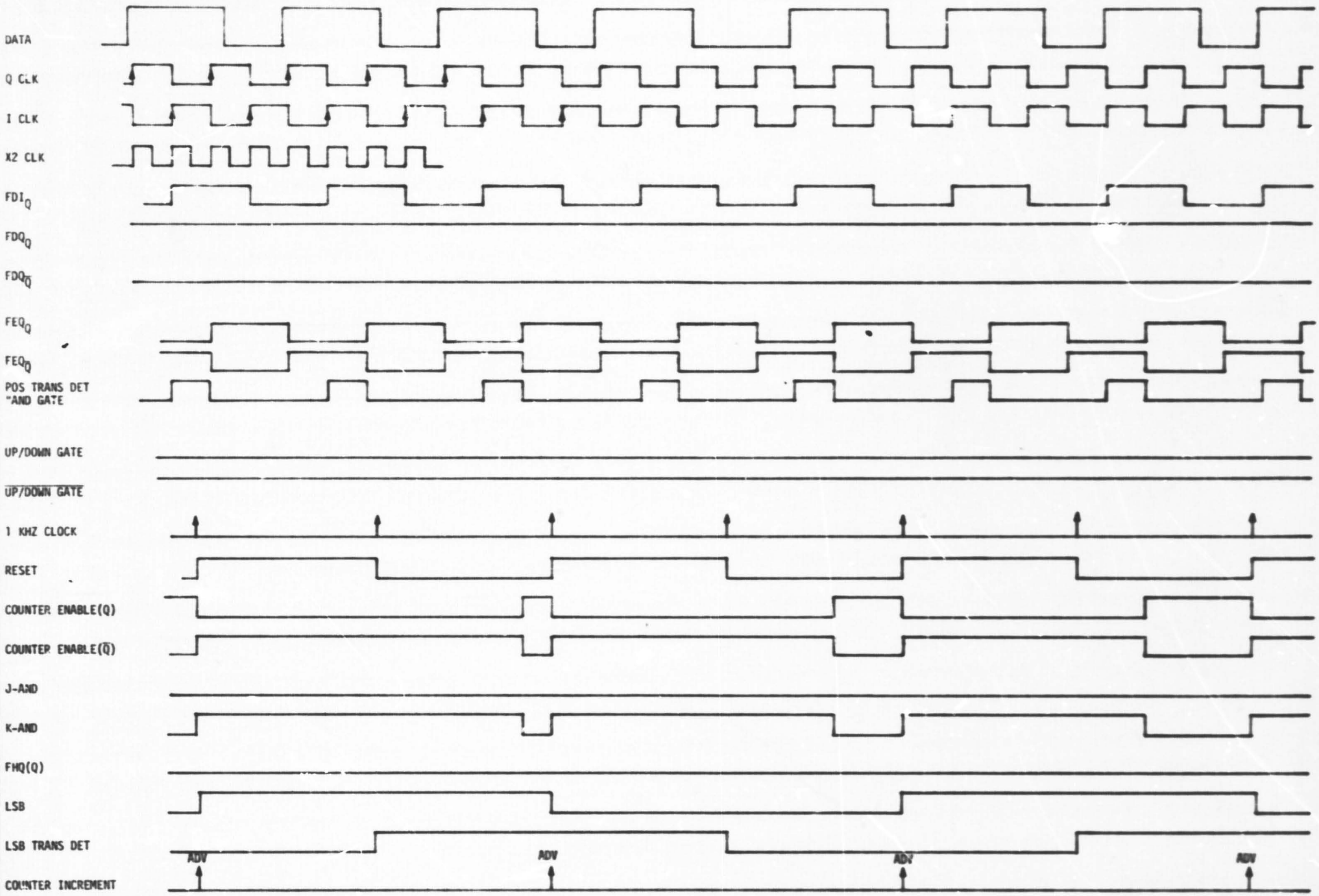

Figure 30 Timing Diagram of the Bit Synchronizer Illustrating the Case of 25% Asymmetry and the Data Leading the Q-Samples by 22.5°

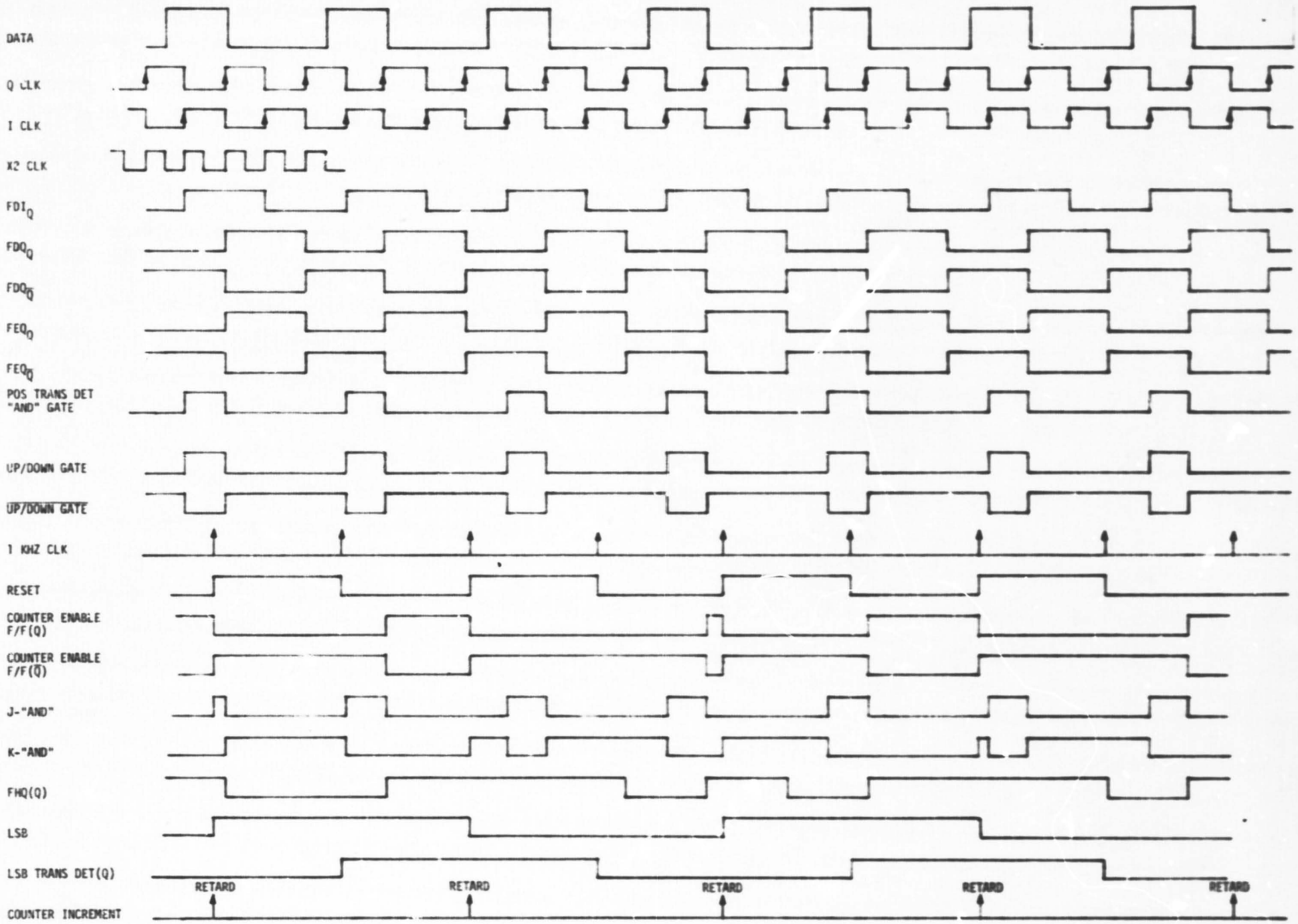

Figure 3: Timing Diagram of the Bit Synchronizer Illustrating the Case of 25% Asymmetry and the Data Lagging the Q-Samples by 100°

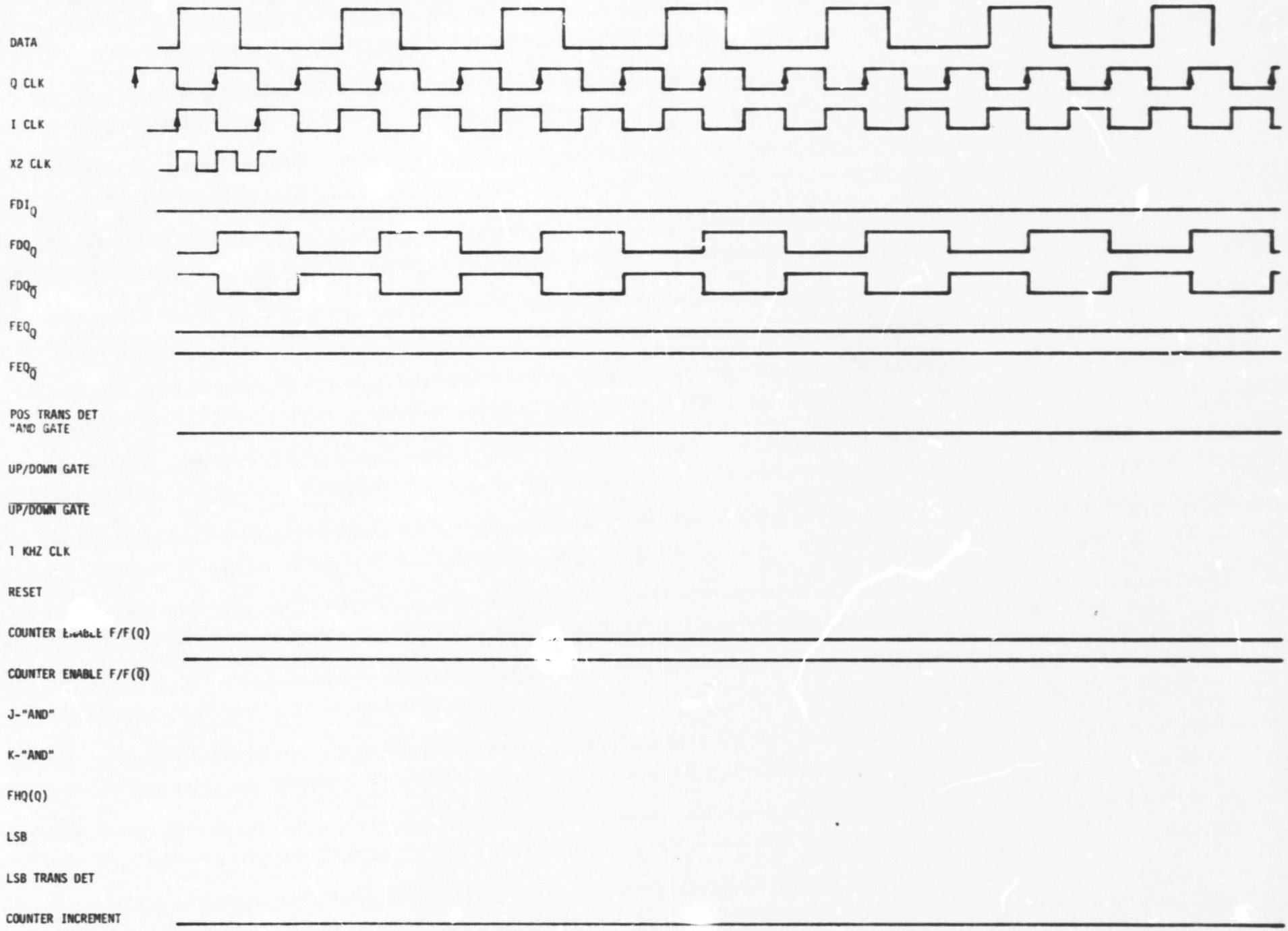

Figure 32 Timing Diagram of the Bit Synchronizer Illustrating the Case of 25% Asymmetry with the Data Lagging the Q-Samples by 190°

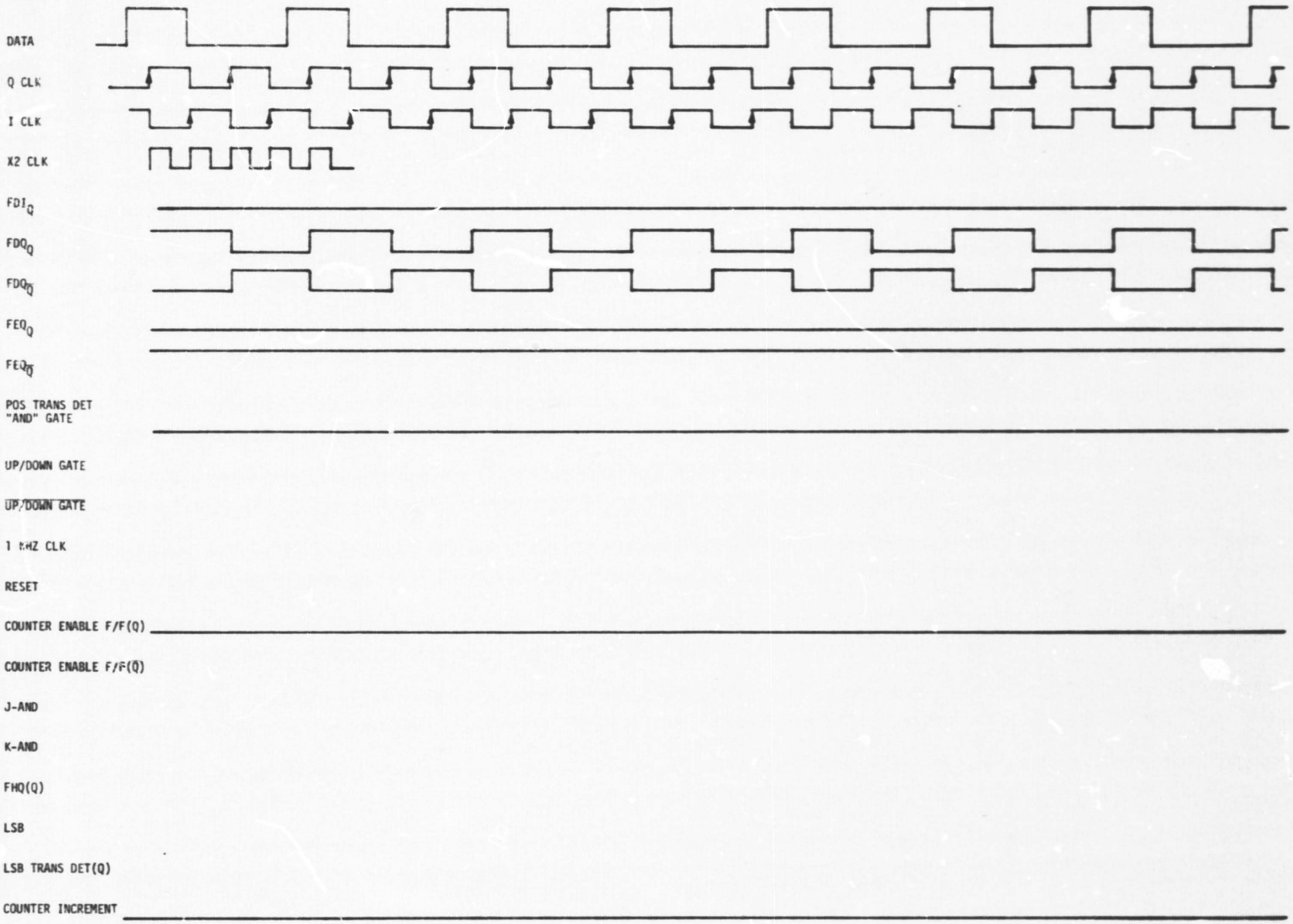

Figure 2: Timing Diagram of the Bit Synchronizer Illustrating the Case of 25% Asymmetry

otherwise, false lock is assumed. If false lock is detected, the digital-to-analog converter (DAC) voltage is set to provide 0 DC bias into the loop filter, which allows the loop to reacquire in true lock.

The bit synchronizer loop is composed of a Motorola high-frequency phase-frequency detector (ϕ-F) [9&13] which is capable of detecting both phase and frequency errors and is used to track the received clock, as well as a bit timing detector, based on positive data transitions.

The phase-frequency detector has been discussed in some detail in [11] and will not be discussed here except to say that its function is to act as a discriminator in a frequency lock loop during frequency acquisition and as a phase detector during tracking.

In effect, the ϕ-F detector removes the frequency error between the VCO and the received clock, then removes the phase error. The function of the flip-flops, least significant bit detector, and counter-DAC unit is to position the clock-generated bit timing so that the Q-clock straddles the leading edge of each bit.

The VCO is run at 4-100 MHz and divided by 2 by the D flip-flop (F/F) following the VCO. From the $\overline{Q}$ output, the Q-clock is generated and, from the Q output, the I-clock is generated. Flip-flop FDI then provides samples of the I sample (mid-bit samples) whereas FDQ outputs the Q samples (or transition samples). The function of FEQ is to delay the I sample by one-half of one bit so that the positive data detector gate will go high when a positive transition occurs. The up/down gate, along with the J-AND and K-AND gates, set the JK flip-flop so as to increase or decrease the counter count and, therefore, the DAC voltage. This voltage is subtracted in the loop filter amplifier, thereby adjusting the loop VCO phase relative to the received clock phase. Both the Q-clock and the X2 clock, plus the resynchronized data, are sent to the convolutional decoder. The function of the least significant bit transition detector is to provide a settling time of 2 ms before a new update can be processed.

Now consider Figure 26, which illustrates how the loop provides corrections so as to align the leading edge of the Q-clock with the leading edge of the bit stream. The top row illustrates an early data stream in the solid line and a late data stream in the dasned line. The next three rows illustrate the I, Q and X2 clocks.

In the 5th row, the FDI D-type flip-flop samples the data stream at the rising edge of the I-clock (CLK), whereas FDQ_Q outputs the Q-CLK sample of the data in row 6. The 7th row indicates that the $FDQ_{\overline{Q}}$ output is simply the complement of FDQ_Q. Notice that both FDQ_Q and $FDQ_{\overline{Q}}$ are dependent on the data timing relative to the Q-CLK timing.

Row 8 illustrates the output of FEQ_Q which is a one-half-bit delay of the I samples. $FEQ_{\overline{Q}}$ is the complement of FEQ_Q. In the 10th row, the positive transition detector output AND-gate is shown. Notice that a pulse occurs one-half a bit after the occurrence of the leading edge of each bit.

The 11th row illustrates the up/down gate output for both late and early data streams. In the 12th row, the count enable flip-flip is indicated. In order for the count enable to be high, the reset input must be at the 0 state and the transition detector must be high when the Q-clock arrives. When the Q-output is high, the up/down counter is free to accept a unit change in its count.

In the 13th row, the 1 kHz clock tick marks are shown, for convenience, at a much higher rate than 1 kHz. The counter enable ($\overline{Q}$) output of the flip-flop of row 14 is the inverse of the 12th row output.

Row 15 depicts the output of the J-AND gate, illustrating the difference for early and late data streams. In the same manner, row 17 illustrates the output of the K-AND gate. In row 16, the inverse of the up/down gate is illustrated.

Row 18 illustrates the least significant bit output of the up/down counter which feeds the LSB delayed flip-flop. This control stays high for 2 ms rather than 1 ms since the up/down counter is enabled just after the next 1 ms clock occurs, which therefore requires 2 ms to change the LSB.

In row 19, the least significant bit detector flip-flop output stays high for 2 ms, as can be seen from the sketch. The reason for the 2 ms duration is the same as for the LSB 2 ms duration. The reset control for the counter enable F/F is just the modulo 2 sum of the LSB and the LSB-delayed F/F, which is shown in row 20.

In the 21st row, the JK F/F called FHQ(Q) provides the advance or retard signal which, when clocked into the up/down counter and converted via the DAC, provides the timing error reduction. This advance or retard

is relative to the Q-clock epoch times. Finally, the last row illustrates the times when the counter is updated to correct the loop timing. Notice that the correction will be an advance of the VCO-generated clock when the leading edge of the bit stream leads the clock and a retard if the data leading edge is retarded from the clock.

4.5.3 Timing Diagrams Under Imperfect Data Streams

In this section, timing diagrams are presented which consider data asymmetry of 25% and various timing errors. In Figure 17, the case of 25% asymmetry is illustrated via a timing diagram. Asymmetry is defined as

$$ASY = \frac{|T_1 - T_0|}{T_1 + T_0} \times 100\%$$

where T_1 is the bit duration of a "one" when preceded and followed by a zero, and T_0 is the bit duration of a "zero" when preceded and followed by a one. It is currently expected that the total asymmetry due to rise time and transmitted asymmetry will be no more than 25% at 50 Mbps, and less at low bit rates.

In the last row of Figure 17, it is seem that the updating is in the correct direction; that is, the Q-clock is advancing. We conclude from Figure 17 that errors up to 90° (data leading edge of the Q-clock) are acceptable to the bit synchronizer when the data "ones" are larger than the data "zeros" with 25% asymmetry.

In Figure 18, the same case as in Figure 17 is illustrated, except that the data lags the Q samples leading edge by 67.5°. As can be seen in row 6, the Q samples are all zero; however, the last row of the timing diagram indicates that the error correction signal retards the timing, which is the proper action for the loop to take. We conclude from Figure 18 that, with errors up to 90° (data lagging the leading edge of the Q-clock) and 25% asymmetry, the bit synchronizer works properly so as to decrease the timing error.

Figure 19 illustrates the same case as Figure 18 except that the phase of the 1 kHz clock has been changed to verify that the loop operates properly, which it does.

In Figure 20, the case when the data leads the Q-clock by 22.5° is illustrated. This figure has the "ones" larger than the "zeros" but, again, the bit synchronizer provides the correct correction so as to reduce the tracking error.

Figure 21 illustrates the case where data lags the Q samples by 100° and has 25% asymmetry with the "zeros" wider than the "ones." As can be seen from the last row, the loop still corrects in the proper direction so as to reduce the timing error.

The point of Figure 22 is to illustrate the fact that the bit synchronizer has limitations as to how large a timing error can be tolerated. With the data lagging the leading edge of the Q sample by 190°, it is seen that the loop has no response; that is, no loop correction occurs since the counter enable is always at 0 or, equivalently, the counter is disabled.

Finally, Figure 23 illustrates the case when, with 25% asymmetry, and the data leading the Q-clock by 100°, the loop is incapable of providing updates to reduce the timing error.

5.0 KU-BAND RADAR PERFORMANCE EVALUATION

5.1 Threshold Analysis

5.1.1 Introduction

In this section and section 5.2, Axiomatix evaluates radar parameters which are difficult to measure experimentally. This effort is covered under Task A4 of the contract, "Critical Design Review and Development Test Evaluation."

The constant false alrm rate (CFAR) thresholding scheme in the Shuttle Ku-band radar is analyzed for the "designated mode" of operation. In particular, both the mean and standard deviations are determined for the threshold level.

In search, there are two basic modes of operation: designated and undesignated. In the designated mode, range being designated, there are two overlapping range gates of width $3\tau/2$, where τ is the transmitted pulse width. Four nonoverlapping range gates of width τ are used in the undesignated mode.

Sixteen pulses are transmitted at each of the five RF frequencies. When range designation is available, the pulse width and pulse repetition frequency are functions of the designated range.

Included below is a glossary of terms used in this section.

I = RF frequency index; $I \epsilon [1, I_{max}]$

L = Range gate index; $\begin{cases} -1: & \text{early gate} \\ +1: & \text{late gate} \end{cases}$

k = Time index for a specified pair (I,L); $k \epsilon [0, N-1]$

m = Doppler filter index; $m \epsilon [0, N-1]$, $N = 16$

$S_R(L,k)$, $S_I(L,k)$ = Real and imaginary parts, respectively, of the signal component at the output of the Lth range gate, at time k.

$N_R(L,k)$, $N_I(L,k)$ = Real and imaginary parts, respectively, of the noise component at the output of the Lth gate, at time k.

$PSI(L,k) = S_R(L,k) + N_R(L,k)$ = Real part of the total output of the Lth gate at time k.

$PSQ(L,k) = S_I(L,k) + N_I(L,k)$ = Imaginary part of the total output of the Lth gate at time k.

$F(L,m)$ = Output of the mth doppler filter following the Lth gate.

$F_R(L,m)$, $F_I(L,m)$ = Real and imaginary parts of $F(L,m)$, respectively.

σ_s^2 = Variance of the in-phase and quadrature phase Gaussian signal components.

σ_n^2 = Variance of the in-phase and quadrature phase Gaussian noise components.

N = Order of the Discrete Fourier Transform (DFT) filter.

$|\cdot|$ = Norm of $(\cdot)$

ρ = Noise correlation coefficient.

$j = \sqrt{-1}$

5.1.2 Designated Mode Threshold

The basic signal processing of the Shuttle Ku-band radar for the designated mode in search is shown in Figure 34. Only those signal processings pertinent to the CFAR threshold formulation are shown. For a more detailed description of the signal processing for the Ku-band radar, see [14].

The output of the IF filter is downconverted to a complex base-band waveform

$$I + jQ = SI(I,J,k) + jSQ(I,J,k) \tag{42}$$

Before A/D, the I and Q waveforms for the kth pulse are given by

$$I + jQ = A_I\, P(t - kT_p)\, \exp\left[j(\omega_d t + \theta_I)\right] + N_c(t) + jN_s(t) \tag{43}$$

where

A_I = the random amplitude of the target return which has the Rayleigh probability density function with parameter σ_s^2, which represents signal power

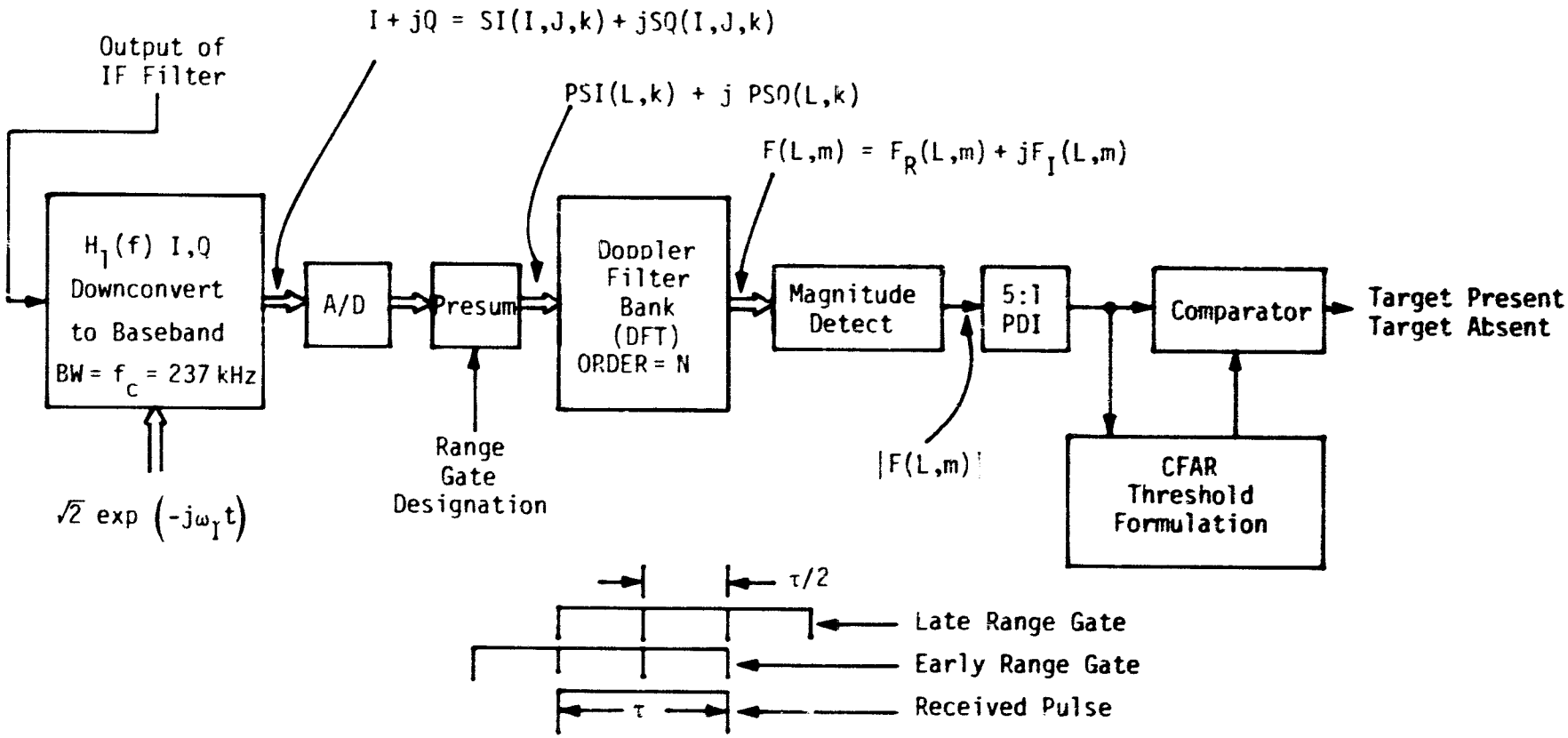

Shuttle Ku-Band Radar

Figure 34. Signal Processing for Designated Mode in Search

θ_I = a random phase uniformly distributed over $(0,2\pi)$

ω_d = the doppler frequency, which is neglected in this analysis. The effect of doppler on the final results is not expected to be appreciable.

$P(t)$ = pulse shape of width τ seconds

$T_p = (PRF)^{-1}$

$N_c(t)$, $N_s(t)$ = independent zero-mean Gaussian processes with one-sided power spectral density N_0 W/Hz and one-sided noise bandwidth f_c (f_c = 237 kHz), which is the 3 dB bandwidth of $H_1(f)$ (see Figure 34).

The noise power in $N_c(t)$ and $N_s(t)$ is therefore given by

$$N_0 \, f_c \tag{44}$$

for each process.

The integration process of the presum is also shown in Figure 34. for the designated mode in search. We assume that the received pulse is ideally designated so that it appears exactly between the two range gates of width $3\tau/2$, as shown in Figure 34. This, coupled with neglecting the doppler effect, maximizes the effect of the signal received from the target on the CFAR threshold.

With these assumptions, the presum output for the k<u></u>th pulse for the L<u></u>th range gate is

$$PSI(L,k) + j\,PSQ(L,k) = \frac{1}{\tau}\int_{t_s}^{t+3\tau/2} \Big[SI(t) + j\,SQ(t)\Big]dt$$

$$= A_I\tau \exp(j\theta_I) + \int_{t_s}^{t_s+3\tau/2} \Big[N_c(t) + j\,N_s(t)\Big]dt \tag{45}$$

where the sum of the samples at the output of the A/D is approximated by analog integration. This is an excellent approximation since the number

of samples in $3\tau/2$ is sufficiently large at long ranges. The starting time of the range gate integration is designated t_s.

The signal part of the presum output is designated

$$A_I \, \tau \exp(j\theta_I) = S_R(L,k) + jS_I(L,k) \tag{46}$$

where S_R and S_I are independent zero-mean Gaussian random variables, with variance σ_s^2. This is the same value found at the input to the presum because of the normalization in our definition.

The noise components of the presum output are designated

$$N_R(L,k) + j\, N_I(L,k) = \frac{1}{\tau}\int_{t_s}^{t_s+3\tau/2} \left[N_c(t) + j\, N_s(t)\right] dt \tag{47}$$

where N_R and N_I are independent Gaussian random variables with variances

$$\sigma_n^2 = \left(\frac{N_0}{2}\right)\frac{3}{2} = \frac{3}{4}\, N_0 \tag{48}$$

Formulation of the CFAR threshold for the designated mode in search is shown in more detail in Figure 35. In particular, the outputs of the DFT doppler filters are given by

$$F(m) = \sum_{k=0}^{N-1} \left[PSI(k) + j\, PSQ(k)\right] \exp\left(-j\, \frac{2\pi mk}{N}\right) \tag{49}$$

for both the early and late range gate outputs. Note that the doppler filter outputs from the early and late range gates are correlated; this affects the evaluation of the variance of this CFAR threshold.

The CFAR threshold, T, is formed via the following average

$$T \triangleq C_1 \sum_{I=1}^{I_{max}} \sum_{L=-1}^{+1} \sum_{m=0}^{N-1} F(L,m,I) \tag{50}$$

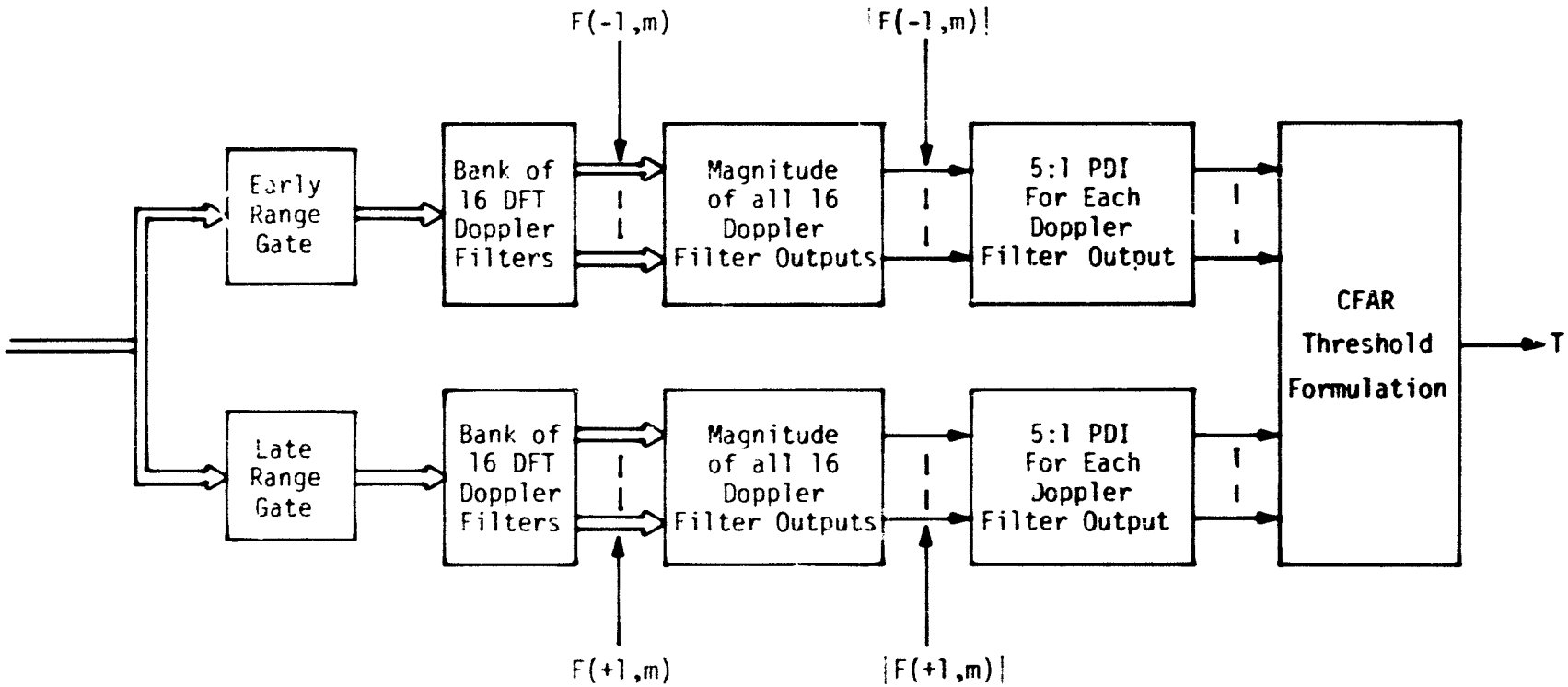

Figure 35. Formulation of Shuttle Ku-Band CFAR Threshold for Designated Mode in Search

where

I = the RF frequency index, $I = 1,\ldots,I_{max}$, $I_{max} = 5$

L = the range gate index, $L = -1$: early gate; $L = +1$: late gate

k = the time or pulse index, $k = 0,\ldots, N-1$, $N = 16$

m = the frequency of doppler filter index, $m = 0,\ldots, N-1$.

In the next section, the results of the statistical analysis of T are discussed.

5.1.3 Performance of CFAR Threshold

The mean (ensemble average) of the CFAR threshold is determined in section 5.1.4 and plotted in Figure 36. In this analysis, any doppler frequency shift away from the center frequency of the nearest doppler filter is neglected. In addition, it is assumed that the range designation is ideal. Both of these assumptions maximize the effect of the signal on the statistics of the CFAR threshold.

Under the above assumptions, the average CFAR threshold value for the designated mode versus the SNR at the output of the presum is plotted in Figure 36, where

$$SNR = \sigma_s^2/\sigma_n^2 \tag{51}$$

As expected, at small values of SNR, the effect of the signal from the target disappears and the threshold becomes the value corresponding to noise only.

Also included in Figure 36 is the result of the simulation reported in [15]. The results of our analysis are normalized in Figure 36 so that the average threshold value at 0 dB coincides with that in [15].

At this time, we have no explanation for the significant difference between the exact analytical and the simulation results since their target dependence is less, even though we assumed maximum target dependence.

In Figure 37, the normalized standard deviation of the CFAR threshold is plotted versus the SNR at the output of the presum. This

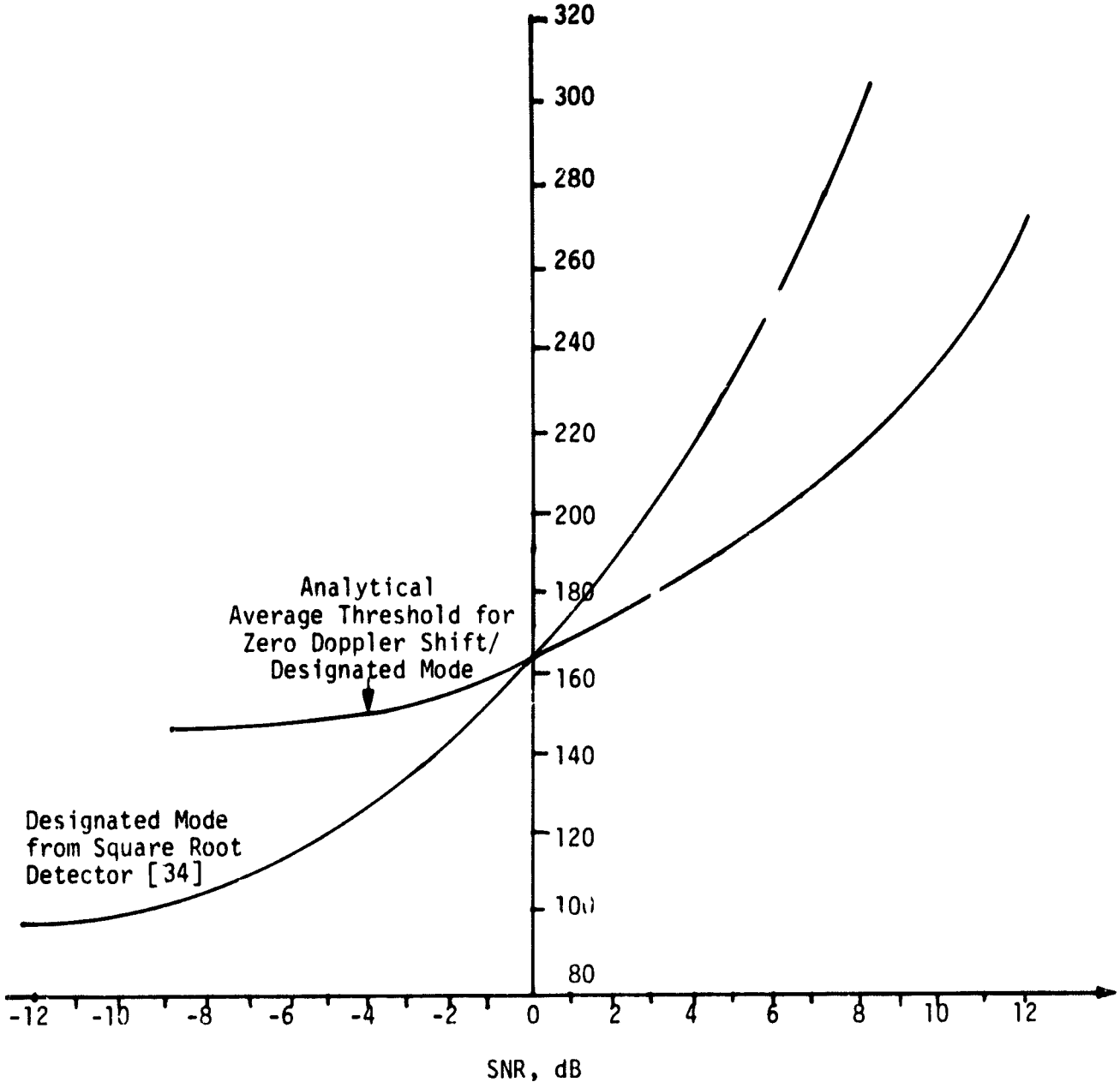

Figure 36. Average Threshold Values for Zero Doppler Shift, Designated Mode

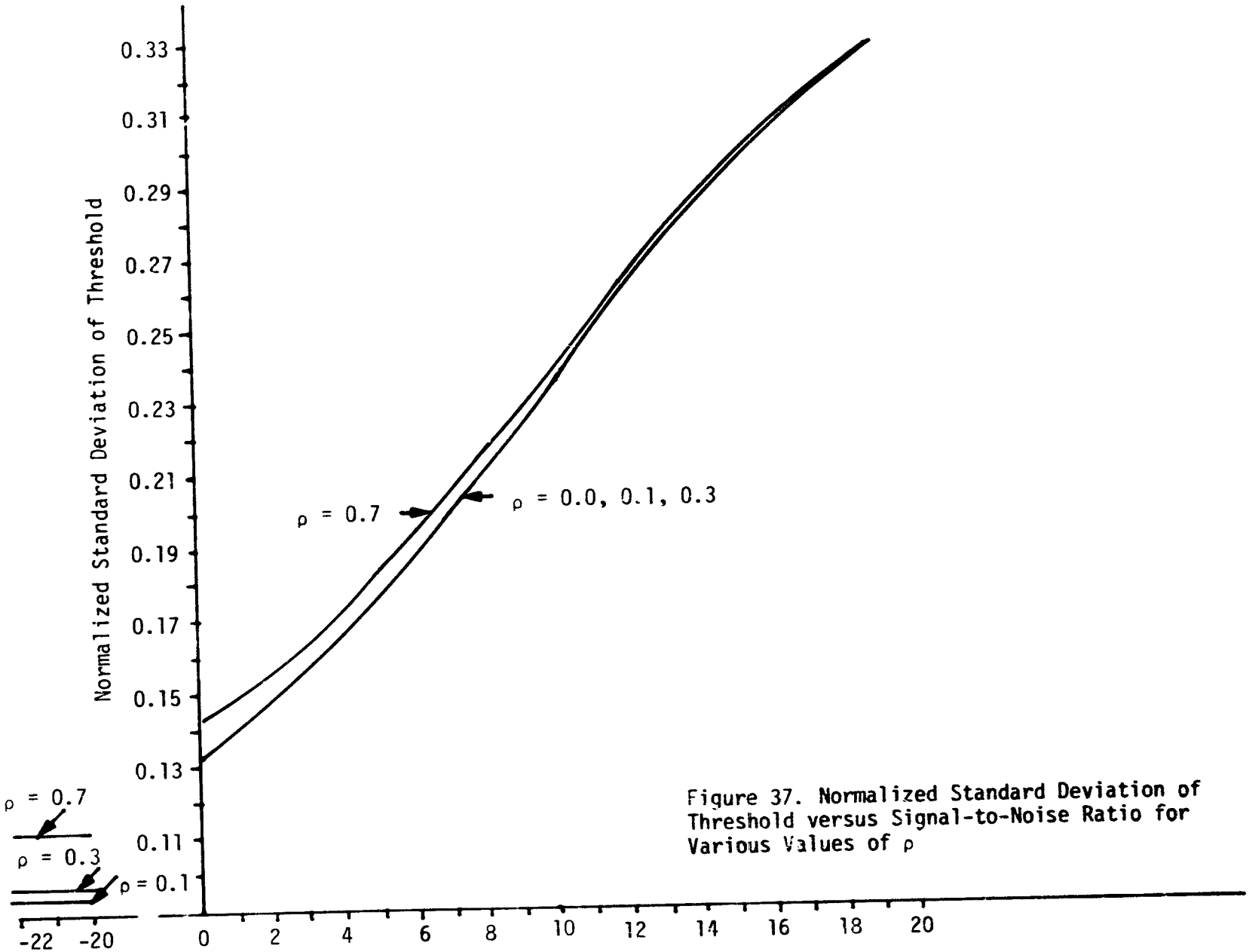

Figure 37. Normalized Standard Deviation of Threshold versus Signal-to-Noise Ratio for Various Values of ρ

exact analytical result shows a significant dependence on SNR and a negligible dependence on the normalized noise correlation coefficient ρ. For the actual case, we have, as described for the range gates in Figure 34,

$$\rho = 2/3.$$

Inspection of the plot in Figure 37, however, shows little variation as ρ varies from 0 to 0.7.

It is worthy to note the substantial variation in the CFAR threshold, particularly at large values of SNR where the normalized standard deviation is greater than 0.3. No attempt has been made to determine the effects of this variation on the probability of detection. On the optimistic side, the threshold setting and the target return are correlated; this leads us to conjecture that this variation may not appreciably affect the probability of detection. On the pessimistic side, there is a substantial variation of the CFAR threshold setting away from that developed from the noise-only condition.

5.1.4 Derivation of Threshold Mean

Here we wish to derive the expected value E(T) of the random variable T, defined as (see Figures 34 and 35):

$$T \triangleq C_1 \cdot \sum_{I=1}^{I_{max}} \sum_{L=-1}^{1} \sum_{m=0}^{N-1} |F(L,m,I)| \tag{52}$$

where the dependence of F on the frequency range I is explicitly shown in (52) and where C_1 is a normalizing constant.

Before we proceed, let us first list the assumptions entailed in the following derivations.

<u>Assumptions</u>

(1) The in-phase and quadrature-phase components of the signal and noise are zero-mean, independent, Gaussian random variables (rv).

(2) For different RF frequencies, all rv's are independent. We can therefore confine our interest to one specific frequency.

(3) For the same range gate (L) and different time slots (k), the noise variables are independent, i.e.,

$$N_R(L,k_1) \perp N_R(L,k_2) \qquad \text{for } k_1 \neq k_2$$
$$N_I(L,k_1) \perp N_I(L,k_2)$$

(4) Real and imaginary parts of either signal or noise are always independent, i.e.,

$$N_R \perp N_I \ , \qquad S_R \perp S_N \ .$$

(5) For the <u>same</u> k but different gate, the noise components are correlated. The covariance matrix is

$$R = \{\text{cov } N_R(-1,k), N_I(-1,k), N_R(1,k), N_I(1,k)\} = \sigma_n^2 \cdot \begin{bmatrix} 1 & 0 & \rho & 0 \\ 0 & 1 & 0 & \rho \\ \rho & 0 & 1 & 0 \\ 0 & \rho & 0 & 1 \end{bmatrix}$$

Therefore, for different k's, the noise rv's are independent, regardless of the value of L.

(6) For both range gates and all times k associated with one RF frequency, the parts of the signal are identical, i.e.,

$$S_R(-1,k_1) = S_R(-1,k_2) = S_R(1,k_3) = S_R(1,k_4).$$

for every k_1,k_2,k_3,k_4 [0 , N]. Likewise for the imaginary parts of the signal S_I.

As an immediate result of assumption (2), the frequency dependence can be dropped and T can be written as

$$\begin{aligned} T &= C_1 \cdot I_{max} \cdot \sum_{L=-1}^{1} \sum_{m=0}^{N-1} |F(L,m)| \\ &= C \sum_{m=0}^{N-1} \sum_{L=-1}^{1} |F(L,m)| \\ &= C \cdot \sum_{m=0}^{N-1} X(m) \end{aligned} \tag{53}$$

where $C = C_1 \cdot I_{max}$ and we have defined the rv X(m) by

$$X(m) = |F(-1,m)| + |F(1,m)| \tag{54}$$

In the following, we shall derive the expected value of X(m). From (54), it follows that

$$E\{X(m)\} = E\{|F(-1,m)|\} + E\{|F(1,m)|\} \tag{55}$$

and, because of the symmetry existing between the two gates, (54) simplifies to

$$E\{X(m)\} = 2E\{|F(1,m)|\} \tag{56}$$

It is obvious from (56) and the assumptions made that the first moment

(ensemble average) is not a function of the range gate. Henceforth, we will drop the gate-index dependence from the symbols listed before in order to simply matters.

Let us call

$$y(m) \triangleq |F(m)| = \sqrt{F_R^2(m) + F_I^2(m)} \tag{57}$$

so that, from (53), (56) and (57),

$$E\{T\} = 2C \cdot \sum_{m=0}^{N-1} E\{y(m)\} \tag{58}$$

Since F(m) is the output of a DFT filter whose input is the set $\{PSI(k) + jPSQ(k)\}$, we have that

$$F(m) = \sum_{k=0}^{N-1} \{PSI(k)+jPSQ(k)\} \cdot e^{-j\frac{2\pi mk}{N}}$$

which means that

$$F_R(m) = \sum_{k=0}^{N-1} PSI(k) \cos \frac{2\pi mk}{N} + PSQ(k) \sin \frac{2\pi mk}{N} \tag{59a}$$

$$F_I(m) = \sum_{k=0}^{N-1} - PSI(k) \sin \frac{2\pi mk}{N} + PSQ(k) \cos \frac{2\pi mk}{N} \tag{59b}$$

Since PSI(k), PSQ(k) are Gaussian rv's, (both signal and noise are Gaussian), so are their linear combinations $F_R(m)$ and $F_I(m)$, which are also zero mean.

We will need the covariance matrix of $\{F_R(m), F_I(m)\}$. From (59a), we have that

$$E\left\{F_R^{\,2}(m)\right\} = E\left\{\sum_{k=0}^{N-1}\left(PSI(k)\cos\frac{2\pi mk}{N} + PSQ(k)\sin\frac{2\pi mk}{N}\right)^2\right.$$

$$+ \sum_{\substack{k=0\\k\neq\tau}}^{N-1}\sum_{\tau=0}^{N-1}\left(PSI(k)\cos\frac{2\pi mk}{N} + PSQ(k)\sin\frac{2\pi mk}{N}\right)$$

$$\left.\cdot\left(PSI(\tau)\cos\frac{2\pi m\tau}{N} + PSQ(\tau)\sin\frac{2\pi m\tau}{N}\right)\right\} \tag{60}$$

But

$$E\left\{PSI^2(k)\right\} = E\left\{S_R^{\,2}(k) + N_R^{\,2}(k) + 2S_R(k)\,N_R(k)\right\} = \sigma_s^{\,2} + \sigma_n^{\,2} \tag{61a}$$

and, similarly,

$$E\left\{PSQ^2(k)\right\} = \sigma_s^{\,2} + \sigma_n^{\,2} \tag{61b}$$

For $k \neq \tau$,

$$E\{PSI(k)\cdot PSI(\tau)\} = E\left\{\left(S_R(k) + N_R(k)\right)\left(S_R(\tau) + N_R(\tau)\right)\right\} \quad \text{(Assumption 1)}$$

$$= E\left\{S_R(k)\cdot S_R(\tau)\right\} + E\left\{N_R(k)\,N_R(\tau)\right\} \quad \text{(Assumptions 3,6)}$$

$$= \sigma_s^{\,2} \tag{62a}$$

and, similarly,

$$E\{PSQ(k)\cdot PSQ(\tau)\} = \sigma_s^{\,2} \tag{62b}$$

Also, from Assumption 4,

$$E\{PSI(k)\cdot PSQ(k)\} = E\{PSI(k)\cdot PSQ(\tau)\} = E\{PSI(\tau)\cdot PSQ(k)\} = 0 \tag{63}$$

Substituting (61), (62), and (63) into (60) and after some manipulations, we get

$$E\left\{F_R^{\,2}(m)\right\} = \left(\sigma_s^{\,2}+\sigma_n^2\right)\cdot\sum_{k=0}^{N-1}\left(\cos^2\frac{2\pi mk}{N}+\sin^2\frac{2\pi mk}{N}\right)^{=1}$$

$$+\,\sigma_s^{\,2}\sum_{\substack{k=0\\k\neq\tau}}^{N-1}\sum_{\tau=0}^{N-1}\left[\cos\frac{2\pi m}{N}(k-\tau)\right]$$

or

$$E\left\{F_R^{\,2}(m)\right\} = N\left(\sigma_s^{\,2}+\sigma_n^{\,2}\right) + 2\sigma_s^{\,2}\sum_{\xi=1}^{N-1}(N-\xi)\cos\frac{2\pi m\xi}{N} \tag{64}$$

The corresponding result for $E\left\{F_I^{\,2}(m)\right\}$ is easily shown to be the same as in (64).

Before we examine (64) closer, let us calculate the cross-covariance term:

$$E\left\{F_R(m)\cdot F_I(m)\right\} = E\left\{\sum_{k=0}^{N-1}\sum_{\tau=0}^{N-1}\left(PSI(k)\cos\frac{2\pi mk}{N}+PSQ(k)\sin\frac{2\pi mk}{N}\right)\right.$$

$$\left.\times\left(-PSI(\tau)\sin\frac{2\pi m\tau}{N}+PSQ(\tau)\cos\frac{2\pi m\tau}{N}\right)\right\} \quad \text{(Assumption 4)}$$

$$= E\left\{\sum_{k=0}^{N-1}\sum_{\tau=0}^{N-1}\left(-PSI(k)\,PSI(\tau)\sin\frac{2\pi m\tau}{N}\cos\frac{2\pi mk}{N}\right.\right.$$

$$\left.\left.+\,PSQ(k)\,PSQ(\tau)\cos\frac{2\pi m\tau}{N}\sin\frac{2\pi mk}{N}\right)\right\}$$

$$= \sigma_s^{\,2}\sum_{\substack{k=0\\k\neq\tau}}^{N-1}\sum_{\tau=0}^{N-1}\sin\frac{2\pi m}{N}(k-\tau) \tag{65}$$

We now notice in (65) that, to each term $\xi = k-\tau>0$ in the double summation, there exists a corresponding term $-\xi=\tau-k<0$ which, because of the sine function being an odd function, cancels with the former term. Hence,

$$E\left\{F_R(m)\cdot F_I(m)\right\} = 0 \text{ , for all } m\varepsilon[0,15] \tag{66}$$

and this holds independently of N. The covariance matrix of $F_R(m)$, $F_I(m)$ can now be written as

$$\Lambda \triangleq \operatorname{cov}\left\{F_R(m),F_I(m)\right\} = N \begin{bmatrix} A(m)\cdot\sigma_s^{\,2} + \sigma_n^{\,2} & 0 \\ 0 & A(m)\cdot\sigma_s^{\,2} + \sigma_n^{\,2} \end{bmatrix} \tag{67}$$

where, from (64) and (67), it follows that

$$A(m) = 1 + 2\sum_{\xi=1}^{N-1}\left(1 - \frac{\xi}{N}\right)\cos\frac{2\pi m\xi}{N} \tag{68}$$

We will briefly examine A(m). We have that, for m=0,

$$A(0) = 1 + 2\sum_{\xi=1}^{N-1}\left(1 - \frac{\xi}{N}\right) = 1 + 2\left[(N-1) - \frac{1}{N}\sum_{\xi=1}^{N-1}\xi\right]$$

$$= 1 + 2\left[N-1 - \frac{N(N-1)}{2N}\right] = N. \tag{69}$$

To study the case $m\neq 0$, let us assume that N is divisible by 4. Then, if we call $\xi' = N - \xi$, it follows that

$$\cos\frac{2\pi m\xi'}{N} = \cos\frac{2\pi m}{N}(N-\xi) = \cos\frac{2\pi m\xi}{N}$$

so that (68) reduces to

$$A(m) = 1 + 2\left[\sum_{\xi=1}^{N/2-1}\left(1 - \frac{\xi}{N} + 1 - \frac{N-\xi}{N}\right)\cos\frac{2\pi m\xi}{N} + \frac{\cos m\pi}{2}\right]$$

or

$$A(m) = 1 + 2\sum_{\xi=1}^{N/2-1}\cos\frac{2\pi m\xi}{N} + \cos m\pi \tag{70}$$

If we now call $\xi' = N/2-1$, it follows that

$$\cos\frac{2\pi m\xi'}{N} = \cos\frac{2\pi m(N/2-\xi)}{N} = (-1)^m\cos\frac{2\pi m\xi}{N}$$

so that (70) yields

$$A(m) = 1 + 2\left[\sum_{\xi=1}^{N/4-1}\left(1+(-1)^m\right)\cos\frac{2\pi m\xi}{N} + \cos\frac{m\pi}{2}\right] + \cos m\pi \tag{71}$$

An immediate conclusion of (71) is that $A(m) = 0$ for m = odd. For m = even, (53) reduces to

$$A(m) = 2\left[1 + (-1)^{m/2} + 2\sum_{\xi=1}^{N/4-1}\cos\frac{2\pi m\xi}{N}\right] \tag{72}$$

The above holds for an arbitrary N divisible by 4. In the general case, (72) might yield a nonzero value of A(m), which nevertheless will be small. However, it is straightforward to show that, if N is a power of 2 (which is almost always the case in practice), A(m) of (72) identically vanishes. Below we summarize the conclusion for the covariance matrix Λ:

$$\Lambda = \mathrm{cov}\left\{F_R(m), F_I(m)\right\} = \begin{cases} N\begin{bmatrix} N\sigma_s^2 + \sigma_n^2 & 0 \\ 0 & \sigma_s^2 + \sigma_n^2 \end{bmatrix} & ; m = 0 \\ N\begin{bmatrix} \sigma_n^2 & 0 \\ 0 & \sigma_n^2 \end{bmatrix} & ; m \neq 0 \end{cases} \tag{73}$$

From (73), some useful conclusions can be drawn. First, we notice that the noise components at the input affect all doppler filter outputs, while the effect of the signal is confined to the $m = 0$ doppler filter only. Furthermore, the effect of the signal on that term is enhanced by a factor of N as compared to the noise. Hence, for the moderate-to-high signal-to-noise ratio (SNR) environment, we can claim that the zeroth filter output is produced by the signal only and the other outputs by the noise only. Finally, we notice that, in all cases and for every doppler filter output, the real and imaginary parts of the output are independent. This enables us to conclude that $y(m)$ of (57) is a Rayleigh rv with mean

$$E\{y(m)\} = \sqrt{\frac{\pi}{2}} \cdot \gamma(m) \tag{74}$$

where

$$\gamma(m) = \begin{cases} \sqrt{N^2\sigma_s^2 + N\sigma_n} & ; m = 0 \\ \sqrt{N\sigma_n^2} & ; m \neq 0 \end{cases} \tag{75}$$

From (58), (74) and (75), it follows that

$$E\{T\} = C\sqrt{2\pi} \cdot \left[\sqrt{N^2\sigma_s^2 + N\sigma_n^2} + (N-1) \cdot \sqrt{N\sigma_n^2}\right]$$

or

$$E\{T\} = C \cdot N\sqrt{2\pi}\left[\sqrt{\sigma_s^2 + \sigma_n^2/N} + \frac{N-1}{\sqrt{N}} \cdot \sigma_n\right] \tag{76}$$

or in terms of the signal-to-noise ratio $SNR = \sigma_s^2/\sigma_n^2$,

$$\boxed{E\{T\} = C\cdot\sqrt{2\pi}\cdot N\cdot\sigma_n\left[\sqrt{SNR + \frac{1}{N}} + \frac{N-1}{\sqrt{N}}\right]} \tag{77}$$

Typically, the constant C_1 in (1) is defined as

$$C_1 = \frac{1}{2NI_{max}} \tag{78}$$

In this case, $C = C_1\cdot I_{max} = 1/2N$, and (77) modifies to

$$\boxed{E\{T\} = \sqrt{\frac{\pi}{2}}\cdot\sigma_n\cdot\left[\sqrt{SNR + \frac{1}{N}} + \frac{N-1}{\sqrt{N}}\right]} \tag{79}$$

For the specific application considered, $N = 16$, so that the factor $1/N \approx 0.06$ can be neglected for even very moderate SNR (say, $SNR \geq 0$ dB). In this case, we conclude that $E\{T\}$ varies linearly with $(SNR)^{1/2}$.

A final comment pertains to the values of SNR and σ_n^2 of (79). These are the values of the signal-to-noise ratio and noise power at the input of the doppler filters. Since an A/D converter precedes these filters, the values of these parameters at the input of the A/D converter, denoted here by $(SNR)_i$ and σ_{n_i}, respectively, relate to the A/D output parameters (which are the inputs to the filters) by [14]

$$SNR = \frac{SNR_i}{L_{A/D}} \tag{80a}$$

and

$$\sigma_n = \sigma_{n_i}\sqrt{L_{A/D}} \tag{80b}$$

where

$$L_{A/D} = 1.0129 + 0.0129\cdot SNR_i \tag{81}$$

If we incorporate (80) and (81) into (79), we get

$$\boxed{E\{T\} = \sqrt{\frac{\pi}{2}} \cdot \sigma_{n_1} \cdot \sqrt{L_{A/D}} \left[\sqrt{\frac{SNR_1}{L_{A/D}}} + \frac{N-1}{\sqrt{N}} \right]} \tag{82}$$

which is plotted in Figure 36 for $N = 16$ as a function of SNR_1 in dB.

5.1.5 Derivation of Threshold Standard Deviation

We evaluate herein the variance σ_T^2 of the random variable T, as defined in equation (52).

From (53), it follows that:

$$E\left\{T^2\right\} = C^2 \cdot \left[\sum_{m=0}^{N-1} X^2(m) + \sum_{\substack{m_1=0 \\ m_1 \neq m_2}}^{N-1} \sum_{m_2=0}^{N-1} X(m_1)\, X(m_2)\right] \tag{83}$$

where

$$X(m) = \sqrt{F_R^2(-1,m) + F_I^2(-1,m)} + \sqrt{F_R^2(1,m) + F_I^2(1,m)} \tag{84}$$

To simplify matters, we will examine two distinct cases: moderate-to-high and low SNR.

5.1.5.1 Moderate-to-High SNR

According to the previous comments of this section, we can justifiably assume in this case that the zeroth doppler filter output X(0) is produced by the signal part of the DFT input only, while all other X(m), $m \neq 0$ are produced by noise only.

5.1.5.1.1 Signal Output (m=0)

$$E\left\{X^2(0)\right\} = \left(\text{from (2)}\right) = E\left\{F_R^2(-1,0) + F_I^2(-1,0) + F_R^2(1,0) + F_I^2(1,0) + 2\sqrt{\left(F_R^2(-1,0) + F_I^2(-1,0)\right)\left(F_R^2(1,0) + F_I^2(1,0)\right)}\right\} \tag{85}$$

Since we have assumed that all random variables appearing in (85) are exclusively signal functions, we can further invoke Assumption 6 according to which

$$F_R(-1,0) = F_R(1,0) \quad \text{and} \quad F_I(-1,0) = F_I(1,0).$$

Substituting the above into (85) yields

$$E\left\{X^2(0)\right\} = 4E\left\{F_R^{\,2}(-1,0)\right\} + 4E\left\{F_I^{\,2}(-1,0)\right\} \tag{86}$$

From (73), we have $\left(\text{setting } \sigma_s^{\,2} \gg \sigma_n^{\,2}\right)$ that

$$E\left\{F_R^{\,2}(-1,0)\right\} = E\left\{F_I^{\,2}(-1,0)\right\} = N^2\sigma_s^{\,2} \tag{87}$$

so that (86) and (87) combine to give

$$E\left\{X^2(0)\right\} = 8N^2\sigma_s^{\,2} \tag{88}$$

5.1.5.1.2 Noise Outputs ($m \neq 0$)

$$E\left\{\underset{m\neq 0}{X^2(m)}\right\} = E\left\{F_R^{\,2}(-1,m) + F_I^{\,2}(-1,m) + F_R^{\,2}(1,m) + F_I^{\,2}(1,m) + 2\sqrt{\left(F_R^{\,2}(-1,m) + F_I^{\,2}(-1,m)\right)\left(F_R^{\,2}(1,m) + F_I^{\,2}(1,m)\right)}\right\} \tag{89}$$

Since all random variables are produced by noise, it follows from (73) that

$$E\left\{F_R^{\,2}(-1,m)\right\} = E\left\{F_I^{\,2}(1,m)\right\} = E\left\{F_R^{\,2}(1,m)\right\} = E\left\{F_I^{\,2}(1,m)\right\} = N\sigma_n^{\,2} \triangleq \sigma^2$$

so that

$$E\left\{\underset{m\neq 0}{X^2(m)}\right\} = 4N\sigma_n^{\,2} + 2\,D \tag{90}$$

where

$$D \triangleq E\left\{\sqrt{\left(F_R^{\,2}(-1,m) + F_I^{\,2}(-1,m)\right)\left(F_R^{\,2}(1,m) + F_I^{\,2}(1,m)\right)}\right\} \tag{91}$$

We now proceed to evaluate D. To do this, we need the joint statistics of the zero-mean, Gaussian rv's appearing in (91). Let us find the covariance matrix R of $\{F_R(-1,m),\ F_I(-1,m),\ F_R(1,m),\ F_I(1,m)\}$, $m \neq 0$.

From (59a), we have that (assuming only noise input),

$$E\left\{F_R^{\,2}(-1,m)\right\} = E\left\{\left[\sum_{k=0}^{N-1}\left(N_R\ (k,-1)\cos\frac{2\pi mk}{N} + N_I(k,-1)\sin\frac{2\pi mk}{N}\right)\right]^2\right\}$$

(because of assumption 4)

$$= \sigma_n^{\,2}\sum_{k=0}^{N-1}\left(\cos^2\frac{2\pi mk}{N} + \sin^2\frac{2\pi mk}{N}\right) = N\sigma_n^{\,2} = \sigma^2 \qquad (92)$$

and similarly for the others.

Furthermore,

$$E\left\{F_R(-1,m)\cdot F_R(1,m)\right\} = E\left\{\sum_{k=0}^{N-1}\sum_{\tau=0}^{N-1}\left(N_R(-1,k)\cos\frac{2\pi mk}{N} + N_I(-1,k)\sin\frac{2\pi mk}{N}\right)\right.$$

$$\left.\left(N_R(1,\tau)\cos\frac{2\pi m\tau}{N} + N_I(1,\tau)\sin\frac{2\pi m\tau}{N}\right)\right\} \qquad (93)$$

which, because of Assumptions 4 and 5, reduces to

$$E\left\{F_R(-1,m).F_R(1,m)\right\} = E\left\{\sum_{k=0}^{N-1} N_R(-1,k)N_R(1,k)\cos^2\frac{2\pi mk}{N}\right.$$

$$\left. + N_I(-1,k)\cdot N_I(1,k)\sin^2\frac{2\pi mk}{N}\right\} = N\cdot\sigma_n^{\,2}\cdot\rho = \rho\sigma^2 \qquad (94)$$

Hence, the covariance matrix R is

$$R = \mathrm{cov}\left\{F_R(-1,m),F_I(-1,m),F_R(1,m),F_I(1-m)\right\} = \sigma^2\begin{bmatrix}1 & 0 & \rho & 0\\ 0 & 1 & 0 & \rho\\ \rho & 0 & 1 & 0\\ 0 & \rho & 0 & 1\end{bmatrix} \qquad (95)$$

Comparing (95) and Assumption 5, we draw the interesting conclusion that the noise statistics remain unaltered after passing through the complex DFT doppler filters.

We are now in a position to evaluate D. If we change to polar coordinates

$$F_R(-1,m) = V_E \cos \phi_E \qquad F_R(1,m) = V_L \cos \phi_L$$
$$\text{and} \tag{96}$$
$$R_I(-1,m) = V_E \sin \phi_E \qquad F_I(1,m) = V_L \sin \phi_L$$

then (91) is simply written as

$$D = E\{V_E \cdot V_L\} \tag{97}$$

The joint distribution of the envelopes V_E and V_L, for the four Gaussian rv's correlated as in (95), is found from [16] to be

$$\rho(V_E,V_L) = \begin{cases} \dfrac{V_E V_L}{|R|^{1/2}} \cdot I_0\left\{\dfrac{V_E V_L \cdot \sigma^2 \rho}{|R|^{1/2}}\right\} \cdot \exp\left\{-\dfrac{\sigma^2(V_E^2+V_L^2)}{2|R|^{1/2}}\right\} & , \text{ for } V_E,V_L \geq 0 \\ 0 & , \text{ elsewhere} \end{cases} \tag{98}$$

where $I_0(\cdot)$ is the zeroth-order modified Bessel function. From (97) and (98), it follows that

$$D = \int_0^\infty\int_0^\infty \frac{V_E^2 V_L^2}{|R|^{1/2}} \cdot I_0\left(\frac{V_E V_L \sigma^2 \rho}{|R|^{1/2}}\right) \cdot \exp\left\{-\frac{\sigma^2(V_E^2+V_L^2)}{2|R|^{1/2}}\right\} dV_E dV_L \tag{99}$$

If we make the transformation

$$V_E^2 = \frac{|R|^{1/2}}{\sigma^2} \cdot y \cdot \exp\{2z\}$$

$$V_L^2 = \frac{|R|^{1/2}}{\sigma^2} \cdot y \exp\{-2z\}$$

whose Jacobian is

$$|J| = \frac{|R|^{1/2}}{\sigma^2}$$

and, upon substituting into (99), we get

$$D = \frac{|R|}{\sigma^6}\int_0^\infty dy \cdot y^2 \cdot I_0(y\rho)\cdot\left(\int_{-\infty}^{\infty} dz \cdot \exp\{-y \cosh (2z)\}\right) \quad (100)$$

The inner integral equals $K_0(y)$ [17], where $K_0(y)$ is the zeroth-order modified Hankel function. Therefore, from (100),

$$D = \frac{|R|}{\sigma^6}\int_0^\infty y^2 \, J_0(j\rho y) \, k_0(y) \, dy \quad (101)$$

where we have used the fact that $I_0(n) = J_0(jn)$ ($J_0(\cdot)$ is the zeroth-order Bessel function).

The integral of (101) can be evaluated. From [18], we find that

$$\int_0^\infty . \, K_\alpha(az) \, J_\beta(bz)\cdot z^{-\gamma} \, dz$$

$$= b^\beta . \Gamma\left(\frac{\beta-\gamma+\alpha+1}{2}\right)\cdot\Gamma\left(\frac{\beta-\gamma-\alpha+1}{2}\right)\cdot 2^{-(\gamma+1)} \cdot a^{\gamma-\beta-1} \, \Gamma^{-1}(\beta+1)$$

$$\cdot {}_2F_1\left(\frac{\beta-\gamma+a+1}{2} \, ; \, \frac{\beta-\gamma-\alpha+1}{2} \, ; \, \beta+1; \, -\frac{b^2}{a^2}\right) \quad (102)$$

where ${}_2F_1(\cdot)$ is the Gaussian hypergeometric function [18]. Applying (102) for $\alpha = 0$, $\beta = 0$, $\gamma = -2$, $a = 1$, $b = j\rho$, we get from (101) that

$$D = \frac{|R|}{\sigma^6} \cdot \frac{\pi}{2} \cdot {}_2F_1(3/2; \, 3/2; 1; \rho^2) \quad (103)$$

From [18], we find that

$$ {}_2F_1(3/2;\ 3/2;\ 1;\ \rho^2) = (1-\rho^2)^{-2}\cdot {}_2F_1(-1/2;\ -1/2;\ 1;\ \rho^2) $$

$$ = (1-\rho^2)^{-2}\cdot\left[\frac{4}{\pi}\,E(\rho^2) - \frac{2}{\pi}(1-\rho^2)\cdot k(\rho^2)\right] \qquad (104) $$

where $k(\cdot)$ and $E(\cdot)$ are the complete elliptic integrals of the first and second kind [19].

Upon substitution of (104) into (103), we find that

$$ D = \frac{|R|}{\sigma^6}\cdot(1-\rho^2)^{-2}\left[2E(\rho^2) - (1-\rho^2)\,k(\rho^2)\right] \qquad (105) $$

From (95), the determinant $|R|$ can be evaluated to be

$$ |R| = \sigma^8(1-\rho^2) = N^4\sigma_n^{\,8}(1-\rho^2)^2 \qquad (106) $$

From (105) and (106), we finally get

$$ D = N\sigma_n^{\,2}\left[2E(\rho^2) - (1-\rho^2)\,k(\rho^2)\right] \qquad (107) $$

From (90) and (107), we derive that

$$ \underset{m\neq 0}{E}\left\{X(m)^2\right\} = 2N\sigma_n^{\,2}\left[2 + 2E(\rho^2) - (1-\rho^2)\,k(\rho^2)\right] \qquad (108) $$

Equations (88) and (108) yield the result for the first summation in (83). The second term (double summation) is now evaluated.

First let us assume that $m_1 \neq m_2$ and none of them equals zero. In this case, both $X(m_1)$ and $X(m_2)$ are produced by noise, and from (84)

$$E\left\{\underset{0\neq m_1\neq m_2\neq 0}{X(m_1)\ X(m_2)}\right\} = E\left\{\sqrt{\left(F_R^2(-1,m_1)+F_I^2(-1,m_1)\right)\cdot\left(F_R^2(-1,m_2)+F_I^2(-1,m_2)\right)}\right\}$$
$$+ E\left\{\sqrt{\left(F_R^2(1,m_1)+F_I^2(1,m_1)\right)\cdot\left(F_R^2(1,m_2)+F_I^2(1,m_2)\right)}\right\}$$
$$+ E\left\{\sqrt{\left(F_R^2(-1,m_1)+F_I^2(-1,m_1)\right)\cdot\left(F_R^2(1,m_2)+F_I^2(1,m_2)\right)}\right\}$$
$$+ E\left\{\sqrt{\left(F_R^2(1,m_1)+F_I^2(1,m_1)\right)\left(F_R^2(-1,m_2)+F_I^2(-1,m_2)\right)}\right\} \quad (109)$$

We will now show that all random variables under the same square root are mutually independent. To do this, let us evaluate

$$E\left\{\underset{m_1\neq m_2}{F_R(-1,m_1)\cdot F_R(-1,m_2)}\right\} = E\left\{\sum_{k=0}^{N-1}\sum_{\tau=0}^{N-1}\left(N_R(-1,k)\cos\frac{2\pi m_1 k}{N}+N_I(-1,k)\sin\frac{2\pi m_1 k}{N}\right)\right.$$
$$\left.\cdot\left(N_R(-1,\tau)\cos\frac{2\pi m_2\tau}{N}+N_I(-1,\tau)\sin\frac{2\pi m_2\tau}{N}\right)\right\}$$

(Assumption 4)

$$= E\left\{\sum_{k=0}^{N-1} N_R^2(-1,k)\cos\frac{2\pi m_1 k}{N}\cos\frac{2\pi m_2 k}{N}\right.$$
$$\left.+ N_I^2(-1,k)\sin\frac{2\pi m_1 k}{N}\sin\frac{2\pi m_2 k}{N}\right\}$$
$$= \sigma_n^2\sum_{k=0}^{N-1}\cos\frac{2\pi k(m_1-m_2)}{N} \quad (110)$$

For N a power of 2 and $m_1 \neq m_2$, it is easy to show that the summation in (110) vanishes which in turn means that $F_R(-1,m_1)$ and $F_R(-1,m_2)$ are independent. Identically, we show that $F_I(-1,m_1) \perp F_I(-1,m_2)$. Similarly,

$$E\left\{F_R(-1,m_1)\cdot F_R(1,m_2)\right\} = \rho\sigma_n^{\,2}\sum_{k=0}^{N-1}\cos\frac{2\pi k(m_1-m_2)}{N} = 0\ .$$

Finally, by interchanging 1 and -1, we get the symmetrical results for both gates, which justify our earlier claim that all rv's in (109) are independent. Therefore,

$$E\left\{\underset{0\neq m_1\neq m_2\neq 0}{X(m_1)\,X(m_2)}\right\} = 4E^2\left\{\sqrt{F_R^{\,2}(-1,m_1)+F_I^{\,2}(-1,m_1)}\right\}$$

$$= 4\cdot\left(\sigma\sqrt{\frac{\pi}{2}}\right)^2 = 2\pi N\sigma_n^{\,2} \tag{111}$$

Second, assume that $m_1 = m_2 = m \neq 0$. Because $X(0)$ is produced by the signal, $X(m)$ by the noise and, due to the high SNR assumption, we get

$$E\{\underset{m\neq 0}{X(m)}\ X(0)\} = E\{X(m)\}\cdot E\{X(0)\} \quad (\text{see } (73))$$

$$= \sqrt{2\pi}\cdot\sqrt{N^2\sigma_s^{\,2}}\cdot\sqrt{2\pi}\cdot\sqrt{N\sigma_n^{\,2}} = 2\,N\sqrt{N}\,\sigma_s\sigma_n \tag{112}$$

From the N^2 terms involved in (85), one term is given by (88), N-1) terms are given by (108), 2(N-1) terms are given by (112) and (N-1)·(N-2) terms are given by (111). Summarizing, we get that

$$E\{T^2\} = C^2\cdot\Big[8N^2\sigma_s^{\,2} + (N-1)\cdot 2N\sigma_n^{\,2}\left[2+2E(\rho^2)-(1-\rho^2)\,k(\rho^2)\right]$$

$$+2(N-1)\cdot 2\pi N\sqrt{N}\,\sigma_s\sigma_n + (N-1)(N-2)\,2\pi N\sigma_n^{\,2}\Big]$$

$$= 2C^2N^2\sigma_n^{\,2}\Big[4\cdot SNR + \left(1-\frac{1}{N}\right)\left[2+2E(\rho^2)-(1-\rho^2)\,K(\rho^2)\right]$$

$$+\frac{2\pi(N-1)}{\sqrt{N}}\sqrt{SNR} + \left(1-\frac{1}{N}\right)\cdot(N-2)\cdot\pi\Big] \tag{113}$$

But from (79), we have that (for high SNR)

$$E\{T\} = C \cdot N\sqrt{2\pi} \cdot \sigma_n \left[\sqrt{SNR} + \left(\frac{N-1}{\sqrt{N}}\right)\right]$$

therefore,

$$E^2\{T\} = 2C^2N^2 \cdot \sigma_n \cdot \left[\pi\ SNR + \frac{\pi(N-1)^2}{N} + \frac{2\pi(N\cdot 1)\cdot\sqrt{SNR}}{\sqrt{N}}\right] \tag{114}$$

From (113) and (114), it follows that

$$\begin{aligned} \mathrm{var}\{T\} &= \sigma_T^{\ 2} \\ &= E\{T^2\} - E^2\{T\} \\ &= 2C^2N^2\sigma_n^{\ 2}\Big[(4-\pi)\ SNR + \left(1-\frac{1}{N}\right)\Big[2 + 2E(\rho^2) - (1-\rho^2)\ K(\rho^2) \\ &\qquad + (N-2)\pi - (N-1)\pi\Big]\Big] \end{aligned}$$

or

$$\boxed{\begin{aligned} \sigma_T^{\ 2} &= 2C^2N^2\sigma_n^{\ 2}\left[(4-\pi)\ SNR + \left(1-\frac{1}{N}\right) H(\rho)\right] \\ &\text{where} \\ H(\rho) &= 2-\pi + 2E(\rho^2) - (1-\rho^2)\ K(\rho^2) \end{aligned}} \tag{115}$$

(Moderate-to-high SNR)

The primary quantity of interest is the ratio $\sigma_T/E\{T\}$ which, for case 1.1 is given by

$$\frac{\sigma_T}{E\{T\}} = \frac{\sqrt{2}C\,N\,\sigma_n \cdot \sqrt{(4-\pi)\ SNR + \left(1-\frac{1}{N}\right) H(\rho)}}{C\,N_0\sqrt{2\pi}\cdot G_n\left(\sqrt{SNR} + \frac{N-1}{\sqrt{N}}\right)}$$

or

$$\boxed{\frac{\sigma_T}{E\{T\}} = \frac{1}{\sqrt{\pi}} \cdot \frac{\sqrt{(4-\pi)\ \mathrm{SNR} + \left(1 - \frac{1}{N}\right) H(\rho)}}{\left(\sqrt{\mathrm{SNR}} + \frac{N-1}{\sqrt{N}}\right)}} \tag{116}$$

(Moderate-to-high SNR)

5.1.5.2 Very Low SNR (or Signal Absent)

In this case, all the doppler filter outputs are produced by noise. If signal is also present (in order for this assumption to be valid, even for the $m = 0$ filter), we must have that

$$N\sigma_s^2 << \sigma_n^2 \rightarrow \frac{\sigma_s^2}{\sigma_n^2} << \frac{1}{N} .$$

For $N = 16$, such an inequality is satisfied for SNR in the order of -20 dB or less.

From (108)(which also holds for $m = 0$ now) and (111)(which is now restricted only to $m_1 \neq m_2$), we get that

$$\begin{aligned} E\{T^2\} &= C^2\left[2N^2\sigma_n^2\left[2 + 2E(\rho^2) - (1-\rho^2)\ k(\rho^2)\right] + N(N-1)\ 2\pi N\sigma_n^2\right] \\ &= 2C^2N^2\sigma_n^2\left[2 + (N-1) + 2E(\rho^2) - (1-\rho^2)\ K(\rho^2)\right] \end{aligned} \tag{117}$$

For very low SNR, we have from (79) that

$$E\{T\} = C \cdot \sqrt{2\pi} \cdot N \cdot \sqrt{N\sigma_n^2}$$

therefore

$$E^2\{T\} = 2\pi\ C^2 N^3 \sigma_n^2$$

and

$$\mathrm{var}\{T\} = \sigma_T^{\,2} = 2C^2N^2\sigma_n^{\,2}\left[2 + (N-1)\pi + 2E(\rho^2) - (1-\rho^2)\,k(\rho^2) - N\pi\right]$$

or

$$\mathrm{var}\{T\} = 2C^2N^2\sigma_n^{\,2} \cdot H(\rho) \tag{118}$$

where $H(\rho)$ has been defined in (115). The ratio $\sigma_T/E\{T\}$ for this case (2.0) is found to be

$$\frac{\sigma_T}{E\{T\}} = \frac{\sqrt{2}N\,C\,\sigma_n\sqrt{H(\rho)}}{\sqrt{2}\cdot C\cdot N\sqrt{N}\cdot\sigma_n}$$

or

$$\boxed{\frac{\sigma_T}{E\{T\}} = \sqrt{\frac{H(\rho)}{N\pi}}} \tag{119}$$

(Very low SNR)

independent of the SNR, as expected. The ratios of (118) and (119) have been plotted in Figure 37 for various values of ρ. The function $H(\rho)$ depends on the complete elliptic integrals $E(\rho^2)$ and $K(\rho^2)$, which have been tabulated for different values of the argument ρ^2 [19]. In Table 2, we give some values of $H(\rho)$ as a function of ρ.

Table 2. $H(\rho)$ versus ρ

ρ	0.0	0.1	0.2	0.3	0.4	0.5	0.6	0.7	0.8	0.9	0.99
$H(\rho^2)$	0.42920	0.43313	0.44495	0.46475	0.49269	0.52902	0.57409	0.72843	0.69280	0.76850	0.84851

5.2 Degradation of Shuttle Radar Performance due to Pejorative Antenna Scan Overlap

5.2.1 Introduction

Stability considerations of the deployed assembly (DA) fixed base on the Shuttle may cause the antenna scan overlap to fall below the recommended value for off-zenith-centered scans. A lower antenna scan overlap will cause a lower antenna gain and can lead to shorter target dwell times. This will cause a corresponding decrease in the probability of target detection when the worst-case detection scenario is considered, i.e., detection in the center of the overlap region.

This section will present the relationship between the antenna overlap, dwell time and antenna gain, and their effects on the received target signal-to-noise ratio (SNR) and resulting probabilities of detection.

5.2.2 Target Dwell Time Considerations

The target dwell time is a function of the total allowed scan time, the scan frequency and the antenna overlap between consecutive scans. The spiral scan geometry is shown in Figure 38 including the antenna overlap region. It should be observed that the overlap region and, consequently, the chord corresponding to the dwell time are defined in terms of the null-to-null beamwidth, θ_n, instead of the half-power beamwidth, θ_B. This has been done to account for the possibility of overlap below the 3 dB point.

Following the procedure outlined in [20], the dwell time, t_d, for a hybrid spiral scan is given by

$$t_d = \frac{T_s \theta_n \theta_0 (1-\Delta) + \theta_0 \sqrt{\left[T_s \theta_n f_s (1-\Delta)\right]^2 - \left[\theta_m - \frac{\theta_n}{2}(1-\Delta)\right]^2}}{2\pi \left[\theta_m - \frac{\theta_n}{2}(1-\Delta)\right]^2} \qquad (120)$$

where T_s = total scan time = 60 sec

θ_n = null-to-null beamwidth = 2.08°

θ_0 = antenna chord sweeping across the target

Δ = antenna overlap with respect to θ_n

f_s = scan frequency = 2 Hz

θ_m = maximum scan limit = 30°

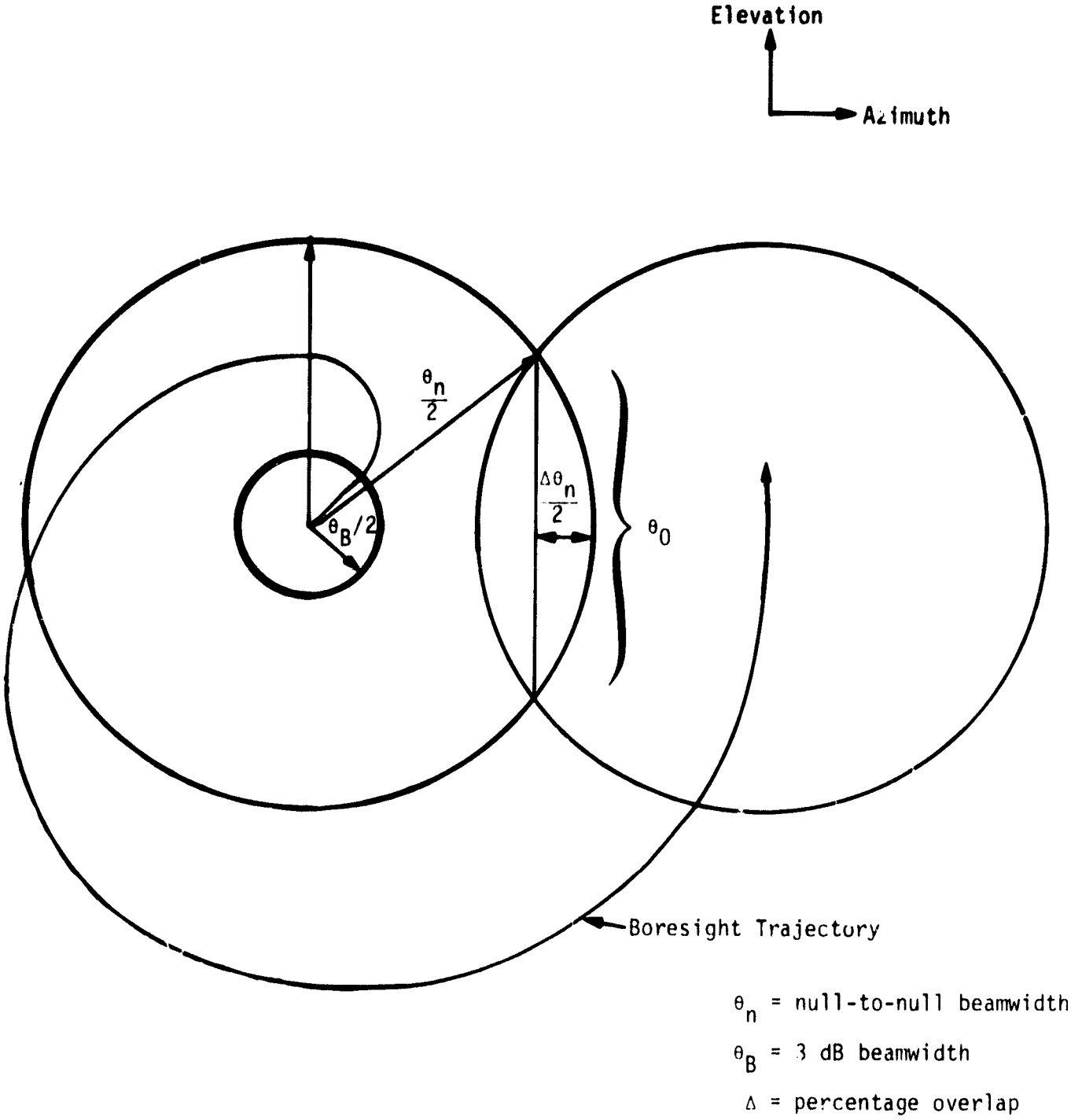

Figure 38. Geometry of Spiral Scan, Including Overlap

A high target dwell time is desirable since it increases the received target energy. However, it should be noted that the dwell time in this case is constrained by the total scan time allowed; too high an antenna overlap precludes completing the volume to be scanned and is physically impossible. A graph of the dwell time is given in Figure 39 as a function of the antenna overlap. As expected, the time on target is equal to zero when no overlap occurs. Maximization of the dwell time, ignoring related effects such as antenna gain, is seen at a scan overlap of 25-30% when measured with respect to the null-to-null beamwidth.

5.2.3 Calculation of Peak Antenna Loss

Since the worst-case detection will occur in the center of the overlap region at some point down the antenna mainlobe, a loss must be computed to account for the degraded peak antenna gain illuminating the target. This is not the same as the beamshape loss, which is incurred as the beam sweeps across the target and is included in the system loss budget.

For small values of off-boresight antenna angles and excluding the sidelobes, the antenna mainlobe weighting function may be approximated by

$$W(\theta) = \left[\frac{\sin\left(\frac{\pi\theta}{\theta_B}\right)}{\left(\frac{\pi\theta}{\theta_B}\right)}\right]^2 \tag{121}$$

where θ = angle off-boresight = $(1-\Delta)\theta_n/2$

θ_B = 3 dB beamwidth = 1.6^o

θ_n = null-to-null beamwidth = 2.08^o

For $\Delta = 1$, corresponding to complete overlap or the on-boresight case, the weighting function is equal to one and the mainlobe is fully weighted. As the scan overlap moves away from the center of the beam, the antenna gain is weighted less. A revised value of the antenna peak can be found as a function of the scan overlap, Δ. A plot of this modified peak gain is given in Figure 40. As noted above, instances when $\Delta = 0.7$ or higher are physically unrealizable and are shown as limiting cases only.

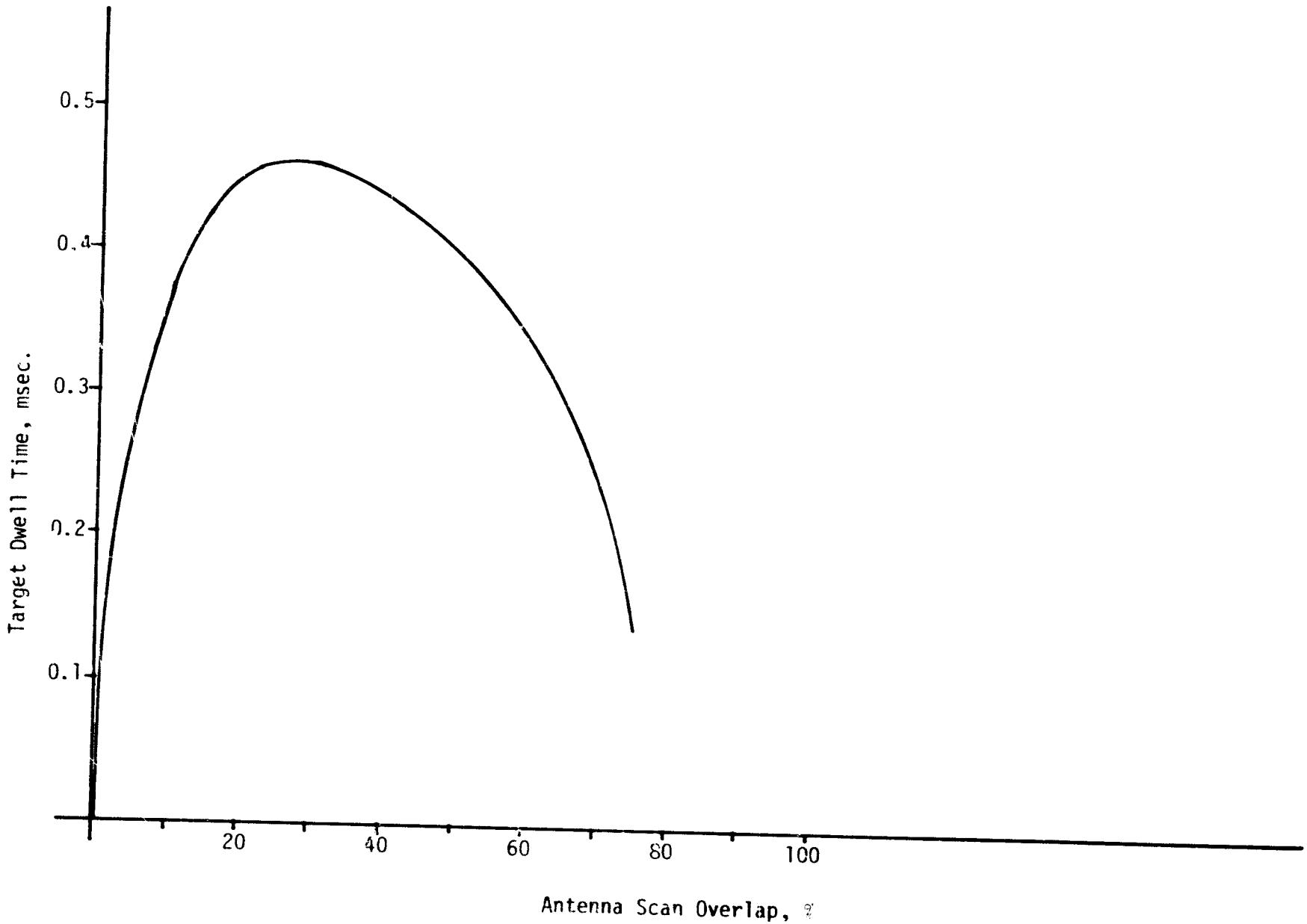

Figure 39. Target Dwell Time as a Function of Antenna Scan Overlap

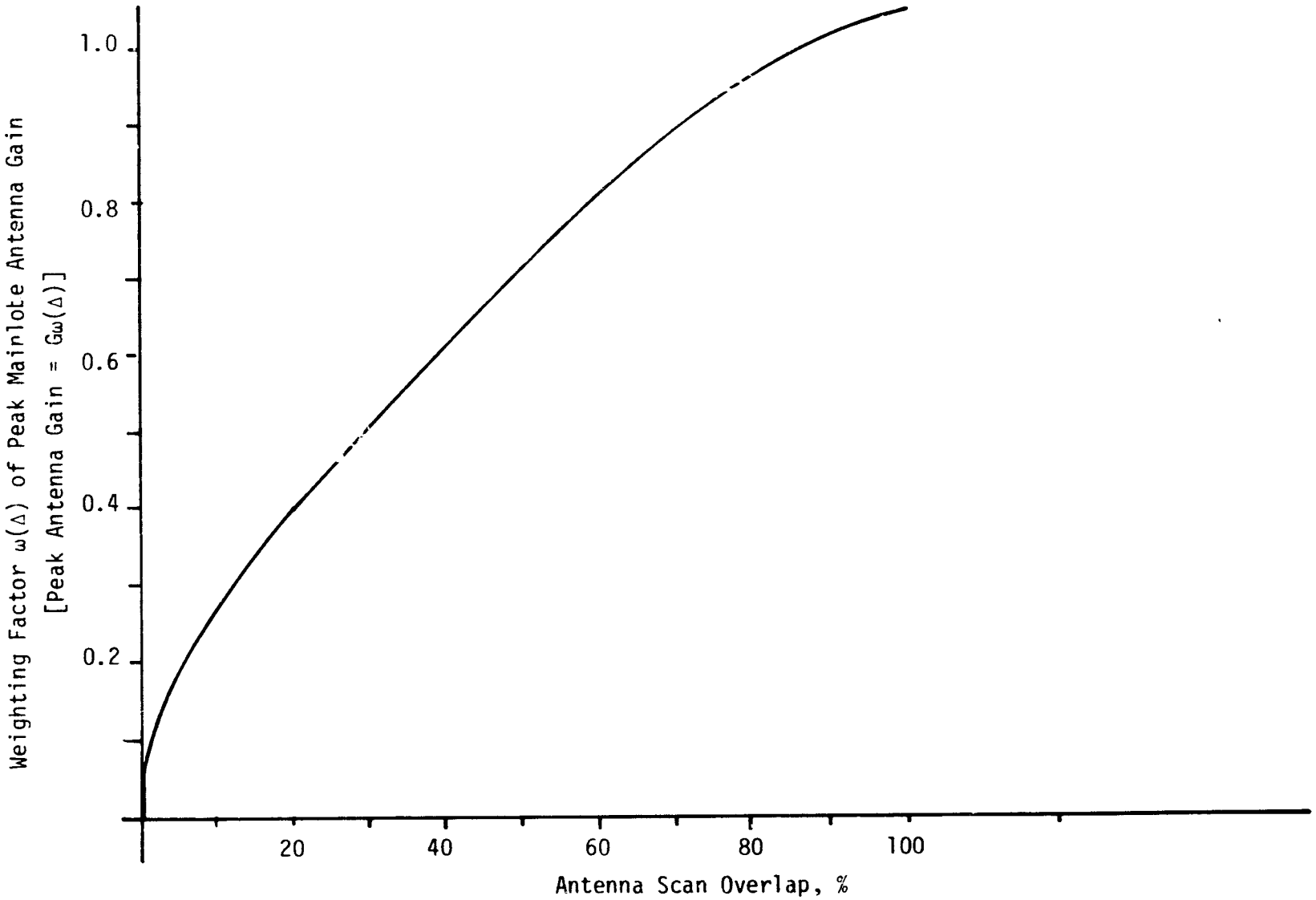

Figure 40. Weighting Factor of Peak Mainlobe Gain as a Function of Scan Overlap

5.2.4 Pulsewidth and Pulse Repetition Frequency (PRF)

The pulse duration, τ, of the RF pulse and the PRF are functions of the designated range to target in the Shuttle Ku-band radar. These signal parameters are summarized according to range in Table 3.

Table 3. Radar Pulsewidth and PRF as a Function of Target Range

Range to Target, nmi	τ(μsec)	PRF (Hz)
7.2 +	66.4	2987
3.8 - 7.2	33.2	6970
1.9 - 3.8	16.6	6970
0.95 - 1.9	8.3	6970
0.42 - 0.95	4.15	6970
- 0.42	0.122	6970

5.2.5 Calculation of Average SNR

The average SNR, including coherent integration, is found from the radar equation in the following form. The effects of the variable scan overlap are included implicitly via the target dwell time and the peak antenna gain loss, L_B.

$$\overline{SNR} = \frac{P_p \, \tau \, PRF \, t_d \, G^2 \, \lambda^2 \, \bar{\sigma}}{(4\pi)^3 \, R^4 \, kT_i \, LL_B} \tag{122}$$

where P_p = peak transmitter power = 60W

G = antenna gain = 38.5 dB

λ^2 = transmitted wavelength = 0.216 m

$\bar{\sigma}$ = average target cross section = 1 m^2

R = range to target

k = Boltzmann's constant = 1.38×10^{-23} J/°K

T_1 = system noise temperature = 1500°K

L = system losses = 13.88 dB

L_B = loss in peak antenna gain

and all other parameters were defined previously.

5.2.6 Probability of Target Detection

Frequency agility, using five RF frequencies, has been used in both the search and track modes of the radar to minimize target scintillation effects. Therefore, the target is modeled assuming Swerling II scintillation statistics, i.e., a fast fluctuating target. The single-scan probability of detection for this case is given by

$$P_{ss} = 1 - \int_0^{Y_b/(1+\overline{SNR})} \frac{x^{N-1} e^{-x}}{(N-1)!} dx \tag{123}$$

$$= 1 - I\left[\frac{Y_b}{\sqrt{N}\,(1+\overline{SNR})}, N-1\right] \tag{124}$$

where Y_b is the receiver bias level, N is the number of pulses integrated noncoherently and $I[\cdot]$ refers to the incomplete gamma function.

Radar performance is judged by the probability of detection over two scans. This cumulative probability can be approximated by

$$P_{cum} = 1 - (1 - P_{ss})^2 = 2P_{ss} - P_{ss}^2 \tag{125}$$

if it is assumed that the target range between scans has not changed appreciably. Figure 41 shows the cumulative P_d for different scan overlaps, measured with respect to the antenna 3 dB beamwidth. For example, $\Delta = 0.3$ means that the beam overlap is 30% higher than the half-power beamwidth point, with a probability of detection on one of two scans equal to 0.76 at 10 nmi.

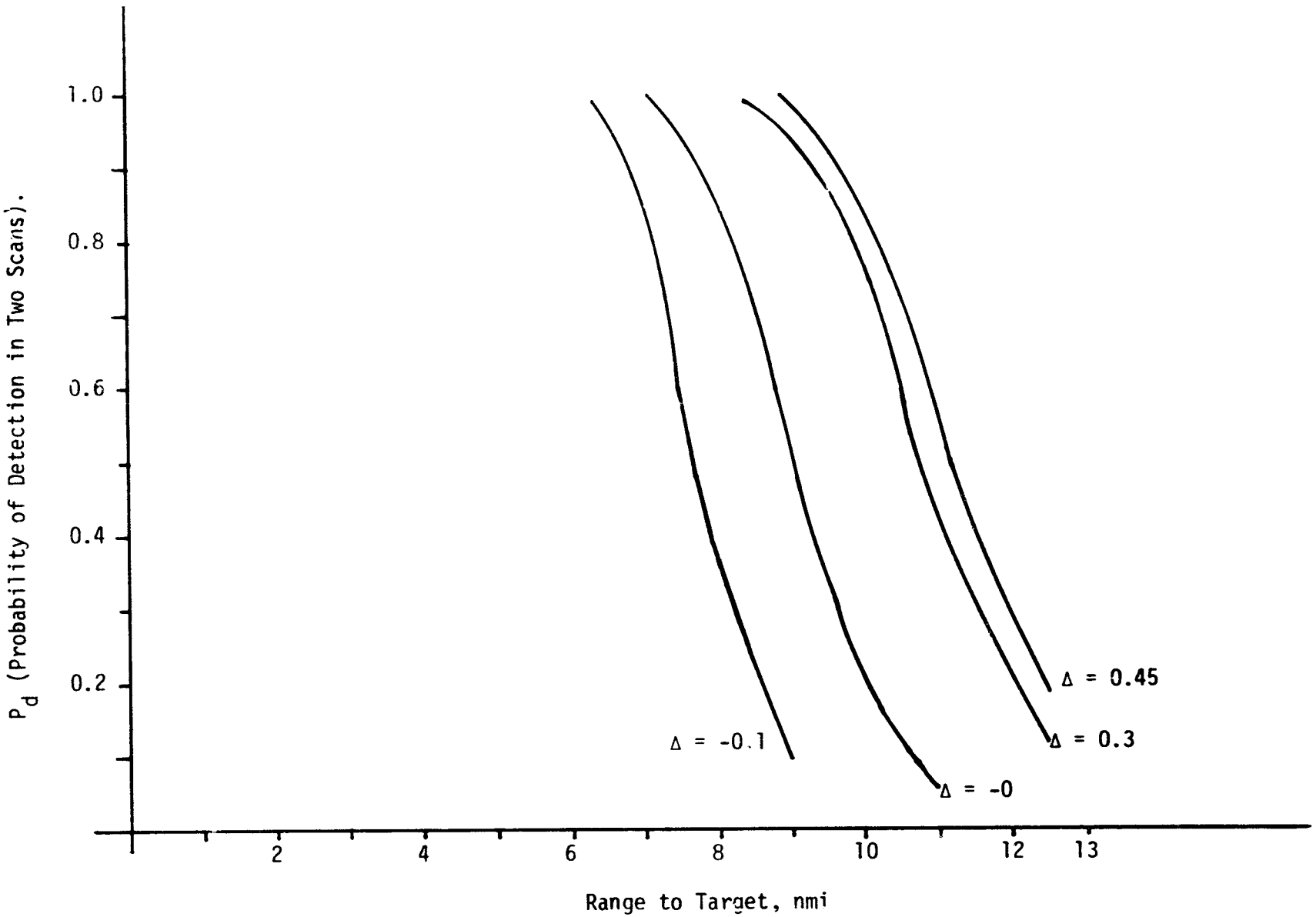

Figure 41. Probability of Target Detection, Servo Bandwidth = 2 Hz.

5.2.7 Conclusions

Maximum target energy is received when the antenna scan overlap is approximately 45% when measured with respect to the half-power beamwidth. This compares reasonably with the commonly accepted value of 30% when the approximate nature of the antenna mainlobe model is considered. Probability of detection decreases with lower values of scan overlap until zero detection is "achieved" with no overlap. These results should be considered when deciding which values of scan overlap are tolerable.

6.0 EVALUATION OF KU-BAND SPA AND EA-1 SOFTWARE

6.1 Introduction

This report covers Task No. 2 of Axiomatix contract number NAS 9-15795A. Task No. 2 is an evaluation of the Ku-band SPA and EA1 software. This report addresses the EA1 software only as no documentation has been made available by HAC on the SPA software. The intent of this task is to augment the HAC documentation and provide a clearer understanding of the software algorithms and programming techniques as well as provide recommendations for improved efficiency and reliability.

The initial phase of this effort entailed a detailed study of HAC documentation, primarily References 21 and 22. Additionally, Reference 23 was needed to correlate software input/output flags and commands with hardware response. Understanding of the software was hampered by the lack of a cross-reference listing of variables, particularly flags used to transfer status between software routines. As part of the task requirement to augment the HAC documentation as well as facilitate our own understanding of the software, a cross-reference table of inter-routine flags has been generated. After the familiarization phase, the software was examined for potential problem areas and possible sub-optimal coding techniques. A bug was discovered in the procedure termination routine and the technique used to store status flags is not as efficient as possible, from both the standpoints of memory usage and processing time. Self-test routines were examined with the intent of providing a more detailed description of MDM and D&C outputs.

6.1.1 Summary

A minor bug has been found in the procedure termination routine, SWTCH. The alpha and beta position loop integrators are not zeroed, as is claimed. Rather, they are loaded with hex 6060. The fix is to insert an LDI :00 after the LOADR S1, BINTGR+1 at location 0932.

In section 6.2, we have generated a cross-reference table of status flags. This should aid in tracing the functional activity of software modules, as a description of where a flag is used, set or reset indicates how routines interact. Reconfiguration is one of the more complex executive functions. An example of a reconfiguration is presented in section 6.3, with a block diagram to indicate the critical

paths. In section 6.4, we dissect the self-test tasks and include a series of tables which give the MDM outputs after each task as a function of pass or fail. These tables are more detailed than those in [22].

The techniques used to store flags and status information, e.g., storage of up to eight bits per word, requires that each access strip the flag from the word. This means that extra memory and time is required for each access. In section 6.5, we present an alterate technique for flag storage. Memory usage and processing time are not critical yet, but proposed changes to the software to accommodate feed-forward may require more stringent optimization.

6.2 Flag Cross-Reference Table

6.2.1 Introduction

Table 4 lists flags, or status bits, which carry information between software routines or between software and external hardware. The flags are listed alphabetically, followed by the module number, as defined in [21] and Table 5, and the section within a module where the flag is accessed. A letter following the module and section number indicates the action which is taken with the flag. A flag can be tested (T), set (S), reset (R) or toggled (X). A combination of letters indicates several actions being taken, in the order given. However, if a flag is acted upon several times within one module, only the first of each type is listed. For example, the entry

DETECT 12.6:S,R 20.1:T

indicates that DETECT is set and reset in module 12.6, the set status flag routine, and tested in module 20.1, the self-test task 7. Local flags, e.g., flags used within one routine, are not listed. Those flags which are set by hardware input or used to output status information are appended with the name of the appropriate input/output word. These names are indications of the function: OMDM1 is MDM output word 1, and PIW1 is parallel input word 1.

Table 4. Flag Cross-References

ACQEN	3.1:R,S
ACQINH	12.6:S,R 13.4:T
ANGTRK OIRAD1)	3.1:T 18.5:T 20.1:T
ASTOP	2.5:T,S,R 14.1:T
ATIME	2.1:T,S
ATTEN1 (POW5)	2.3:R 18.5:R 19.3:R 20.1:R 21.1:S
ATTEN2 (POW5)	2.3:R 18.5:R 19.3:R 20.1:R 21.1:R
AUTO (PIW1)	3.1:T, 5.1:T 12.3:T 12.6:T 13.1:T 13.4:T
BOOM (PIW4)	3.1:T
BSTOP	2.5:T,R,S 14.1:T
BTIME	2.5:T,S
COASTA (PIW2)	3.1:T 12.6:T
COMON (PIW4)	3.1:T 12.6:T
COMSTB (PIW4)	3.1:T 12.6:T
CTIME	2.3:R 16.2:R,T,S
DATAGO	12.6:S,R 13.1:T
DATAP (PIW2)	12.6:T 13.4:T
DATEST	2.3:R 13.1:T 18.1:R 21.1:S,T
DETECT	12.5:S,R 13.1:T 20.1:T
DOPOS	1.4:T 18.1:R 19.1:S,R 19.2:R,S 22.1:S,R
DOWN (PIW3)	15.1:T
DPLYF	1.2:T 14.1:R 15.3:S
DWELL	5.1:S,R 6.2:T
EAST (IMDM1)	3.1:T
EBW2	0.1:T 2.1:S 3.1:S
EBW3	0.1:T 2.1:S 3.1:S
EDW1	3.1:S,T
EDW2	2.3:T 3.1:S
EDW3	2.3:R 3.1:R,S,T
EVEODD	0.1:R,T 0.2:R 2.5:X 15.2:T
EVW1	0.1:T 0.2:S 2.1:S 3.1:S
E1TEST	2.3:R 13.1:T 18.1:R 21.1:S,T
E2TEST	2.3:R 13.1:T 18.1:R 21.1:S,T
FAST (PIW3)	15.1:T
FSTSLO	3.1:T 12.0:T 13.4:T 15.1:S,R

Table 4. Flag Cross-References (Cont'd)

GAIN3	12.1:R,S
GPCACQ (PIW1)	3.1:T 7.2:T 12.3:T 12.6:T 13.1:T 13.4:T
GPCDES (PIW1)	1.2:S 3.1:T 7.2:T 12.3:T 12.6:T 13.1:T 13.4:T
GPCLS	12.3:T
INCDEC	5.1:R,T,S 6.1:T
INIT	0.2:S 2.1:S,R 3.1:T
INSTAB	1.2:R 2.3:R 7.1:T 7.4:T 12.3:R 19.1:R 19.2:R
KOUNTL	5.1:S,T
LAMP	18.1:R 21.1:S 21.3:T
LATCH (PIW2)	3.1:T,R 12.5:R
LEFT (PIW3)	15.1:T
LINEAR (POW1)	12.5:R,S
MAIN	13.4:R,T
MAMINI	5.1:T,S,R 13.4:T
MANUAL (PIW1)	2.6:T
MCOMP	2.3:R
MFIRST	1.4:T 2.1:T,S 3.1:R,S 5.1:T 14.1:T 15.1:T 16.2:T
MINIST	0.8:T 2.3:R 3.1:S 5.1:T,R
MINI2 (IRAD2)	5.1:T
MODE	0.2:S 2.1:T 3.1:T,S
MOTON (POW4)	2.2:R 2.3:S 14.1.S,R 19.3:R 20.1:R
NEWA (PIW4)	13.1:T 14.1:T
NEWB (PIW4)	13.1:T 14.1:T
NEWMDM (PIW1)	0.1:T 0.3:T 0.4:T 3.1:T 7.1:T
OPER (PIW2)	13.1:T 19.3:T
OUTFLG	1.4:T,R 2.3:R 18.1:S 18.4:S 18.5:S 19.1:S 19.2:S 19.3:S 20.1:S 21.1:S
PFLAG	7.1:R,S 7.2:T 7.3:T,S
PNTTRK	2.1:S 3.1:S,R
PSON (POW1)	2.1:S 3.1:R
PTIME	2.3:R 3.1:T,S
RADACT (PIW1)	12.5:T 13.4:T
RADCOM	1.1:T 3.1:T 5.1:T 12.5:T 12.6:S,R,T 13.1:T 13.3:T 13.4:T 16.2:T
RADON (PIW1)	3.1:T 12.6:T

Table 4. Flag Cross-References (Cont'd)

RADSTB (PIW4)	3.1:T 12.6:T
RDETCT (IRAD2)	12.6:T
RGOOD (IRAD1)	13.1:T 18.5:T,S 19.3:R 20.1:T 22.1:R
RIGHT (PIW3)	15.1:T
ROPER (IRAD1)	18.4:T
RRGOOD (IRAD1)	13.1:T 18.5:T,S 19.3:R 20.1:T 22.1:R
RTRACK (IRAD2)	12.6:T
SCANNG	2.3:R 3.1:T 5.1:T,S,R 13.1:T 13.4:T 21.3:S
SCANRC	5.1:T,R,S 6.2:T
SCWARN	2.4:R 4.2:R,S 13.1:T 21.3:S
SELF	2.3:R 13.1:T 18.1:S
SIGEN (POW5)	2.3:R 18.2:S 18.5:S 19.3:R 20.1:S 21.1:S
SIGNAL	12.6:R,S,T 13.4:T
SIGPC (IMDM1)	3.1:T
SIMAN (PIW2)	3.1:T
SKEY (PIW3)	11.6:T 15.3:T
SLEINT	15.1:S 15.2:T,R
SLEWNG	2.3:R 3.1:T 7.1:T 12.3:T 12.6:T 13.4:T 15.1:S,T,R
SLOW (PIW3)	15.1:T
STCON1 (POW5)	2.3:R 18.5:R 19.3:S 20.1:R 21.1:R,S
STCON2 (POW5)	2.3:R 18.5:S,R 19.3:S 20.1:S 21.1:S,R
STCON3 (POW5)	2.3:R 18.5:S 19.3:S 20.1:S 21.1:S
STCON4 (POW5)	2.3:R 18.5:R 19.3:R 20.1:R 21.1:R
STEST (IMDM1)	3.1:T
STON (POW5)	2.3:R 18.5:S 19.3:S 20.1:S 21.1:S
STOWM (POW3)	2.1:R 14.1:R,S
STUNST	3.1:S,R 14.1:T
STWAIT	2.3:R 18.1:S 18.S:T 18.5:S 19.1:S 19.2:S 19.3:S 20.1:S 21.1:S 22.1:R
SYSTST	2.3:R 13.1:T 18.1:R 21.1:S
TARGET	2.3:R 18.4:T 18.1:S 19.3:R 20.1:S,R
TDEAST	3.1:T,S,R 13.1:T 13.4:T
TDWEST	3.1:R,T,S 13.1:T 13.4:T
TIMOUT	2.3:R 3.1:T,S,R 5.1:T

Table 4. Flag Cross-References (Cont'd)

TRACK	12.6:S,R 13.1:T 20.1:T 21.1:T 21.3:S
TRKING	2.3:R 3.1:T 12.6:T 16.2:S
UNLOCK (POW3)	14.1:S 15.3:R
UNSTOD	3.1:T 14.1:T
UP (PIW3)	15.1:T
WAITF	0.1:T,R 0.2:S 2.5:S
WEST (IMDM1)	3.1:T
XMIT (PIW4)	3.1:T
ZERDIS	2.1:S 2.2:S 2.3:R 13.1:T
ZONEI	3.1:T 5.1:R 7.2:S,R 12.3:T 15.3:T 19.1:R,T 19.2:R,T 22.1:R
ZONEO	3.1:T 7.2:S,R 12.6:T 15.3:R,S

Table 5. Software Module Index

0.1	INTERRUPT/EXEC RTN
0.2	POWER UP RTN
0.3	INITIALIZE PROC
0.4	POINT PROC
0.5	IDLE PROC
0.6	PROC TERM PROC
0.7	SLEW PROC
0.8	SCAN PROC
1.1	TRACK PROC
1.2	DEPLOY PROC
1.3	RECOVER PROC
1.4	SELF TEST PROC
2.1	INITIALIZE ROUTINE
2.2	IDLE ROUTINE
2.3	PROC TERM ROUTINE
2.4	OUTPUT STATUS ROUTINE
2.5	WAIT ROUTINE
3.1	CONFIGURE ROUTINE
4.1	ANGLE RATE XFORM
4.2	OBSCURATION CALC
5.1	SCAN1 ROUTINE
6.1	SCAN2 ROUTINE
6.2	SCAN3 ROUTINE
6.3	SCAN4 ROUTINE
7.1	POSITION LOOP, MOD1
7.2	POSITION LOOP, MOD2
7.3	POSITION LOOP, MOD3
7.4	POSITION LOOP, MOD4
11.6	SHORT SHUTTLE TO GIMBAL TRANSFORM
12.1	ENCODER ROUTINE
12.2	ANALOG ROUTINE
12.3	INERT ROUTINE
12.4	INPUT DISCRETE ROUTINE
12.5	OUTPUT DISCRETE ROUTINE
12.6	SET STATUS FLAGS ROUTINE
13.1	MDM/D&C OUTPUT ROUTINE
13.3	INPUT LRU SERIAL ROUTINE
13.4	OUTPUT LRU SERIAL ROUTINE
14.1	DEPLOY ROUTINE
15.1	SLEW GENERATION ROUTINE
15.2	SLEW INTERPOLATION ROUTINE
15.3	DEPLOY ROUTINE

Table 5. Software Module Index (Cont'd)

16.2	TRACK ROUTINE
18.1	SELF TEST INITIALIZATION ROUTINE
18.2	SELF TEST SEQUENCER
18.3	SELF TEST TASK2 CPU
18.4	SELF TEST TASK3 POWER FORM
18.5	SELF TEST TASK8 ANGLE TRACK
19.1	SELF TEST TASK4 INITIALIZE ANTENNA
19.2	SELF TEST TASK5 ANTENNA SERVO
19.3	SELF TEST TASK6 TRANSMITTER POWER CHECK
20.1	SELF TEST TASK7 RANGE AND RANGE RATE CHECK
21.1	SELF TEST TASK9 RECEIVER SENSITIVITY CHECK
21.2	SELF TEST TASK10 COMPILE TEST RESULTS
21.3	SELF TEST TASK11 LAMP TEST
22.1	SELF TEST PAUSE ROUTINE

6.3 Example of Reconfiguration

6.3.1 Introduction

In order to facilitate an understanding of the software and to bridge the gap between the HAC-supplied listing and block diagrams, a hybrid block diagram, Figure 42, was generated to provide an example of a reconfiguration. Reconfiguration is probably the most complex of the executive functions, and an understanding of this function will aid in understanding the executive structure.

For purposes of the example, a reconfiguration from IDLE to SELF TEST is illustrated. Four interrupt cycles are covered which demonstrate the function of the termination procedure and the initialization routine for self-test. Each interrupt cycle is a separate diagram. Each block is labeled with the absolute hexadecimal address of the routine in ROM and contains descriptive text as to the function to be performed. Action on variables or flags is underlined in the blocks. Blocks are grouped within modules in order to ease cross-referencing with the software listing.

6.3.2 Description of Reconfiguration

Initially, in the IDLE routine, executive data word 1 equals MIDLE (=2), executive branch word 1 (EBW1) = 12, EBW2 = 15 and EBW3 = 18. The latter are the absolute memory locations of the long branches to the 0.1-second sequence, the even and odd sequences of the idle procedure. The 0.1-second sequence tests the even/odd flag, EVEODD, branches to EVEN, executes INDIS (input discrete), executes MSDIN (input MDM), then executes CONF, the configure routine on module 3. The configure routine tests the status flags, notes that STEST is set, and sets EDW1 = MSELF. Configure then notes that MODE is not equal to EDW1; hence, a new procedure is to be initiated. Since the current mode is not the termination procedure, MODE and EDW4 are set to 8 to indicate that the termination procedure is to be executed, MFIRST is set to 3 for the first pass through and EBW1 is set to 51, EBW2 to 54 and EBW3 to 57.

After configure, the executive takes the even leg of the procedure, which is now the termination procedure, MTRM2. This procedure executes TRS2G, the Shuttle-to-gimbal transform, then executes the

termination routine, MTERMR, which sets EDW3 equal to 0, and returns to the procedure. The termination procedure outputs discrete data, then executes WAIT, which toggles the even/odd flag to odd and idles for the next interrupt.

During the next interrupt, the executive branches to the termination procedure odd leg, which executes TRG2S, transform gimbal-to-Shuttle, executes MSDOUT, MDM output, and finally executes WAIT, which toggles the even/odd flag back to even.

During the third interrupt, the self-test procedure is executed for the first time. Configure tests EDW1 and MODE for equality. Since they are not equal and the current MODE is 8, the termination procedure, configure again sets MFIRST, the first pass flag, to 1 and configures for self-test by setting the executive branch words. Upon return to the executive, a long branch to the even leg of the self-test procedure is executed. The self-test initialization is rather busy. With MFIRST equal to 1, STST2 executes self-test initialization, STINIT, which does a long branch to BEGIN. Various flags and buffers are initialized, including the step counter, STPCNT, and LAMP. BEGIN returns to the self-test procedure which inputs LRU serial data, then executes the self-test task sequences. With STWAIT equal to 1 and STPCNT equal to 0, a ten-second pause is initiated and WAIT is executed.

Finally, the fourth interrupt results in the execution of the odd leg of the self-test procedure. After the gimbal-to-Shuttle transform, task 11 is executed. Since LAMP was initialized to 0, the D&C lamps are not lit. Task 11 returns to the odd leg of the self-test procedure, which outputs discrete, outputs LRU serial, and outputs MDM data since OUTFLG was set to 1 by STINIT. WAIT is executed and the even/odd cycle repeats. A more detailed discussion of the self-test routines is covered in the next section.

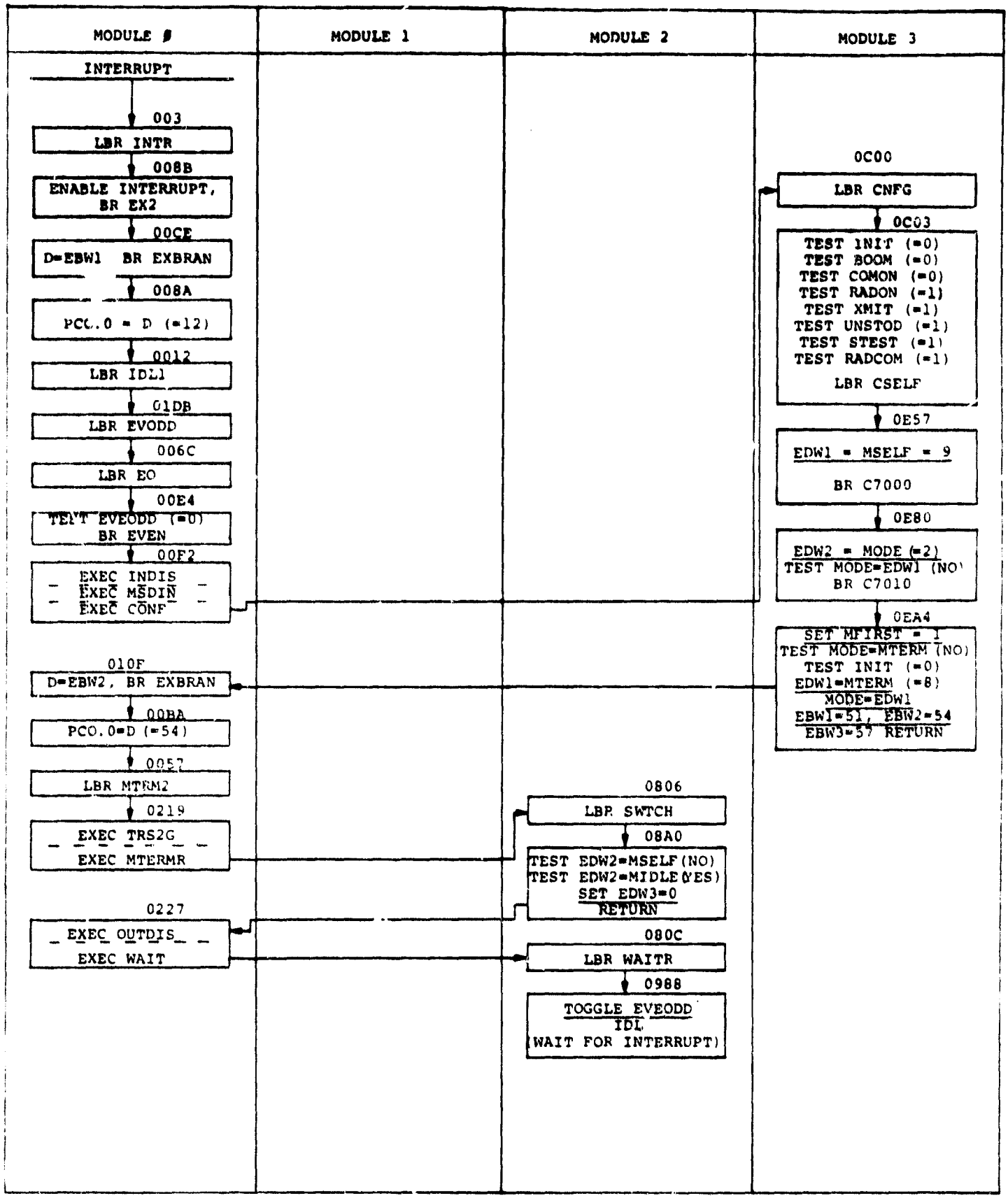

INITIAL CONDITIONS: EDW1 = MIDLE = MODE = EDW2 = 2,
EBW1 = 12, EBW2 = 15, EBW3 = 18
EVEODD = Ø (EVEN)

Figure 42. 0.1-Second Interrupt; Configure from Idle to Self-Test

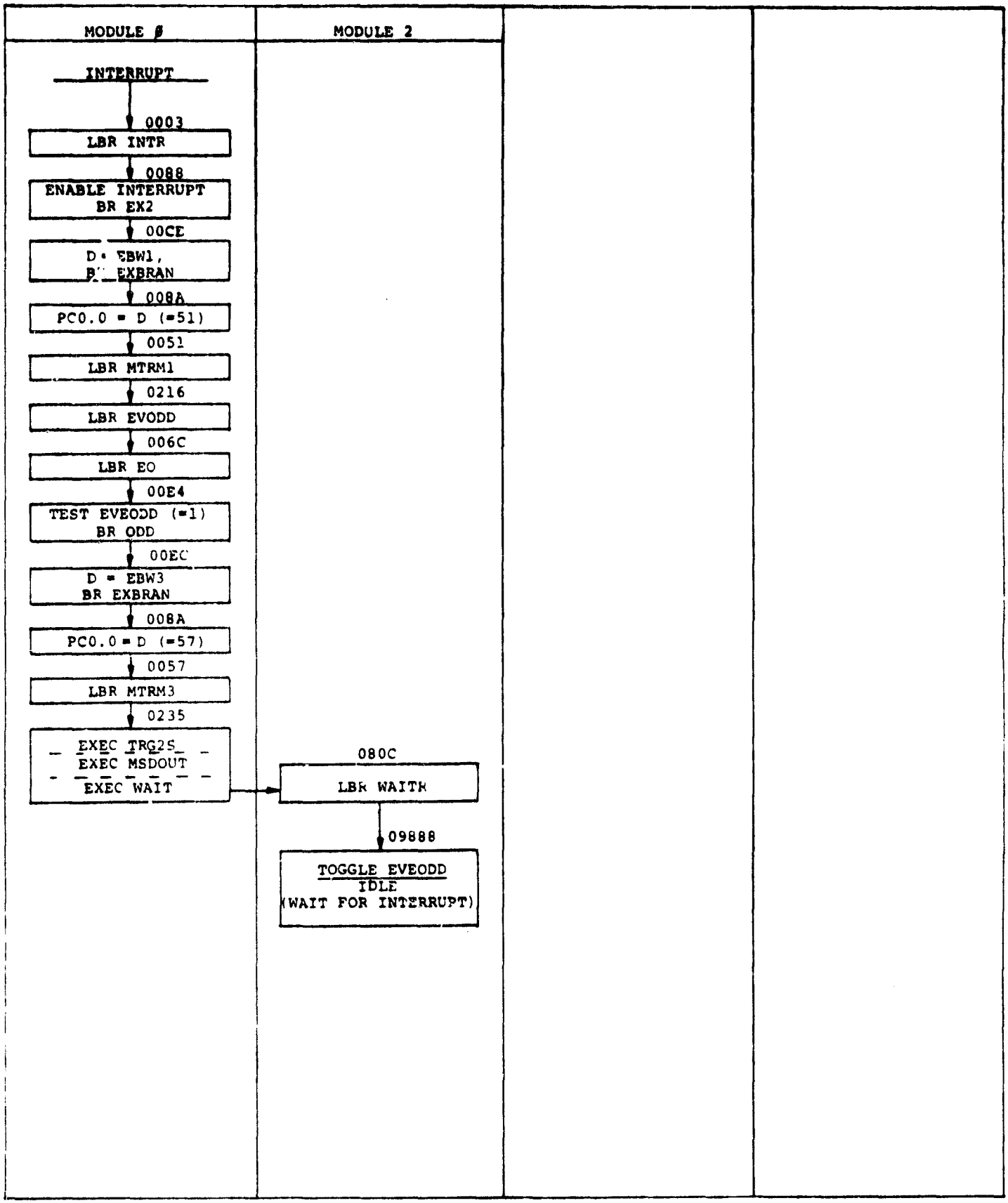

Figure 42. (Cont'd)

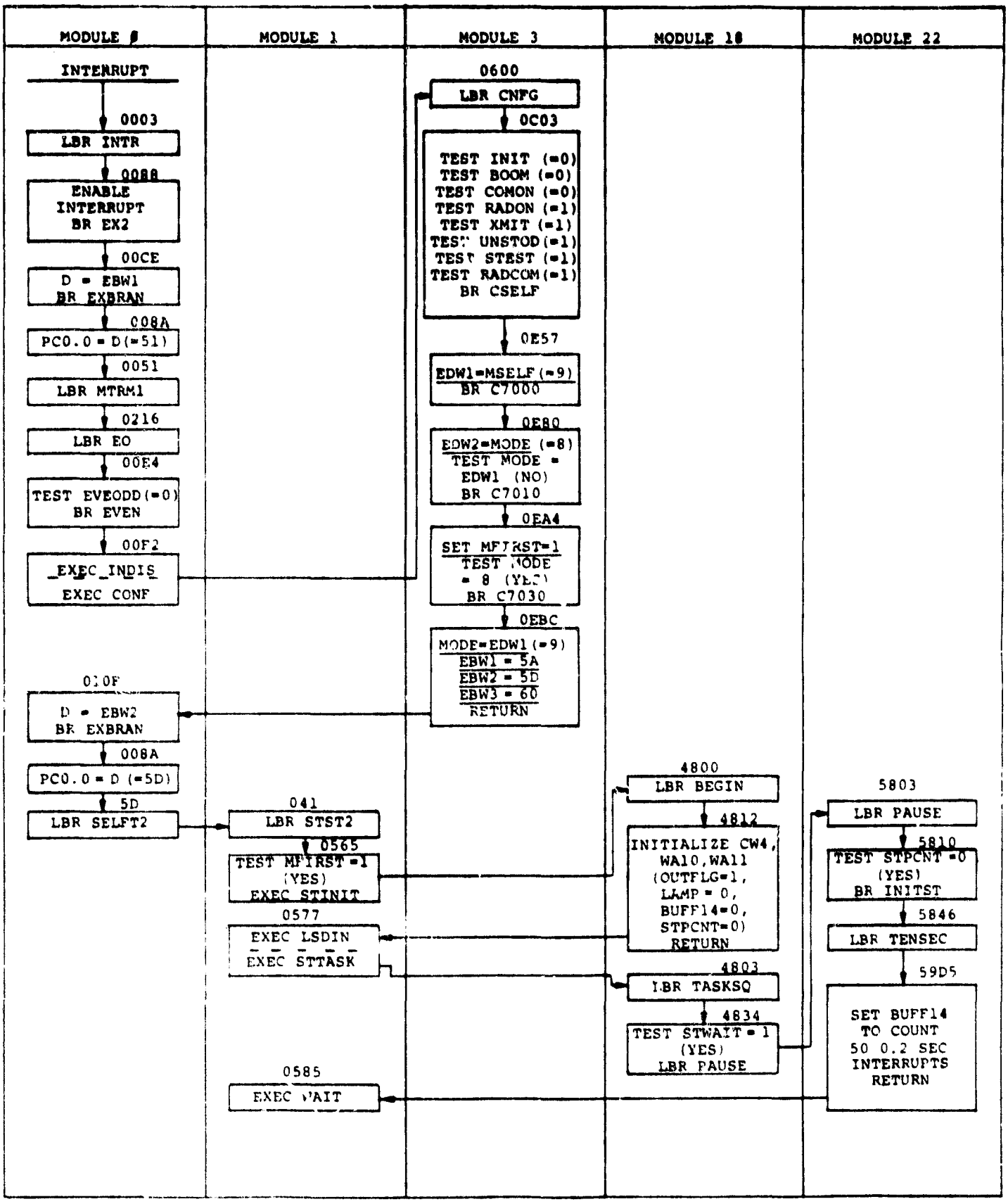

Figure 42. (Cont'd)

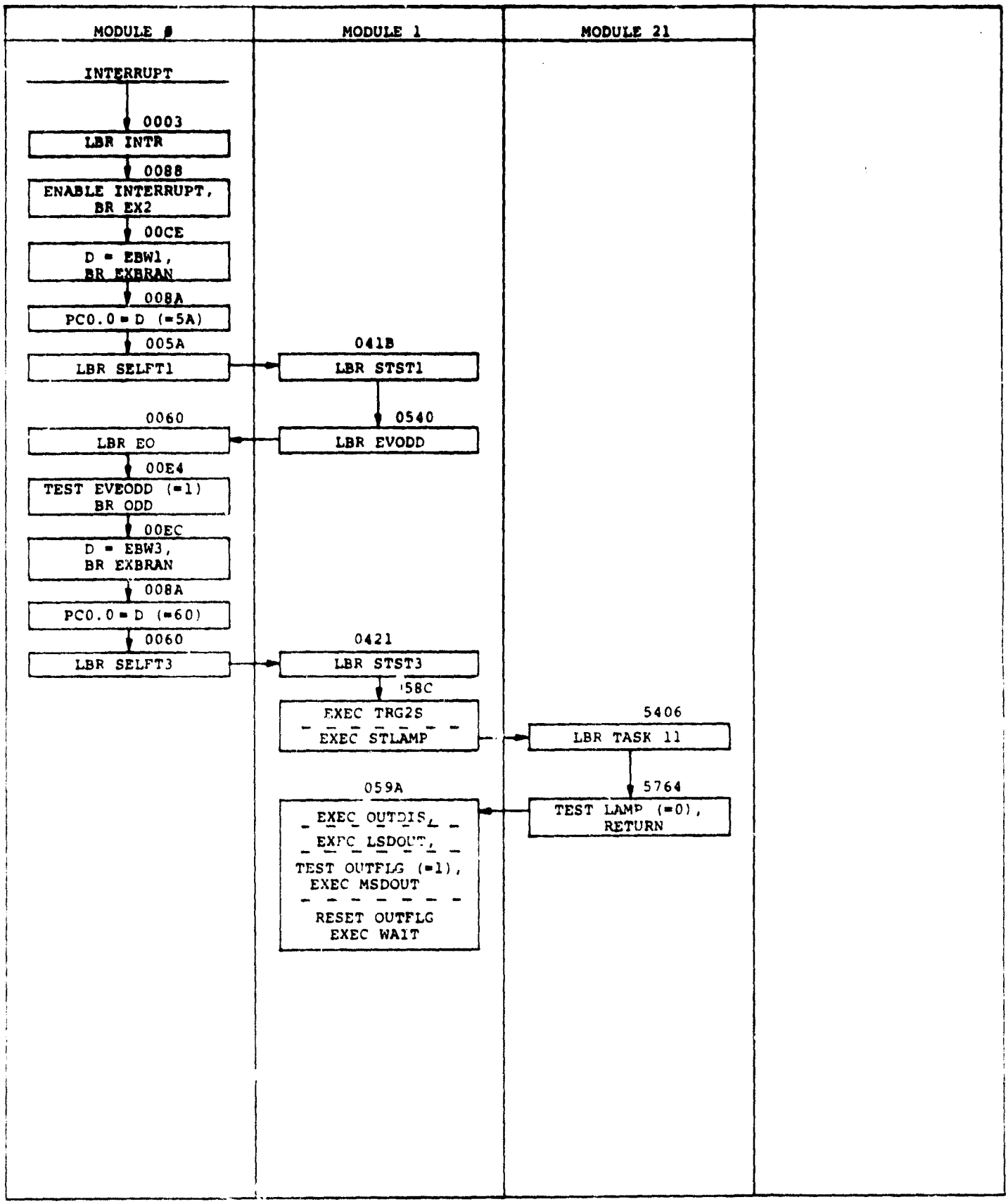

Figure 42. (Cont'd)

6.4 Self-Test Tasks

6.4.1 Introduction

Operation of the self-test portion of the EA-1 software is examined with emphasis on the outputs generated at the completion of each self-test task. The intent is to provide a reference to augment the HAC description of the outputs, as well as a guide to modification of the software, should it be considered desirable to change the output format. As an example, the present implementation does not provide an unambiguous indication as to which task is currently in progress during self-test. This would be changed by modification of a few memory locations, as described in subsequent paragraphs.

Self-test tasks are discussed in chronological order, with key routines and parameters referenced to their absolute memory locations. MDM outputs are summarized at the conclusion of this section in Tables 7 through 14.

The self-test routines make extensive use of macros specific to self-test. These macros are explicitly defined in the self-test portion of [21]. Macro CONFIG A,B loads parallel input word one (PIW1), bits 4 through 8, with the value A and bits 1 through 5 and 7 with the value B. Macro RANG A,B,C loads values A,B,C into EA2 serial input words IRAD3, IRAD4 and IRAD5. Similarly, RANGRT A,B loads A and B into IRAD6 and IRAD7. These two macros allow the software to output specified values of the range and range rate to the MDM's and D&C using the MDM output routine, MDMO (340F), which transfers data from the EA2 input to the MDM and D&C output registers. ANGRTE A,B,C,D transfers the specified data to the MDM output registers OMDM17 through OMDM20 in order to force display of angle rates. Macro POSIT A,B,C,D stores the data A-D in IMDM3 through IMDM6, the MDM input registers. This allows the software to position the antenna to roll specified by A,B and pitch specified by C and D, overriding angle designates read in from the MDM's. Macro DAVOLT A,B outputs A and B to the digital-to-analog converter. This voltage is used by the self-test multiplexer/comparator to determine if specified signals exceed the voltage threshold. Macro ANDATA A,B,C,D is similar in that it loads A and B into the analog output registers ADAM and ADAL for setting the alpha axis rates and C and D into BDAM and BDAL to set the beta axis rates. Actual output is done using the subroutine ANALOG, also called SERVO, at location 3084.

The self-test MUX selects one of four analog inputs, as defined in Table 6, and compares the voltage with the output of the alpha axis rate D/A converter. During this test, the motors are turned off. The difference of the two analog voltages is sent to the processors event flag, EF3, for test.

In general terms, each self-test task uses a sequence counter, SEQUEN, zeroed by the previous task, to govern which phase of the task to execute. Typically, with SEQUEN equal to 0, the task initializes itself and sets a flag, STWAIT, to pause 10 seconds for display of MDM and D&C output from the last sequence of the prior task.

All self-test tasks, with the exception of the lamp test, are executed during the even cycle of the self-test procedure. The first pass through the self-test procedure (MFIRST = 1) will result in the execution of the initialization routine. This is entered via

```
0570              EXEC      PC1,STINIT
4800              LBR       BEGIN
4812     BEGIN    LOADR     IOP,CW4 .
```

BEGIN, the initialization routine for the self-test procedure, resets RAM WA10, WA11 and sets various flags:

```
SELF = 1          indicate in self-test
TARGET = 1        turn on test target
DATEST = 0        reset status flags
E2TEST = 0
E1TEST = 0
SYSTST = 0
STWAIT = 1        set for 10-sec pause
OUTFLG = 1        set to output MDM.
```

The self-test task sequencer, TASKSQ, uses the variable STPCNT to control the sequence of self-test routines. STPCNT is reset to 0 by virtue of being located in WA10. BEGIN returns to the self-test procedure via SET PCØ.

The self-test tasks are entered via

```
057E              EXEC      PC1,STTASK
4803              LBR       TASKSQ
4834     TASKSQ   SETT      IOP,SIGEN.
```

Initially, with STWAIT set, TASKSQ branches to PAUSE, which implements a 10-sec wait. At the conclusion of 10 seconds, PAUSE resets STWAIT to enable the first self-test routine. During the final pass through PAUSE,

Table 6. Self-Test MUX Control

Function	STCON1	STCON2	STCON3
BETA ERROR	0	0	1
SIGNAL STRENGTH	0	1	1
ALPHA ERROR	1	0	1
XMIT RF POWER	1	1	1

STPCNT is tested and the routine branches to INITST (location 5846), which initializes the MDM output. Data-good flags are reset and MDM words are set as follows:

RANG	(range) set to all 1's
RANGRT	(range rate) set to all 1's
ANGRTE	(angle rate) set to 0's.

Values of the angles are not modified by INITST.

During the first pass through the odd leg of the self-test procedure, MDM output is initiated since OUTFLG had been initialized to 1.

6.4.2 Tasks 1 and 2

At the conclusion of the first 10-sec pause, TASKSQ tests STPCNT (=0) and branches to TSKCPU,

```
484E              LBZ       TSKCPU
5800              LBR       TASK1
5806     TASK1    LOADR     TO,STPCNT
```

Task 1, the CPU self-test, has been eliminated. The net effect of TASK1 is to set STPCNT equal to 1 and return. Thus, during the next pass through the even leg of the self-test procedure, TASKSQ will branch to TSKPCS, the PROM self-test,

```
4854              LBA       TSKPCS
4809              LBR       TASK2
489C     TASK2    LOADRS    IOP,SEQUEN.
```

At the conclusion of the PROM test, the PROM check sum flag is set and STPCNT is set to 2 (task 3) if the test is successful. Otherwise, the flag is reset, STPCNT is set to go to task 10, and self-test will be prematurely terminated. New MDM output is not initiated after PROM test.

6.4.3 Task 3

During the next pass through the even leg of the self-test procedure, the EA2 power form task is executed:

```
484A              LBA       TSKPFC
480C              LBR       TASK3
4914     TASK3    LOADRS    IOP,IRAD1
```

Task 3 first resets the four data-good flags, sets range and range rate to all 1's and sets the angle rates to 0. MDM output is not conditioned

on the results of the power form test. The radar operate bit from the EA2 is tested and, if true, PFC flag is set to 80. STPCNT is set to 3 for task 4, OUTFLG is set to initiate MDM output, and control is returned to the even leg of the self-test procedure. MDM (and D&C) data will be output during the next pass through the odd leg of the self-test procedure. However, STWAIT has not yet been set, and the first pass through Task 4 will be executed without undergoing a 10-sec pause.

6.4.4 Task 4

The first pass through Task 4, which initializes the antenna to zenith, again resets the data-good flags, sets range and range rates to all 1's and the angle rates to 0's. Mode is set to GPC designate. SEQUEN is tested to determine if this is the first or a subsequent pass. SEQUEN is 0 during the first pass, having been cleared as part of work area 10 (WA10+17). STWAIT is set to enable the 10-sec pause and control is returned to the self-test procedure. After the first pass through Task 4, the task sequencer will branch to PAUSE, which tests STPCNT to determine the current task. STPCNT is 3, which causes PAUSE to branch to ZEN1 (5883). Using the POSIT macro, ZEN1 loads 0's into the angle designates IMDM3 through IMDM4 and branches to POSLOP (5983). POSLOP sets the position loop flag, DOPOS, and starts the 10-sec pause. With DOPOS set, the position loop routine is executed every 100 ms prior to executing either the even or odd leg of the self-test procedure. At the conclusion of the 10-sec pause, DOPOS is reset, as is the ZONEI inner zone flag.

During the second and subsequent calls to Task 4, SEQUEN is set and TASK4 branches to DES (4C7B). DES again sets the angle designates to 0, tests ZONEI to determine if the antenna is within 0.3° of the designate and sets the position loop flag. BUFF5, initially cleared as part of work area 10, is tested for excessive time to reach zenith. Ten seconds after the end of the 10-sec pause are allowed for the antenna to reach zenith. If the limits are exceeded, DES branches to ABORT (4CD0), which sets STPCNT to skip Tasks 5 and 6 and sets OUTFLG to initiate MDM output. Measured pitch and roll angles are stored in the MDM and D&C output words, OMDM5 through OMDM8, and ODC1 through ODC6, by the gimbal-to-Shuttle transform routine G2S1 (2C0C), executed prior to MDM

output. If the antenna is successfully positioned at zenith, DES branches to READY (4CAA), which resets the position loop flag. The ZONEI inner zone flag, the sequence counter SEQUEN, sets STPCNT for Task 5 and sets OUTFLG for MDM output. In either case, no flag is set to indicate the results of Task 4. However, if Task 4 fails and Tasks 5 and 6 are not executed, ASD and TPLF will be 0 since they are in WA11 and an EA1 or DA error will be indicated. ASD (WA11+4) is set by Task 5 and TPLF (WA11+5) is set by Task 6.

6.4.5 Task 5

Task 5 (4CDE) tests the ability of the servos to point the antenna to designated positions within a specified time. This task is divided into four sequences--0 through 3. Sequence 0 is initialization, sequence 1 points to pitch = 30°, roll = 0°; sequence 2 points to pitch = 30°, roll = -30°; and sequence 3 points back to zenith. There are three possible results of the Task 5 tests: unconditional pass if the antenna reaches designate within 7 sec, conditional failure if it reaches designate within 7 to 10 sec in pitch or roll, and unconditional failure if it fails to reach designate within 10 sec. During sequence 0, STWAIT is set for the 10-sec pause and the sequence number is set to 1. The 10-sec pause routine tests STPCNT (4) and branches to ANT (5899), which tests the sequence number, SEQUEN. With SEQUEN equal to 1, ANT branches to ZEN1 (5883), which positions the antenna to zenith prior to the pitch test. If the test passes or fails conditionally at the conclusion of sequence 1, pitch output should read 30° and roll 0°. If the test fails unconditionally, Task 5 is terminated, STPCNT is set to go to Task 7, OUTFLG is set to initiate MDM output, but STWAIT is not set for the 10-sec pause--this is set in sequence 0 of Task 7. The 10-sec pause prior to the roll test (Task 2) designates the antenna to the pitch position attained in Task 1 and the 10-sec pause prior to the zenith test (Task 3) designates the antenna to the roll position from Task 2. As in sequence 1, the designate positions are read out during the 10-sec pause following sequences 2 and 3.

6.4.6 Task 6

Task 6 (4EAC), the transmitter power level test, consists of three sequences. The first is initialization, the second tests the DA operate bit, and the third verifies that the transmitted power exceeds threshold. The initialization sequence sets the range and range rate to all 1's and the angle rate to all 0's, as well as resetting the data-good flags, as in prior tasks. Estimated range is set to 10,250 ft in IMDM7 through IMDM10 (6167-616A) for output to the EA2. STWAIT is set for the 10-sec pause, which again sets an estimated range of 10,250 ft. After the first 10-sec pause, Task 6 branches to CHKOPB (4F41), which tests the DA operate bit. The logic of the DA operate bit is depicted in Figure 43. If the operate bit is true, bit 8 of TPLP (61E5) is set. The transmitter is enabled by the commands:

```
4F4F            RESETS     IOP,SIGEN
4F58            RESETS     IOP,ATTEN1
4F61            RESETS     IOP,ATTEN2.
```

Transmitter power level is selected by the following commands:

```
4F6A            SETS       IOP,STCON1
4F71            SETS       IOP,STCON2
4F78            SETS       IOP,STCON3.
```

Comparator voltage threshold is set by the macro:

```
4F8F            DAVOLT     TRP1,TRP2 .
```

OUTFLG is set, STWAIT is set and control is returned to the even leg of the self-test procedure. The MDM output, pass or fail, will be the same as sequence 3 of Task 5--range and range rate all 1's, angle rate all 0's, pitch and roll 0's. After the second 10-sec pause, TASK6 branches to CHKVLT (4FBA), which tests the status of external flag 3, EF3, which will be true if the transmit power exceeds threshold. OUTFLG is set and MDM output will remain the same as sequence 1, whether the test passes or fails. STPCNT is set to 6 for task 7 and OUTLFG is set for MDM output.

6.4.7 Task 7

Task 7 consists of four sequences: initialization, radar active, test target off, and radar passive. During the initialization sequence, mode is set to manual by the macro

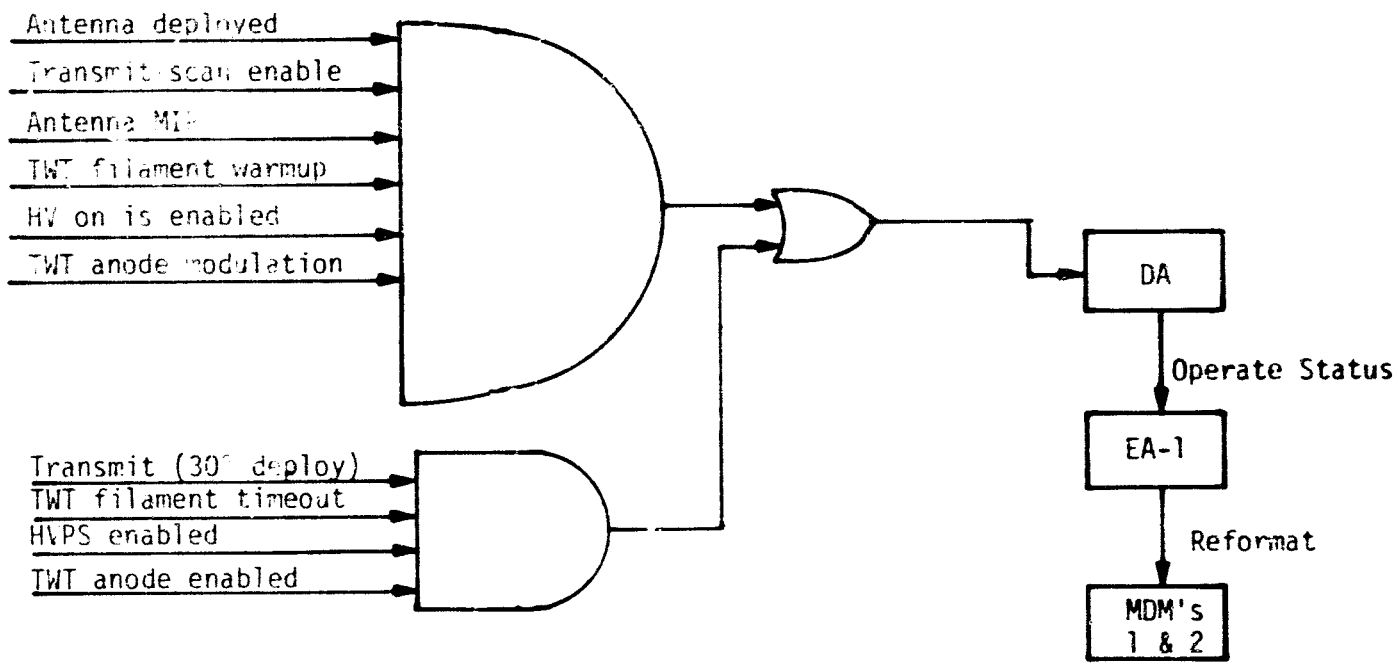

Figure 43. Operate Signal Logic Diagram

500C TASK7 CONFIG :88,:40.

Angle and angle rate flags are cleared, estimated range of 10,250 ft is stored in the MDM input buffer, and TARGET is set. The TARGET flag is sent to the EA2 during LRU serial output to turn on the test target. POW5 is set to 8D, which sets the test dipole to -17.5 dBm. SEQUEN is set to 1, gimbal motors are turned off, and STWAIT is set to provide the 10-sec wait for display of Task 6 results. The pause routine branches to RRWAIT (58DC), which again sets the estimated range to 10,250 ft and configures the system to manual-active mode. After the first 10-sec pause, TASK7 branches to ACTIVE (507A). Bit 8 of ACTFLG (61E6) is set if the track status flag is true and bit 7 is set if the angle track flag is false. ACTIVE then executes a call to RNGACT (5295) to test if the measured range is within limits. The range limits are 5570 and 5070 ft. A 1 is returned in BUFF7 if range is within limits. ACTIVE in turn sets bit 6 of ACTFLG if the range is valid and sets bit 5 if the range-good flag, RGOOD, is true. ACTIVE then calls RRATE (52C2) to determine whether or not the range rate data is within limits of ±3 ft/s. If the high-order bits of range rate (1RAD6) are 0, 3 ft/s (3C) is subtracted from the low-order bits. A negative or 0 result indicates that range rate is less than 3 ft/s. Conversely, if the high-order bits are all 1's, -3 ft/s is subtracted from the low-order bits. A negative result indicates that the velocity is greater in magnitude than the limit. Passing the limit test results in bit 4 of ACTFLG being set, and bit 3 is set if RRGOOD, the range rate good status flag, is true. Signal strength from the test target is compared with thresholds S1 and S2. If greater than S1, bit 2 of ACTFLG is set and, if less than S2, bit 1 is set. The test target is turned off and OUTFLG and STWAIT are set. Note that output to the MDM and D&C will reflect the actual range and range rate computed by the EA2, as well as the state of the data-good flags. That is, the range and range rate flags will be 1 unless the test fails. Pitch and roll will be 0° if Tasks 5 and 6 are successful. Otherwise, pitch and roll will reflect the actual pitch and roll as computed by the gimbal-to-Shuttle routine, reflecting the measured gimbal angles. Angle rates will be 0 since they had been set to 0 by previous routines and the angle rate routine has not been called.

The third phase of Task 7, sequence 2, tests the detect and track flags with the target off. If DETECT is false, bit 8 of OFFRRR (61E7) is set and, if TRACK is false, bit 7 is set. The test target is turned back on, SEQUEN is set to 3 and OUTFLG and STWAIT are set. Range and range rate data-good flags to the MDM will be 0 if the test passes, as will angle and angle rate-good flags. Range and range rate will be 0 if the test passes since, from [24], EA-2 serial output is forced to 0 unless tracking. Pitch and roll will be as in the prior sequence and angle rate will be 0.

Sequence 3 of Task 7, radar passive, starts at PASIVE (5194). Bit 8 of PASFLG (61E8) is set if the track flag is true and bit 7 is set if ANGTRK is false. PASIVE then calls RNGPAS (5260) to check if the measured range is 10.240 ± 250 ft. Bit 6 of PASFLG will be set if this test is successful. Bit 5 is set if the range data-good flag is true. PASIVE then calls RRATE to determine if the measured range rate is 0 ± 3 ft/s. If successful, bit 4 of PASFLG is set and bit 3 is set if the range rate data-good flag, RRGOOD, is true. Signal strength is compared with thresholds S3 and S4. If it is greater than S3, bit 2 of PASFLG is set and, if less than S4, bit 1 is set. STPCNT is set to 7 for Task 8 and OUTFLG is set for MDM output. Range and range rate data-good will be 1 if the test passes, range will be measured range, 10,240 ± 250 ft, and range rate will be between ±3 ft/s if the test passes. Angle rates will be 0 and pitch and roll will be as in the prior sequences. Note that tasks subsequent to Task 7 do not explicitly turn on the test target but rely on TARGET being set by TASK7. This would be important if the tasks were to be shuffled for some reason.

6.4.8 Task 8

Task 8 (496D) has four parts: initialization, data-good flag test, alpha error signal within limits, and beta error signal within limits. During initialization, the system is configured to auto-track by the macro:

```
496D    TASK8    CONFIG    :40,:0.
```

Estimated range is set to 10,250 ft and angle and angle rate good flags are set to 1. SEQUEN is set to 1, POW5 is set to 8D to provide -17.5 dBm at the test dipole, and STWAIT is set for the 10-sec pause to display the

results of Task 7, sequence 3. The task 8 pause merely reestablishes the estimated range of 10,250 ft. Sequence 1 of Task 8, starting at RFLG (49C5), sets bit 8 of ANTR (61E9) if range rate data-good is true and sets bit 7 if range data is good. POW5 is set to 95 to command the self-test MUX to measure the alpha error signal with the test dipole at maximum power. OUTFLG and STWAIT are set, and control is returned to the even leg of the self-test procedure. MDM output will consist of range and range rate data-good flags equal to 1 if the test passes. Angle and angle rate data-good flags are set by software and will be 1 unconditionally. Range and range rate will be that provided by the test target, presumably close to 10,240 ft and 0 ft/s. Angle rates will be 0, pitch and roll will be 0 if Tasks 5 and 6 were successful; otherwise, the angles are not predetermined.

Sequence 2, starting at DELELE (4A07) tests if the alpha error is within limits Y1 and Y2. The comments [21, pp. 536 and 537] are misleading with regard to pass/fail conditions. Bit 6 of ANGR will be set if the test passes and delta alpha is greater than Y1. Bit 5 will be set by EL2FAL (4A49) if delta alpha is less than Y2. EL2FAL and EL2PAS are misnamed. This is not a program error, just a confusion factor. If delta alpha is within limits, measured roll angle rate output to the MDM will be set to all 1's; otherwise, it will be set to 0's. Pitch angle rate will remain 0. Range and range rate data-good flags will be the same as in sequence 1, angle and angle rate data-good flags will be as provided by the EA2, presumably 1 if the test is successful. Range, range rate, pitch and roll will be as in sequence 1. The self-test MUX is set to measure delta beta with POW5 set to 85 and OUTFLG and STWAIT are set. Sequence 3, the beta test, compares the measured delta beta with thresholds Y3 and Y4. Bit 4 of ANTR is set if the delta beta is greater than Y3 and bit 3 is set if less than Y4. Bit 2 is set if the angle track enable test is true. STPCNT is set to 8 for Task 9 and OUTFLG is set. Pitch rate will be set to all 1's if the test succeeds or all 0's if it fails. All other outputs will remain the same as in sequence 2.

6.4.9 Task 9

Task 9 (5409) is the receiver sensitivity test. This uses the test dipole at less than full power. During the first pass, the system is configured to GPC acquisition mode by the macro

5409 TASK9 CONFIG :10,:00.

Estimated range is set to 10,250 ft, angle and angle rate data-good flags are forced to 1, SEQUEN is set to 1, and STWAIT is set for the 10-sec pause. After the pause, a sequence equal to 1 causes a branch to TRKFLG (545E). If TRACK is true, bit 8 of RSTY is set. SEQUEN is set to 2 and the test target is set by loading hex CD into POW5. This sends the radar signal strength to the comparator, sets ATTEN1 = 1 and ATTEN2 = 0 for a nominal output of -45 dBm to the dipole. All MDM outputs will be the same as they were during the previous pause, except the mode flag will be GPC ACQ and angle and angle rate data-good flags will be 1's. Sequence 2 goes to SIGSTV (548E), which compares the signal strength with thresholds R1 and R2. If signal strength is greater than R1, bit 7 of RSTY is set, and bit 6 is set if signal strength is less than R2. POW5 is set to D5 to measure delta alpha error voltage, SEQUEN is set to 3, OUTFLG is set, and STWAIT is set. MDM output will be identical to that of sequence 1. Sequence 3 goes to ALPHA (54F4) to compare the delta alpha error signal with thresholds ALP1 and ALP2. If the error signal is greater than ALP1, bit 5 of RSTY is set, and bit 4 is set if the error signal is less than ALP2. POW5 is set to 4, OUTFLG is set, and STWAIT is set. Again, MDM output is identical to Tasks 1 and 2. Sequence 4 goes to BETA (5555) to compare the delta beta error with thresholds BETA1 and BETA2. If delta beta is greater than BETA1, bit 3 is set and, if less than BETA2, bit 2 is set. Range and range rate limits are tested using routines RNGPAS and RRATE, the same routines used by sequence 3 of Task 7. Bit 8 of RSTYRR is set if the range is 10,240 ft ± 250 ft, and bit 7 is set if the range rate is within ±3 ft/s. STPCNT is set to 9 for TASK10, OUTFLG is set and STWAIT is set. MDM outputs will be identical to those of sequence 3, with the exception of range and range rate which will reflect the values measured by the EA2 using the lower power test target.

6.4.10 Task 10

Task 10 tests the flags set in the prior tasks and sets E1TEST, E2TEST, DATEST and SYSTST, accordingly. SYSTST is set if all tests were successful and resets otherwise. These four flags are output to the MDM in status word 3. Range data to the MDM and D&C is set to 100,000 ft if

all tests pass, or 1,000 ft if any test fails. During the first pass through task 10, MDM output is initiated with OUTFLG set to 1. LAMP is set, and subsequent passes through task 10 will set SCANNG, TRACK and SCWARN flags which, in turn, will light the search, track and scanwarn lights in the D&C panel. Task 10 will continue to be executed until self-test conditions are reset.

A synopsis of D&C output is presented in Figure 44. Two cumulative times are given. The maximum cumulative time assumes that all tests pass, and the minimum assumes that Task 4 fails to point the antenna to zenith within 10 seconds, in which case Tasks 5 and 6 are not exercised. There is more than a minute variability in time to complete self-test, depending on which tests fail, if any. Even if all tests pass, there is a 28-second variability due to uncertainties in Tasks 4 and 5, the antenna gimbal/servo tests.

The status of range and angle are shown in Figure 44; however, they share a common display and only one can be displayed at any given time.

Table 7. MDM Output at Conclusion of Power Form Test
Tasks 1-3, Sequence 1

MDM Output	Pass	Fail
Mode	Existing mode prior to self-test	Same
Range Data Good	0	Same
Range Rate Data Good	0	Same
Angle Data Good	0	Same
Angle Rate Data Good	0	Same
Range	All 1's (2,621,440 ft)	Same
Range Rate	All 1's (1638.35 fps)	Same
Roll Angle Rate	All 0's	Same
Pitch Angle Rate	All 0's	Same
Roll	Indeterminate	Same
Pitch	Indeterminate	Same

Table 8. MDM Output at Conclusion of Zenith Positioning Test
Task 4

MDM Output	Pass	Fail
Mode	GPC Designate	Same
Range Data Good	0	Same
Range Rate Data Good	0	Same
Angle Data Good	0	Same
Angle Rate Data Good	0	Same
Range	All 1's (2,621,440 ft)	Same
Range Rate	All 1's (1638.35 fps)	Same
Roll Angle Rate	All 0's	Same
Pitch Angle Rate	All 0's	Same
Roll	0°	Indeterminate
Pitch	0°	Indeterminate
Comment		Go to task 7

Table 9a. MDM Output at Conclusion of Servo Test
Task 5, Sequence 1

MDM Output	Pass	Fail
Mode	GPC Designate	Same
Range Data Good	0	Same
Range Rate Data Good	0	Same
Angle Data Good	0	Same
Angle Rate Data Good	0	Same
Range	All 1's (2,621,440 ft)	Same
Range Rate	All 1's (1638.35 fps)	Same
Roll Angle Rate	All 0's	Same
Pitch Angle Rate	All 0's	Same
Roll	0°	0°
Pitch	30°	Indeterminate
Comment		Go to task 7

Table 9b. MDM Output at Conclusion of Servo Test
Task 5, Sequence 2

MDM Output	Pass	Fail
Mode	GPC Designate	Same
Range Data Good	0	Same
Range Rate Data Good	0	Same
Angle Data Good	0	Same
Angle Rate Data Good	0	Same
Range	All 1's (2,621,440 ft)	Same
Range Rate	All 1's (1638.35 fps)	Same
Roll Angle Rate	All 0's	Same
Pitch Angle Rate	All 0's	Same
Roll	-30°	Indeterminate
Pitch	30°	30°
Comment		Go to task 7

Table 9c. MDM Output at Conclusion of Servo Test
Task 5, Sequence 3

MDM Output	Pass	Fail
Mode	GPC Designate	Same
Range Data Good	0	Same
Range Rate Data Good	0	Same
Angle Data Good	0	Same
Angle Rate Data Good	0	Same
Range	All 1's (2,621,440 ft)	Same
Range Rate	All 1's (1638.35 fps)	Same
Roll Angle Rate	All 0's	Same
Pitch Angle Rate	All 0's	Same
Roll	0°	Indeterminate
Pitch	0°	Indeterminate
Comment		Go to task 7

Table 10a. MDM Outout at Conclusion of Power Test
Task 6, Sequence 1

MDM Output	Pass	Fail
Mode	GPC Designate	Same
Range Data Good	0	Same
Range Rate Data Good	0	Same
Angle Data Good	0	Same
Angle Rate Data Good	0	Same
Range	All 1's (2,621,440 ft)	Same
Range Rate	All 1's (1638.35 fps)	Same
Roll Angle Rate	All 0's	Same
Pitch Angle Rate	All 0's	Same
Roll	0°	Same
Pitch	0°	Same

Table 10b MDM Output at Conclusion of Power Test
Task 6, Sequence 2

MDM Output	Pass	Fail
Mode	GPC Designate	Same
Range Data Good	0	Same
Range Rate Data Good	0	Same
Angle Data Good	0	Same
Angle Rate Data Good	0	Same
Range	All 1's (2,621,440 ft)	Same
Range Rate	All 1's (1638.35 fps)	Same
Roll Angle Rate	All 0's	Same
Pitch Angle Rate	All 0's	Same
Roll	0°	Same
Pitch	0°	Same

Table 11a. MDM Output at Conclusion of R,Ṙ Test
Task 7, Sequence 1

MDM Output	Pass	Fail
Mode	Manual	Same
Range Data Good	1	0 or 1
Range Rate Data Good	1	0 or 1
Angle Data Good	0 or 1	Same
Angle Rate Data Good	0 or 1	Same
Range	5,320 ± 250 ft	Indeterminate if range check fails
Range Rate	0 ± 3 fps	Indeterminate if range rate check fails
Roll Angle Rate	All 0's	Same
Pitch Angle Rate	All 0's	Same
Roll	0° if tasks 4 and 5 pass Indeterminate otherwise	Same
Pitch	0° if tasks 4 and 5 pass Indeterminate otherwise	Same

Table 11b. MDM Output at Conclusion of R,$\dot{R}$ Test
Task 7, Sequence 2

MDM Output	Pass	Fail
Mode	Manual	Same
Range Rate Good	0	0 or 1
Range Rate Data Good	0	0 or 1
Angle Data Good	0	0 or 1
Angle Rate Data Good	0	0 or 1
Range	All 0's	Indeterminate
Range Rate	All 0's	Indeterminate
Roll Angle Rate	All 0's	Same
Pitch Angle Rate	All 0's	Same
Roll	0° if tasks 4 and 5 pass Indeterminate otherwise	Same
Pitch	0° if tasks 4 and 5 pass Indeterminate otherwise	Same
Comment	EA2 to EA1 serial data forced to 0 unless tracking	

Table 11c. MDM Output at Conclusion of R,$\dot{R}$ Test
Task 7, Sequence 3

MDM Output	Pass	Fail
Mode	Manual	Same
Range Data Good	1	0 or 1
Range Rate Data Good	1	0 or 1
Angle Data Good	0 or 1	0 or 1
Angle Rate Data Good	0 or 1	0 or 1
Range	10,240 ± 250 ft	Indeterminate if range check fails
Range Rate	0 ± 3 fps	Indeterminate if range rate check fails
Roll Angle Rate	All 0's	Same
Pitch Angle Rate	All 0's	Same
Roll	0° if tasks 4 and 5 pass Indeterminate otherwise	Same
Pitch	0° if tasks 4 and 5 pass Indeterminate otherwise	Same

Table 12a. MDM Output at Conclusion of Servo Angle Track Test
Task 8, Sequence 1

MDM Output	Pass	Fail
Mode	Autotrack	Same
Range Data Good	1	0 or 1
Range Rate Data Good	1	0 or 1
Angle Data Good	1	Same
Angle Rate Data Good	1	Same
Range	Should be close to 10,240 ft	Same
Range Rate	Should be close to 0 fps	Same
Roll Angle Rate	All 0's	Same
Pitch Angle Rate	All 0's	Same
Roll	0° if tasks 4 and 5 pass Indeterminate otherwise	Same
Pitch	0° if tasks 4 and 5 pass Indeterminate otherwise	Same
Comment	Range and range rate as provided by test target	

Table 12b. MDM Output at Conclusion of Servo Angle Track Test
Task 8, Sequence 2

MDM Output	Pass	Fail
Mode	Autotrack	Same
Range Data Good	0 or 1 (same as sequence 1)	Same
Range Rate Data Good	0 or 1 (same as sequence 1)	Same
Angle Data Good	1	Same
Angle Rate Data Good	1	Same
Range	Should be close to 10,240 ft	Same
Range Rate	Should be close to 0 fps	Same
Roll Angle Rate	All 1's (-16.38°/s)	All 0's
Pitch Angle Rate	All 0's	All 0's
Roll	0° if tasks 4 and 5 pass Indeterminate otherwise	Same
Pitch	0° if tasks 4 and 5 pass Indeterminate otherwise	Same
Comment	Range and range rate as provided by test target	Same

Table 12c. MDM Output at Conclusion of Servo Angle Track Test
Task 8, Sequence 3

MDM Output	Pass	Fail
Mode	Autotrack	Same
Range Data Good	0 or 1 (same as sequence 1)	Same
Range Rate Data Good	0 or 1 (same as sequence 1)	Same
Angle Data Good	1	Same
Angle Rate Data Good	1	Same
Range	Should be close to 10,240 ft	Same
Range Rate	Should be close to 0 fps	Same
Roll Angle Rate	All 0's or all 1's depending on outcome of sequence 2	Same
Pitch Angle Rate	All 1's (-16.38°/s)	All 0's
Roll	0° if tasks 4 and 5 pass Indeterminate otherwise	Same
Pitch	0° if tasks 4 and 5 pass Indeterminate otherwise	Same

Table 13a. MDM Output at Conclusion of Receiver Sensitivity Test
Task 9, Sequence 1

MDM Output	Pass	Fail
Mode	GPC Acquisition	Same
Range Data Good	0 or 1 (same as task 8, sequence 1)	Same
Range Rate Data Good	0 or 1 (same as task 8, sequence 1)	Same
Angle Data Good	1	Same
Angle Rate Data Good	1	Same
Range	Should be close to 10,240 ft (same as task 8, sequence 1)	Same
Range Rate	Should be close to 0 fps (same as task 8, sequence 1)	Same
Roll Angle Rate	All 0's or all 1's depending on outcome of task 8, sequence 2	Same
Pitch Angle Rate	All 0's or all 1's depending on outcome of task 8, sequence 3	Same
Roll	0° if tasks 4 and 5 pass Indeterminate otherwise	Same
Pitch	0° if tasks 4 and 5 pass Indeterminate otherwise	Same

Table 13b. MDM Output at Conclusion of Receiver Sensitivity Test
Task 9, Sequence 2-4

MDM Output	Pass	Fail
Mode	GPC Acquisition	Same
Range Data Good	0 1	Same
Range Rate Data Good	0 or 1	Same
Angle Data Good	1	Same
Angle Rate Data Good	1	Same
Range	10,240 ± 250 ft	Indeterminate
Range Rate	0 ± 3 fps	Indeterminate
Roll Angle Rate	All 0's or all 1's, depending on outcome of task 8, sequence 2	Same
Pitch Angle Rate	All 0's or all 1's, depending on outcome of task 8, sequence 3	Same
Roll	0° if tasks 4 and 5 pass Indeterminate otherwise	Same
Pitch	0° if tasks 4 and 5 pass Indeterminate otherwise	Same
Comment	Range, range rate and range data good flags may differ from seq. 1 due to lower power	Same

Table 14. MDM Output at Conclusion of Flag Compilation
Task 10

MDM Output	Pass	Fail
[illegible]	Manual	Same
Range Data Good	0 or 1	Same
Range Rate Data Good	0 or 1	Same
Angle Data Good	1	Same
Angle Rate Data Good	0	Same
Range	100,000 ft	1,000 ft
Range Rate	Should be close to 0 fps (same as task 9, sequence 4)	Indeterminate
Roll Angle Rate	All 0's	Same
Pitch Angle Rate	All 0's	Same
Roll	0°	0° if tasks 4 and 5 pass Indeterminate otherwise
Pitch	0°	0° if tasks 4 and 5 pass Indeterminate otherwise
DA	1	0 or 1
E1	1	0 or 1
E2	1	0 or 1
SYS	1	0

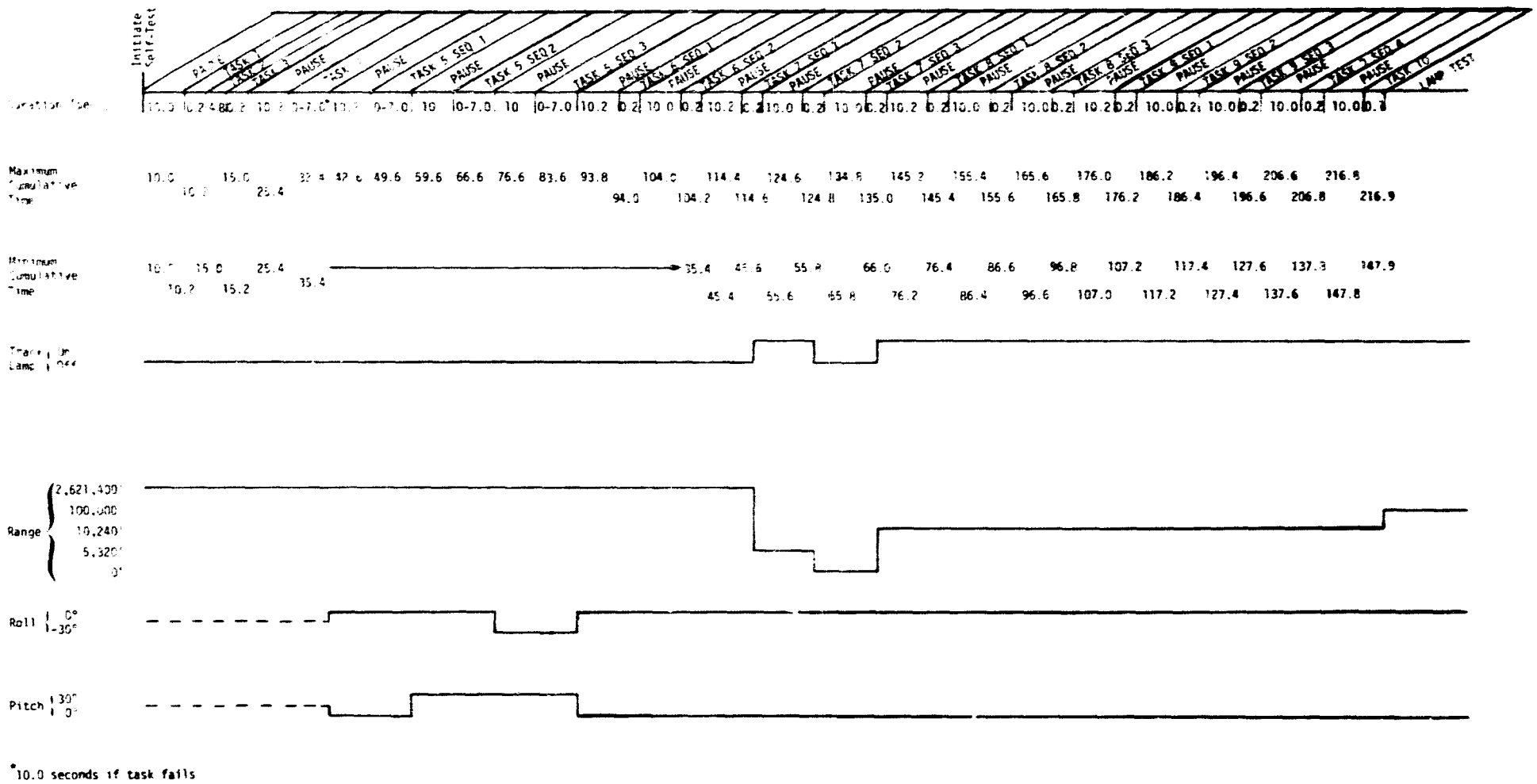

*10.0 seconds if task fails

Figure 44. D&C Status During Self-Test

6.5 Memory Usage Optimization

6.5.1 Introduction

In the present hardware configuration, the RCA processor is not limited by available memory space. If feed-forward for the antenna servo is implemented, however, time considerations may play an important role in the processor's ability to perform the required functions. Initial estimates by HAC indicate a timing margin of 3-6% if feed-forward is implemented.

One way to improve the efficiency of the present software from the standpoints of both execution time and memory requirements, would be to redefine the multitude of flags in terms of one flag/word rather than eight/word. This has the effect of requiring more memory to store flags but effects a net increase in memory due to the simplified software required to test or modify flags. An additional benefit is that computational speed is increased.

6.5.2 Suggested Modifications

With the current implementation, one flag word may hold as many as eight flag bits. In order to access an arbitrary flag bit, assembler macro instructions are used which generate inline code as the program is assembled. These macro instructions are used to GET, SET, RESET or TOGGLE flag bits. For example, the instruction

```
RESETS  REGISTER,FLAG
```

is expanded to the following inline code:

```
LDI  (low-order address of flag word)
PLO  REGISTER
LDN  REGISTER
ORI  (flag bit to be reset)
XRI  (flag bit to be reset)
STR  REGISTER.
```

This macro uses nine memory words and 12 machine cycles, with the high-order byte of REGISTER preset to the high-order address of the flag word. By contrast, if one word contained one flag, the flag would be reset merely by clearing the word. This could be done with four instructions, versus six, using six memory words and eight machine cycles. Similarly, the SETS macro, which takes seven memory locations, five instructions and 10 cycles, could be implemented with five memory locations, four instructions and eight cycles.

The use of one-bit flag words would require about 120 additional memory words for flags; however, these would be gained back by the savings of memory in one routine, CONFIGURE, which makes extensive use of flags. Additional space would be required in input/output routines to format the bit flags; however, this can be done with relative efficiency since the flag access is not random as it is with the GET, SET and RESET macros. Parallel output word 5 (POW5) could remain parallel since all bits of POW5 are typically loaded at the same time.

While there is no point in modifying the existing software if it is adequate to do the job, in the event that feed-forward requires too much time, this technique could be tried. The effect of the suggested changes can easily be tested merely by redefining the macros, allocating storage for the flags and redefining the input/output bit mapping.

6.6. Conclusions and Recommendations

The EA1 software is well documented and annotated, with the exception of the omission of a cross-reference listing in the documentation. In this report, Axiomatix has provided a cross-reference listing of status flags to partially fill this gap. A minor bug in the procedure termination routine has been found and the fix is discussed in section 6.1.1. Executive reconfiguration and self-test are examined and appear to perform as expected. Discussion of the MDM output during self-test is very brief in the HAC documentation; a more complete discussion of the MDM outputs is provided in this report. A change in the method of flag storage is recommended if processing time becomes a critical factor in future versions of the EA1 software.

7.0 DELIVERABLE TEST EQUIPMENT EVALUATION

7.1 Introduction

As per NASA Contract NAS 9-15795B, Task 3, this section reviews and evaluates the Hughes Aircraft Company's Ku-band test equipment which will be delivered to both the Avionic Development Laboratory (ADL) and the Electronic System Test Laboratory (ESTL). This test equipment was previously known as the Deliverable Test Equipment (DTE); however, the present nomenclature is the Deliverable System Test Equipment (DSTE).

The DSTE is capable of performing system level developmental testing of the Ku-Band Integrated Radar and Communications Equipment and is functionally organized into LRU test panels similar to the Ku-band system with the addition of a microcomputer system, a Ku-band signal conditioner, power control panel and general-purpose test equipment. Figure 45 is a functional block diagram of the DSTE.

The Hughes test philosophy entailed a cost-effective approach wherein the LRU test equipment would be readily adapted for use in the DSTE. Three individual panels, the EA-1 LRU, the EA-2 LRU and the SPA LRU test panel, were developed and are being used as the primary signal sources and signal detection circuits for the respective LRU's. Upon completion of the EA-1, EA-2 and SPA LRU testing, the three LRU test panels were integrated into a console to form the basis of the DSTE.

While the DSTE is capable of operating in an RF link mode where radiation is coupled between the Ku-band system antenna and a simulated TDRS satellite, the more typical operational mode is to use the Ku-band Test Signal Conditioner (TSC). The TSC provides numerous functions but, essentially, the TSC upconverts the simulated forward link data generated by the EA-1 test panel or the simulated radar target return signals generated by the EA-2 test panel to Ku-band frequencies. The upconverted signals are, in turn, injected into the deployed assembly (DA) via RF connectors. Also, the TSC demodulates the return link QSPK or FM signal which is input into the SPA test panel for data comparison and validation.

The DSTE utilizes a power control panel that monitors the voltage and current supplied to the Ku-band system. The power control panel provides protection circuitry to guard against bus reversal, overvoltage and short-circuit conditions, and provides the logic circuitry to perform the power-up/down procedures.

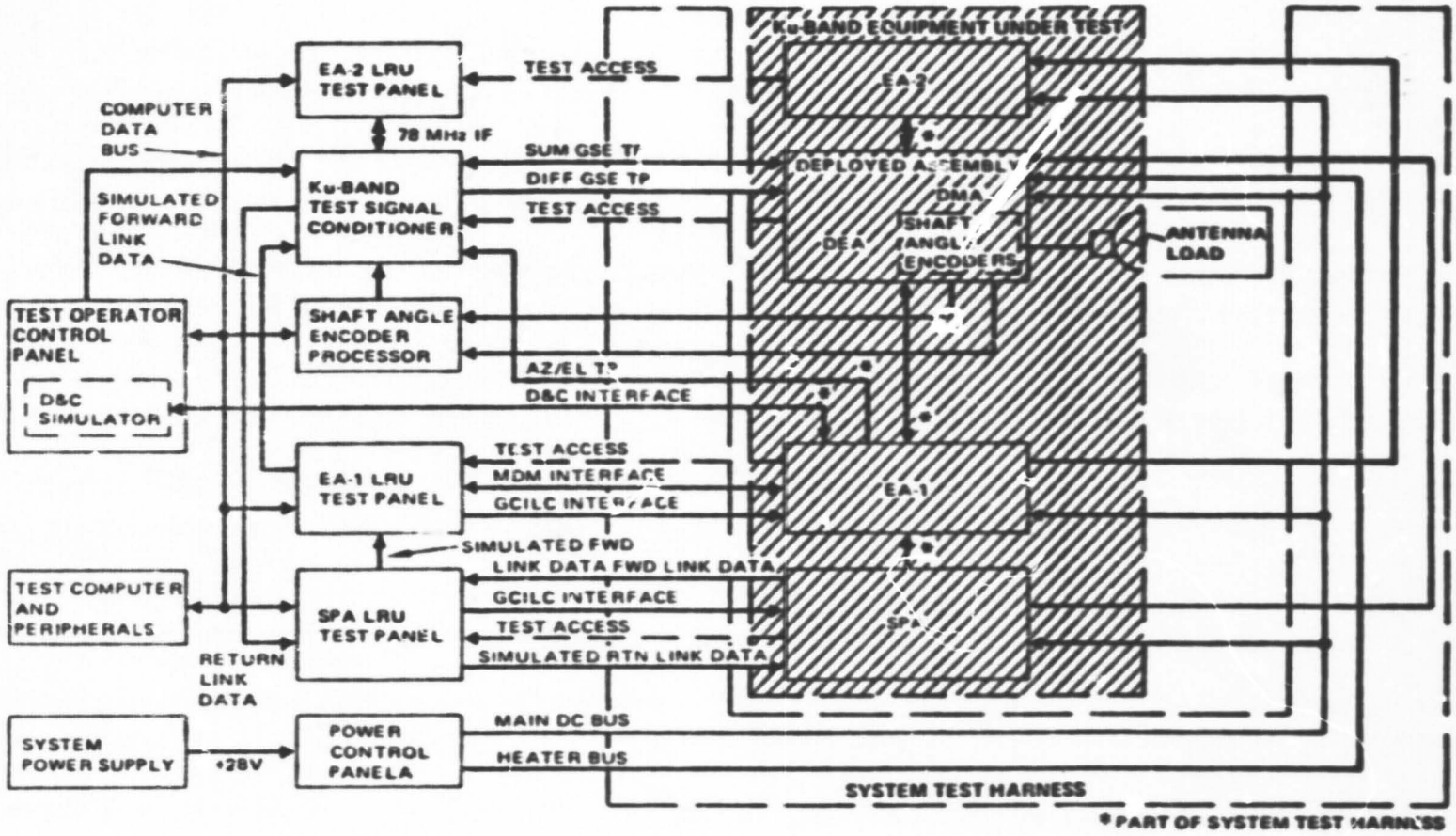

Figure 45. DSTE Functional Block Diagram

The last major features of the DSTE are the test operator interface and the test computer system. The DSTE is basically semiautomatic, with primary control of the test operations by the test operator. The test computer primarily performs the role of monitoring nonreal-time functions, data logging, and management of the Ku-band system operating modes. The test computer system includes a minicomputer, a dual floppy disc system, a hard disc system (ESTL only), a CRT display terminal, a high-speed line printer, and a test control/computer interface panel.

The DSTE was built into a modularized configuration being grouped functionally to minimize intercabling and to facilitate system and LRU level testing. Figure 46 shows the DSTE physical configuration which consists of the following:

(1) A three-and-one-half bay console housing the three LRU test panels (EA-1, EA-2 and SPA), power supplies, the system-unique panels (power control, test operator panel and shaft angle encoder processor), commercial measuring equipment and the test computer system. Note: The ESTL configuration will be a four-bay console so that the hard disc system and additional cooling blowers may be added.

(2) A mobile stand for mounting the DA LRU and housing the TSC panel.

(3) A two-bay, low-boy console with cold plates for mounting the EA-1, EA-2 and SPA LRU's.

(4) A line printer on a stand.

(5) An additional three-bay console for user-supplied commercial test equipment.

Since the DSTE is semiautomated, Hughes generated a number of computer programs to test the Ku-band system. The 14 communications mode tests and the 17 radar mode tests and described in detail in Hughes document TP32090-001, "Subsystem Development Test Procedures for the Ku-Band Integrated Radar/Communications Equipment," dated October 23, 1979. The 31 test modules will be discussed in greater detail later in this report.

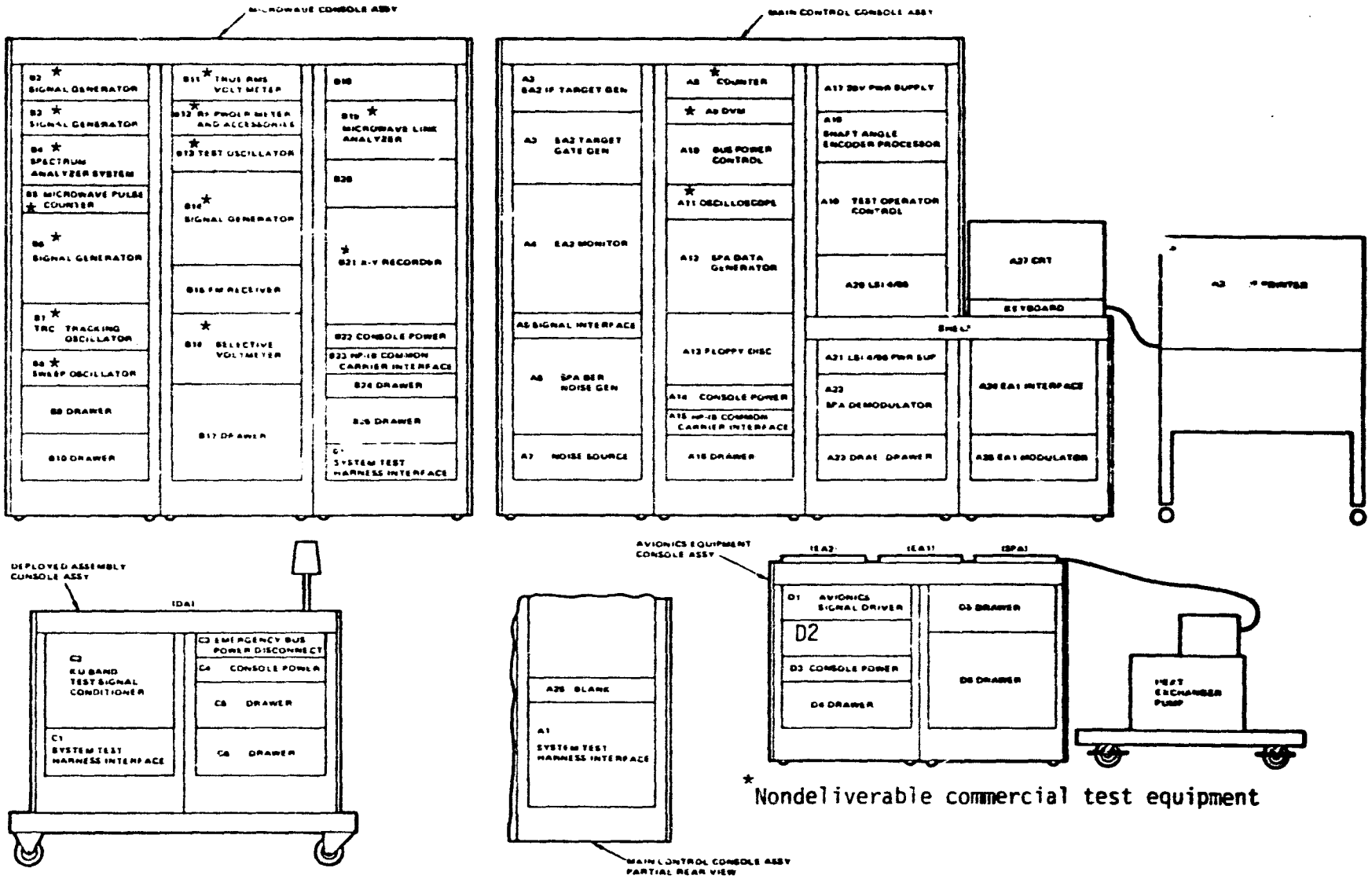

Figure 46. DSTE Configuration

Note: The ESTL DSTE will consist of a four-bay main control assembly so that additional cooling blowers and hard disc system may be added.

7.2 Approach

To date, there is no existing document describing the DSTE in detail. So, in order to understand the capabilities, a number of documents were reviewed. First, there is Hughes document HS237-528, "Verification Plan for Ku-Band Integrated Radar and Communications Equipment," dated September 14, 1979. This Hughes document, which is sometimes referred to as "TM01," is a Rockwell contractually required plan that permits Rockwell to evaluate the Hughes method of verifying the Ku-band system requirements. In TM01, a number of system tests are described, and there is a discussion of the system test equipment (STE). The STE is similar to, but not the same as, the DSTE.

Second, there is Hughes document TP32090-001 (previously mentioned) that describes the 31 test modules. This specification will be used in this report to determine the basic capabilities of the DSTE.

Third, Hughes document TP32012-074, "Ku-Band Sell-Off Test Procedure," dated May 19, 1980, is used to sell off the ADL and ESTL DSTE's. This procedure outlines which of the 31 test modules will be used for sell-off.

Fourth, Rockwell document MC409-0025, "Integrated Communications and Radar Equipment, Ku-Band," Rev B with changes, dated July 21, 1978, is the Ku-band system specification. This document describes in detail all of the system requirements and methods that must be used to verify compliance to the specification.

The basic approach was to generate a matrix to compare the Ku-band system requirements as detailed in the Rockwell specification to the 31 test modules described in TP32090-001. Ideally, the modules should test a majority of the Rockwell system requirements. In this same matrix, the modules used for DSTE sell-off will also be identified.

733 Findings

The first task was to determine exactly what each of the 14 communications test modules and the 17 radar test modules actually verify. This was accomplished by reviewing TP32090-001 and TM01.

7.3.1 Test Module Descriptions

The reader must remember that originally there were no requirements for Hughes to perform system testing. The 31 test modules were intended for system developmental tests only. When system testing was eventually required, these modules were used to test the system, even though they were not initially designed for that task.

7.3.1.1 Communications Test Module Descriptions

7.3.1.1.1 Communications power up/down consumption

The Ku-band communications subsystem power up/down sequence will be tested to verify that the subsystem responds properly to the standby and power on modes.

The test begins with the system switched to COMM STDBY from the OFF condition. MDM status bits will be verified for correct mode. In the COMM STDBY mode, the following power will be measured:

(1) Avionics power
(2) DA power
(3) HTR power.

Upon completion of the standby power measurements, the system will then be commanded to COMM ON. The antenna unstowing procedure, along with initialization of the angle designation register, will be verified via the MDM pitch and roll data and the shaft angle encoder data. With the antenna in the unstowed condition, the following power will be measured:

(1) Avionics power
(2) DA power
(3) HTR power.

Upon completion of the power measurement, the antenna stowing procedure will be verified via MDM pitch and roll data and discrete signals (BOOM STOW ENABLE I and II--high) The system will then be commanded off and the avionics and DA currents measured.

7.3.1.1.2 Communications subsystem slant range

The purpose of this test is to demonstrate the capability of the Ku-band system to acquire and lock on to a TDRS simulated signal.

The test consists of transmitting a 13.775 GHz CW signal from an antenna located atop the south end of Hughes building #355 (Bird House) to the Ku-band system located in the radome-enclosed area in building #358.

The Ku-band system antenna is manually slewed until a maximum reading occurs, indicating that the DA antenna is pointing at the simulated target. The Ku-band antenna is then positioned away from the simulated target, but within the 10° half-cone search angle. Search is initiated in GPC ACQUISITION antenna steering mode, and the Ku-band system capability to acquire and lock up on the simulated target is verified. Search is visually verified by the antenna motion. After the antenna motion has stopped, system status is verified by reading the MDM status.

7.3.1.1.3 Forward link signal strength test

The objective of this test is to verify the Ku-band communications subsystem capability to provide acceptable conditioned AGC voltage representing communications signal strength.

The Ku-band communications subsystem input signal level will be varied and the corresponding signal strength voltage measured. The signal level will be input at the DA test access connector and the MDM-3 signal strength voltage measured at the signal interface panel.

7.3.1.1.4 Forward link tracking threshold test

The tracking threshold level for the specified modulation types will be verified for the communications subsystem, as follows:

(1) Unmodulated carrier
(2) Data modulation on the carrier
(3) PN modulation on the carrier
(4) Data and PN modulation on the carrier.

The test starts with the Costas and PN (when PN is present) loops tracking a known input signal of sufficient strength to cause lock-on. The signal level will be reduced by 0.5 dB steps and held constant for 60 seconds. The point where each loop loses lock will be recorded (does not apply to the PN loop when PN is absent).

7.3.1.1.5 Forward link acquisition time test

Acquisition and lock-on time for the Costas loop, PN loop, frame synchronization and data present (lock-on and dropout) are measured for the following classes of forward link input signals:

(1) Unmodulated carrier
(2) Data modulation on the carrier
(3) PN modulation only on the carrier
(4) Data and PN modulation on the carrier.

The forward link acquisition time measurements are made on an electronics counter set for time interval measurement. Unless otherwise specified, each test is repeated 10 times for the high input signal level (upper C/N range) and 100 times for the low input signal level (lower C/N range).

(1) The Costas loop acquisition and lock indication (within 330 ms) after the input signal is applied is measured for all four specified modulation types. Test is performed in mode 1.

(2) The PN loop acquisition and lock indication (within 10 seconds) after the input signal is applied is measured for the PN modulation on carrier and data and PN modulation on carrier modulation types. Test is performed in mode 1.

(3) Frame synchronization acquisition within two seconds after PN acquisition when PN data are present and within two seconds after Costas lock when PN data are not present is measured. Test is performed in mode 1.

(4) The time for the data present signal to go high, within two seconds after PN lock is acquired when PN data are present and within two seconds after Costas lock when PN data are not present, is measured. The test is performed in mode 2 and at rates of 32 kbps and 216 kbps.

(5) The data present signal drop-out time ($\leq$ 11 seconds) for data interrupt on the forward link will be measured. The test is performed in mode 2 and at the 216 kbps rate. The test is repeated 10 times with high input signal rate.

7.3.1.1.6 Forward link acquisition BER tests

Acceptable BER for the communications forward link input signal levels and output data RMS jitter will be verified.

The bit error for various forward link input signal levels is measured on the electronic counter. Signal detection is verified at the start of each test and the bit error measured at the end of 60 seconds. The test is performed for data modulation on carrier and data and PN modulation on carrier. The mode 1, NSP 1 forward link output data RMS jitter is measured on the electronic counter set for time interval measurement.

7.3.1.1.7 Functional test (return link)

The return link functional test objectives are as follows:

(1) To verify acceptable signal isolation and correct configuration for return link data channels in response to management commands.

(2) To verify acceptable signal conditioning in response to an asymmetrical HDR clock.

The functional tests will be conducted as follows:

(1) Signal isolation and correct configuration will be verified by injecting 125 kHz square-wave signal into two of the SPA return link data channels while the third or selected data channel is provided with the normal signal. The output signal shall be verified for the selected normal signal and rejection of the nonselected signals. The test will be repeated for all combinations of the return link data channels and selectable data source.

(2) Acceptable signal conditioning in the face of clock asymmetry will be verified by first using an HDR clock with +20% asymmetry and insuring that the HDR bit stream output of the DA does not exceed 10% asymmetry. The test will be repeated for -20% HDR clock asymmetry.

7.3.1.1.8 BER test (return link)

The communications return link BER test objective is to verify acceptable BER levels for all return link digital channels for normal and abnormal inputs (asymmetrical convolutional encoder clock).

Generally, BER can be determined directly by comparing the bit stream out of the test device to the bit stream fed into the test device and dividing the number of times a bit error occurs (extra bit due to noise or loss of bit due to noise) by the total number of input bits occurring during the time period of observation. However, because the BER for the return link is normally too low to determine directly in a reasonably short time period, a known amount of noise will be injected into the test channel in order to raise the BER.

By measuring the BER corresponding to each of several known levels of noise, then plotting these points, the resulting curve can be extrapolated to obtain the S/N ratio corresponding to a BER of 10^{-6}. This S/N ratio shall not be different from an S/N ratio measured for the calibration configuration by more than a specified amount.

Additionally, the BER test will include measurement of BER for the HDR channel 3, mode 1, clock in response to asymmetry in the convolutional recorder clock signal.

7.3.1.1.9 Communications mode antenna stow/unstow test

The antenna is deployed to its unstowed position and directed to the zenith, where roll and pitch gimbal encoder angles are verified. The antenna is then directed to the stowed position and the roll and pitch encoders are verified for the gimbal's stowed angular values.

7.3.1.1.10 Communications mode antenna stow/unstow test

The antenna's obscuration area is verified using values for roll and pitch gimbal angles computed from the data in the obscuration boundary table.

7.3.1.1.11 Communications mode antenna stability test

The antenna's drift rate in inertial stabilization and the antenna's drift and pointing accuracy in body stabilization are measured. The antenna's angular position is set for different pointing designates and the accuracy is checked. After two minutes at each pointing designate, the antenna's angular position is again read. From this data, the drift rates in inertial stabilization mode and the angular drift in body stabilization mode are computed.

7.3.1.1.12 Communications mode antenna slew test

The antenna's manual fast and slow slew rates are checked in elevation (up and down directions) and in azimuth (left and right directions). A plot is made to verify the antenna search scan.

The antenna wraparound rate is checked at various beta gimbal positions. The antenna is positioned 5° from the alpha gimbal stop and directed to go to a position 5° on the other side of the alpha gimbal stop. Since the gimbal cannot go through its stop, the gimbal whips around at the super slew rate to the designate angle. This rate is measured to verify that it is within the slew maximum and minimum tolerances.

7.3.1.1.13 Communications mode target acquisition and track test

The target acquisition and track functions of the antenna servo system are performed to verify angular track accuracy, the main scan TDRS acquisition and track stability requirements, the low signal level TDRS acquisition requirements and the loss in antenna gain during TDRS track. The resultant data is either processed by the test equipment computer or analyzed off-line to determine requirements compliance.

7.3.1.1.14 Communications antenna scan volume

Proper response to an invalid start scan commanded during GPC DESIG, MANUAL, GPC ACQ and AUTOTRACK antenna steering modes is verified. The operator then selects either the ambient scan volume test or the thermal vacuum scan volume test. These tests use the X-Y plotter to record the antenna scan trajectory for off-line analysis. Parameters to be verified off-line are: number of scan circles, scan volume, 30% scan overlap, scan time, scan dwell time and scan rates. The thermal vacuum scan volume test consists of a search scan at each of four scan centers. The scan centers in (ALPHA, BETA) are (0,0), (45,0), (-75,0) and (0,45). The search cone is 20°. The ambient scan volume test consists of a 20° scan cone.

7.3.1.2 Radar Test Module Description

7.3.1.2.1 Radar power up/down consumption

The Ku-band radar subsystem power up/down sequence will be tested to verify that the subsystem responds properly to the standby and power-on modes.

The test begins with the system switched to RADAR STDBY from the OFF condition. MDM status bits will be verified for correct mode. In the RADAR STDBY mode, the following power will be measured: avionics power, DA power and HTR power. Upon completion of the standby power measurements, the system will then be commanded to RADAR ON. The antenna unstowing procedure, along with initialization of the angle designation register, will be verified via the MDM pitch and roll data and the shaft angle encoder data. With the antenna in the unstowed condition, the following power will be measured: avionics power, DA power and HTR power. Upon completion of the power measurement, the antenna stowing procedure will be verified via MDM pitch and roll data and discrete signals (BOOM STOW ENABLE I & II--HIGH) from the system.

The system will then be commanded off and the avionics current and DA current measured.

7.3.1.2.2 Radar self-test

The radar self-test begins with an invalid start command. The response is noted and is followed by a correct initiation of the self-test mode. The test operator evaluates the response of the D&C displays while the DSTE evaluates the S/T information available at the MDM. The combined evaluations determine the self-test validity.

Available to the operator at his discretion is a printout of all the MDM data that was taken during S/T by the DSTE.

7.3.1.2.3 Antenna stow/unstow test

The antenna is commanded to execute the stow and unstowing process. Along with visual verification, the stow and unstow angle positions are measured and verified against known values.

7.3.1.2.8 Radar waveform test

This test verifies the radar waveform design by measuring the pulse width, PRF, power and frequency management of the transmitted waveforms. These parameters are obtained from 19 operator-selectable tests. These tests are derived from appropriate combinations of GPC DESIGNATE and MANUAL operation in the active or passive modes for both search and track, along with designating the range. A simulated target return is provided to obtain the track waveforms. In addition, the frequencies of the 156 MHz (T.O. reference) and 49.2 MHz (range clock reference) signals are measured.

7.3.1.2.9 Radar range accuracy test

This test module verifies the radar subsystems's measurement of range in the active and passive modes. Two verification approaches are provided: developmental and acceptance. The developmental approach uses many data samples (1000 nominal, but operator controlled) to determine the statistical mean, variance and three sigma values of the data. These computer-calculated statistical reports are then compared to the system specification values. The acceptance approach uses a single data sample which is compared to the combined random and bias specification values. Fourteen range accuracy tests make up the test module. The tests are configured to verify the radar subsystem's measuring capability through the specified regime of operation.

7.3.1.2.10 Radar range rate accuracy test

This test module verifies the radar subsystem's measurement of range rate in the active and passive modes. Two verification approaches are provided: developmental and acceptance. The developmental approach uses many data samples (1000 nominal, but operator controlled) to determine the statistical mean, variance and three-sigma values of the data. These computer-calculated statistical reprots are then compared to the system specification values. The acceptance approach uses a single data sample which is compared to the combined random and bias specification values. Twenty-three range rate accuracy tests make up this test module. The tests are configured to verify the radar subsystem's measuring capability through the specified regime of operation.

7.3.1.2.4 Antenna obscuration zone test

The obscuration profile for the A side is checked out. The antenna is positioned to seven locations, five of which are in the obscuration area. The scan warn limit indicator on the MDM and D&C outputs are monitored for the correct responses.

7.3.1.2.5 Antenna stabilization test

This portion consists of several tests. The drift rate in the inertial stabilization mode and the antenna drift while in the Orbiter stabilized mode are measured and verified to be within specification. The slew modes are verified by measuring the antenna slew rate for both fast and slow rates in the azimuth and elevation planes. Finally, the antenna is scanned about the -Z axis in a 12° cone.

7.3.1.2.6 Radar target track test

This test verifies radar target tracking in both angle-tracking and nonangle-tracking modes. The passive mode is used in both tests.

The Ku-band radar subsystem signal strength indicator is dynamically exercised by varying the input signal level. In addition, the transmitted signal strength indicator is characterized by measuring the response to all three transmitter power settings.

7.3.1.2.7 Radar antenna scan volume test

Proper response to invalid start scan commanding during GPC DESIGNATE, MANUAL, GPC ACQUISITION and AUTOTRACK antenna steering modes is verified. The operator then selects either the ambient scan volume test or the thermal vacuum scan volume test. These tests use an X-Y plotter to record the antenna scan trajectory for off-line analysis. Parameters to be verified off-line are: number of scan circles, scan volume, 30% scan overlap and scan time of one minute maximum. The thermal vacuum scan volume test consists of five scan cones for each of three scan centers. Scan centers (pitch, roll) are (0,0), (30,30) and (-30,-30). Search cones are approximately 60, 50, 40, 20 and 10°. The ambient scan volume test consists of a 10° scan cone centered at (0,0).

7.3.1.2.11 Radar target acquisition test

The radar target acquisition test module contains three test segments: nonscanning acquisition, the sidelobe test and the mainscan acquisition. This test module verifies that the radar subsystem will properly transition from acquisition to target track. A brief description of the three test segments in this module is as follows:

(1) Nonscanning acquisition. This test verifies that the radar system will detect and angle track a target placed within the 3 dB beamwidth. The operator selects the antenna pointing direction, the location of the target relative to the antenna, the mode (active or passive), and whether the target is at short or long range.

The range will determine the settling time of the acquisition loop. The antenna is not scanned during this test.

(2) Sidelobe test. The sidelobe logic of the radar operation is verified. The operator designates the location of the target relative to the antenna boresight. A default position for the target is available and is set to 2.5°.

The test is conducted in the GPC DESIGNATE mode rather than an angle-tracking mode. The nonangle-tracking mode will permit target track (i.e., range and range rate track) but would preclude the antenna servos from nulling out the target position. This enables the radar subsystem to determine that the target is in the sidelobe and provide a steady indication of this status.

(3) Mainscan acquisition. The mainscan acquisition tests the system for target lock-on when the scanning antenna encounters a target within the scan trajectory. The operator designates the scan center location, the target location relative to the scan center, and the scan volume.

There are only 10 scan volumes, and not all scan volumes need be employed; this choice is left to the operator.

Verification of target acquisition leading to track with all related Ku-band system designators (e.g., track, detect status bits) correctly responding will determine test acceptance.

7.3.1.2.12 Radar moving-target acquisition test

This test consists of a target moving inward toward the scan center as the antenna is scanning. Successful acquisition results in stopping the antenna scan and ending in target track. There are five test profiles that can be selected on the basis of test number, as listed below:

Test No.	Scan Volume (°)	Target Velocity (°/sec)
1	30	0.1
2	25	0.2
3	11	0.3
4	8	0.6
5	6	1.1

In each test, two signal levels maximum or minimum must be designated corresponding to a 1 square meter or 10,000 square meter target. A third quantity must also be given and allows for fine correction of the test signal conditioner panel RF output level. The value is specified in decibels of attenuation. A positive value decreases the signal level whereas a negative value increases it. Specifying 0 dB does not change the programmed levels.

7.3.1.2.13 Radar recovery time test

The test consists of the Ku-band system locking on to a moving target. Target eclipse takes place for a predetermined time interval; the target then reappears. The test observes whether or not reacquisition occurs.

The four selectable tests are listed below:

Test No.	Loss Time
1	0.1 sec
2	0.2 sec
3	0.3 sec
4	Operator designated

The target is at 12 nm with 1 square meter cross-section and moves normal to the line of sight. In addition to selecting the test number, the operator must specify the following parameters:

CF Correction factor for the RF signal level, given in decibels of attenuation

RB Range bias correction for test equipment, given in feet

V Target loss rate in °/sec; 2°/sec maximum.

7.3.1.2.14 Radar gimbal pointing control

The tests involve the Ku-band servo system capability to accurately point the antenna, hold the designated position and verify part of its dynamic response. In all tests, selected test locations are given. The operator has, in most of the tests, the option of designating the test location. The tests are partitioned into three sections and are described as follows:

(1) Gimbal pointing and stabilization test. There are four selectable positions to which the gimbals are designated, with an option for the operator to designate a fifth location. After reaching the designate, the position holding test can be selected in either the body stabilized or inertial stabilized mode. The test positions in the alpha-beta coordinates are:

1. 0, 0
2. 0, 30
3. 0, 60
4. -45, 45
5. Operator designated.

(2) Gimbal slew test. The test consists of measuring gimbal slew rates as the antenna moves between designates. Two types of designates are used. The difference is whether or not the wraparound logic is exercised. Straight slew has operator option of selecting the pointing designates.

(a) Gimbal straight slew test. Test position for alpha and beta (°) are:

Test	Initial Alpha	Initial Beta	Final Alpha	Final Beta
1	0	65	0	0
2	0	-85	0	0
3	Operator supplied			

(b) Gimbal slew test with wraparound logic involved. Wraparound primarily exercises the alpha gimbal with the beta gimbal held constant. Alpha moves from 145° to -205°.

Test No.	Beta (°)
1	0
2	60
3	75
4	-60
5	-85
6	Operator supplied

7.3.1.2.15 Radar angle track--servo convergence test

The servo convergence test will verify the radar servo loop bandwidth. Several parameters are supplied to define the test.

Test No.	Mode	Bandwidth (Hz)
1	Passive	0.12
2	Passive	0.075
3	Passive	0.027
4	Active	0.075
5	Active	0.027

The test numbers are selected in addition to the following:

CF — Correction factor for the RF signal level, given in decibels of attenuation

RB — Range bias correction for test equipment, given in feet

V — Target LOS rate in °/sec

A,B — Antenna location expressed in degrees

AR,BR — Target location relative to the antenna, expressed in degrees.

The angle error signals are recorded on a strip chart recorder or equivalent equipment.

7.3.1.2.16 Radar angle track--dynamic tracking test

There are two major tests. The first measures the Ku-band systems's capability to angle-track a target into the antenna pole locations. The second test verifies the capability of tracking a target accelerating normal to the line-of-sight (LOS). In the second test, the operator has the option of specifying the test parameters in addition to a preselected case.

7.3.1.2.17 Radar angle track--angle track statistics test

The angle-track statistics test derives statistical angle parameters when the Ku-band system is in radar angle-track. There are two tests, as follows:

(1) Static angle-track. Antenna is positioned at coordinates designated by operator. Angle-track is established. MDM and SAE angle data are collected (500 samples). Mean and 3-sigma values are derived.

(2) Dynamic angle-track. 500 samples of angle rate data from MDM are collected with the Ku-band system tracking a target moving with constant velocity. A baseline velocity of 0.06°/second can be selected. Other rates up to 0.5°/second can be designated by the operator.

7.3.2 Rockwell Specification versus the DSTE Test Module Matrix

After reviewing the 14 communications and 17 radar test modules, the next task was to compare the module capabilities to the Rockwell specification. Even though this task initially appeared to be straightforward, some problems developed.

The first problem is that TP32090-001 gives very general test descriptions. In the radar tests, for example, the system is initialized to the GPC DESIGNATE mode, but it is not clear whether or not the test module automatically switches to the GPC ACQUISITION mode in the course of the test. In order to determine the answer to this question, it would be necessary to review each software step for every test module. There is no convenient intermediate Hughes document between the software and TP3209-001.

The second problem is that the test modules were generated approximately two years ago, primarily for developmental testing. The modules were not intended to be used to verify system performance.

7.3.3 DSTE Sell-Off Procedures

The previously mentioned Hughes document TP32012-074 describes the test modules to be used for DSTE sell-off. There are a number of DSTE check-out tests but, essentially, Hughes is taking the ADL Ku-band system after the LRU's have passed their respective ATP's and connecting the ADL LRU's to the ESTL DSTE. Also, the ESTL LRU's will be connected to the ADL DSTE. The assumption is that, since the LRU's have passed their acceptance tests, if the same results are achieved using the ADL LRU's with the ESTL DSTE and vice-versa, the DSTE's must be functioning properly.

Hughes will be using two of the 14 communications test modules and four of the 17 radar test modules to conduct the DSTE sell-off. The sell-off modules are listed as follows:

1. COMMUNICATIONS MODE

   Forward Link Acquisition Time Test
   Communications Mode Target Acquisition and Track Test

2. RADAR MODE

   Radar Power Up/Down Consumption Test
   Antenna Obscuration Zone Test
   Antenna Stabilization Test
   Radar Target Track Test.

By examining the Rockwell specification versus the DSTE test module matrix, the two communications tests and the four radar tests simply do not exercise the Ku-band system or, for that matter, the DSTE to any great extent. Granted that many of the DSTE components had been used for the LRU ATP's, it is the opinion of Axiomatix that a more extensive sell-off procedure is required.

7.4. Conclusions/Recommendations

The 31 test modules provide a good cross-section of tests with which to exercise the Ku-band system. However, based on the test modules currently available, the DSTE is very limited when being used to verify the Ku-band system performance as per the Rockwell specification. Additional test modules or utilizing the MCP mode would greatly increase the present capabilities.

Because reviewing the software in great detail would be too costly and time-consuming and because the modules are for developmental testing, some interpretation and judgments were used in generating the matrix. While Hughes may take exceptions to the matrix in some areas, Axiomatix feels that the matrix is fairly representative of the test module capabilities.

The matrix is shown in section 7.5 but, before discussing it, some explanations are required. The Rockwell specification paragraphs are listed along the left-hand side and the communications or radar tests are listed across the top. Listed along the right-hard side are the verification methods required per the Rockwell specification. Of special interest is the column just to the left of the test module columns which indicates whether or not the test module completely tests a particular Rockwell paragraph.

The reader must be cautioned that, because numerous asterisks appear in the "not completely tested by the development test module" column, this does not mean that requirement never gets tested. It simply means that the test module itself does not completely test the paragraph.

In reviewing the matrix, it is evident that the test modules do not completely verify system performance with respect to the Rockwell specification. It must be noted, however, that the DSTE may be placed in a manual mode.

This manual mode is accomplished by loading the Manual Control Program (MCP) into the computer; now the test operator is allowed to manually key-in test parameters and commands. In conversations with various personnel, it has been stated that, with this manual mode, the DSTE can simulate almost any Ku-band function or operating situation.

Since the test modules were never really intended to be used to verify the entire system performance, the manual mode or, perhaps, additional test modules should be explored in more detail. Unfortunately, at this time, there appears to be no document which fully describes the DSTE capabilities. While the present test modules seem inadequate to fully verify system performance as required per the Rockwell specification, generating new modules or utilizing the MCP so that parameters and commands may be input manually would increase the present DSTE performance capabilities.

It is recommended that a DSTE capabilities document be generated by Hughes which discusses in detail the DSTE performance characteristics. With this document, the DSTE end users, NASA and Rockwell, could more easily generate new tests to meet specific needs.

It is further recommended that TP32090-001, "Subsystem Development Test Procedure for the Ku-Band Integrated Radar/Communications Equipment," be expanded to include a more detailed test description. The reader and test module user will now have a better understanding as to exactly which Ku-band modes are really tested by the module.

A major area of concern is the DSTE sell-off procedure. In Axiomatix's opinion, the present procedure is inadequate, and it is recommended that a more detailed sell-off procedure be used.

7.5 Ku-Band Radar Subsystem Tests Cross-Reference Matrix

Rockwell Specification Paragraph RL409-0025 Rev B	RADAR Specification Title/Test Criteria	Not Completely Tested by Dev. Test Modules	Radar Power Up/Down Consumption Test	Radar Self-Test	Antenna Stow/ Unstow Test	Antenna Obscurat'n Zone Test	Antenna Stabiliza-tion Test	Radar Target Track Test	Radar Antenna Scan Volume Test	Radar Waveform Test	Radar Range Accuracy Test	Radar Range Rate Accuracy Test	Radar Target Acquisition Test	Radar Moving Target Acquisition Test	Radar Recovery Time Test	Radar Gimbal Pointing Test	Radar Angle Track-Servo Convergence Test	Radar Angle Track-Dynam. Track'g Test	Radar Angle Track-Angle Track Statistics Test	N/A	To Be Verified By Analysis	To Be Verified By Assessment	To Be Verified By Test
3.2.1.3	Rendezvous Radar Requirements	•						X			X	X	X	X		X					X	X	X
3.2.1.3.1	Pass. Targ. Sig. Decorrelation Enhancement	•																			X	X	X
3.2.1.3.2	Antenna Angle Servo Requirements	•															X	X	X		X	X	X
3.2.1.3.2.1	Target Inertial Angle Rate for Detection																				X	X	X
3.2.1.3.2.1.1	Target Motion Direction Constrained	•																			X	X	X
3.2.1.3.2.1.2	Target Motion Direction Unconstrained	•																			X	X	X
3.2.1.3.2.2	Target Inertial Angle Rate for Tracking																			X			
	• 0 to 0.5°/second																		X		X	X	X
	• 0.5 to 1.1°/second																	X			X	X	X
3.2.1.3.3	Radar Operating Modes	•					X				X	X	X			X			X		X	X	X
3.2.1.3.3.1	GPC Acquisition Mode																			X			
	• GPC Designates used for Antenna Position'g													X		X			X		X	X	X
	• Automatic Angle Track							X					X								X	X	X
	• Variable Search Volume								X				X								X	X	X
	• Output Range and Range Rate Data	•																			X	X	X
	• Output Range & Range Rate Data-Good Flag													X	X						X	X	X
	• Output Angle Data (Gimbal) Roll; Pitch							X													X	X	X
	• Output Angle Rate Data, Roll; Pitch							X													X	X	X
	• Output Angle & Angle Rate Data-Good Flag												X	X	X				X		X	X	X
	• Inertial Stabilization	•																			X	X	X
	• Sidelobe Lock Test	•																			X	X	X
3.2.1.3.3.2	GPC Designate Mode																			X			
	• GPC Designates used for Antenna Position'g															X					X	X	X
	• Output Range and Range Rate Data										X	X									X	X	X
	• Output Range & Range Rate Data-Good Flag										X	X									X	X	X
	• Output Angle Data (Gimbal) Roll; Pitch															X			X		X	X	X
	• Inertial Stabilization						X									X					X	X	X
	• Body Axis Stabilization															X					X	X	X
3.2.1.3.3.3	Manual Mode																			X			
	• Respond-to-Slew Switches						X														X	X	X
	• Output Range and Range Rate Data	•																			X	X	X
	• Output Range & Range Rate Data-Good Flag	•																			X	X	X
	• Output Angle Data (Gimbal) Roll; Pitch	•																			X	X	X
	• Body Axis Stabilization						X														X	X	X

KU-BAND RADAR SUBSYSTEM TESTS CROSS-REFERENCE MATRIX

Rockwell Specification Paragraph MC409-0025 Rev B	RADAR Specification Title/Test Criteria	Not Completely Tested by Dev. Test Modules	Radar Power Up/Down Consumption Test	Radar Self-Test	Antenna Stow/ Unstow Test	Antenna Obscurat'n Zone Test	Antenna Stabiliza-tion Test	Radar Target Track Test	Radar Antenna Scan Volume Test	Radar Waveform Test	Radar Range Accuracy Test	Radar Range Rate Accuracy Test	Radar Target Acquisition Test	Radar Moving Target Acquisition Test	Radar Recovery Time Test	Radar Gimbal Pointing Test	Radar Angle Track-Servo Convergence Test	Radar Angle Track-Dynam. Track'g Test	Radar Angle Track-Angle Track Statistics Test	N/A	To Be Verified By Analysis	To Be Verified By Assessment	To Be Verified By Test
3.2.1.3.3.4	Auto Mode																			X			
	• Automatic Angle Tracking	*																			X	X	X
	• Programmed Search	*																			X	X	X
	• Respond-to-Slew Switches	*																			X	X	X
	• Output Range and Range Rate Data	*																			X	X	X
	• Output Range & Range Rate Data-Good Flag	*																			X	X	X
	• Output Angle Data (Gimbal) Roll; Pitch	*																			X	X	X
	• Output Angle Rate Data, Roll; Pitch	*																			X	X	X
	• Output Angle Data-Good Flag	*																			X	X	X
	• Output Angle Rate Data-Good Flag	*																			X	X	X
	• Inertial Stabilization	*																			X	X	X
	• Sidelobe Lock Test	*																			X	X	X
3.2.1.3.4	Vectored Search	*							X				X								X	X	X
3.2.1.3.4.1	Target Coordinate Designation																			X			
3.2.1.3.4.2	Search Volume																			X			
	• GPC Acquisition Mode	*							X														
	• GPC Designate Mode (Scan Inhibited)								X												X	X	X
	• Manual Mode	*																			X	X	X
	• Auto Mode	*																			X	X	X
3.2.1.3.4.3	Search Time																				X	X	X
3.2.1.3.4.4	Angle Rates During Search	*																			X	X	X
3.2.1.3.4.5	Search Angle Scan Mechanization	*							X					X							X	X	X
3.2.1.3.4.5.1	Search Angle Scan Pattern	*							X												X	X	X
3.2.1.3.4.5.2	Search Scan Angular Velocity Limit	*																			X	X	X
3.2.1.3.4.6	Manual Target Coordinate Designation	*																				X	X
3.2.1.3.4.6.1	Auto Mode																			X			
	• Search Initiation by Manual Control	*																			X	X	X
	• Auto. Target Detect. & Acq. following Manual Designate or Search Initiate	*																			X	X	X
	• Auto. Target Track'g Following Detect.	*																			X	X	X
	• Inertial Space Angular Drift Rate 4°/Min. for Specified Conditions	*						X													X	X	X

KU-BAND RADAR SUBSYSTEM TESTS CROSS-REFERENCE MATRIX

Rockwell Specification Paragraph MC409-0025 Rev B	RADAR Specification Title/Test Criteria	Not Completely Tested by Dev. Test Modules	Radar Power Up/Down Consumption Test	Radar Self-Test	Antenna Stow/ Unstow Test	Antenna Obscurat'n Zone Test	Antenna Stabilization Test	Radar Target Track Test	Radar Antenna Scan Volume Test	Radar Waveform Test	Radar Range Accuracy Test	Radar Range Rate Accuracy Test	Radar Target Acquisition Test	Radar Moving Target Acquisition Test	Radar Recovery Time Test	Radar Gimbal Pointing Test	Radar Angle Track-Servo Convergence Test	Radar Angle Track-Dynam. Track'g Test	Radar Angle Track-Angle Track Statistics Test	N/A	To Be Verified By Analysis	To Be Verified By Assessment	To Be Verified By Test
3.2.1.3.4.6.2	Manual Mode																			X			
	• Auto Angle Track'g Servos Disabled								X												X	X	X
	• After Target Detection, Auto Target Tracking in Range and Range Rate	*																			X	X	X
	• Antenna Position in Orbiter Coordinates	*																			X	X	X
	• ±0.3° when Orbiter coordinates selected						X																
	• Angle Data Output to GPC and D&C	*																			X	X	X
3.2.1.3.5	Prob. of Detection & False Alarm Rate	*																			X	X	X
3.2.1.3.5.1	Ground Clutter	*																			X	X	X
3.2.1.3.6	Acquisition																			X			
	• GPC Acquisition/Auto Modes	*											X	X							X	X	X
	• GPC Designate/Manual Modes	*											X								X	X	X
3.2.1.3.6.1	Auxiliary Search								X													X	X
3.2.1.3.6.2	Automatic Track							X					X									X	X
3.2.1.3.7	Radar Operation Interruption	*																			X	X	X
3.2.1.3.8	Radar Parameter Measurement Limits										X	X									X	X	X
3.2.1.3.9	Radar Parameter Measurement Accuracies										X	X									X	X	X
3.2.1.3.9.1	Radar Param. Meas. Accur. Convergence Time												X		X						X	X	X
3.2.1.3.9.2	Meas. Accuracies & Output Data Update Rate	*																			X	X	X
3.2.1.3.10	Break-Track Condition							X					X		X							X	X
3.2.1.3.11	Radar System Power-Up/Down Procedure		X																			X	X
3.2.1.3.12	Radar System Operation Sequence	*							X				X									X	X
3.2.1.3.13	Received Signal Strength Indication							X														X	X
3.2.1.3.14	Radar System Design Requirements																			X			
3.2.1.3.14.1	Transmitter	*								X											X	X	X
3.2.1.3.14.2	Microwave Losses	*																			X	X	X

KU-BAND RADAR SUBSYSTEM TESTS CROSS-REFERENCE MATRIX

Rockwell Specification Paragraph MC409-0025 Rev B	RADAR Specification Title/Test Criteria	Not Completely Tested by Dev. Test Modules	Radar Power Up/Down Consumption Test	Radar Self-Test	Antenna Stow/ Unstow Test	Antenna Obscuration Zone Test	Antenna Stabilization Test	Radar Target Track Test	Radar Antenna Scan Volume Test	Radar Waveform Test	Radar Range Accuracy Test	Radar Range Rate Accuracy Test	Radar Target Acquisition Test	Radar Moving Target Acquisition Test	Radar Recovery Time Test	Radar Gimbal Pointing Test	Radar Angle Tracking Servo Convergence Test	Radar Angle Tracking Dynamic Tracking Test	Radar Angle Track Angle Track Statistics Test	N/A	To Be Verified By Analysis	To Be Verified By Assessment	To Be Verified By Test
3.2.1.3.14.3	Antenna	*																				X	X
3.2.1.3.14.3.1	Antenna Error Detection																					X	
3.2.1.3.14.3.2	Antenna Beam Sidelobe Lock-On																					X	
3.2.1.3.14.3.3	Stabilization						X														X	X	X
3.2.1.3.14.3.4	Polarization									X											X	X	X
3.2.1.3.14.3.5	Gimbal Arrangements																					X	
3.2.1.3.14.3.6	Antenna Control Servos																					X	
3.2.1.3.14.4	Receiver																					X	
3.2.1.3.14.4.1	Receive Signal Dynamic Range	*																			X	X	X
3.2.1.3.14.4.2	IF Preamplifiers	*																			X	X	X
3.2.1.3.14.4.3	Operating Modes Compatibility	*																			X	X	X
3.2.1.3.15	Radar Self-Test			X																	X	X	X
3.2.1.3.16	Radar System Power Consumption		X																		X	X	X
3.2.1.3.16.1	Power Consumption in Operating Modes and Conditions		X																		X	X	X
3.2.1.3.16.2	LRU Heater Power		X																		X	X	X

KU-BAND RADAR SUBSYSTEM TESTS CROSS-REFERENCE MATRIX

Rockwell Specification Paragraph MC409-0025 Rev B	COMMUNICATIONS Specification Title/Test Criteria	Not Completely Tested by Dev. Test Modules	Comm. Power Up/Down Consumption	Comm. Subsystem Slant Range	Forward Link Signal Strength Test	Forward Link Tracking Threshold Test	Forward Link Acquisition Time Test	Forward Link BER Test	Functional Test (Return Link)	BER Test (Return Link)	Comm. Mode Antenna Stow/Unstow Test	Comm. Mode Obscuration Zone Test	Comm. Mode Antenna Stability Test	Comm. Mode Antenna Slew Test	Comm. Mode Target Acq. Track Test	Comm. Antenna Scan Volume Test	N/A	To Be Verified by Analysis	To Be Verified By Assessment	To Be Verified By Test
3.2.1.2	Communication Subsystem Performance	*		X											X	X			X	X
3.2.1.2.1	Angle Search, Signal Detection and Track Requirements	*		X											X				X	X
3.2.1.2.1.1	TDRS Forward Link Signal						X												X	X
3.2.1.2.1.2	Antenna Angle Coverage for Communications																X			
3.2.1.2.1.2.1	Acquisition Coverage											X						X	X	X
3.2.1.2.1.2.2	Tracking Coverage											X						X	X	X
3.2.1.2.1.3	Orbiter-TDRS Link Acquisition & Handover																X			
3.2.1.2.1.3.1	Link Acquisition Mode Definition	*																X	X	X
3.2.1.2.1.3.1.1	Primary Acquisition Mode	*																X	X	X
3.2.1.2.1.3.1.2	Alternate Acquisition	*																X	X	X
3.2.1.2.1.3.2	Handover Requirements	*																X	X	X
3.2.1.2.1.3.2.1	Return Link Data																X			
3.2.1.2.1.3.2.2	Data Transfer Sequencing	*																X	X	X
3.2.1.2.1.3.3	Detection IF Bandwidth	*																X	X	X
3.2.1.2.1.3.4	Detection Requirements	*	X												X	X		X	X	X
3.2.1.2.1.3.4.1	Signal Uncertainties for Detection																	X	X	
3.2.1.2.1.3.4	Link Acquisition Time																X			
3.2.1.2.1.3.5.1	TDRS Signal Acquisition	*					X									X			X	X
3.2.1.2.1.3.5.2	Signal Processing Time						X												X	X
3.2.1.2.1.4	Antenna Control Servos	*													X	X		X	X	X
3.2.1.2.1.4.1	Open-Loop Operation	*																X	X	X
3.2.1.2.1.4.1.1	Angle Search															X			X	X
3.2.1.2.1.4.1.2	Search Scan Mechanization															X		X	X	X
3.2.1.2.1.4.1.3	GPC Designate Tracking	*				X									X				X	X
3.2.1.2.1.4.1.4	Wide-Angle Antenna Characteristics	*																X	X	X
3.2.1.2.1.4.2	Closed-Loop Operation																X			

KU-BAND RADAR SUBSYSTEM TESTS CROSS-REFERENCE MATRIX

Rockwell Specification Paragraph MC409-0025 Rev B	COMMUNICATIONS Specification Title/Test Criteria	Not Completely Tested by Dev. Test Modules	Comm. Power Up/Down Consumption	Comm. Subsystem Slant Range	Forward Link Signal Strength Test	Forward Link Tracking Threshold Test	Forward Link Acquisition Time Test	Forward Link BER Test	Functional Test (Return Link)	BER Test (Return Link)	Comm. Mode Antenna Stow/Unstow Test	Comm. Mode Obscuration Zone Test	Comm. Mode Antenna Stability Test	Comm. Mode Antenna Slew Test	Comm. Mode Target Acq. Track Test	Comm. Antenna Scan Volume Test	N/A	To Be Verified By Analysis	To Be Verified By Assessment	To Be Verified By Test
3.2.1.2.1.4.2.1	Angle Tracking Accuracy												X		X			X	X	X
3.2.1.2.1.4.2.2	Angle Tracking Limitations												X	X	X			X	X	X
3.2.1.2.1.4.2.3	Break Track Condition	*																X	X	X
3.2.1.2.2	Forward Link Data Subsystem	*					X												X	X
3.2.1.2.2.1	Forward Link Data Subsystem Characteristics	*					X												X	X
3.2.1.2.2.1.1	Forward Link Subsystem Characteristics	*						X											X	X
3.2.1.2.2.2	Data Characteristics																X			
3.2.1.2.2.2.1	Information Signal Characteristics																X			
3.2.1.2.2.2.1.1	Mode 1 Forward Link Data	*																X	X	X
3.2.1.2.2.2.1.2	Mode 2 Forward Link Data	*																X	X	X
3.2.1.2.2.2.2	Spread Spectrum						X											X	X	X
3.2.1.2.2.2.3	Unspread Spectrum						X											X	X	X
3.2.1.2.2.3	Data Output	*				X	X												X	X
3.2.1.2.2.4	Data Quality Estimation	*			X	X	X											X	X	X
3.2.1.2.2.4.1	Data Quality Estimate Duration	*			X	X	X											X	X	X
3.2.1.2.2.5	Forward Link Performance	*			X	X	X	X										X	X	X
3.2.1.2.3	Ku-Band Comm. Transmit Subsystem																X			
3.2.1.2.3.1	Transmit Subsystem Description	*							X										X	X
3.2.1.2.3.2	Return Link Data Requirements	*							X									X	X	X
3.2.1.2.3.2.1	Mode 1 Data Requirements	*																X	X	X
3.2.1.2.3.2.2	Mode 2 Data Requirements	*																X	X	X
3.2.1.2.3.2.3	Data Source Selection	*							X										X	X
3.2.1.2.3.3	Return Link Characteristics																X			
3.2.1.2.3.3.1	Modulation Type																		X	
3.2.1.2.3.3.2	Data Channelization	*																X	X	X
3.2.1.2.3.3.3	Return Link Operational Characteristics	*							X									X	X	X
3.2.1.2.3.3.4	Return Link Data Throughput	*																X	X	X

KU-BAND RADAR SUBSYSTEM TESTS CROSS-REFERENCE MATRIX

Rockwell Specification Paragraph MC409-0025 Rev B	COMMUNICATIONS Specification Title/Test Criteria	Not Completely Tested by Dev. Test Modules	Comm. Power Up/Down Consumption Test	Comm. Subsystem Slant Range	Forward Link Signal Strength Test	Forward Link Tracking Threshold Test	Forward Link Acquisition Time Test	Forward Link BER Test	Functional Test (Return Link)	BER Test (Return Link)	Comm. Mode Antenna Stow/Unstow Test	Comm. Mode Obscuration Zone Test	Comm. Mode Antenna Stability Test	Comm. Mode Antenna Slew Test	Comm. Mode Target Acq. Track Test	Comm. Antenna Scan Volume Test	N/A	To Be Verified By Analysis	To Be Verified By Assessment	To Be Verified By Test
3.2.1.2.3.3.4.1	Digital Data Throughput	*																X	X	X
3.2.1.2.3.3.4.1.1	Bit Transition Density	*																X	X	
3.2.1.2.3.3.4.1.2	Data Asymmetry	*							X									X	X	X
3.2.1.2.3.3.4.2	Analog Data Throughput	*																X	X	X
3.2.1.2.3.4	Modulation																		X	
3.2.1.2.3.4.1	Mode 1 Modulation	*																	X	X
3.2.1.2.3.4.2	Mode 2 Modulation	*																	X	X
3.2.1.2.3.4.3	Analog Data via Channel 2	*																	X	X
3.2.1.2.3.4.4	Unmodulated Carrier																		X	X
3.2.1.2.3.5	Data Degradation ~~Deleted~~																			
3.2.1.2.3.5.1	Mode 1 Degradation																			
3.2.1.2.3.5.2	Mode 2 Degradation																			
3.2.1.2.4	Communications B Subsystem																		X	
3.2.1.2.5	Comm. System Self-Test ~~Deleted~~																			
3.2.1.2.6	Comm. System Power Consumption		X																	

KU-BAND RADAR SUBSYSTEM TESTS CROSS-REFERENCE MATRIX

8.0 SYSTEM TEST EVALUATION

8.1 Introduction

As per NASA Contract NAS 9-15795A, Task 3, this section reviews and evaluates the data obtained by Hughes Aircraft Company (HAC) during the Ku-band system testing. The Hughes testing involved verifying the performance of the Ku-band system, composed of the EA-1, EA-2, SPA and DA LRU's, by utilizing the system test equipment (STE).

To perform system testing, Hughes has manufactured three sets of test equipment. One set, the STE, will be retained by Hughes. The second and third sets, referred to as the deliverable system test equipment (DSTE), will be delivered to the Avionics Development Laboratory (ADL) at Rockwell, Downey, and to the Electronic System Test Laboratory (ESTL) at JSC, Houston, respectively.

The STE and ESTL DSTE are both the same configuration, whereas the ADL DSTE has a slightly different configuration. All three sets of test equipment are semiautomatic and computer controlled with a number of test programs, known as test modules, that may be loaded into the respective computers via a floppy disk. The reader should reference section 7.0 for a more detailed description of the DSTE and test module capabilities.

Hughes has also manufactured two sets of LRU's--one set for the ADL and the other set for the ESTL. This section will review the ADL Ku-band system tests as conducted with the STE by Hughes.

8.2 Approach

The system tests were based upon Hughes document TP32090-001, "Subsystem Development Test Procedure for the Ku-Band Integrated Radar/Communications Equipment," dated October 23, 1979. This test procedure and the 31 test modules it describes have previously been reviewed and the results disclosed in Section 7.0

The reader should also review section 8.5, which is composed of matrices comparing the Ku-band system requirements as detailed in Rockwell document MC409-0025, "Integrated Communications and Radar Equipment, Ku-Band," Rev. B with changes, dated July 21, 1978, to the 31 test modules described in TP32090-001. These matrices will provide the basis for the remainder of this report.

The approach involved discussions with cognizant Rockwell and Hughes personnel to determine which tests from TP32090-001 and which additional tests were used by Hughes for system verification. After ascertaining which tests were conducted, the section 7.5 matrices were used to determine the Rockwell Rev. B specification paragraphs substantiated by Hughes.

8.3 Findings

Hughes document TP32090-001, along with the test modules, were originally developed for system development tests and were never intended for system verification. Once system testing was required of Hughes, the already developed test modules provided a number of reasonable system tests. To prepare new test modules specifically designed to verify the Rockwell Rev. B specification would have been costly and time consuming.

The initial plan for system verification, therefore, was to run the 31 test modules, 14 communications mode tests and 17 radar mode tests, as outlined in TP32090-001. As the tests progressed, a number of software and hardware problems developed with the test equipment and, in addition, some LRU problems also developed. Because of these problems, the number of tests were reduced by the mutual consent of Rockwell and Hughes personnel. Also, some tests were conducted manually instead of computer controlling the STE with a test module.

A total of eight communications mode test modules, six radar mode test modules and six additional tests were used for system verification.

8.3.1 Communications Mode System Verification Test Modules

As previously mentioned, eight of the 14 communications mode test modules were used. Detailed test descriptions are included in Appendix A and, therefore, the eight tests will be listed as follows with the appropriate Section 7.0 reference paragraphs:

		Reference Paragraph
1.	Communications power up/down consumption	7.3.1.1.1
2.	Forward link signal strength test	7.3.1.1.3
3.	Forward link tracking threshold test	7.3.1.1.4
4.	Forward link BER tests	7.3.1.1.6
5.	BER test (return link)	7.3.1.1.8
6.	Communications mode obscuration zone test	7.3.1.1.10
7.	Communications mode antenna stability test	7.3.1.1.11
8.	Communications antenna scan volume	7.3.1.1.14

The ADL LRU's eventually passed the eight communications mode tests; however, some tests were modified. Because of problems with the STE SPA data generator, both the forward and return link BER tests were changed. Tests equivalent to those described in paragraphs 7.3.1.1.6 and 7.3.1.1.8, were conducted using a Hewlett-Packard data generator and the BER detector.

The forward link tracking threshold test, as discussed in paragraph 7.3.1.1.4, was not completely run. Only Costas loop data was gathered, with no PN loop threshold data being collected.

The communication tests used for system verification have been identified on pages 5 - 7 of section 8.5, the Ku-band subsystem tests cross-reference matrix. This matrix references the test modules to the Rockwell Rev. B specification.

8.3.2 Radar Mode System Verification Test Modules

As stated earlier, six of 17 radar mode tests were utilized. Detailed test descriptions are included in section 7.5 and therefore the six tests will be listed as follows with the appropriate section 7.0 reference paragraphs.

		Reference Paragraph
1.	Radar power up/down consumption test	7.3.1.2.1
2.	Antenna obscuration zone test	7.3.1.2.4
3.	Antenna stabilization test	7.3.1.2.5

4.	Radar waveform test	7.3.1.2.8
5.	Radar range accuracy test	7.3.1.2.9
6.	Radar range rate accuracy test	7.3.1.2.10

The ADL LRU's passed the six radar mode tests. There were some initial problems with the range and range rate tests but the LRU's passed the tests after the STE was placed in the manual mode. In addition, the radar waveform tests were also conducted manually.

The radar tests used for system verification have been identified on pages 1-4 of section 8.5. Notice that no angle-tracking tests were performed since the new servo design has not been implemented.

8.3.3 Additional System Verification Tests

Besides the eight communications mode and six radar mode tests, six additional tests were also conducted. While no definitive test procedure exists at this time, each test will be briefly described as follows:

1. The power consumption of each LRU while in various system operating modes was measured.

2. The ability to hold track in the active mode with a target at 300 nmi accelerating directly towards the system was verified.

3. In the passive mode, the target size was changed in a step function manner to determine the change magnitude required to break track.

4. With the system in angle tracking, a small jerk in α or β was introduced to determine the system response.

5. Proper TWT bypass operation was substantiated.

6. The system was placed in AUTOTRACK and proper scan and acquisition were ascertained.

Tests 2 through 6 were conducted primarily out of curiosity by the test personnel to observe the system response. Hughes is presently documenting these test results and producing a more definitive test procedure for future use.

8.4 Conclusions/Recommendations

As already mentioned in Section 7.0, the 31 test modules provide a good cross-section of tests with which to exercise the Ku-band system, but these tests are very limited when used to verify the Rockwell Rev. B specification By examining the matrices in section 8.5, the number of Rev. B paragraphs actually substantiated during system tests may be determined.

Because of the existing servo problem, no radar mode target acquisition, antenna scan volume, target track or angle track tests and no communications mode target acquisition, forward link acquisition time or slew tests were conducted. Additionally, while the Costas loop tracking threshold was measured, the PN tracking threshold was not determined.

If compliance to the Rockwell Rev. B specification was to have been confirmed during system tests, then the tests were very superficial since only a small number of Rev. B paragraphs were verified, as shown in the section 8.5 matrices. If the purpose of the system tests was to gain additional confidence that the system was functioning, the tests served their purpose.

It is Axiomatix's opinion that, at some time, compliance to the Rockwell Rev. B specification must be demonstrated, and the longer it takes for this demonstration, the more potential exists for serious system problems. It is recommended that additional test modules be generated for the STE and DSTE's which are capable of specification compliance verification.

Once the present servo problem has been resolved, it will be imperative to conduct detailed system tests immediately to determine that the new servo functions properly. It is recommended that the servo redesign and testing be closely monitored since servo performance is so critical to the system operation.

8.5 Ku-Band Radar Subsystem Tests Cross-Reference Matrix

Rockwell Specification Paragraph MC409-0025 Rev B	RADAR Specification Title/Test Criteria	Not Completely Tested by Dev. Test Modules	Radar Power Up/Down Consumption Test	Radar Self-Test	Antenna Stow/ Unstow Test	Antenna Obscurat'n Zone Test	Antenna Stabiliza-tion Test	Radar Target Track Test	Radar Antenna Scan Volume Test	Radar Waveform Test	Radar Range Accuracy Test	Radar Range Rate Accuracy Test	Radar Target Acquisition Test	Radar Moving Target Acquisition Test	Radar Recovery Time Test	Radar Gimbal Pointing Test	Radar Angle Track-Servo Converg. Test	Radar Angle Track-Dynam. Track'g Test	Radar Angle Track-Angle Track Statistics Test	N/A	To Be Verified By Analysis	To Be Verified By Assessment	To Be Verified By Test
	Modules used for system tests		X			X	X			X	X	X											
3.2.1.3	Rendezvous Radar Requirements	*						X			X	X	X	X		X					X	X	X
3.2.1.3.1	Pass. Targ. Sig. Decorrelation Enhancement	*																			X	X	X
3.2.1.3.2	Antenna Angle Servo Requirements	*															X	X	X		X	X	X
3.2.1.3.2.1	Target Inertial Angle Rate for Detection																				X	X	X
3.2.1.3.2.1.1	Target Motion Direction Constrained	*																			X	X	X
3.2.1.3.2.1.2	Target Motion Direction Unconstrained	*																			X	X	X
3.2.1.3.2.2	Target Inertial Angle Rate for Tracking																			X			
	• 0 to 0.5°/second																		X		X	X	X
	• 0.5 to 1.1°/second																	X			X	X	X
3.2.1.3.3	Radar Operating Modes	*					X				X	X	X			X			X		X	X	X
3.2.1.3.3.1	GPC Acquisition Mode																			X			
	• GPC Designates used for Antenna Position'g													X		X			X		X	X	X
	• Automatic Angle Track							X					X								X	X	X
	• Variable Search Volume								X				X								X	X	X
	• Output Range and Range Rate Data	*																			X	X	X
	• Output Range & Range Rate Data-Good Flag													X	X						X	X	X
	• Output Angle Data (Gimbal) Roll; Pitch							X													X	X	X
	• Output Angle Rate Data, Roll; Pitch							X													X	X	X
	• Output Angle & Angle Rate Data-Good Flag												X	X	X				X		X	X	X
	• Inertial Stabilization	*																			X	X	X
	• Sidelobe Lock Test	*																			X	X	X
3.2.1.3.3.2	GPC Designate Mode																			X			
	• GPC Designates used for Antenna Position'g															X					X	X	X
	• Output Range and Range Rate Data										X	X									X	X	X
	• Output Range & Range Rate Data-Good Flag										X	X									X	X	X
	• Output Angle Data (Gimbal) Roll; Pitch															X			X		X	X	X
	• Inertial Stabilization						X									X					X	X	X
	• Body Axis Stabilization															X					X	X	X
3.2.1.3.3.3	Manual Mode																			X			
	• Respond-to-Slew Switches						X														X	X	X
	• Output Range and Range Rate Data	*																			X	X	X
	• Output Range & Range Rate Data-Good Flag	*																			X	X	X
	• Output Angle Data (Gimbal) Roll; Pitch	*																			X	X	X
	• Body Axis Stabilization						X														X	X	X

KU-BAND RADAR SUBSYSTEM TESTS CROSS-REFERENCE MATRIX

Rockwell Specification Paragraph MC409-0025 Rev B	RADAR Specification Title/Test Criteria	Not Completely Tested by Dev. Test Modules	Radar Power Up/Down Consumption Test	Radar Self-Test	Antenna Stow/ Unstow Test	Antenna Obscurat'n Zone Test	Antenna Stabilization Test	Radar Target Track Test	Radar Antenna Scan Volume Test	Radar Waveform Test	Radar Range Accuracy Test	Radar Range Rate Accuracy Test	Radar Target Acquisition Test	Radar Moving Target Acquisition Test	Radar Recovery Time Test	Radar Gimbal Pointing Test	Radar Angle Track-Servo Convergence Test	Radar Angle Track-Dynam. Track'g Test	Radar Angle Track-Angle Track Statistics Test	N/A	To Be Verified By Analysis	To Be Verified By Assessment	To Be Verified By Test
	Modules used for system tests		X			X	X			X	X	X											
3.2.1.3.3.4	Auto Mode																			X			
	• Automatic Angle Tracking	*																			X	X	X
	• Programmed Search	*																			X	X	X
	• Respond-to-Slew Switches	*																			X	X	X
	• Output Range and Range Rate Data	*																			X	X	X
	• Output Range & Range Rate Data-Good Flag	*																			X	X	X
	• Output Angle Data (Gimbal) Roll; Pitch	*																			X	X	X
	• Output Angle Rate Data, Roll; Pitch	*																			X	X	X
	• Output Angle Data-Good Flag	*																			X	X	X
	• Output Angle Rate Data-Good Flag	*																			X	X	X
	• Inertial Stabilization	*																			X	X	X
	• Sidelobe Lock Test	*																			X	X	X
3.2.1.3.4	Vectored Search	*							X				X								X	X	X
3.2.1.3.4.1	Target Coordinate Designation																			X			
3.2.1.3.4.2	Search Volume																			X			
	• GPC Acquisition Mode	*							X														
	• GPC Designate Mode (Scan Inhibited)								X												X	X	X
	• Manual Mode	*																			X	X	X
	• Auto Mode	*																			X	X	X
3.2.1.3.4.3	Search Time																				X	X	X
3.2.1.3.4.4	Angle Rates During Search	*																			X	X	X
3.2.1.3.4.5	Search Angle Scan Mechanization	*							X					X							X	X	X
3.2.1.3.4.5.1	Search Angle Scan Pattern	*							X												X	X	X
3.2.1.3.4.5.2	Search Scan Angular Velocity Limit	*																			X	X	X
3.2.1.3.4.6	Manual Target Coordinate Designation	*																				X	X
3.2.1.3.4.6.1	Auto Mode																			X			
	• Search Initiation by Manual Control	*																			X	X	X
	• Auto. Target Detect. & Acq. following Manual Designate or Search Initiate	*																			X	X	X
	• Auto. Target Track'g Following Detect.	*																			X	X	X
	• Inertial Space Angular Drift Rate 4°/Min. for Specified Conditions	*						X													X	X	X

KU-BAND RADAR SUBSYSTEM TESTS CROSS-REFERENCE MATRIX

Rockwell Specification Paragraph MC409-0025 Rev B	RADAR Specification Title/Test Criteria	Not Completely Tested by Dev. Test Modules	Radar Power Up/Down Consumption Test	Radar Self-Test	Antenna Stow/ Unstow Test	Antenna Obscurat'n Zone Test	Antenna Stabilization Test	Radar Target Track Test	Radar Antenna Scan Volume Test	Radar Waveform Test	Radar Range Accuracy Test	Radar Range Rate Accuracy Test	Radar Target Acquisition Test	Radar Moving Target Acquisition Test	Radar Recovery Time Test	Radar Gimbal Pointing Test	Radar Angle Track-Servo Convergence Test	Radar Angle Track-Dynam. Track'g Test	Radar Angle Track-Angle Track Statistics Test	N/A	To Be Verified By Analysis	To Be Verified By Assessment	To Be Verified By Test
	Modules used for system tests		X			X	X			X	X	X											
3.2.1.3.4.6.2	Manual Mode																			X			
	• Auto Angle Track'g Servos Disabled								X												X	X	X
	• After Target Detection, Auto Target Tracking in Range and Range Rate	•																			X	X	X
	• Antenna Position in Orbiter Coordinates	•																			X	X	X
	• ±0.3° when Orbiter coordinates selected						X																
	• Angle Data Output to GPC and D&C	•																			X	X	X
3.2.1.3.[illegible]	Prob. of Detection & False Alarm Rate	•																			X	X	X
3.2.1.3.5.1	Ground Clutter	•																			X	X	X
3.2.1.3.6	Acquisition																			X			
	• GPC Acquisition/Auto. Modes	•											X	X							X	X	X
	• GPC Designate/Manual Modes	•											X								X	X	X
3.2.1.3.6.1	Auxiliary Search								X													X	X
3.2.1.3.6.2	Automatic Track							X					X									X	X
3.2.1.3.7	Radar Operation Interruption	•																			X	X	X
3.2.1.3.8	Radar Parameter Measurement Limits										X	X									X	X	X
3.2.1.3.9	Radar Parameter Measurement Accuracies										X	X									X	X	X
3.2.1.3.9.1	Radar Param. Meas. Accur. Convergence Time												X		X						X	X	X
3.2.1.3.9.2	Meas. Accuracies & Output Data Update Rate	•																			X	X	X
3.2.1.3.10	Break-Track Condition							X					X		X							X	X
3.2.1.3.11	Radar System Power-Up/Down Procedure		X																			X	X
3.2.1.3.12	Radar System Operation Sequence	•							X				X									X	X
3.2.1.3.13	Received Signal Strength Indication							X														X	X
3.2.1.3.14	Radar System Design Requirements																			X			
3.2.1.3.14.1	Transmitter	•								X											X	X	X
3.2.1.3.14.2	Microwave Losses	•																			X	X	X

KU-BAND RADAR SUBSYSTEM TESTS CROSS-REFERENCE MATRIX

Rockwell Specification Paragraph MC409-0025 Rev B	RADAR Specification Title/Test Criteria	Not Completely Tested by Dev. Test Modules	Radar Power Up/Down Consumption Test	Radar Self-Test	Antenna Stow/ Unstow Test	Antenna Obscurat'n Zone Test	Antenna Stabiliza-tion Test	Radar Target Track Test	Radar Antenna Scan Volume Test	Radar Waveform Test	Radar Range Accuracy Test	Radar Range Rate Accuracy Test	Radar Target Acquisition Test	Radar Moving Target Acquisition Test	Radar Recovery Time Test	Radar Gimbal Pointing Test	Radar Angle Track-Servo Convrg. Test	Radar Angle Track-Dynam. Track'g Test	Radar Angle Track Angle Track Statistics Test	N/A	To Be Verified By Analysis	To Be Verified By Assessment	To Be Verified By Test
	Modules used for system tests		X			X	X			X	X	X											
3.2.1.3.14.3	Antenna	*																				X	X
3.2.1.3.14.3.1	Antenna Error Detection																					X	
3.2.1.3.14.3.2	Antenna Beam Sidelobe Lock-On																					X	
3.2.1.3.14.3.3	Stabilization						X														X	X	X
3.2.1.3.14.3.4	Polarization									X											X	X	X
3.2.1.3.14.3.5	Gimbal Arrangements																					X	
3.2.1.3.14.3.6	Antenna Control Servos																					X	
3.2.1.3.14.4	Receiver																					X	
3.2.1.3.14.4.1	Receive Signal Dynamic Range	*																			X	X	X
3.2.1.3.14.4.2	IF Preamplifiers	*																			X	X	X
3.2.1.3.14.4.3	Operating Modes Compatibility	*																			X	X	X
3.2.1.3.15	Radar Self-Test			X																	X	X	X
3.2.1.3.16	Radar System Power Consumption		X																		X	X	X
3.2.1.3.16.1	Power Consumption in Operating Modes and Conditions		X																		X	X	X
3.2.1.3.16.2	LRU Heater Power		X																		X	X	X

KU-BAND RADAR SUBSYSTEM TESTS CROSS-REFERENCE MATRIX

Rockwell Specification Paragraph MC409-0025 Rev B	COMMUNICATIONS Specification Title/Test Criteria	Not Completely Tested by Dev. Test Modules	Comm. Power Up/Down Consumption	Comm. Subsystem Slant Range	Forward Link Signal Strength Test	Forward Link Tracking Threshold Test	Forward Link Acquisition Time Test	Forward Link BER Test	Functional Test (Return Link)	BER Test (Return Link)	Comm. Mode Antenna Stow/Unstow Test	Comm. Mode Obscuration Zone Test	Comm. Mode Antenna Stability Test	Comm. Mode Antenna Slew Test	Comm. Mode Target Acq. Track Test	Comm. Antenna Scan Volume Test	N/A	To Be Verified by Analysis	To Be Verified By Assessment	To Be Verified By Test
	Modules used for system tests		X		X	X		X		X		X	X			X				
3.2.1.2	Communication Subsystem Performance	*		X											X	X			X	X
3.2.1.2.1	Angle Search, Signal Detection and Track Requirements	*		X											X				X	X
3.2.1.2.1.1	TDRS Forward Link Signal						X												X	X
3.2.1.2.1.2	Antenna Angle Coverage for Communications																X			
3.2.1.2.1.2.1	Acquisition Coverage											X						X	X	X
3.2.1.2.1.2.2	Tracking Coverage											X						X	X	X
3.2.1.2.1.3	Orbiter-TDRS Link Acquisition & Handover																X			
3.2.1.2.1.3.1	Link Acquisition Mode Definition	*																X	X	X
3.2.1.2.1.3.1.1	Primary Acquisition Mode	*																X	X	X
3.2.1.2.1.3.1.2	Alternate Acquisition	*																X	X	X
3.2.1.2.1.3.2	Handover Requirements	*																X	X	X
3.2.1.2.1.3.2.1	Return Link Data																X			
3.2.1.2.1.3.2.2	Data Transfer Sequencing	*																X	X	X
3.2.1.2.1.3.3	Detection IF Bandwidth	*																X	X	X
3.2.1.2.1.3.4	Detection Requirements	*	X												X	X		X	X	X
3.2.1.2.1.3.4.1	Signal Uncertainties for Detection																	X	X	
3.2.1.2.1.3.4	Link Acquisition Time																X			
3.2.1.2.1.3.5.1	TDRS Signal Acquisition	*					X									X			X	X
3.2.1.2.1.3.5.2	Signal Processing Time						X												X	X
3.2.1.2.1.4	Antenna Control Servos	*													X	X		X	X	X
3.2.1.2.1.4.1	Open-Loop Operation	*																X	X	X
3.2.1.2.1.4.1.1	Angle Search															X			X	X
3.2.1.2.1.4.1.2	Search Scan Mechanization															X		X	X	X
3.2.1.2.1.4.1.3	GPC Designate Tracking	*				X									X				X	X
3.2.1.2.1.4.1.4	Wide-Angle Antenna Characteristics	*																X	X	X
3.2.1.2.1.4.2	Closed-Loop Operation																X			

KU-BAND RADAR SUBSYSTEM TESTS CROSS-REFERENCE MATRIX

Rockwell Specification Paragraph MC409-0025 Rev B	COMMUNICATIONS Specification Title/Test Criteria	Not Completely Tested by Dev. Test Modules	Comm. Power Up/Down Consumption	Comm. Subsystem Slant Range	Forward Link Signal Strength Test	Forward Link Tracking Threshold Test	Forward Link Acquisition Time Test	Forward Link BER Test	Functional Test (Return Link)	BER Test (Return Link)	Comm. Mode Antenna Stow/Unstow Test	Comm. Mode Obscuration Zone Test	Comm. Mode Antenna Stability Test	Comm. Mode Antenna Slew Test	Comm. Mode Target Acq. Track Test	Comm. Antenna Scan Volume Test	N/A	To Be Verified By Analysis	To Be Verified By Assessment	To Be Verified By Test
	Modules used for system tests		X		X	X		X		X		X	X			X				
3.2.1.2.1.4.2.1	Angle Tracking Accuracy												X		X			X	X	X
3.2.1.2.1.4.2.2	Angle Tracking Limitations												X	X	X			X	X	X
3.2.1.2.1.4.2.3	Break Track Condition	*																X	X	X
3.2.1.2.2	Forward Link Data Subsystem	*					X												X	X
3.2.1.2.2.1	Forward Link Data Subsystem Characteristics	*					X												X	X
3.2.1.2.2.1.1	Forward Link Subsystem Characteristics	*						X											X	X
3.2.1.2.2.2	Data Characteristics																X			
3.2.1.2.2.2.1	Information Signal Characteristics																X			
3.2.1.2.2.2.1.1	Mode 1 Forward Link Data	*																X	X	X
3.2.1.2.2.2.1.2	Mode 2 Forward Link Data	*																X	X	X
3.2.1.2.2.2.2	Spread Spectrum						X											X	X	X
3.2.1.2.2.2.3	Unspread Spectrum						X											X	X	X
3.2.1.2.2.3	Data Output	*				X	X												X	X
3.2.1.2.2.4	Data Quality Estimation	*			X	X	X											X	X	X
3.2.1.2.2.4.1	Data Quality Estimate Duration	*			X	X	X											X	X	X
3.2.1.2.2.5	Forward Link Performance	*			X	X	X	X										X	X	X
3.2.1.2.3	Ku-Band Comm. Transmit Subsystem																X			
3.2.1.2.3.1	Transmit Subsystem Description	*							X										X	X
3.2.1.2.3.2	Return Link Data Requirements	*							X									X	X	X
3.2.1.2.3.2.1	Mode 1 Data Requirements	*																X	X	X
3.2.1.2.3.2.2	Mode 2 Data Requirements	*																X	X	X
3.2.1.2.3.2.3	Data Source Selection	*							X										X	X
3.2.1.2.3.3	Return Link Characteristics																X			
3.2.1.2.3.3.1	Modulation Type																		X	
3.2.1.2.3.3.2	Data Channelization	*																X	X	X
3.2.1.2.3.3.3	Return Link Operational Characteristics	*							X									X	X	X
3.2.1.2.3.3.4	Return Link Data Throughput	*																X	X	X

KU-BAND RADAR SUBSYSTEM TESTS CROSS-REFERENCE MATRIX

Rockwell Specification Paragraph MC409-0025 Rev B	COMMUNICATIONS Specification Title/Test Criteria	Not Completely Tested by Dev. Test Modules	Comm. Power Up/Down Consumption Test	Comm. Subsystem Slant Range	Forward Link Signal Strength Test	Forward Link Tracking Threshold Test	Forward Link Acquisition Time Test	Forward Link BER Test	Functional Test (Return Link)	BER Test (Return Link)	Comm. Mode Antenna Stow/Unstow Test	Comm. Mode Obscuration Zone Test	Comm. Mode Antenna Stability Test	Comm. Mode Antenna Slew Test	Comm. Mode Target Acq. Track Test	Comm. Antenna Scan Volume Test	N/A	To Be Verified By Analysis	To Be Verified By Assessment	To Be Verified By Test
	Modules used for system tests		X		X	X		X		X		X	X			X				
3.2.1.2.3.3.4.1	Digital Data Throughput	*																X	X	X
3.2.1.2.3.3.4.1.1	Bit Transition Density	*																X	X	
3.2.1.2.3.3.4.1.2	Data Asymmetry	*							X									X	X	X
3.2.1.2.3.3.4.2	Analog Data Throughput	*																X	X	X
3.2.1.2.3.4	Modulation																		X	
3.2.1.2.3.4.1	Mode 1 Modulation	*																	X	X
3.2.1.2.3.4.2	Mode 2 Modulation	*																	X	X
3.2.1.2.3.4.3	Analog Data via Channel 2	*																	X	X
3.2.1.2.3.4.4	Unmodulated Carrier																		X	X
3.2.1.2.3.5	Data Degradation	Deleted																		
3.2.1.2.3.5.1	Mode 1 Degradation	Deleted																		
3.2.1.2.3.5.2	Mode 2 Degradation	Deleted																		
3.2.1.2.4	Communications B Subsystem																		X	
3.2.1.2.5	Comm. System Self-Test	Deleted																		
3.2.1.2.6	Comm. System Power Consumption		X																	

KU-BAND RADAR SUBSYSTEM TESTS CROSS-REFERENCE MATRIX

9.0 LRU INTERCHANGEABILITY

The purpose of this section is to report the findings of the Ku-band LRU interchangeability study. The Ku-band communications and radar system consists of four LRU's: EA-1, EA-2, SPA and DA. Each LRU interfaces with each of the other three LRU's (except that the EA-2 does not interface with the SPA) and with the Orbiter. The interfaces consist of digital data, digital control pulses, discrete commands, discrete status signals, analog information, RF signals and LRU power.

Figures 47 to 55 show the various interfaces between each of the LRU's and between each LRU and the Orbiter. Each figure indicates the signal name, type of signal and corresponding LRU connector number. Because of the sheer number and complexity of the interfaces and, since the LRU is the basic building block of the Ku-band system, it must be assured that each LRU will be interchangeable with another similar LRU.

9.1 Approach

The approach for completing the LRU interchangeability study was to examine each of the signal interfaces shown in Figure 47 to 55 using five documents for baseline information. The five documents are:

(1) Rockwell specification MC409-0025, Revision B, "Integrated Communications and Radar Equipment, Ku-Band."

(2) Hughes specification DS32012-020, November 13, 1978, "Development Specification Radar/Communications A Electronic Assembly, Part 1 for the Ku-Band Integrated Radar and Communications Equipment" (EA-1).

(3) Hughes specification DS32012-022, Revision B, September 19, 1980, "Development Specification, Radar/Communications Electronic Assembly, Part 2 for the Ku-Band Integrated Radar and Communications Electronic Assembly, Part 2 for the Ku-Band Integrated Radar and Communications Equipment" (EA-2).

(4) Hughes specification DS32012-011, Revision A, November 3, 1980, "Development Specification Signal Processor Assembly for the Ku-Band Integrated Radar and Communications Equipment" (SPA).

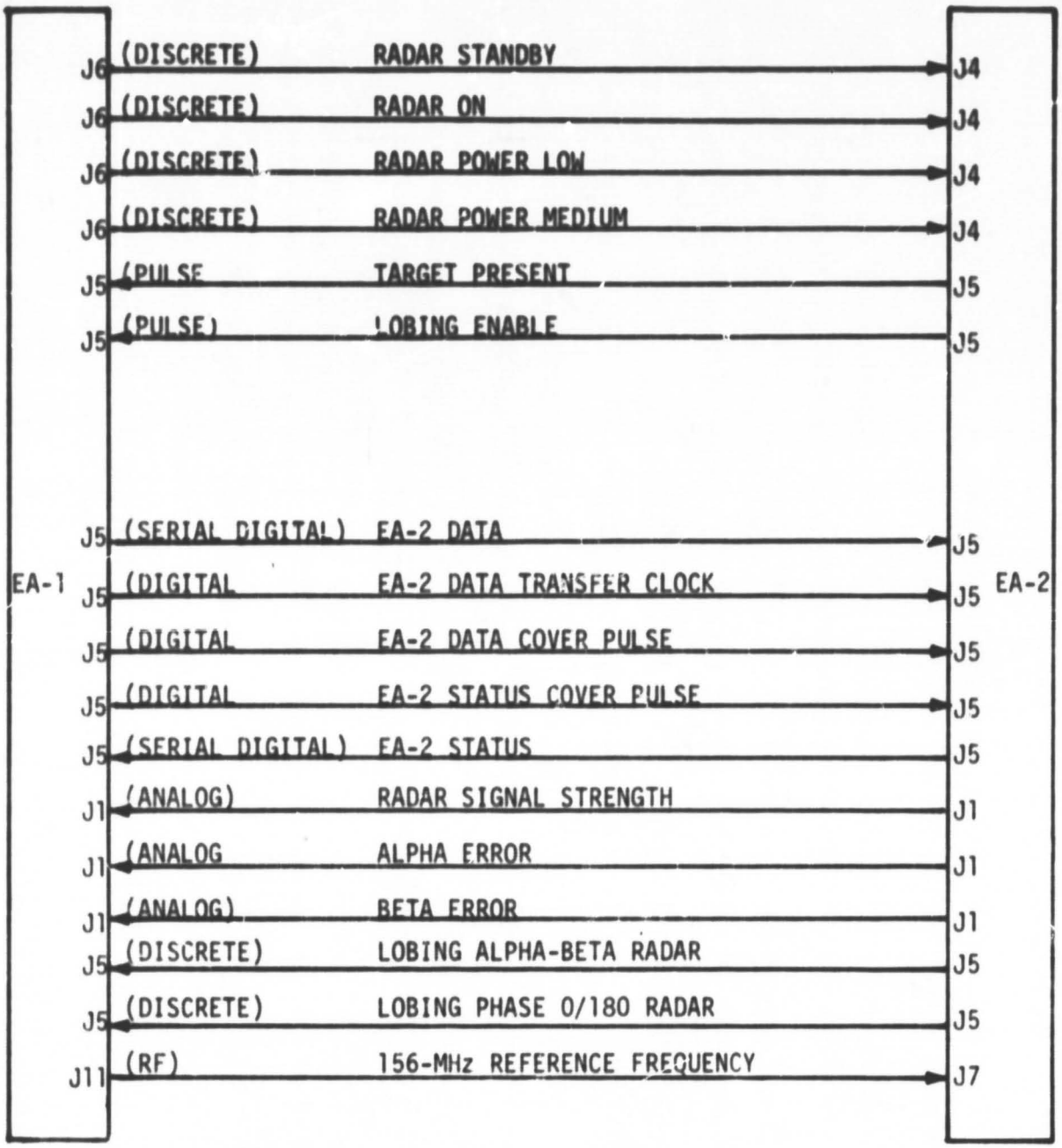

Figure 47. EA-1/EA-2 Signal Interface

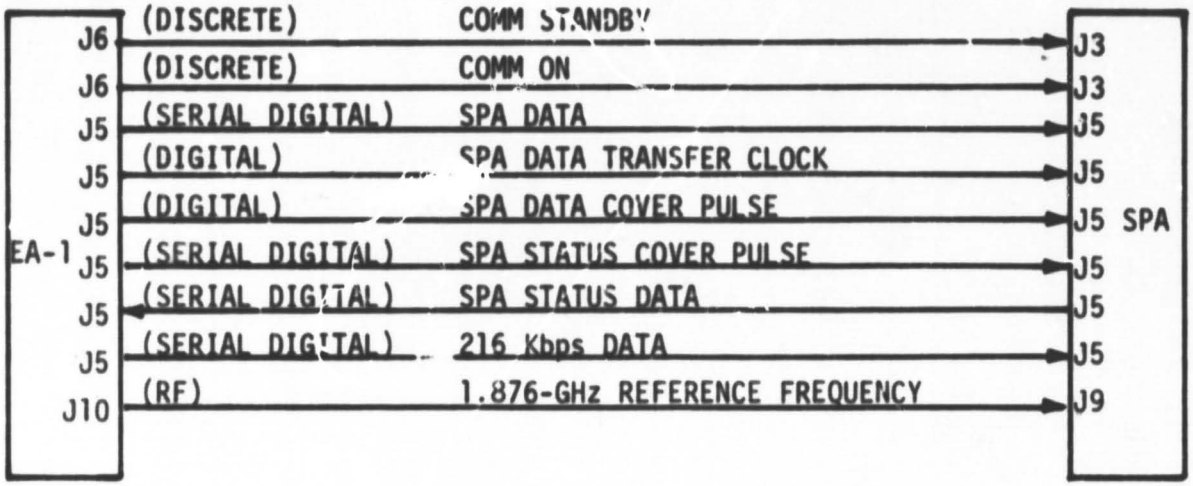

Figure 48. EA-1/SPA Signal Interfaces

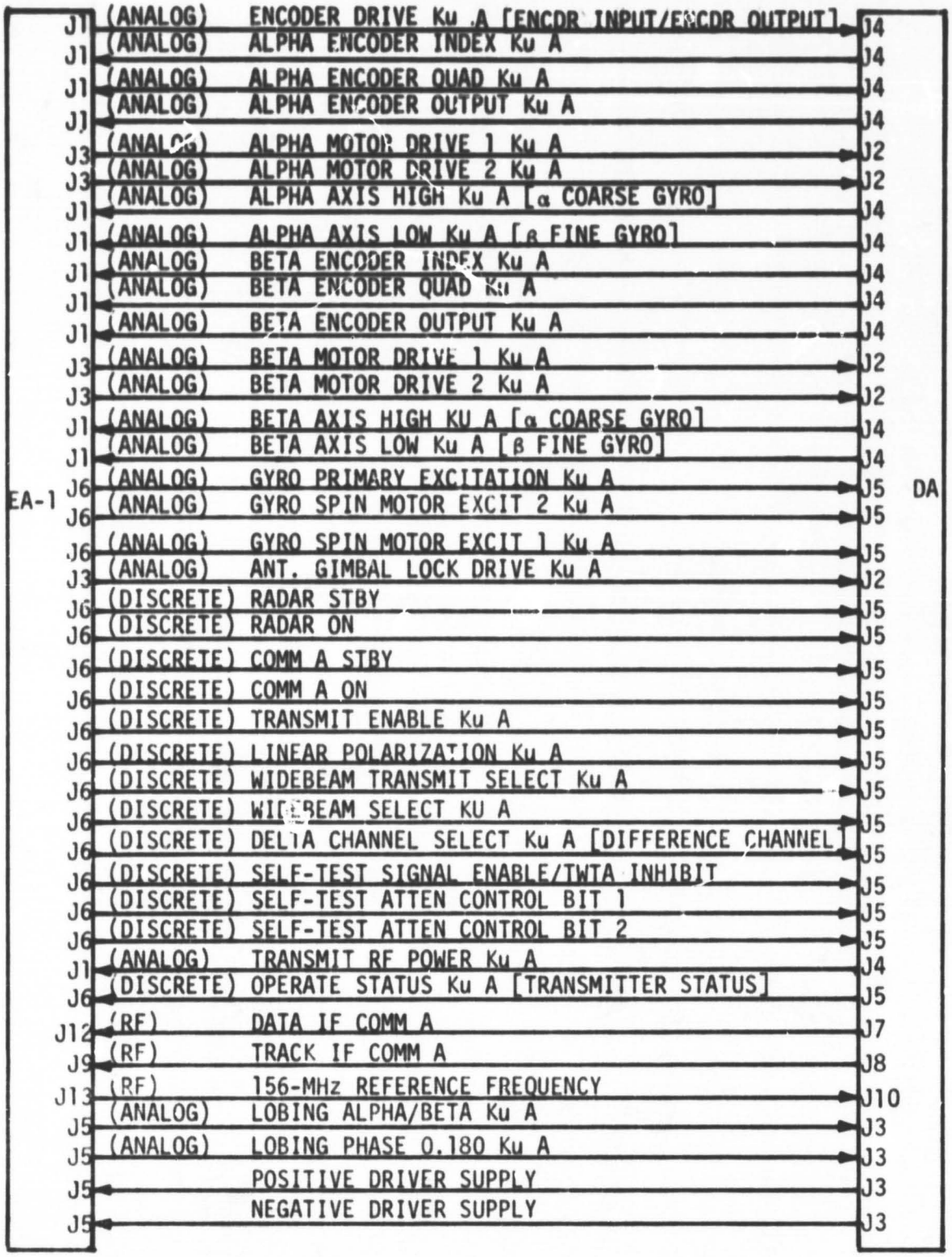

Figure 49. EA-1/DA Signal Interfaces

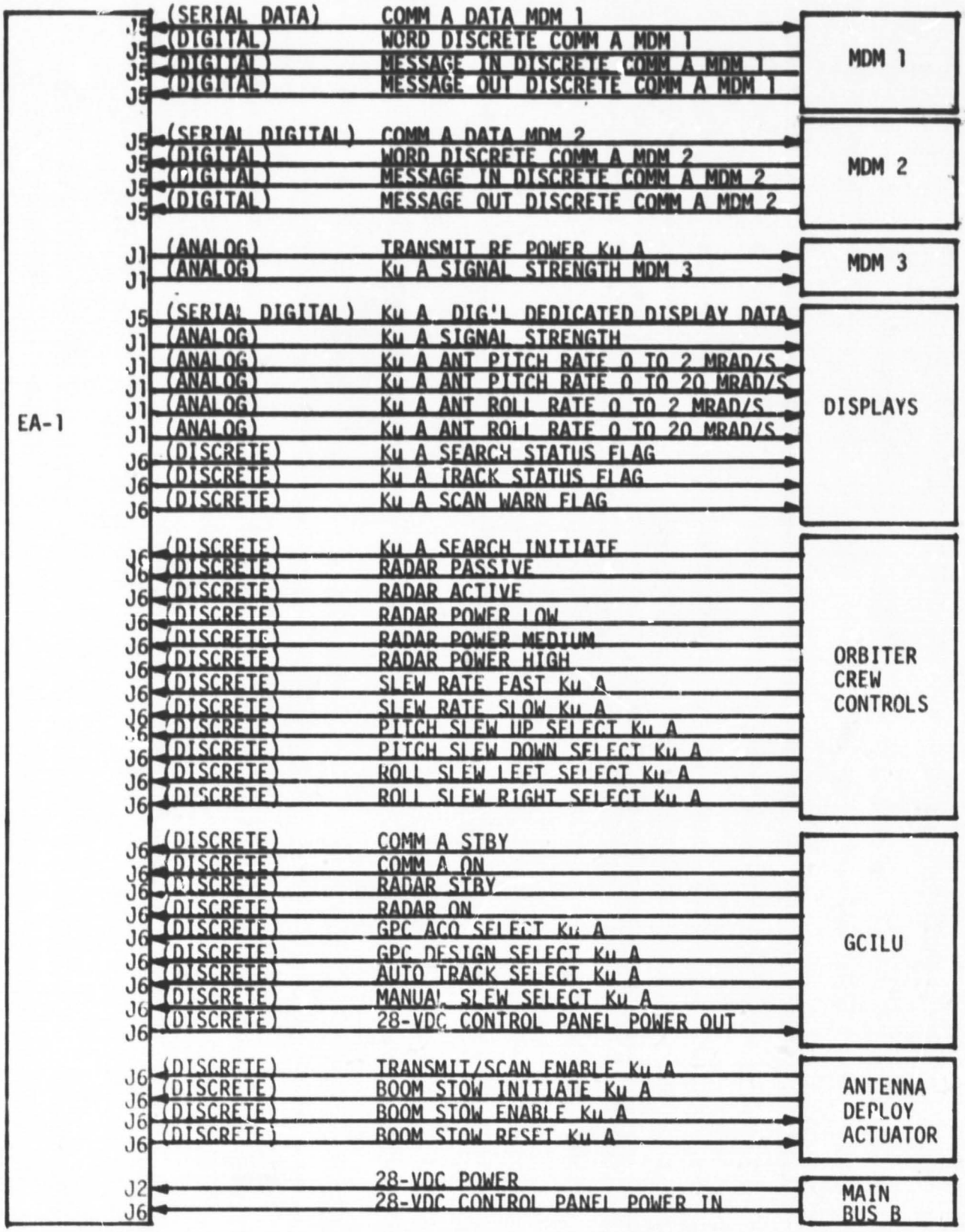

Figure 50. EA-1/Orbiter Signal Interfaces

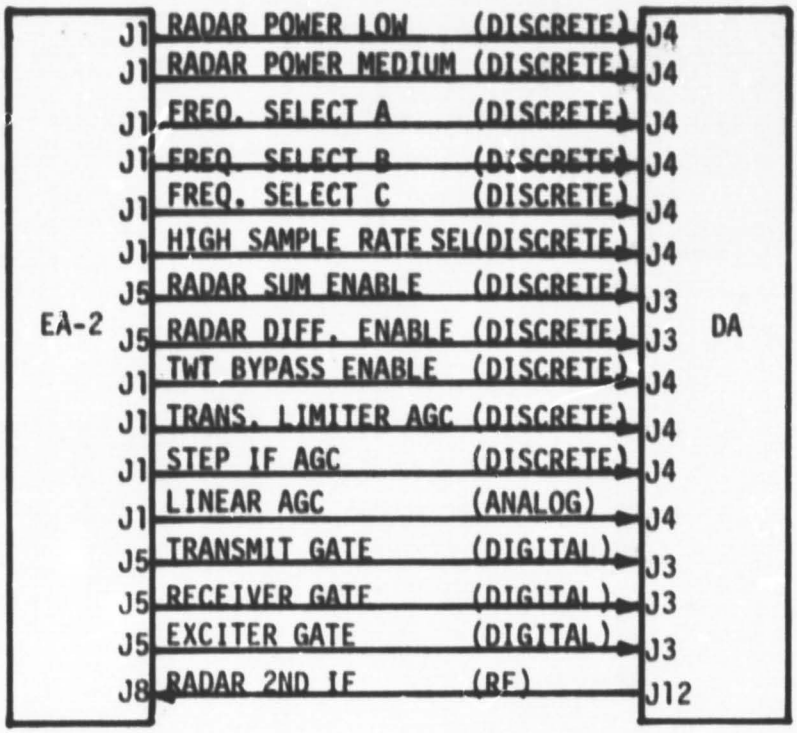

Figure 51. EA-2/DA Interface

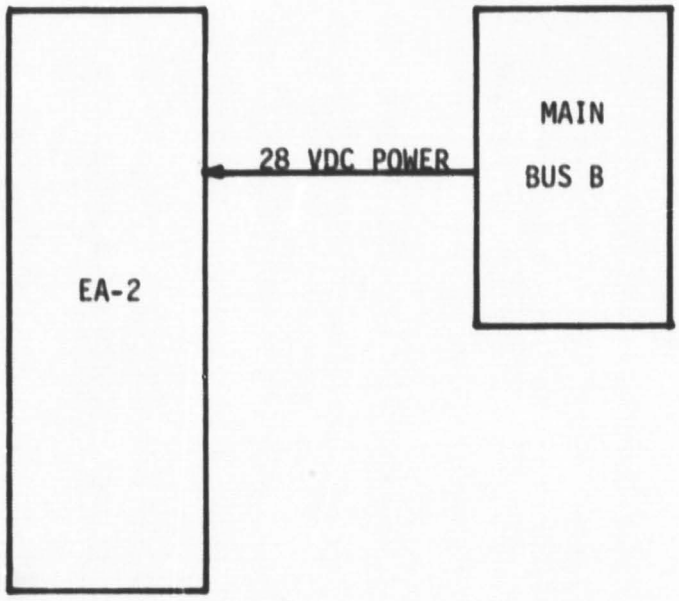

Figure 52 . EA-2/Orbiter Signal Interface

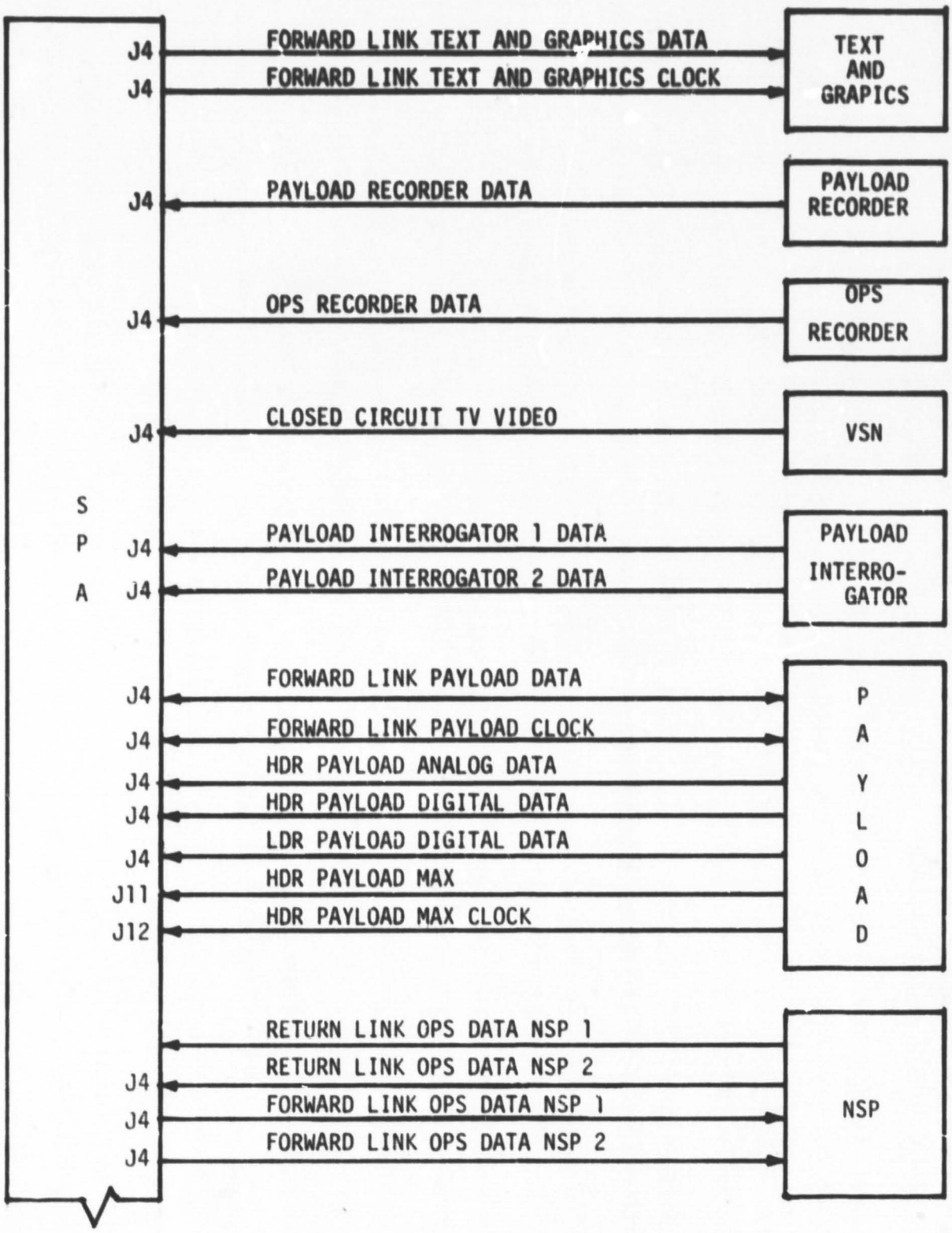

Figure 53a. SPA/Orbiter Signal Interface

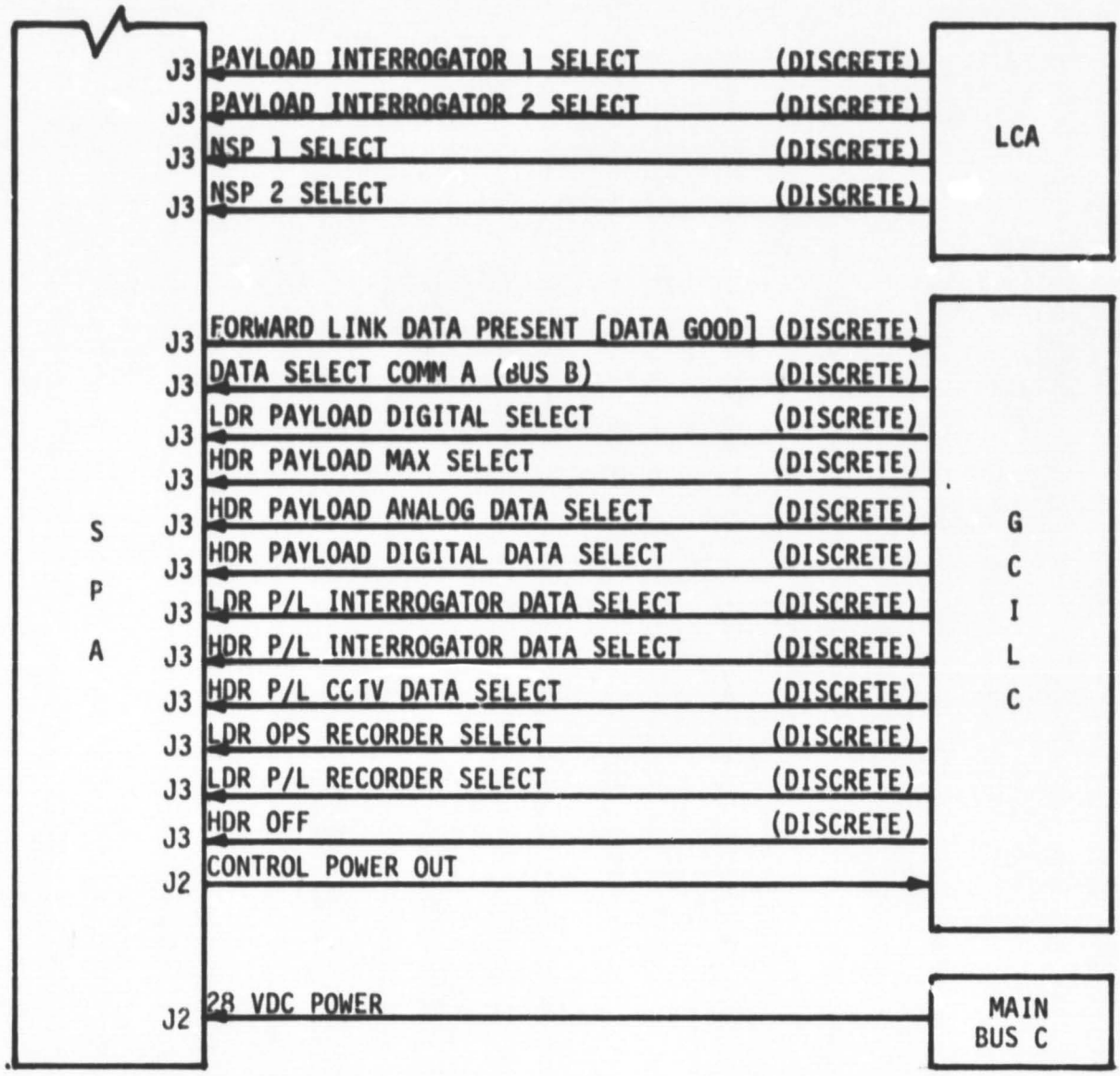

Figure 53b. SPA/Orbiter Signal Interface
(Continued)

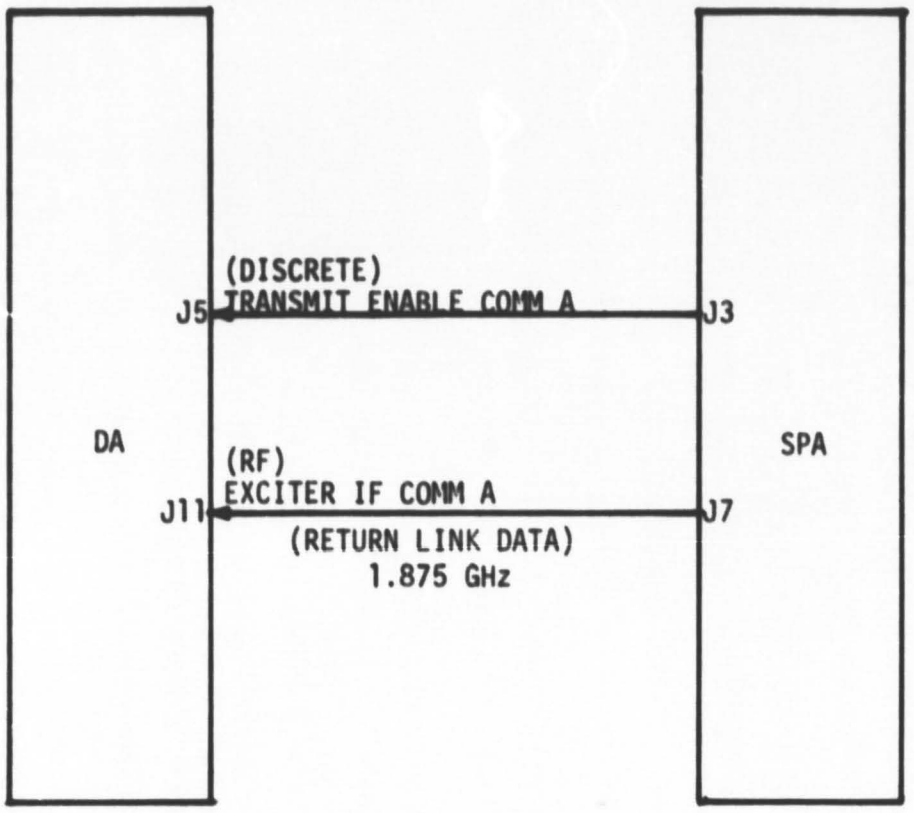

Figure 54. DA/SPA Signal Interface

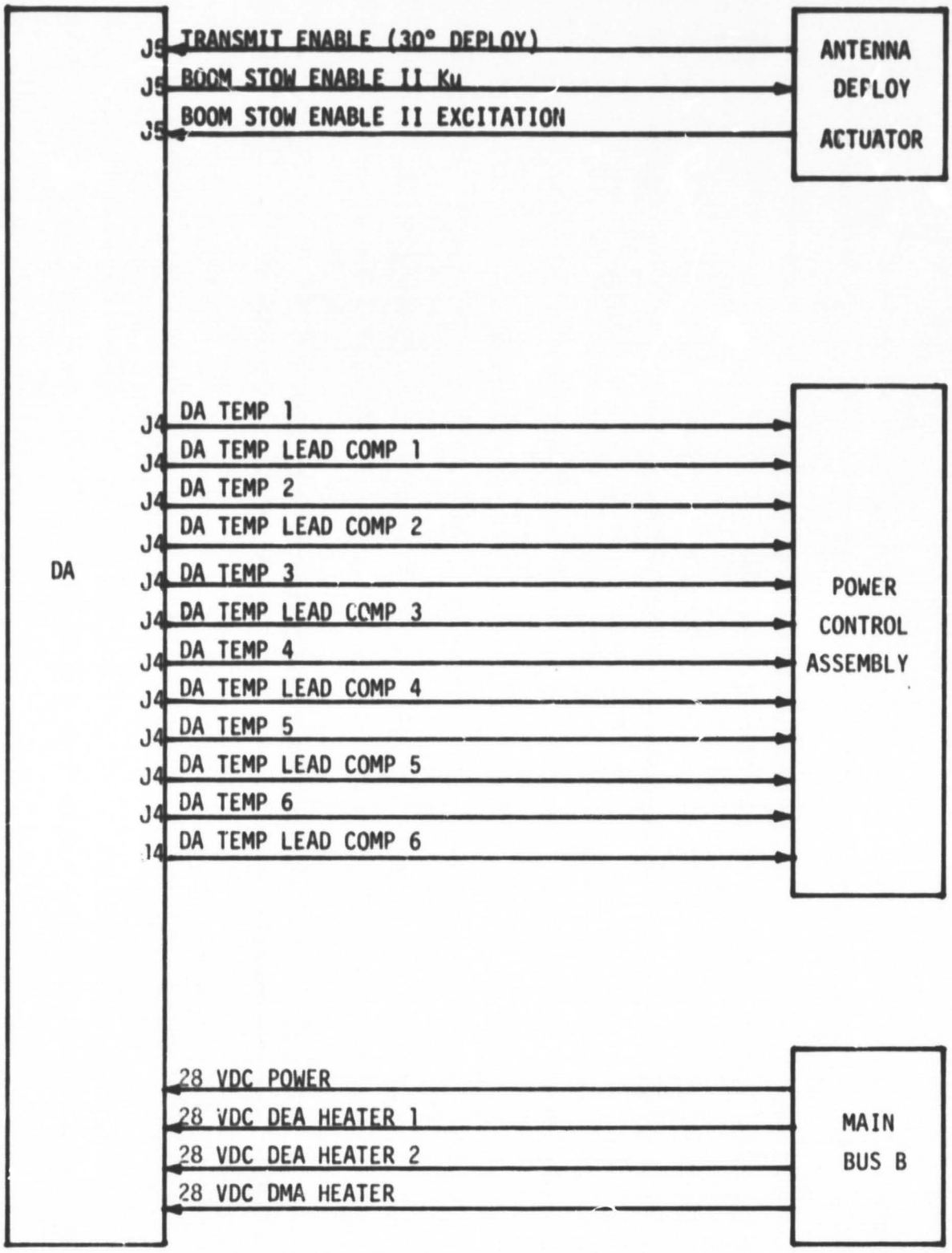

Figure 55 . DA/Orbiter Signal Interface

(5) Hughes specification DS32012-031, Revision A, October 13, 1980, "Development Specification, Deployed Assembly for the Ku-Band Integrated Radar and Communications Equipment" (DA).

All five documents listed reflect the latest system changes with the exception of the EA-1 LRU specification which is still being updated by Hughes.

Each interface was compared with applicable LRU and/or Orbiter specifications to determine electrical compatibility by verifying that the document describing the signal output was consistent with the document specifying the signal input. Since electrical compatibility was the objective of this study, only interface parameters such as input/output impedances, rise/fall times, proper voltage levels and proper power levels were compared. Performance parameters such as SNR, BER, spurious products and phase noise were not included in this study since performance parameters are verified during development, acceptance and qualitative testing. Therefore, this study centered on examining the electrical compatibility of all the interfaces.

9.2 Findings

In the process of examining the various signal interfaces, a number of assumptions were made. The first assumption concerned the tolerances associated with the voltage levels defining a logic "0" and a logic "1". In the SPA and EA-1 LRU specifications, the actual interface circuits are not illustrated whereas, in the DA and EA-2 LRU specifications, most of the actual circuits are shown. Where the circuit is actually shown, as in the case of the DA and EA-2 documentation, it was assumed that the interface driver and receiver would function over voltage tolerances of the logic "1" and "0." For example, Figure 56 illustrates the electro-optical receiver used in a number of the EA-2 interfaces. It is assumed that the device will function over the logic "1" voltage range of +28 ± 4 VDC based on the fact that devices such as the electro-optical receiver have known characteristics which have been documented by the manufacturers and verified by test.

However, where the actual circuit is not illustrated, as in the case of the SPA and EA-1 LRU documentation, a potential problem is flagged when an apparent incompatibility exists. For example, there is a conflict in the requirements defining the signal OPERATE STATUS KuA between the DA

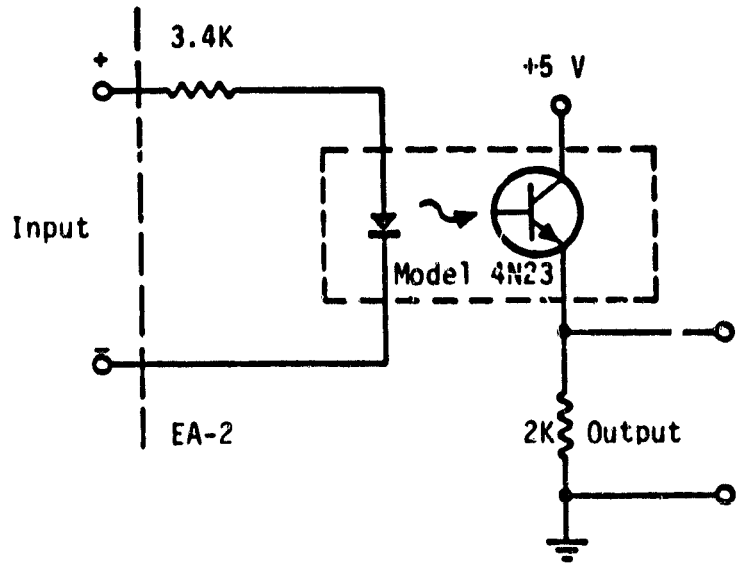

Signal Characteristics

Amplitude:	High State (1) - 28 ± 4 Volts
	Low State (0) - Open Circuit
Rise Time:	< 20 ms
Fall Time:	< 10 ms
Impedance:	Source - < 100Ω
	Load - > 3.3 KΩ

Figure 56. Electro-Optical Receiver for +28 V Discretes

and the EA-1. The DA specification states that the logic "0" supplied to the EA-1 will be an open circuit, but the EA-1 specification states that the logic "0" will be 0 - 2.5 VDC. Since the interface circuit diagram is not readily available to Axiomatix at this time, it is not known if the EA-1 will function properly while supplied with an open circuit instead of a low impedance voltage level for logic "0." Hence, when situations just described arose during the interface study, a potential problem was flagged.

In examining the various interfaces, Axiomatix felt it was useful to identify certain electrical parameters as critical parameters that should be measured. While all parameters defining an interface are important, the second assumption in this report is that, in Axiomatix's opinion, some electrical parameters may be deemed critical while others are not. For example, the logic "1" and "0" voltage tolerances as previously discussed are important but, since the driver and receiver have already been characterized, it is assumed that the interface will function over the voltage tolerance range. Hence, the voltage tolerances are assumed to be noncritical electrical parameters.

On the other hand, the LINEAR AGC signal between the EA-2 and the DA has a specified dynamic range. In this report, the LINEAR AGC has been identified as a critical electrical parameters and the interface should be tested to verify that the output voltage covers the full dynamic range.

Another example of critical and noncritical electrical parameters as defined in this report is the logic timing of the EA-2 serial data output to the EA-1 with respect to the EA-2 data cover pulse. The logic timing is obviously very critical for system performance but, for the purpose of this report (which is to verify the electrical interface compatibility), the logic timing was deemed noncritical since the timing has been demonstrated by previous testing and analysis.

The purpose of identifying critical electrical parameters is to identify areas where an interface should be exercised over its full range to guarantee interface compatibility and, hence, interchangeability.

The third and last assumption deals with the five previously mentioned documents used in this study. Both the Hughes LRU specifications and the Rockwell requirements specify the inter-LRU interface but, if a

signal is between two LRU's, the HAC document is used as the baseline. There was no effort in this study to correlate the LRU interface requirements outlined in the HAC LRU specifications with the same or similar requirements listed in the Rockwell LRU specification appendices. If the interface is between an LRU and the Orbiter, the Rockwell document is used for defining the Orbiter interface, and the Hughes document is used for defining the LRU interface.

Tables 15 - 23 list all the LRU-to-LRU and LRU-to-Orbiter interfaces, showing the signal source and signal destination along with the applicable specification paragraphs. After reviewing each interface, a determination was made as to whether or not the interfaces are compatible, which electrical parameters are critical and, finally, if the critical electrical parameters have been measured during Hughes testing.

The assumptions in dealing with the interface compatibility determination and choosing the critical electrical parameters have already been discussed. To date, Axiomatix has reviewed the SPA and EA-1 CDR LRU test data but has not reviewed the DA and EA-2 data. For this reason, it is unknown at this time whether or not the critical electrical parameters identified in this report have been tested by Hughes for the DA and EA-2.

By studying Tables 15 to 23, it is readily apparent that there are a number of interface inconsistencies, some of which apply to specification or paperwork problems, but some of which are quite serious. The most likely candidate for a paperwork-type problem is where the signal source supplies an open circuit for a logic "0" but the receiver specifies a 0 - 2.5 VDC level. As previously stated, the actual interface circuit schematic was not readily available to Axiomatix at the time of this study. Examination of the schematic will resolve the problem, after which, the appropriate specification may be changed to accurately describe the interface or, possibly, the interface redesigned.

The more serious interface problems highlighted by this study are such items as insufficient drive for the gyros, scale factor mismatch for the α and β axis gyro rate data, the scale factor mismatch for the linear AGC, the unclear alpha/beta lobing requirements, the need to further characterize the track IF signal and the need to clarify the SPA/Orbiter interface requirements.

	SOURCE			DESTINATION					
	LRU	Hughes LRU Spec. Paragraph	Rockwell Spec. Paragraph	LRU	Hughes LRU Spec. Paragraph	Rockwell Spec. Para.	Are Interfaces Compatible?	Critical Electrical Parameters To Be Measured	Have Critical Electrical Parameters Been Tested?
1. Radar Standby Radar On Radar Power Low Radar Power Medium	EA-1 | | EA-1	3.1.2.4.3.4 | | 3.1.2.4.3.4	N/A | | N/A	EA-2 | | EA-2	3.1.2.4.1.2 | | 3.1.2.4.1.2	N/A | | N/A	Perhaps, EA-1 min. "1"=22 V but EA-2 min. "1" reqd=24 V.	None | | None	N/A | | N/A
2. Target Present Lobing Enable	EA-2 EA-2	3.1.2.4.1.2 3.1.2.4.1.2	N/A N/A	EA-1 EA-1	3.1.2.4.4.2 3.1.2.4.4.2	N/A N/A	Yes Yes	None None	N/A N/A
3. EA-2 Data	EA-1	3.1.2.4.2.3	N/A	EA-2	3.1.2.4.1.1.1	N/A	Yes	None	N/A
4. EA-2 Data Transfer Clock	EA-1	3.1.2.4.2.1	N/A	EA-2	3.1.2.4.1.1.2	N/A	Yes	None	N/A
5. EA-2 Data Cover Pulse	EA-1	3.1.2.4.2.2	N/A	EA-2	3.1.2.4.1.1.3	N/A	Yes	None	N/A
6. EA-2 Status Cover Pulse	EA-1	3.1.2.4.2.2	N/A	EA-2	3.1.2.4.1.1.4	N/A	Yes	None	N/A
7. EA-2 Status	EA-2	3.1.2.4.1.1.5	N/A	EA-1	3.1.2.4.2.4	N/A	Yes	None	N/A
8. Radar Signal Strength	EA-2	3.1.2.4.1.3.1	N/A	EA-1	3.1.2.4.7.1	N/A	Yes, provided EA-1 interface is implemented as shown in the EA-2 Spec.	Test over full response range	EA-2, unknown at this time EA-2, No.
9. Alpha Error and Beta Error	EA-2	3.1.2.4.1.3.2	N/A	EA-1	3.1.2.4.5.7	N/A	Yes, provided EA-1 interface is implemented per EA-2 Spec & polarity clearly specified.	Test over full response range and verify polarity.	EA-2, unknown at this time EA-2, Yes
10. Lobing Alpha-Beta Radar Lobing Phase 0/180 Radar	EA-2 EA-2	3.1.2.4.1.2 3.1.2.4.1.2	N/A N/A	EA-1 EA-1	3.1.2.4.4.2 3.1.2.4.4.2	N/A N/A	Yes Yes	None None	N/A N/A
11. 156-MHz Reference Frequency	EA-1	3.1.2.4.7.3 3.2.1.9.1	N/A	EA-2	3.1.2.4.1.3.3	N/A	Perhaps, EA-1 specifies +2.5 +TBS dBM and EA-2, +2.3 +1.0 dBm	This signal should be completely characterized by SMU & LRU Tests	No

Note: EA-1 is Rev. A, not Rev. B.

Table 15. EA-1/EA-2

	SOURCE			DESTINATION					
	LRU	Hughes LRU Spec. Paragraph	Rockwell Spec. Paragraph	LRU	Hughes LRU Spec. Paragraph	Rockwell Spec. Para.	Are Interfaces Compatible?	Critical Electrical Parameters To Be Measured	Have Critical Electrical Parameters Been Tested?
1. Comm Standby Comm On	EA-1 EA-1	3.1.2.4.3.4 3.1.2.4.3.4	N/A N/A	SPA SPA	3.1.2.4.3.2.3 3.1.2.4.3.2.3	N/A N/A	No, EA-1 source is 10 ma nominal & SPA specifies 15.6 ma max. EA-1 logic "0" is an open circuit & SPA specifies 0 V.	None None	N/A N/A
2. SPA Data	EA-1	3.1.2.4.2.3	N/A	SPA	3.1.2.4.3.3.3	N/A	Yes	None	N/A
3. Data Transfer Clock	EA-1	3.1.2.4.2.1	N/A	SPA	3.1.2.4.3.3.4	N/A	Yes	None	N/A
4. Data Cover Pulse	EA-1	3.1.2.4.2.2	N/A	SPA	3.1.2.4.3.3.5	N/A	Yes	None	N/A
5. Status Data	SPA	3.1.2.4.3.3.6	N/A	EA-1	3.1.2.4.2.4	N/A	Unknown, load is unspecified	None	N/A
6. 216 kbps Data	EA-1	3.1.2.4.6.2	N/A	SPA	3.1.2.4.1.1.1	N/A	Unknown, EA-1 voltage output unspecified along with source impedance	Test over data rate range of 32 to 216 kbps	Yes
7. 1.876 GHz Reference	EA-1	3.1.2.4.7.3 3.2.1.9.1	N/A	SPA	3.1.2.4.2.3	N/A	Yes, EA-1 specifies +6 dBm nominal output & SPA specifies -1.2 dBm nominal input. Cable losses account for the apparent power difference. Spec should be clarified to show cable losses.	This signal should be completely characterized by SRU & LRU tests	No

Note: EA-1 Spec is Rev. A instead of Rev. B.

Table 16. EA-1/SPA

	SOURCE			DESTINATION					
	LRU	Hughes LRU Spec. Paragraph	Rockwell Spec. Paragraph	LRU	Hughes LRU Spec. Paragraph	Rockwell Spec. Para.	Are Interfaces Compatible?	Parameters To Be Measured	Have Critical Electrical Parameters Been Tested?
1. Encoder Drive Ku A	EA-1	3.1.2.4.5.3	N/A	DA	3.1.2.4.2.3	N/A	Perhaps*	None	N/A
2. Alpha Encoder Index KuA Alph Encoder Quad KuA Alpha Encdr Output KuA	DA | DA	3.1.2.4.2.4 | 3.1.2.4.24	N/A | N/A	EA-1 | EA 1	3.1.2.4.5.6 | 3.1.2.4.5.6	N/A | N/A	Perhaps. EA-1 does not specify load impedance. DA does not specify that signal is differential.	None | None	N/A | N/A
3. Alpha Motor Drive 1 KuA Alpha Motor Drive 2 KuA	EA-1 EA-1	3.1.2.4.5.1 3.1.2.4.5.1	N A N/A	DA DA	3.1.2.4.19 3.1.2.4.19	N/A N/A	No, EA-1 specifies voltage drive level of 23 to 31 V, but DA is 19 V max*	None None	N/A N/A
4. Alpha Axis High KuA Alpha Axis Low KuA	DA DA	3.1.2.4.22 3.1.2.4.22	N/A N/A	EA-1 EA-1	3.1.2.4.5.5 3.1.2.4.5.5	N/A N/A	No, EA-1 doesn't specify load impedance. EA-1 specifies high scale factor = 12°/sec/volt & low scale factor=0.3°/sec/V. DA specifies high = 0.4165 ±0.021°/sec/V & low = 0.0833 ±0.0042°/sec/V.	Test over full rate range.	DA, unknown at this time. EA-1, yes.
5. Beta Encoder Index KuA Beta ENcoder Quad KuA Beta Encoder Output KuA	DA | DA	3.1.2.4.24 | 3.1.2.4.24	N/A | N/A	EA-1 | EA-1	3.1.2.4.5.6 | 3.1.2.4.5.6	N/A | N/A	Perhaps, ref. item 2.	None | None	N/A | N/A
6. Beta Motor Drive 1 KuA Beta Motor Drive 2 KuA	EA-1 EA-1	3.1.2.4.5.1 3.1.2.4.5.1	N/A N/A	DA DA	3.1.2.4.19 3.1.2.4.19	N/A N/A	No, reference item 3.	None None	N/A N/A
7. Beta Axis High KuA Beta Axis Low KuA	DA DA	3.1.2.4.22 3.1.2.4.22	N/A N/A	EA-1 EA-1	3.1.2.4.5.5 3.1.2.4.5.5	N/A N/A	No, reference item 4.	Test over full rate range.	DA, unknown at this time. EA-1, yes.

Note: EA-1 Spec is Rev A instead of Rev B.

*Cabling IR drop should be specified or accounted for.

Table 17. EA-1/DA

	SOURCE			DESTINATION					
	LRU	Hughes LRU Spec. Paragraph	Rockwell Spec. Paragraph	LRU	Hughes LRU Spec. Paragraph	Rockwell Spec. Para.	Are Interfaces Compatible?	Critical Electrical Parameters To Be Measured	Have Critical Electrical Parameters Been Tested?
8. Gyro Primary Excitation KuA	EA-1	3.1.2.4.5.4	N/A	DA	3.1.2.4.21	N/A	No, EA-1 specifies max. source current 10 ma rms but DA has a max load current spec. of 20 ma rms.	None	N/A
9. Gyro Spin Motor Excitation 2 KuA	EA-1	3.1.2.4.5.4	N/A	DA	3.1.2.4.20	N/A	No, EA-1 specifies max source current of 1.2A rms but DA may require 1.6A rms maximum.	None	N/A
Gyro Spin Motor Excitation 1 KuA	EA-1	3.1.2.4.5.4	N/A	DA	3.1.2.4.20	N/A		None	N/A
10. Antenna Gimbal Lock Drive KuA	EA-1	3.1.2.4.5.2	N/A	DA	3.1.2.4.25	N/A	No, EA-1 doesn't specify output voltage level but DA specifies 14 V +10%, -30%.	None	N/A
11. Radar Standby	EA-1	3.1.2.4.3.4	N/A	DA	Table 3.1.2.4-1	N/A	Yes	None	N/A
Radar On									
Comm A Standby									
Comm A On									
Transmit Enable KuA									
Linear Polarization KuA									
Widebeam Xmit Select KuA	EA-1	3.1.2.4.3.4	N/A	DA	Table 3.1.2.4-1	N/A	Yes	None	N/A
12. Widebeam Select KuA	EA-1	3.1.2.4.5.10	N/A	DA	Table 3.1.2.4-1	N/A	Yes	None	N/A
Delta Channel Select KuA	EA-1	3.1.2.4.5.10	N/A	DA	Table 3.1.2.4-1	N/A	Yes	None	N/A
13. Self-Test Sig. Enable/ TWT Inhibit	EA-1	3.1.2.4.3.4	N/A	DA	Table 3.1.2.4-1	N/A	Yes	None	N/A
Self-Test Atten Ctl Bit 1									
Self-Test Atten Ctl Bit 2	EA-1	3.1.2.4.3.4	N/A	DA	Table 3.1.2.4-1	N/A	Yes	None	N/A

Note: EA-1 Spec is Rev. A instead of Rev. B.

Table 17. EA-1/DA (Cont'd)

	SOURCE			DESTINATION					
	LRU	Hughes LRU Spec. Paragraph	Rockwell Spec. Paragraph	LRU	Hughes LRU Spec. Paragraph	Rockwell Spec. Para.	Are Interfaces Compatible?	Critical Electrical Parameters To Be Measured	Have Critical Electrical Parameters Been Tested?
14. Transmit RF Power KuA	DA	3.2.1.2.1.3	N/A	EA-1	3.1.2.4.7.1	N/A	Unknown, the DA specified only the scale factor with no voltage levels or impedances discussed. EA-1 has TBD for signal level required.	Test over full scale factor range	DA, unknown at this time. EA-1, no
15. Operate Status KuA	DA	Table 3.1.2.4-1	N/A	EA-1	3.1.2.4.3.2	N/A	No, DA specifies a logic "0" as an open but EA-1 A logic "0" as 0-2.5 V.	None	N/A
16. Data IF Comm A	DA	3.1.2.4.1.4.3	N/A	EA-1	3.1.2.4.6.1 3.2.1.2.1.1	N/A	Yes*	This signal should be completely characterized by SRU & LRU tests	DA, unknown at this time. EA-1, no.
17. Track IF Comm A	DA	3.1.2.4.14.2	N/A	EA-1	3.1.2.4.6.1 3.2.1.2.1.2	N/A	Yes*	This signal should be completely characterized by SRU & LRU tests	DA, unknown at this time. EA-1, no.
18. 156-MHz Reference	EA-1	3.1.2.4.7.3	N/A	DA	3.1.2.4.5	N/A	Perhaps, the EA-1 specifies +6+TBS dBm output & the DA specifies +4.7 +1.5 dBm input	This signal should be completely characterized by SRU and LRU tests.	No
19. Lobing Alpha/Beta KuA	EA-1	3.1.2.4.4.3	N/A	DA	Table 3.1.2.4-1	N/A	Unknown, the DA doesn't clearly specify reqmts.	None	N/A

Note: EA-1 Spec is Rev A instead of Rev B.

*Interfaces electrically compatible but performance requirements are an integral part of the interface and should be completely verified. The DA Spec. should present a summary of signal characteristics similar to the summary in the EA-1 Spec.

Table 17. EA-1/DA (Cont'd)

	SOURCE			DESTINATION					
	LRU	Hughes LRU Spec. Paragraph	Rockwell Spec. Paragraph	LRU	Hughes LRU Spec. Paragraph	Rockwell Spec. Para.	Are . erfaces Compatible?	Critical Electrical Parameters To Be Measured	Have Critical Electrical Parameters Been Tested?
20. Lobing Phase 0/180 KuA	EA-1	3.1.2.4.4.3	N/A	DA	Table 3.1.2.4-1	N/A	No, interface shown in DA specification & one described in EA-1 specification are different	None	N/A
21. Positive Driver Supply Negative Driver Supply	DA DA	Table 3.1.2.4-2 Table 3.1.2.4-2	N/A N/A	EA-1 EA-1	3.1.2.4.5.8 3.1.2.4.5.8	N/A N/A	Unknown, DA does not specify voltage level tolerance or load.	None	N/A

Note: EA-1 Spec is Rev. A instead of Rev. B.

Table 17. EA-1/DA (Cont'd)

	SOURCE			DESTINATION					
	LRU	Hughes LRU Spec. Paragraph	Rockwell Spec. Paragraph	LRU	Hughes LRU Spec. Paragraph	Rockwell Spec. Para.	Are Interfaces Compatible?	Critical Electrical Parameters To Be Measured	Have Critical Electrical Parameters Been Tested?
1. Comm A Data MDM 1	MDM EA-1	N/A 3.1.2.4.1.3	120.2.5.2 N/A	EA-1 MDM1	3.1.2.4.1.2 N/A	N/A 120.2.5.2	Yes	None	N/A
2. Word Discrete Comm A MDM 1 Message In Discrete Comm A MDM 1 Message Out Discrete Comm A MDM 1	MDM1 MDM1	N/A N/A	120.2.4 120.2.4	EA-1 EA-1	3.1.2.4.1.1 3.1.2.4.1.1	N/A N/A	Yes Yes	None None	N/A N/A
3. Comm A Data MDM 2	MDM2 EA-1	N/A 3.1.2.4.1.3	120.2.5.2 N/A	EA-1 MDM2	3.1.2.4.1.2 N/A	N/A 120.2.5.2	Yes	None	N/A

Note: EA-1 Spec is Rev. A instead of Rev. B.

Table 18. EA-1/Orbiter

	SOURCE			DESTINATION					
	LRU	Hughes LRU Spec. Paragraph	Rockwell Spec. Paragraph	LRU	Hughes LRU Spec. Para.	Rockwell Spec. Para.	Are Interfaces Compatible?	Critical Electrical Parameters To Be Measured	Have Critical Electrical Parameters Been Tested?
4. Word Discrete Comm A MDM 2	MDM2	N/A	120.2.4	EA-1	3.1.2.4.1.1	N/A	Yes	None	N/A
Message in Discrete Comm A MDM 2									
Message Out Discrete Comm A MDM 2	MDM2	N/A	120.2.4	EA-1	3.1.2.4.1.1	N/A	Yes	None	N/A
5. Transmit RF Power KuA	EA-1	3.1.2.4.7.1 3.2.1.8.4.2	N/A	MDM3	N/A	20.3.1.2.4.2.3	Unknown, EA-1 doesn't specify load impedance or scale factor	Test over scale factor ranges	No
KuA Signal Strength	EA-1	3.1.2.4.7.1 3.1.2.8.4.1	N/A	MDM3	N/A	20.3.1.2.4.2.3			
6. KuA Digital Dedicated Display Data	EA-1	3.1.2.4.7.2	N/A	Disp	N/A	20.3.1.2.4.4.3	Yes	None	N/A
7. KuA Signal Strength	EA-1	3.1.2.4.7.1	N/A	Disp	N/A	20.3.1.2.4.4.2.2	Unknown, EA-1 doesn't specify load impedance or scale factor	Test over scale factor range	No
8. KuA Antenna Pitch Rate 0-2 Mrads/sec	EA-1	3.1.2.4.7.1 3.2.1.8.2.2	N/A	Disp	N/A	20.3.1.2.4.4.2.1	Yes	Test over full response range	Yes
KuA Antenna Pitch Rate 0-2 Mrads/sec	EA-1								
KuA Antenna Roll Rate 0-2 Mrads/sec	EA-1								
KuA Antenna Roll Rate 0-2 Mrads/sec	EA-1	3.1.2.4.7.1 3.2.1.8.2.2	N/A	Disp	N/A	20.3.1.2.4 4.2.1	Yes		Yes
9. KuA Search Status Flag	EA-1	3.1.2.4.3.4	N/A	Disp	N/A	20.3.1.2.4.4.1	Unknown, RI requires logic "0" to be 0 to 4 V & it is unknown if the open circuit the EA-1 supplies for a logic "0" will function.	None	N/A
KuA Track Status Flag									
KuA Scan Warn Flag	EA-1	3.1.2.4.3.4	N/A	Disp	N/A	20.3.1.2.4.4.1		None	N/A

Note: EA-1 Spec is Rev. A instead of Rev. B.

Table 18. EA-1/Orbiter (Cont'd)

	SOURCE			DESTINATION					
	LRU	Hughes LRU Spec. Paragraph	Rockwell Spec. Paragraph	LRU	Hughes LRU Spec. Para.	Rockwell Spec. Para.	Are Interfaces Compatible?	Critical Electrical Parameters To Be Measured	Have Critical Electrical Parameters Been Tested?
10. KuA Search Initiate	Ctls	N/A	20.3.1.2.4.3.1	EA-1	3.1.2.4.3.2	N/A	No, RI specifies logic "0" as 0 - 4 V but EA-1 requires 0 - 2.5 V.	None	N/A
Radar Passive									
Radar Active									
Radar Power Low									
Radar Power Medium									
Radar Power High									
Slew Rate Fast KuA									
Slew Rate Slow KuA									
Pitch Slew Up Select KuA									
Pitch Slew Down Sel. KuA									
Roll Slew Left Sel. KuA									
Roll Slew Right Sel. KuA	Ctls	N/A	20.3.1.2.4.3.1	EA-1	3.1.2.4.3.2	N/A		None	N/A
11. Comm A Standby	GCILU	N/A	20.3.1.2.4.3.2	EA-1	3.1.2.4.3.2	N/A	No, RI specifies logic "0" as 0 - 4 V but EA-1 requires 0 - 2.5 V.	None	N/A
Comm A On									
Radar Standby									
Radar On									
GPC Acq. Select KuA									
GPC Desig. Select KuA									
Auto Track Select KuA									
Manual Slew Select KuA	GCILU	N/A	20.3.1.2.4.3.2	EA-1	3.1.2.4.3.2	N/A		None	N/A
12. 28-VDC Control Panel Power Out	EA-1	3.1.2.4.8.2	N/A	GCILU	N/A	20.3.1.2.4.3.3	Unknown. EA-1 doesn't specify source current	None	N/A
13. Transmit/Scan Ensemble KuA	ADA	N/A	20.3.1.2.4.5.1.1	EA-1	3.1.2.4.3.2	N/A	No, RI specifies logic "1" as 18-32 V and "0" as 0-4 V but EA-1 requires logic "1" as 23-32 V & "0" as 0-2.5V	None	N/A
14. Room Stow Initiate KuA	ADA	N/A	20.3.1.2.4.5.1.2	EA-1	3.1.2.4.3.2	N/A	No, RI specifies logic "0" as 0 - 4 V but EA-1 requires 0 - 2.5 V.	None	N/A

Note: EA-1 Spec is Rev. A instead of Rev. B.

Table 18. EA-1/Orbiter (Cont'd)

	SOURCE			DESTINATION					
	LRU	Hughes LRU Spec. Paragraph	Rockwell Spec. Paragraph	LRU	Hughes LRU Spec. Para.	Rockwell Spec. Para.	Are Interfaces Compatible?	Critical Electrical Parameters To Be Measured	Have Critical Electrical Parameters Been Tested?
15. Boom Stow Enable I, KuA	EA-1	3.1.2.4.3.4	N/A	ADA	N/A	20.3.1.2.4.5.2.1	No, RI specifies a logic "0" as 0-4 V but EA-1 logic "0" is an open circuit. It is not clear if EA-1 can source enough current and maintain logic "1" output voltage.	None	N/A
16. Boom Stow Reset KuA	EA-1	3.1.2.4.3.4	N/A	ADA	N/A	20.3.1.2.4.5.2.1	No, RI specifies logic "0" as 0-4 V but EA-1 logic "0" is an open circuit.	None	N/A
17. 28-VDC Power	Main Bus	N/A	20.3.1.2.1	EA-1	3.1.2.4.9.1 3.1.2.1	N/A	Yes	None	N/A
18. 28-VDC Control Panel Power In	Main Bus	N/A	20.3.1.2.1		3.1.2.4.8.2	N/A	Unknown, EA-1 doesn't specify source current	None	N/A

Note: EA-1 Spec is Rev. A instead of Rev. B.

Table 18. EA-1/Orbiter (Cont'd)

	SOURCE			DESTINATION			Are Interfaces Compatible?	Critical Electrical Parameters To Be Measured	Have Critical Electrical Parameters Been Tested?
	LRU	Hughes LRU Spec. Paragraph	Rockwell Spec. Paragraph	LRU	Hughes LRU Spec. Para.	Rockwell Spec. Para.			
1. Radar Power Low Radar Power Medium Frequency Select A,B,C High Sample Rate Select Radar Sum Enable Radar Difference Enable TWT Bypass Enable Transmitter Limiter AGC First IF Step AGC	EA-2 EA-2	3.1.2.4.2.1 3.1.2.4.2.1	N/A N/A	DA DA	Table 3.1.2.4-1 Table 3.1.2.4-1	N/A N/A	Yes Yes	None None	N/A N/A
2. Linear AGC	EA-2	3.1.2.4.2.2.1	N/A	DA	3.1.2.4.11		No, for EA-2 + 6 V = 40 dB but, for DA, +5 V = 40 dB	Test the linear AGC over its full range	Unknown at this time
3. Transmit Gate	EA-2	3.1.2.4.2.3.1	N/A	DA	3.1.2.4.8	N/A	Yes	None	N/A
4. Receiver Gate	EA-2	3.1.2.4.2.3.2	N/A	DA	3.1.2.4.9	N/A	Yes	None	N/A
5. Exciter Gate	EA-2	3.1.2.4.2.3.3	N/A	DA	3.1.2.4.7	N/A	Yes	None	N/A
6. Radar Second IF	DA	3.1.2.4.14.1	N/A	EA-2	3.1.2.4.2.4	N/A	Yes*	This signal should be completely characterized by SRU & LRU tests	Unknown at this time

*Electrically compatible but performance requirements are an integral part of the interface and should be completely verified. The DA Spec should present a summary of signal characteristics similar to the summary in the EA-1 Spec.

Table 19. EA-2/DA

	SOURCE			DESTINATION			Are Interfaces Compatible?	Critical Electrical Parameters To Be Measured	Have Critical Electrical Parameters Been Tested?
	LRU	Hughes LRU Spec. Paragraph	Rockwell Spec. Paragraph	LRU	Hughes LRU Spec. Para.	Rockwell Spec. Para.			
1. 24-VDC Power	Main Bus	N/A	40.3.1.2.1	EA-2	3.1.2.1	N/A	Yes	None	N/A

Table 20. EA-2/Main Bus B

	SOURCE			DESTINATION					
	LRU	Hughes LRU Spec. Paragraph	Rockwell Spec. Par graph	LRU	Hughes LRU Spec. Para.	Rockwell Spec. Para.	Are Interfaces Compatible?	Critical Electrical Parameters To Be Measured	Have Critical Electrical Parameters Been Tested?
1. Forward Link Text and Graphics Data + Clock	SPA	3.1.2.4.1.2.3	N/A	Text & Graphics	N/A N/A	10.3.1.2.4.1.10 10.3.1.2.4.1.10	Yes, but SPA doesn't specify certain parameters. RI states freq. & clock phase jitters at an input SNR of 13D dB. RI further specifies data-to-clock phase offset of 150 ns and data & clock asymmetry of 10% of bit period.	Effects of asymmetry, jitter and offset	No
2. Payload Recorder Data	PL Recordr	N/A	10.3.1.2.4.1.5	SPA	3.1.2.4.2.1.1	N/A	Yes, but HAC doesn't specify common mode voltage	Test over data range 25.5 - 1024 kbps	Yes
3. OPS Recorder Data	OPS Recordr	N/A	10.3.1.2.4.1.4	SPA	3.1.2.4.2.1.2	N/A	Yes, but HAC doesn't specify common mode voltage	Test over data range 25.5 - 1024 kbps	Yes
4. Closed-Circuit TV Video	VSN	N/A	10.3.1.2.4.1.11	SPA	3.1.2.4.2.1.3	N/A	Yes, but HAC doesn't specify common mode voltage	Test over full bandwidth 0 - 4.5 MHz	Yes
5. Payload Interrogator 1 Data	PL Inter.	N/A	10.3.1.2.4.1.9	SPA	3.1.2.4.2.1.4	N/A	No, RI specifies diff. signal level 2.0 + 0.4 V rms & HAC specifies 2.0 $^{+0.6}_{-0.2}$ V p-p. HAC specifies 35 dB rms SNR & RI specifies nothing.	Test digital over range 16-2000 kbps (NRZ), 16 to 1024 kbps (Bi-ϕ-L), & 0 - 4.5 MHz	Yes

Table 21. SPA/Orbiter

	SOURCE			DESTINATION					
	LRU	Hughes LRU Spec. Paragraph	Rockwell Spec. Paragraph	LRU	Hughes LRU Spec. Para.	Rockwell Spec. Para.	Are Interfaces Compatible?	Critical Electrical Parameters To Be Measured	Have Critical Electrical Parameters Been Tested?
6. Payload Interrogator 2 Data	PI Interr.	N/A	10.3.1.2.4.1.9	SPA	3.1.2.4.2.1.4	N/A	No, same as PI Inter. 1	Same as item 5	Yes
7. Forward Link Payload Data & Clock	SPA	3.1.2.4.1.2.2	N/A	Pay-load	N/A	10.3.1.2.4.1.10	Yes, but ref. item 1	Effects of asymmetry, jitter and offset	No
8. HDR Payload Analog Data	Pay-load	N/A	10.3.1.2.4.1.12.4	SPA	3.1.2.4.2.1.8	N/A	Perhaps, RI specifies 0 to 1.0V p-p +10% diff. signal & HAC specifies 1.0V p-p +10% diff. signal	Effects on SPA over full signal amplitude range. Test over range 0 - 4.5 MHz	Yes
9. HDR Payload Digital Data	Pay-load	N/A	10.3.1.2.4.1.12.2	SPA	3.1.2.4.2.1.7	N/A	No, RI specifies 1.8 - 5.0V p-p, 1-1, and HAC specifies +1.8V p-p, 1-1. HAC doesn't specify max. rise and fall time of 50 ns or common mode voltage	Test over range 16 to 4000 kbps	Yes
10. LDR Payload Digital Data	Pay-load	N/A	10.3.1.2.4.1.12.3	SPA	3.1.2.4.2.1.6	N/A	No, RI specifies 1.8-5.0 V p-p, 1-1 and HAC specifies +1.8V p-p, 1-1 min. HAC does not specify max. rise & fall time of 50 ns or common mode voltage.	Test over ranges of 16-4000 kbps	Yes

Table 21. SPA/Orbiter (Cont'd)

	SOURCE			DESTINATION					
	LRU	Hughes LRU Spec. Paragraph	Rockwell Spec. Paragraph	LRU	Hughes LRU Spec. Para.	Rockwell Spec. Para.	Are Interfaces Compatible?	Critical Electrical Parameters To Be Measured	Have Critical Electrical Parameters Been Tested?
11. HDR Payload Max & Clock	Pay-load	N/A	10.3.1.2.4.1.12.1	SPA	3.1.2.4.2.1.5	N/A	No, this interface will be undergoing extensive test'g. Significant differences exist in RI vs HAC spec. for rise/fall time & input logic levels but this is a known deficiency.	Test over range of 2 to 50 Mbps; rise/fall times input logic level variations	Extensive tests planned
12. Return Link OPS Data NSP 1	NSP	N/A	10.3.1.2.4.1.7.2	SPA	3.1.2.4.2.1.9	N/A	Yes	None	N/A
13. Return Lin OPS Data NSP 2	NSP	N/A	10.31.2.4.1.7.2	SPA	3.1.2.4.2.1.9	N/A	Yes	None	N/A
14. Forward Link OPS Data NSP 1	SPA	3.1.2.4.1.2.1	N/A	NSP	N/A	10.3.1.2.4.1.7.1	Perhaps, RI specifies 75 direct-coupled source & HAC specifies <1.4k AC-coupled source. RI does not specify rise/fall time.	Test over range of 32 - 216 kbps & voltage input range (100 mV to 260 mV)	Yes
15. Forward Link OPS Data NSP 2	SPA	3.1.2.4.1.2.1	N/A	NSP	N/A	10.3.1.2.4.1.7.1	Same as 14.	Same as 14.	Same as 14.
16. Payload Interr. 1 Select Payload Interr. 2 Select NSP 1 Select NSP 2 Select	LCA , | LCA	N/A | | N/A	10.3.1.2.4.1.8 | | 10.3.1.2.4.1.8	SPA | | SPA	3.1.2.4.3.1.1.1 | | 3.1.2.4.3.1.1.1	N/A | | N/A	Yes | | Yes	None | | None	N/A | | N/A

Table 21. SPA/Orbiter (Cont'd)

	SOURCE			DESTINATION					
	LRU	Hughes LRU Spec. Paragraph	Rockwell Spec. Paragraph	LRU	Hughes LRU Spec. Para.	Rockwell Spec. Para.	Are Interfaces Compatible?	Critical Electrical Parameters To Be Measured	Have Critical Electrical Parameters Been Tested?
17. Forward Link Data Pres.	SPA	3.1.2.4.3.1.2.1	N/A	GCILC	N/A	10.3.1.2.4.1.6.3	Perhaps, RI specifies rise & fall times of 1 ms and HAC specifies 10 ms	None	N/A
18. Data Select Comm A (Bus 2)	GCILC	N/A	10.3.1.2.4.1.6.1	SPA	3.1.2.4.3.1.1.1	N/A	Yes	None	N/A
LDR Payload Digital Sel.									
HDR Payload Digital Sel.									
HDR Payload Max Select									
HDR Payld Anlg Data Sel.									
HDR Pyld Dig. Data Sel.									
LDR P/L Inter. Data Sel.									
HDR P/L Inter. Data Sel.									
HDR P/L CCTV Data Select									
LDR OPS Recorder Select									
LDR P/L Recorder Select									
HDR Off	GCILC	N/A	10.3.1.2.4.1.6.1	SPA	3.1.2.4.3.1.1.1	N/A	Yes	None	N/A
19. Control Power Out	SPA	3.1.2.1.2	N/A	GCILC	N/A	10.3.1.2.4.1.6.2	Yes	None	N/A
20. 28-VDC Power	Main Bus	N/A	10.3.1.2.1	SPA	3.1.2.1.1	N/A	Yes	None	N/A

Table 21. SPA/Orbiter (Cont'd)

	SOURCE			DESTINATION			Are Interfaces Compatible?	Critical Electrical Parameters To Be Measured	Have Critical Electrical Parameters Been Tested?
	LRU	Hughes LRU Spec. Paragraph	Rockwell Spec. Paragraph	LRU	Hughes LRU Spec. Para.	Rockwell Spec. Para.			
1. Transmit Enable Comm A	SPA	3.1.2.4.3.2.2	N/A	DA	Table 3.1.2.4-1	N/A	Yes	None	N/A
2. Exciter IF Comm A	SPA	3.1.2.4.2.2.2	N/A	DA	3.1.2.4.6	N/A	Yes, but SPA power output level is 13.4 dBm +1.5 dBm & DA power input level is 5.25 +2.25 dBm. Difference is accounted for by cable losses. Specifications should be clarified to show cable losses.	This signal should be completely characterized by SRU and LRU tests.	No

Table 22. DA/SPA

(Headings same as above)

1. Xmit Enable (30° Deploy)	ADA	N/A	30.3.1.2.4.1.2	DA	Table 3.1.2.4-1	N/A	Yes	None	N/A
2. Boom Stow Enable II Ku	DA	3.1.2.4.2.6	N/A	ADA	N/A	30.3.1.2.4.3.3	Yes	None	N/A
3. Boom Stow Enable II Excitation	ADA	N/A	30.3.1.2.4.1.3	DA	Table 3.1.2.4-1	N/A	Yes	None	N/A
4. DA Temp 1	DA	3.1.2.4.27	N/A	PCA	N/A	30.3.1.2.4.7.2	Yes	Verify measurement range	Unknown at this time
DA Temp Lead Comp 1									
DA Temp 2									
DA Temp Lead Comp 2									
DA Temp 3									
DA Temp Lead Comp 3									
DA Temp 4									
DA Temp Lead Comp 4									
DA Temp 5									
DA Temp Lead Comp 5									
DA Temp 6									
DA Temp Lead Comp 6	DA	3.1.2.4.27	N/A	PCA	N/A	30.3.1.2.4.7.2	Yes		
5. 28 VDC Power	Main Bus	N/A	30.3.1.2.1	DA	3.1.2.1	N/A	Yes	None	N/A
28 VDC DEA Heater 1									
28 VDC DEA Heater 2									
28 VDC DMA Heater	Main Bus	N/A	30.3.1.2.1	DA	3.1.2.1	N/A	Yes	None	N/A

Table 23. DA/Orbiter

9.3 Conclusions/Recommendations

Tables 15 - 23 provide the results summary for the LRU interchangeability study. Even though some LRU's are presently functioning as a system, the conclusions from Tables 15 - 23 are that some serious interface deficiencies exist which must be corrected in order to assure LRU interchangeability. The conclusion of this study, therefore, is that, at the present time, the LRU's are not interchangeable.

In order to assure LRU interchangeability, Axiomatix makes the following recommendations:

- Each interface discrepancy listed in Tables 15 to 23 must be addressed by Rockwell and/or Hughes and resolved. Full resolution includes making the appropriate documentation changes to the Rockwell and/or Hughes LRU specifications.

- In this study, Axiomatix reviewed only the Rockwell systems specification and the four Hughes LRU specifications. Careful attention must be given to determine that the LRU's are built per their respective specifications, and it is recommended that the development and acceptance tests be reviewed to assure hardware conformance.

- Most interfaces specify some input/output voltage tolerance and, to assure LRU interchangeability, the effects of bus voltage variations must be tested. It is recommended that the acceptance tests and development test exercise the interfaces over the bus voltage range of +24 VDC to +32 VDC. The EA-1 ATP already performs some tests as a function of bus voltage; however, each ATP should be reviewed in detail to verify that such bus voltage tests are conducted and, if so, which interfaces or performance parameters are tested.

The reader should remember that this study examined only electrical compatibility of the interfaces. The performance parameters will be verified by development, acceptance and qualification testing, and have not been addressed in this report.

10.0 CDR DEVELOPMENT TEST EVALUATION

10.1 SPA ADL LRU Test Data Evaluation

10.1.1 Introduction

The purpose of this section is to evaluate and assess the SPA ADL LRU test data presented by Hughes Aircraft Company (HAC) on September 16-17, 1980. The majority of these tests can be divided into two categories: return link and forward link tests. The tests were conducted in accordance with HAC preliminary test procedure YP32090-005 and were performed at room temperature only.

The test equipment used to test the SPA ADL LRU is comprised of the following Hughes-built test panels:

- Data generator panel
- Noise generator panel
- Demodulator panel

A brief description of the SPA tester and its relationship to the SPA LRU are discussed in the following sections.

10.1.1.1 SPA Return Link LRU Test Configuration

SPA LRU return link tests require the use of all three previously mentioned test panels. Figure 57 illustrates the return link test setup.

In LRU testing, the data generator is the control center. At the heart of the data generator is the PROM-stored program SPAR. Through SPAR, all conditions required by the SPA LRU are initiated automatically, depending upon the specific test selected by the operator via the front panel. These conditions include: (1) serial data, (2) GCILC (discrete) commands, (3) channel selection, and (4) the data for each channel. The data is then sent to the SPA LRU.

The 1.875425 GHz RF signal at the SPA output is sent to the SPA demodulator test panel where it is demodulated back to baseband, then returned to the data generator (for monitoring purposes) and to the BER generator (for bit detection).

The BER noise generator, under the direction of SPAR, performs all the necessary switching to channel the demodulated signal and the noise through the appropriate summer and bit detector.

Before bit detection, the signal and noise are adjusted to the desired levels via controls on the front panel of the BER noise generator. The bit-detected signal leaves the BER noise generator to return to the

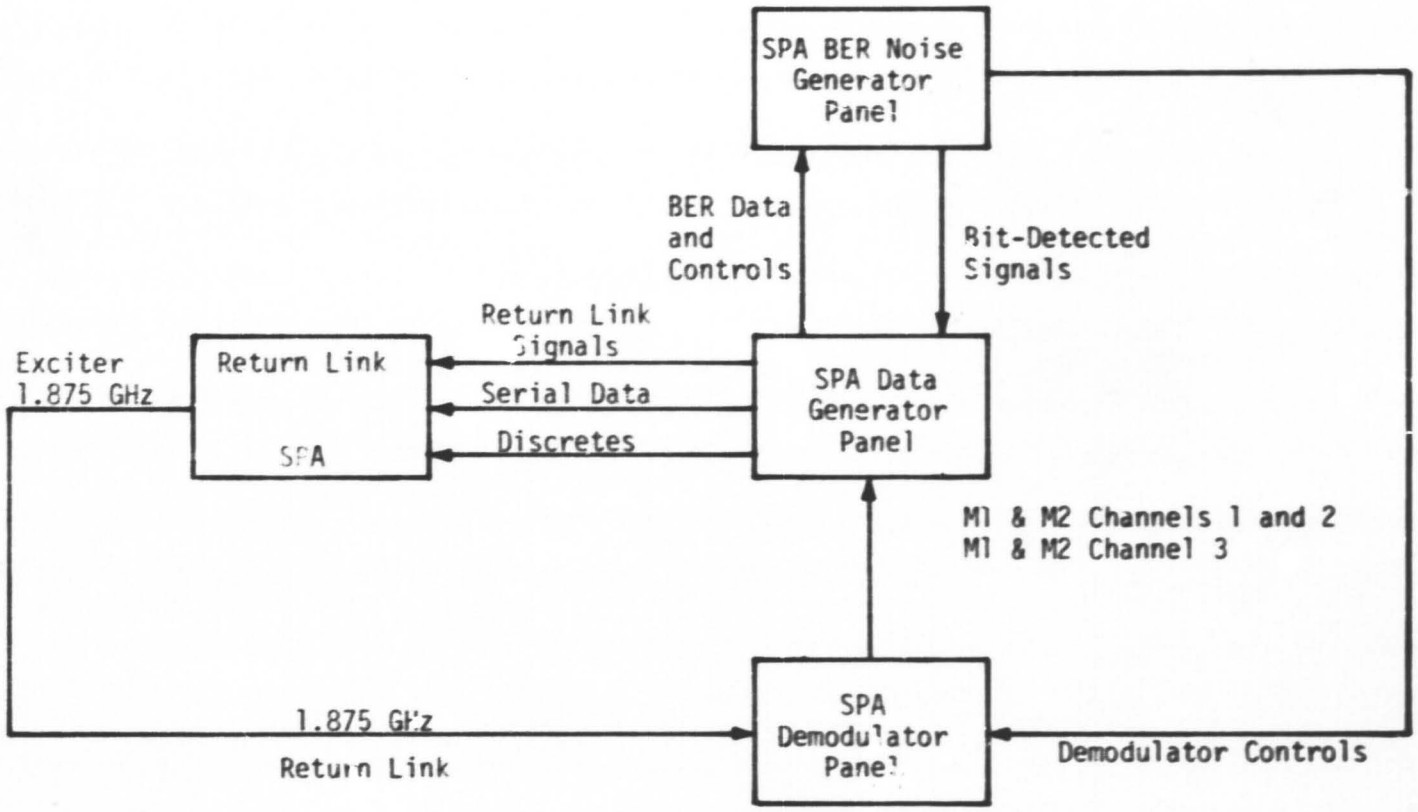

Figure 57. SPA LRU Test Configuration

data generator, where it is compared to the adjustable delayed reference data. After comparison, the errors are channeled to the front panel of the data generator, where they are counted with an external counter.

10.1.1.2 SPA Forward Link LRU Test Configuration

The test setup shown in Figure 58 is used to verify the performance and functional requirements of the SPA forward link. The tester generates a 216 kbps biphase-L signal for input to the SPA; data, clock and frame synchronization lock status SPA output signals are monitored at the tester to verify data and clock quality.

10.1.2 ADL SPA Test Data

Hughes utilized six tests to successfully verify the management/handover logic. The six tests are listed as follows:

(1) HAC test 000 - Q Test
(2) HAC test 001 - Transmit Enable Test, Comm A On
(3) HAC test 002 - Transmit Enable Test, Comm B On
(4) HAC test 003 - Transmit Enable Test, Handover
(5) HAC test 004 - Data Present Test
(6) HAC test 006 - Modulation On/Off Test

The majority of the tests, however, concentrated on the return and forward links.

10.1.2.1 SPA ADL LRU Return Link Data

Figures 59 through illustrate the signal paths used to verify return link performance and also briefly describe each test. In addition, each figure indicates the data rate and hexadecimal data utilized for that test, along with the data rate ranges which each input is required to process.

Hughes tested all the various signal combinations and, except for one case (16 kbps, mode 2), exercised each channel at minimum and maximum data rates and analog frequencies. Of the 30 return link tests, the SPA passed 20, but failed 10. Table 24 summarizes the return link test failures.

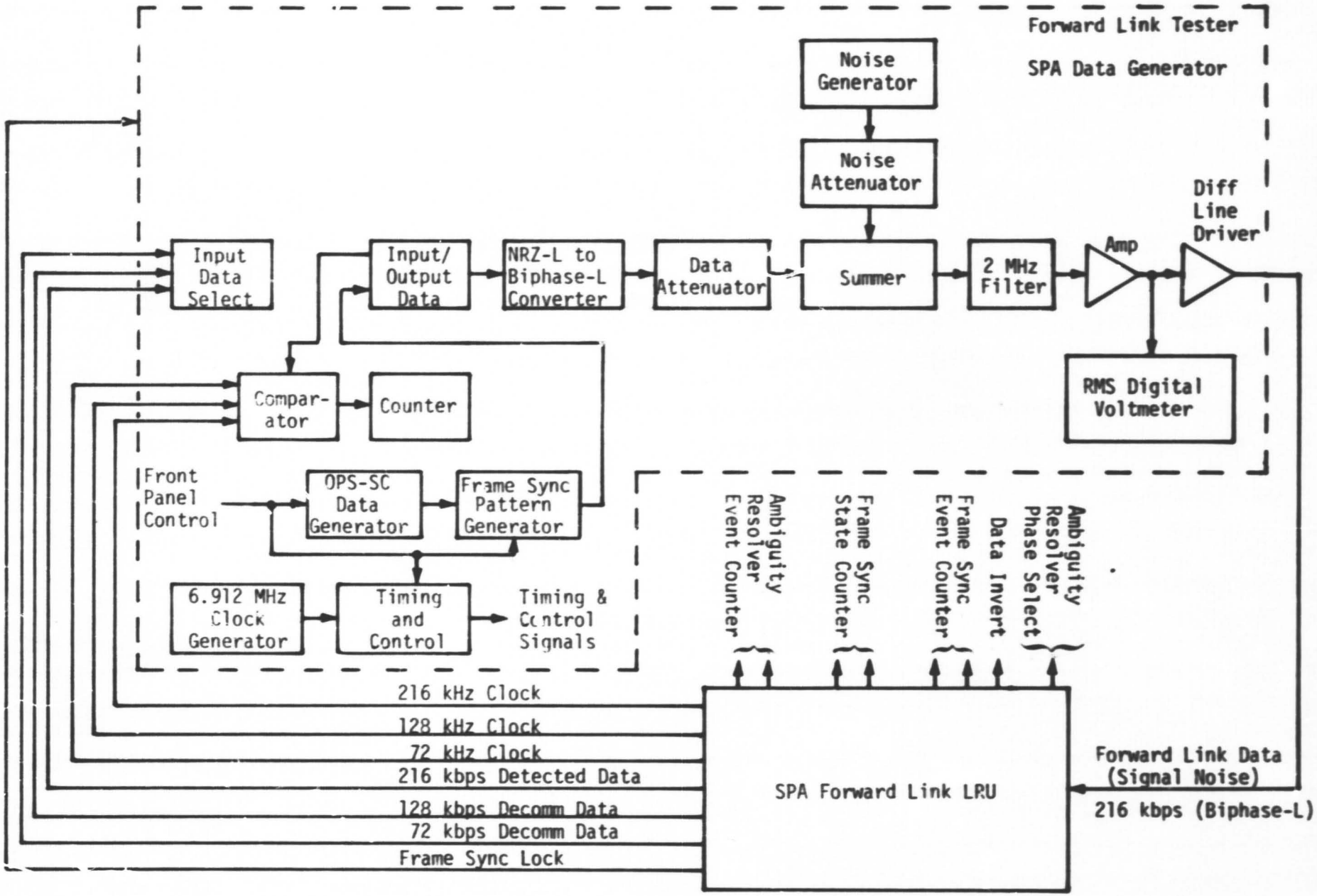

Figure 58. Forward Link Test Setup

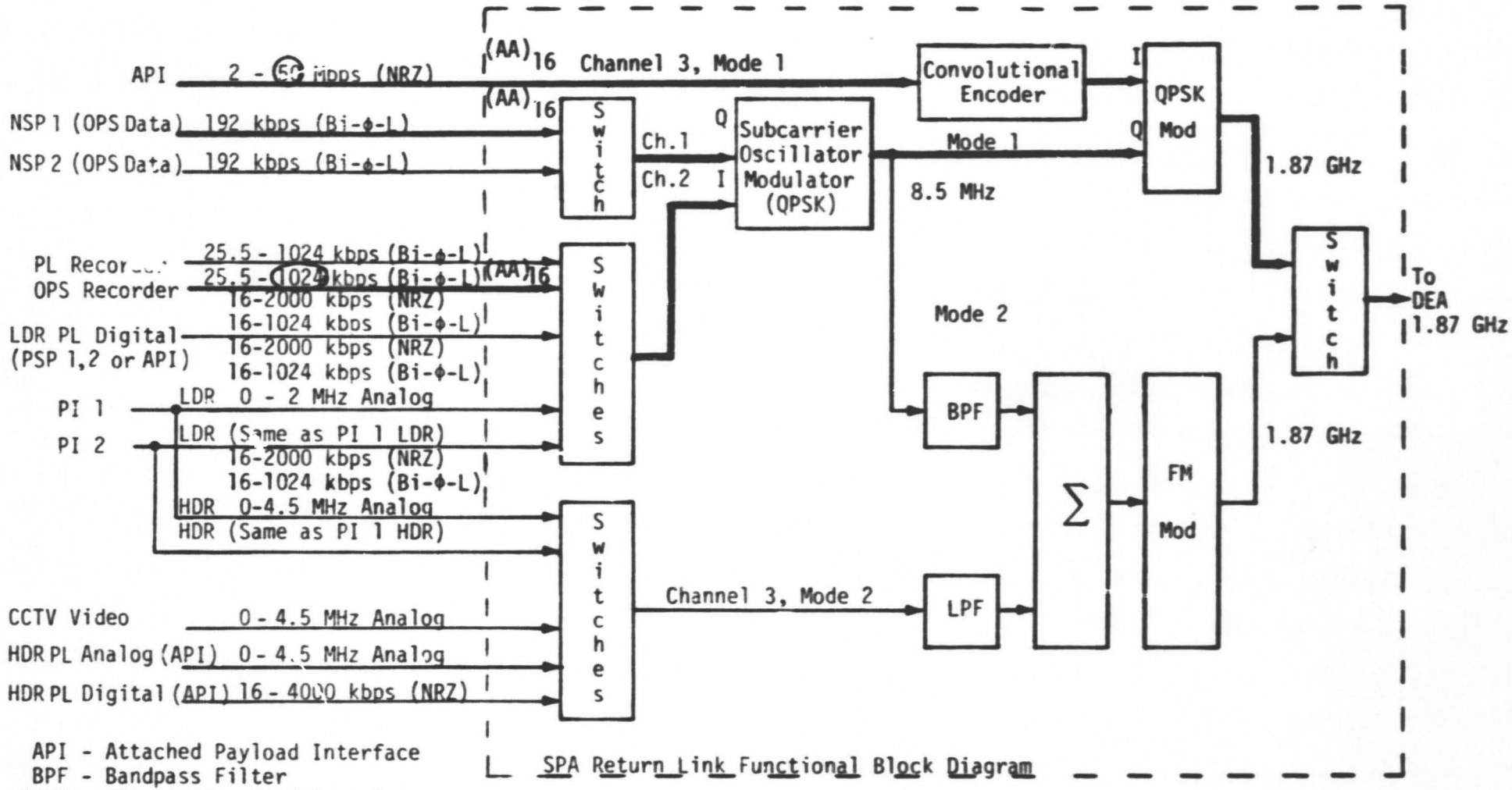

SPA Return Link Functional Block Diagram

API - Attached Payload Interface
BPF - Bandpass Filter
CCTV - Closed-Circuit Television
HDR - High Data Rate
LDR - Low Data Rate
LPF - Lowpass Filter
NSP - Network Signal Processor
OPS - Operations
PI - Payload Interrogator
PL - Payload
PSP - Payload Signal Processor

Test 005

Purpose: To verify spectral purity of 1.875425 GHz with PN modulation.

Results: Passed

Figure 29

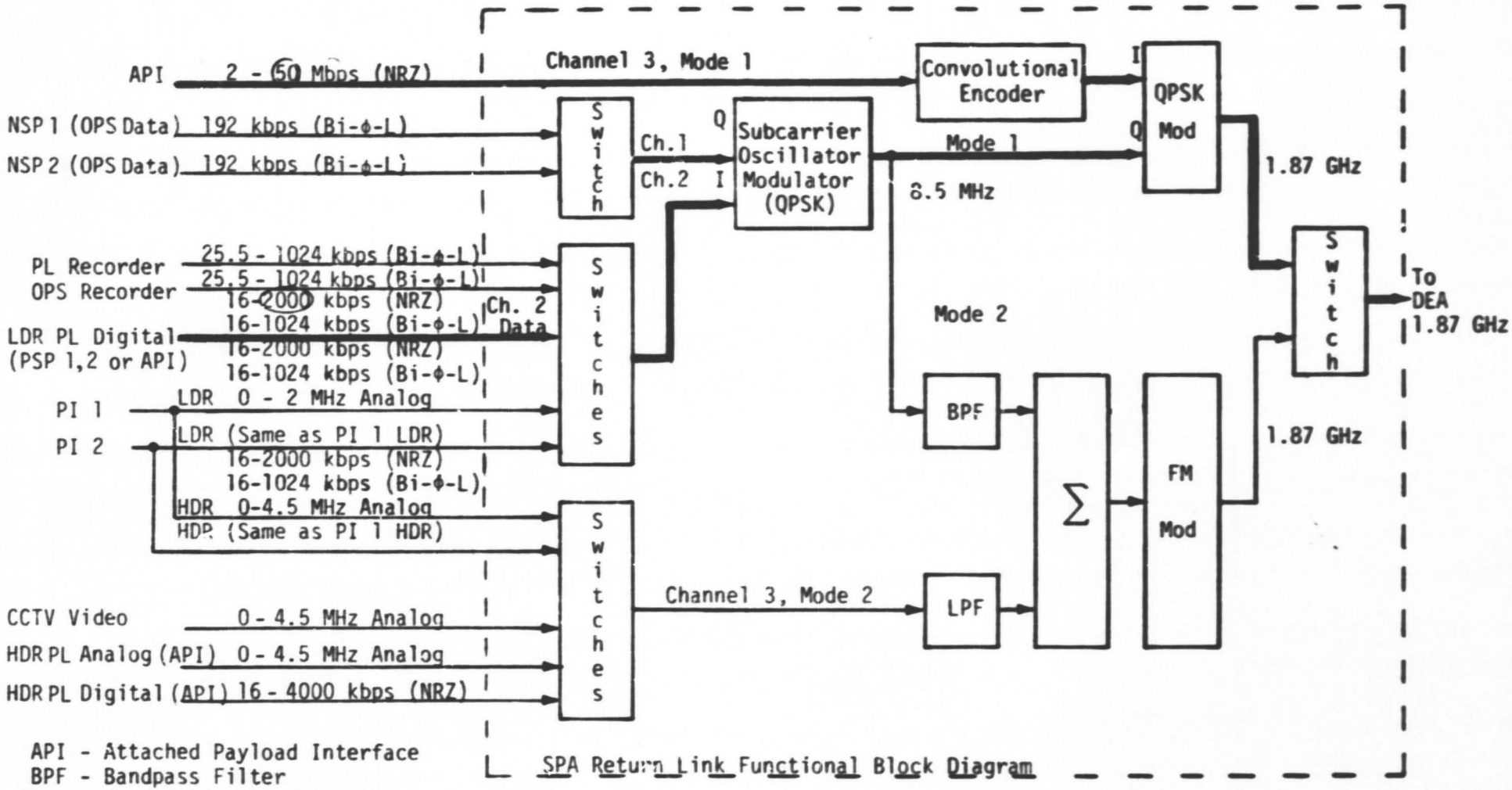

SPA Return Link Functional Block Diagram

API - Attached Payload Interface
BPF - Bandpass Filter
CCTV - Closed-Circuit Television
HDR - High Data Rate
LDR - Low Data Rate
LPF - Lowpass Filter
NSP - Network Signal Processor
OPS - Operations
PI - Payload Interrogator
PL - Payload
PSP - Payload Signal Processor

Note: (1) Test 006 was conducted during management/handover logic tests
(2) There were no tests 008 & 009.

Tests: 007, 010, 011, 012

Purpose: (1) Statically measure the spectral power density out of the QPSK modulator to verify the 80/20 power ratio
(2) Perform transmission and reflection measurements so that various network parameters such as gain, attenuation, insertion loss, SWR, return loss and impedance may be calculated from the data

Results: Failed, improper phase states and VSWR

	Ch. 2 Data	Ch. 3 Data
Test 007	$(FF)_{16}$	$(FF)_{16}$
Test 010	$(FF)_{16}$	$(00)_{16}$
Test 011	$(FF)_{16}$	$(00)_{16}$
Test 012	$(00)_{16}$	$(FF)_{16}$

Figure 60.

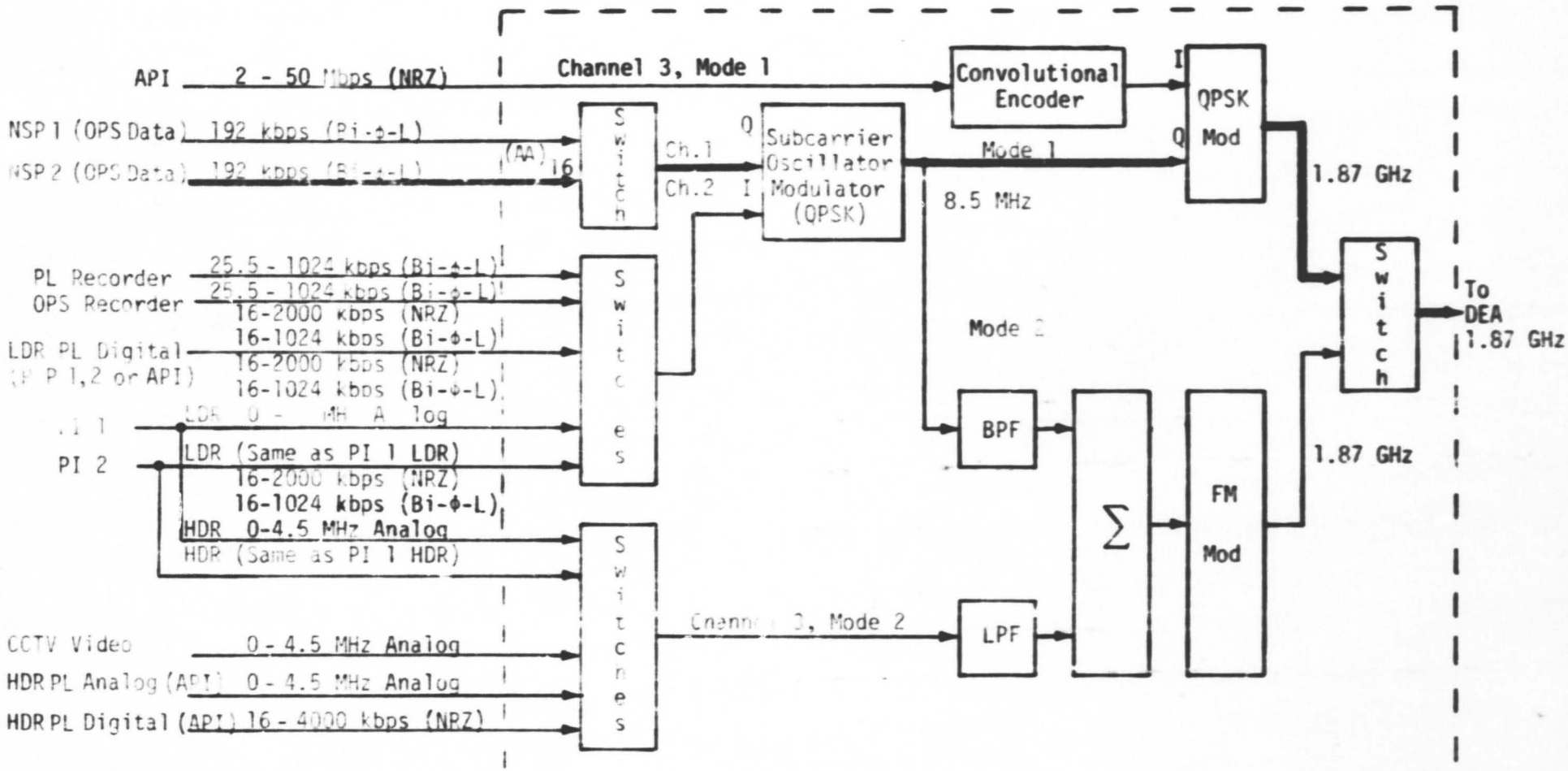

SPA Return Link Functional Block Diagram

API - Attached Payload Interface
BPF - Bandpass Filter
CCTV - Closed-Circuit Television
HDR - High Data Rate
LDR - Low Data Rate
LPF - Lowpass Filter
NSP - Network Signal Processor
OPS - Operations
PI - Payload Interrogator
PL - Payload
PSP - Payload Signal Processor

Test 013

Purpose: (1) Evaluate the FM baseband generator and QPSK modulator performance by comparing demodulated data with the input data.

(2) Verify proper switching and interfacing by management/handover.

Results: Passed.

Figure 61

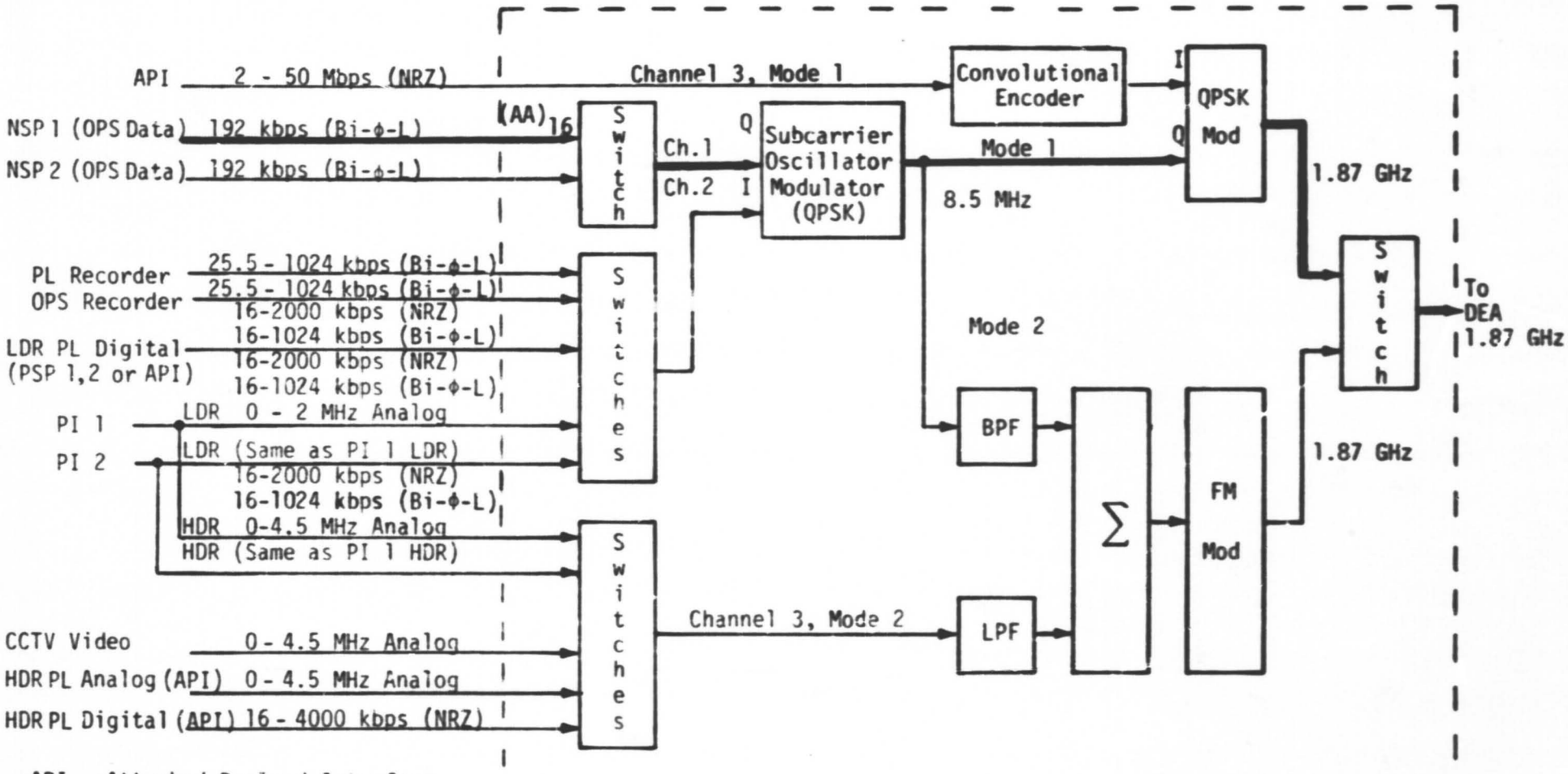

SPA Return Link Functional Block Diagram

API - Attached Payload Interface
BPF - Bandpass Filter
CCTV - Closed-Circuit Television
HDR - High Data Rate
LDR - Low Data Rate
LPF - Lowpass Filter
NSP - Network Signal Processor
OPS - Operations
PI - Payload Interrogator
PL - Payload
PSP - Payload Signal Processor

Test 014

Purpose: Same as Test 013

Result: Hughes states that the SPA passed this test. The test data indicates that the unit failed since the measured fall time was 900 ms but should have been < 600 ms.

Figure 62.

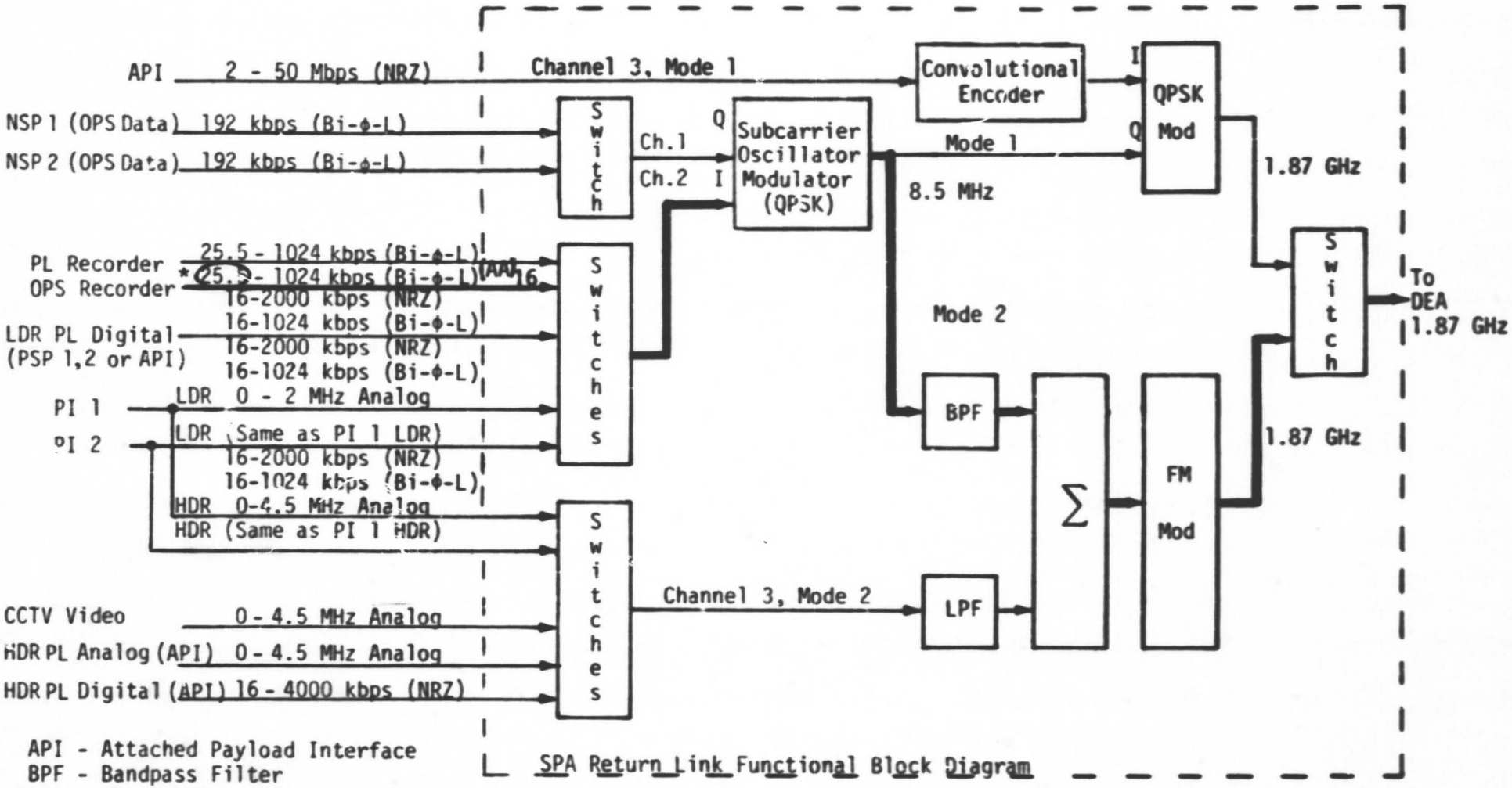

SPA Return Link Functional Block Diagram

API - Attached Payload Interface
BPF - Bandpass Filter
CCTV - Closed-Circuit Television
HDR - High Data Rate
LDR - Low Data Rate
LPF - Lowpass Filter
NSP - Network Signal Processor
OPS - Operations
PI - Payload Interrogator
PL - Payload
PSP - Payload Signal Processor

Test 015

Purpose: (1) Evaluate the FM baseband generator and FM modulator overall performance by comparing demodulated data with the input data.
(2) Verify proper switching and interfacing by management/handover.

Results: Passed

*Note: Minimum required input rate is 25.5 kbps for the OPS recorder. This test was conducted by 24.0 kbps; however, the minimum required input rate is 16.0 kbps for Channel 2, and Channel 2 mode 2 was not exercised at that low rate.

Figure 63.

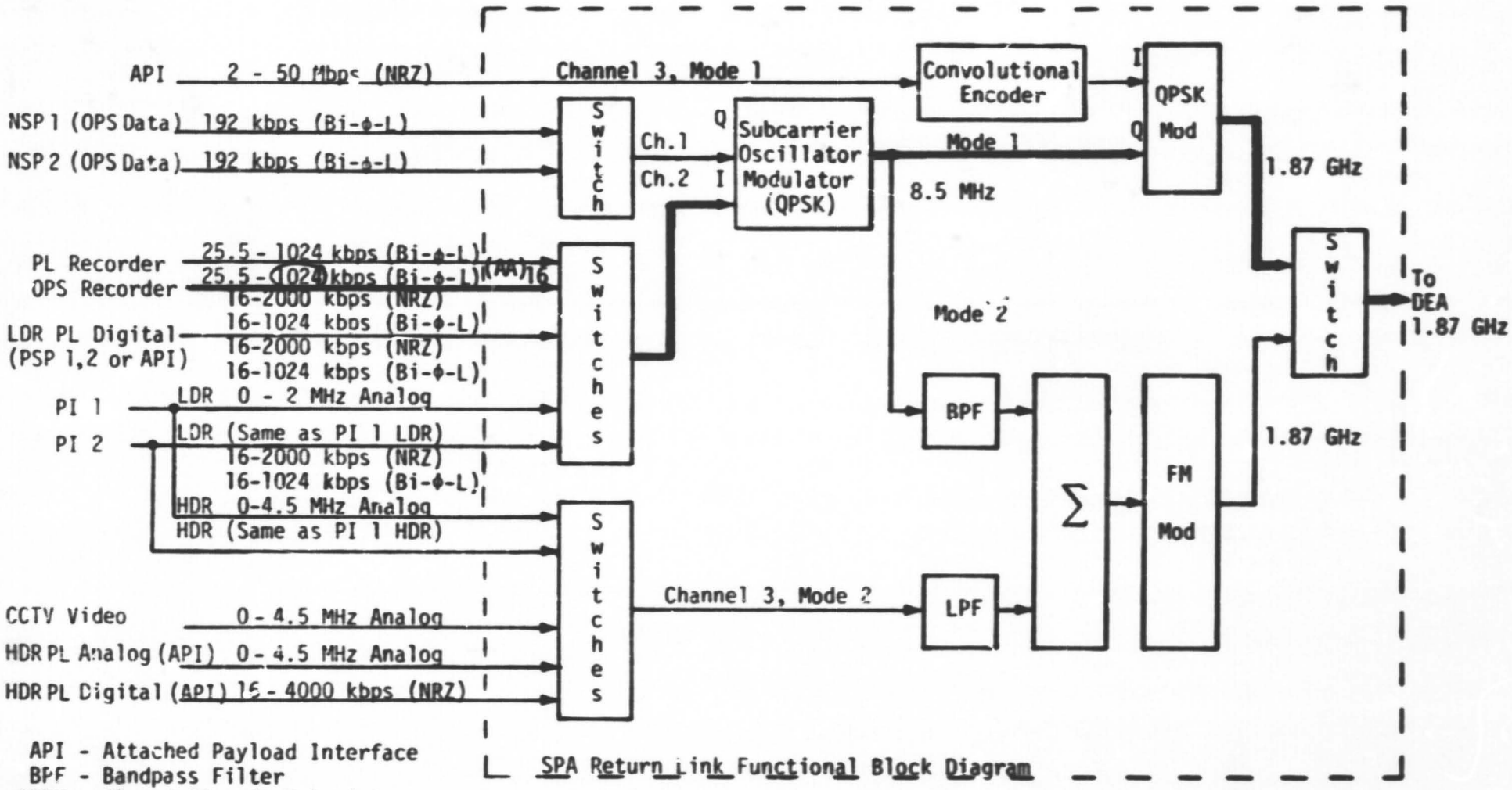

SPA Return Link Functional Block Diagram

API - Attached Payload Interface
BPF - Bandpass Filter
CCTV - Closed-Circuit Television
HDR - High Data Rate
LDR - Low Data Rate
LPF - Lowpass Filter
NSP - Network Signal Processor
OPS - Operations
PI - Payload Interrogator
PL - Payload
PSP - Payload Signal Processor

Test 016

Purpose: Same as Test 013

Result: Passed

Figure 64.

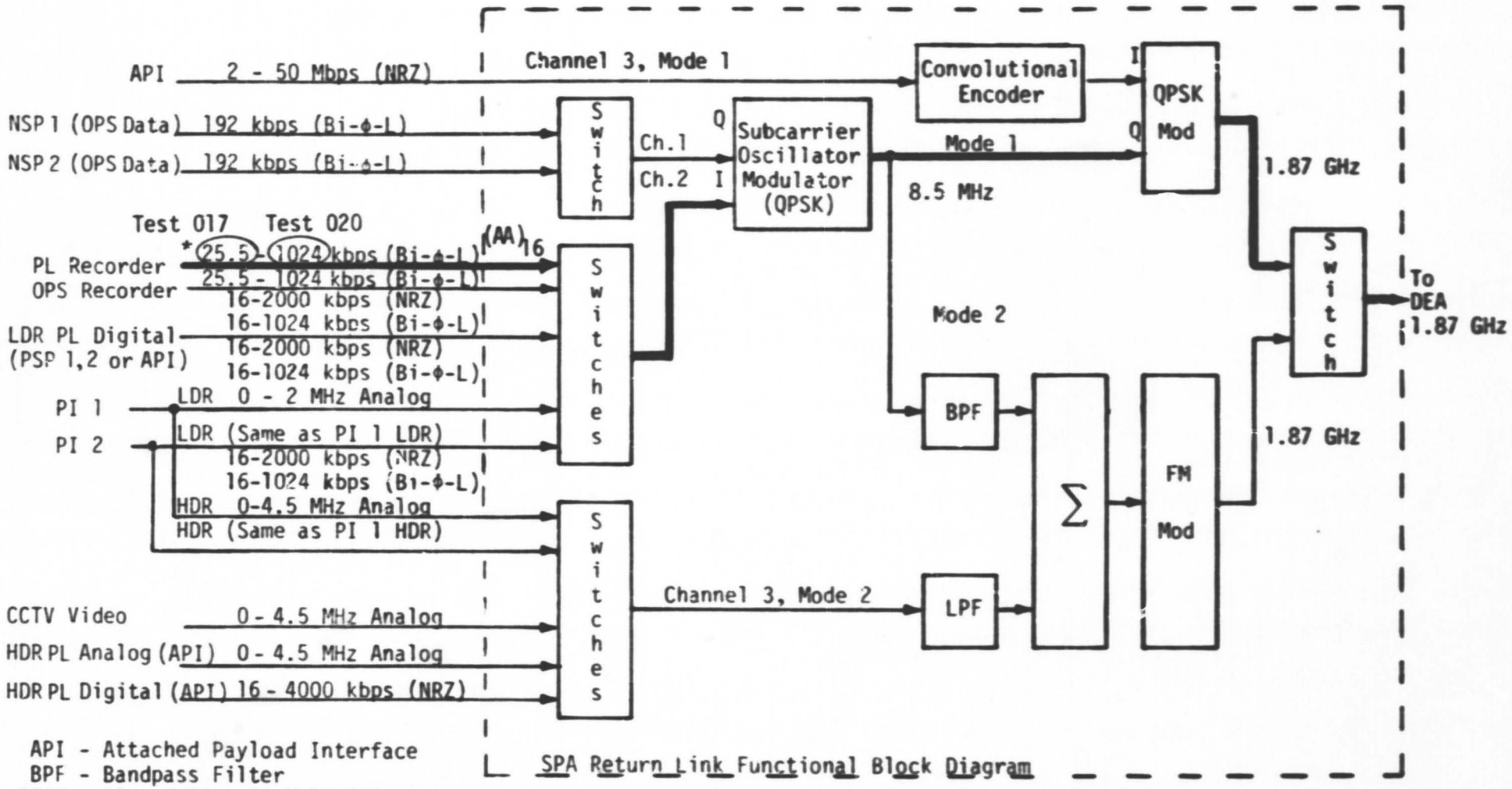

SPA Return Link Functional Block Diagram

API - Attached Payload Interface
BPF - Bandpass Filter
CCTV - Closed-Circuit Television
HDR - High Data Rate
LDR - Low Data Rate
LPF - Lowpass Filter
NSP - Network Signal Processor
OPS - Operations
PI - Payload Interrogator
PL - Payload
PSP - Payload Signal Processor

Tests 017 and 020

Purpose: Same as Test 013

Result: Passed

Note: There were no tests 018 and 019

*Test 017 conducted at 24.0 kbps.

Figure 65.

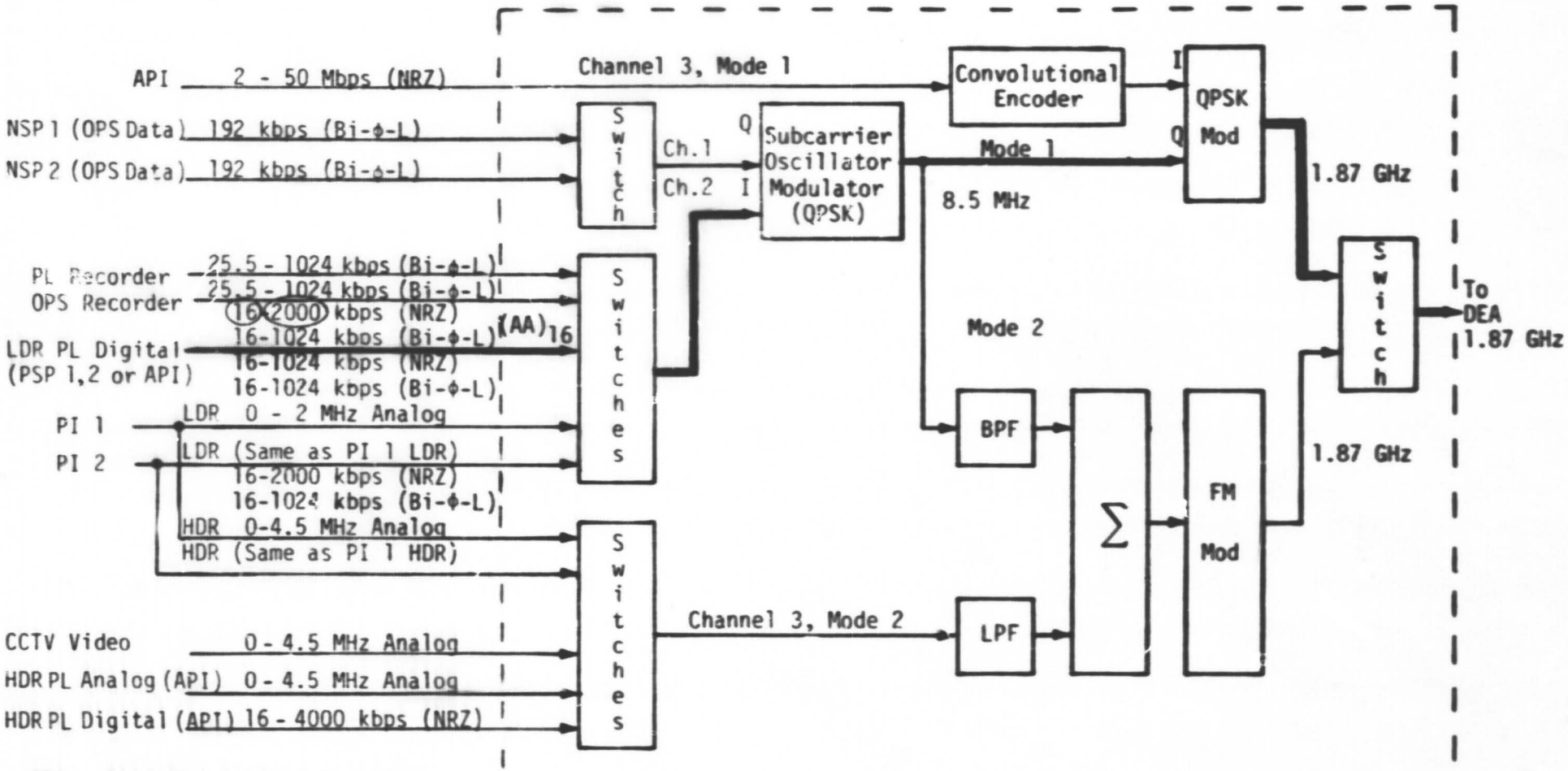

SPA Return Link Functional Block Diagram

API - Attached Payload Interface
BPF - Bandpass Filter
CCTV - Closed-Circuit Television
HDR - High Data Rate
LDR - Low Data Rate
LPF - Lowpass Filter
NSP - Network Signal Processor
OPS - Operations
PI - Payload Interrogator
PL - Payload
PSP - Payload Signal Processor

Tests 021 and 022

Purpose: Same as Test 013

Results: Passed, but Test 022 results state that the output is 2.4V p-p; however, the oscilloscope traces indicate that the output is actually 4.8V p-p.

Test 021 - Data rate 16 kbps

Test 022 - Data rate 2000 kbps

Figure 66.

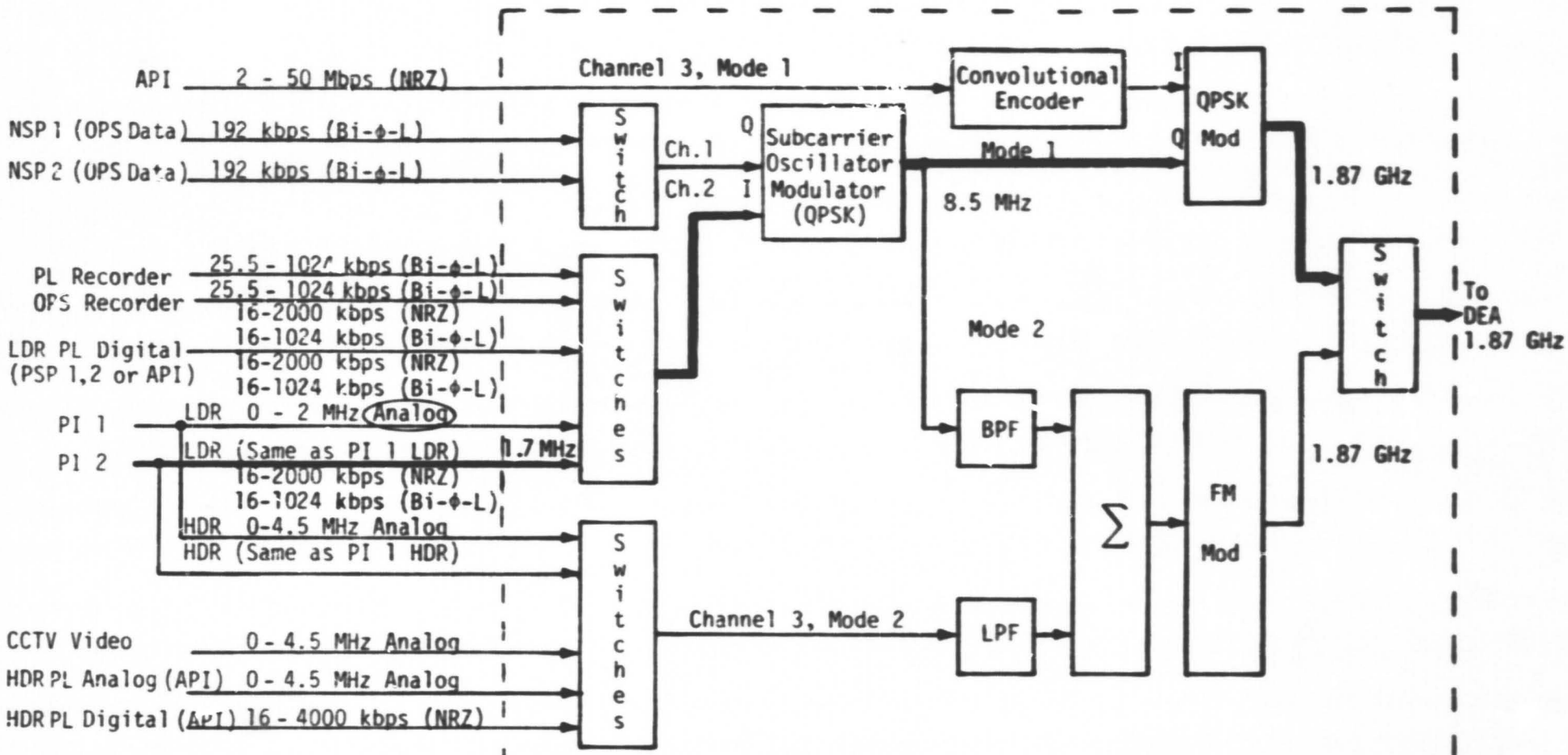

SPA Return Link Functional Block Diagram

API - Attached Payload Interface
BPF - Bandpass Filter
CCTV - Closed-Circuit Television
HDR - High Data Rate
LDR - Low Data Rate
LPF - Lowpass Filter
NSP - Network Signal Processor
OPS - Operations
PI - Payload Interrogator
PL - Payload
PSP - Payload Signal Processor

Test 023

Purpose: Same as Test 013

Results: Passed

Figure 67.

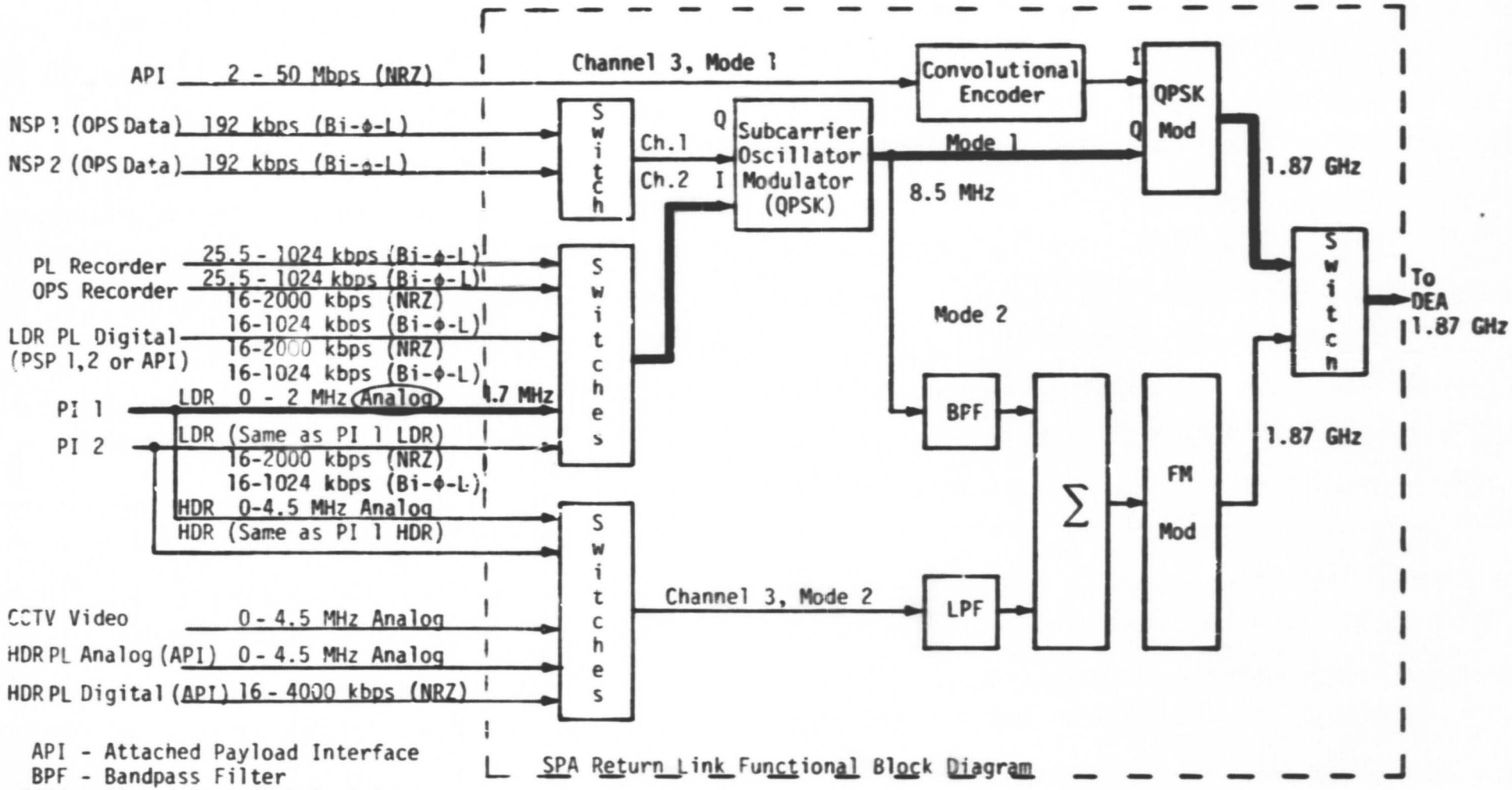

SPA Return Link Functional Block Diagram

API - Attached Payload Interface
BPF - Bandpass Filter
CCTV - Closed-Circuit Television
HDR - High Data Rate
LDR - Low Data Rate
LPF - Lowpass Filter
NSP - Network Signal Processor
OPS - Operations
PI - Payload Interrogator
PL - Payload
PSP - Payload Signal Processor

Test 024

Purpose: Same as Test 013

Result: Passed

Figure 68.

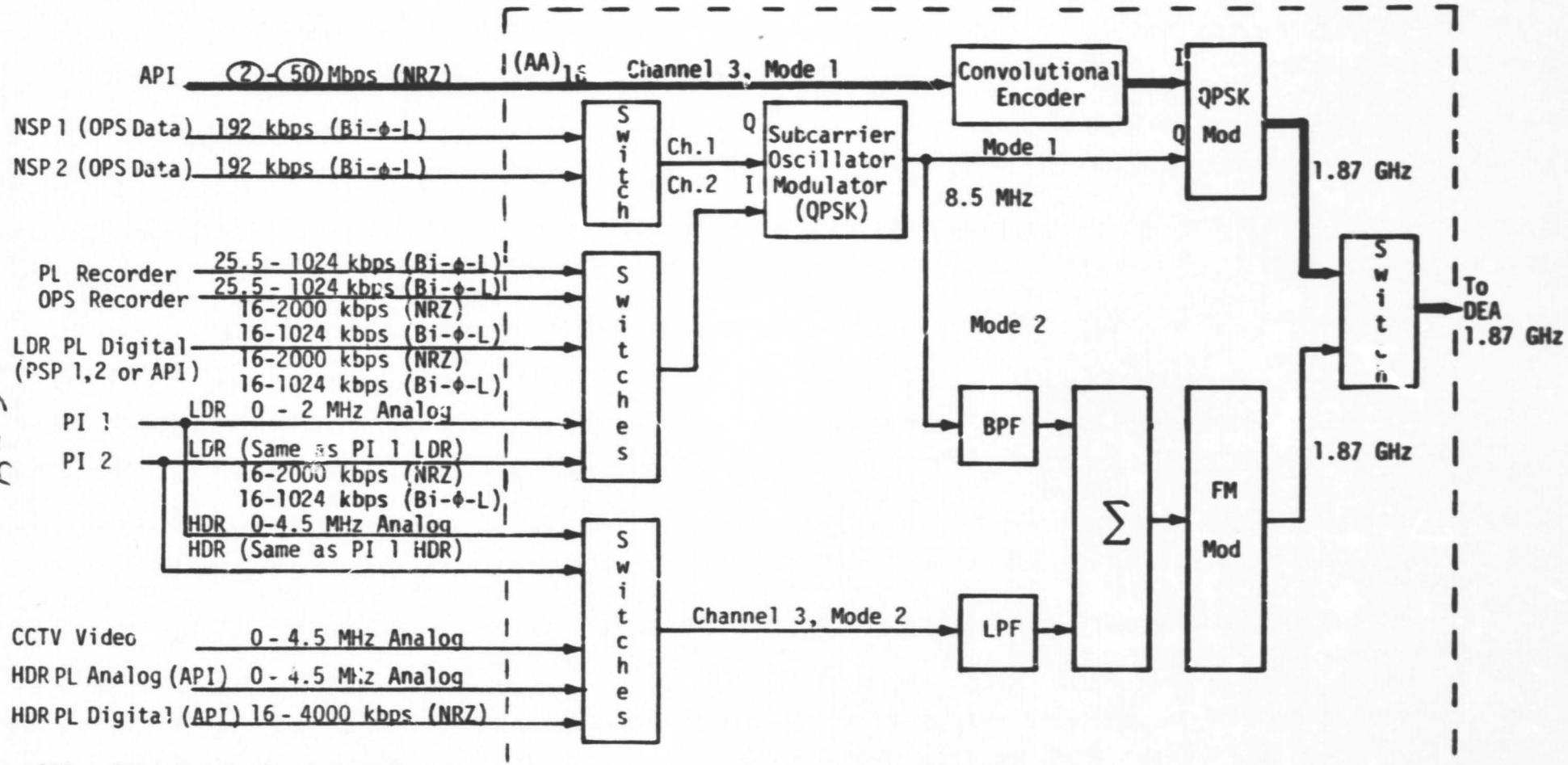

API - Attached Payload Interface
BPF - Bandpass Filter
CCTV - Closed-Circuit Television
HDR - High Data Rate
LDR - Low Data Rate
LPF - Lowpass Filter
NSP - Network Signal Processor
OPS - Operations
PI - Payload Interrogator
PL - Payload
PSP - Payload Signal Processor

SPA Return Link Functional Block Diagram

Tests 025 and 026

Purpose: Evaluate the QPSK modulator I channel overall performance by comparing the demodulated data with the input data.

Results: Passed

Test 025 - Data input 2 Mbps

Test 026 - Data input 50 Mbps

Figure 69.

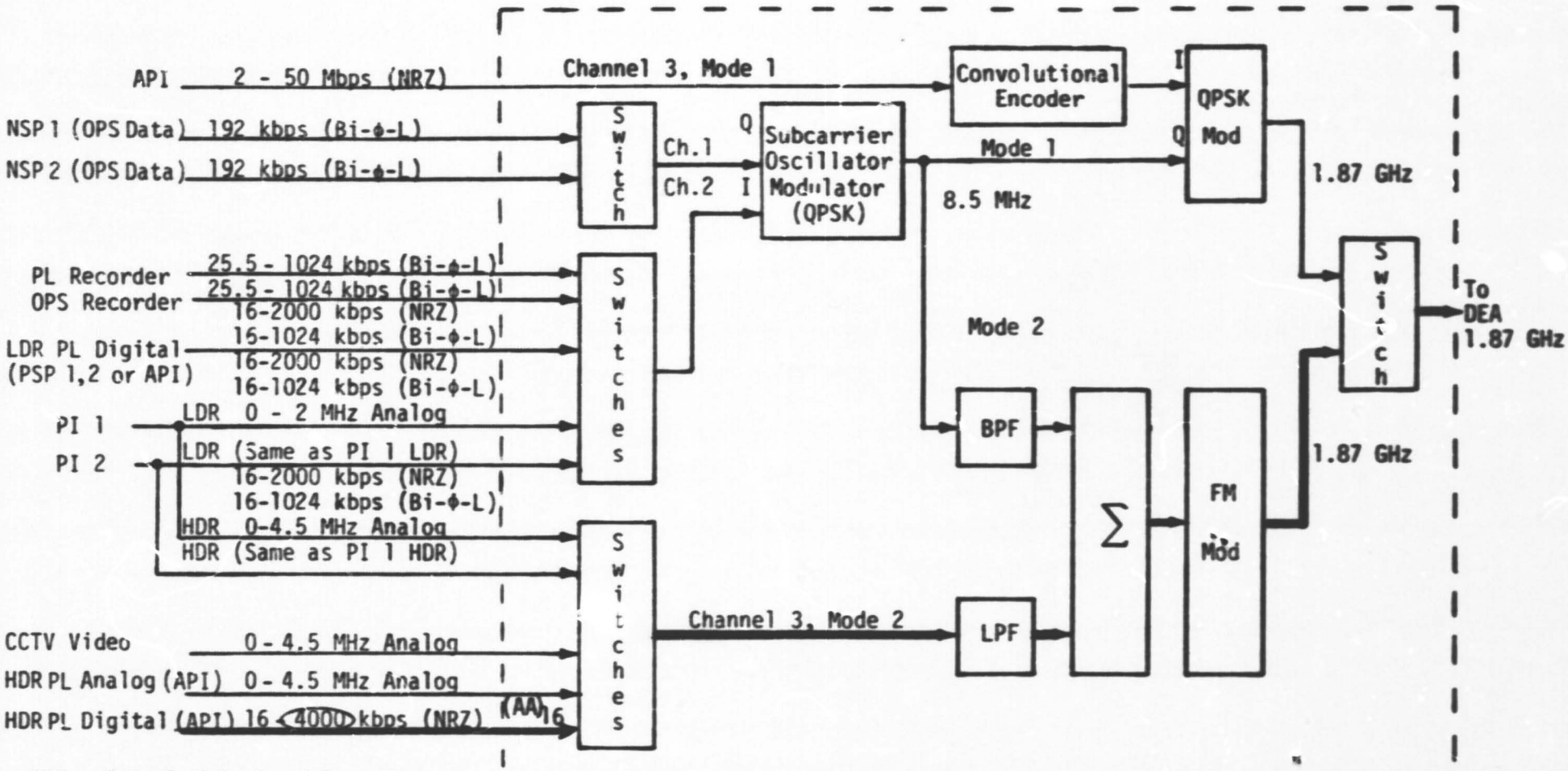

SPA Return Link Functional Block Diagram

API - Attached Payload Interface
BPF - Bandpass Filter
CCTV - Closed-Circuit Television
HDR - High Data Rate
LDR - Low Data Rate
LPF - Lowpass Filter
NSP - Network Signal Processor
OPS - Operations
PI - Payload Interrogator
PL - Payload
PSP - Payload Signal Processor

Test 027

Purpose: Same as Test 015

Results: Failed; voltage output 1-3V p-p, but should be >1-8V p-p.

Figure 70.

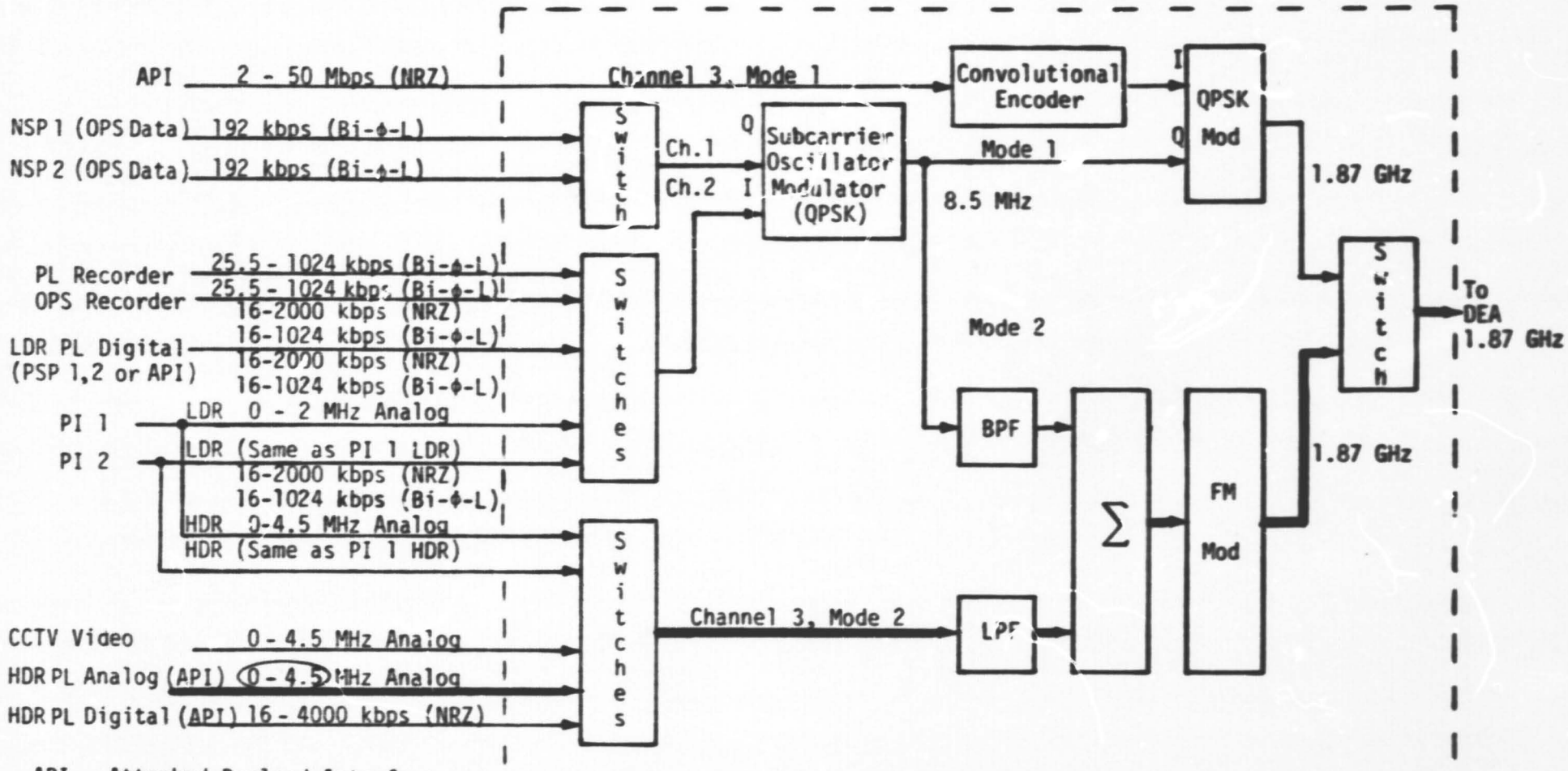

SPA Return Link Functional Block Diagram

API - Attached Payload Interface
BPF - Bandpass Filter
CCTV - Closed-Circuit Television
HDR - High Data Rate
LDR - Low Data Rate
LPF - Lowpass Filter
NSP - Network Signal Processor
OPS - Operations
PI - Payload Interrogator
PL - Payload
PSP - Payload Signal Processor

Test 030

Purpose: (1) Measure incidental FM and AM of the baseband generator and FM modulator.
(2) Take a mode 2 frequency response
(3) Measure FM deviation
(4) Measure static linearity of the FM VCO

Results: Failed--(1) excessive incidental AM
(2) nonuniform frequency response, +4.2 dB at 550 kHz.

Note: There were no tests 028 and 029.

Figure 71.

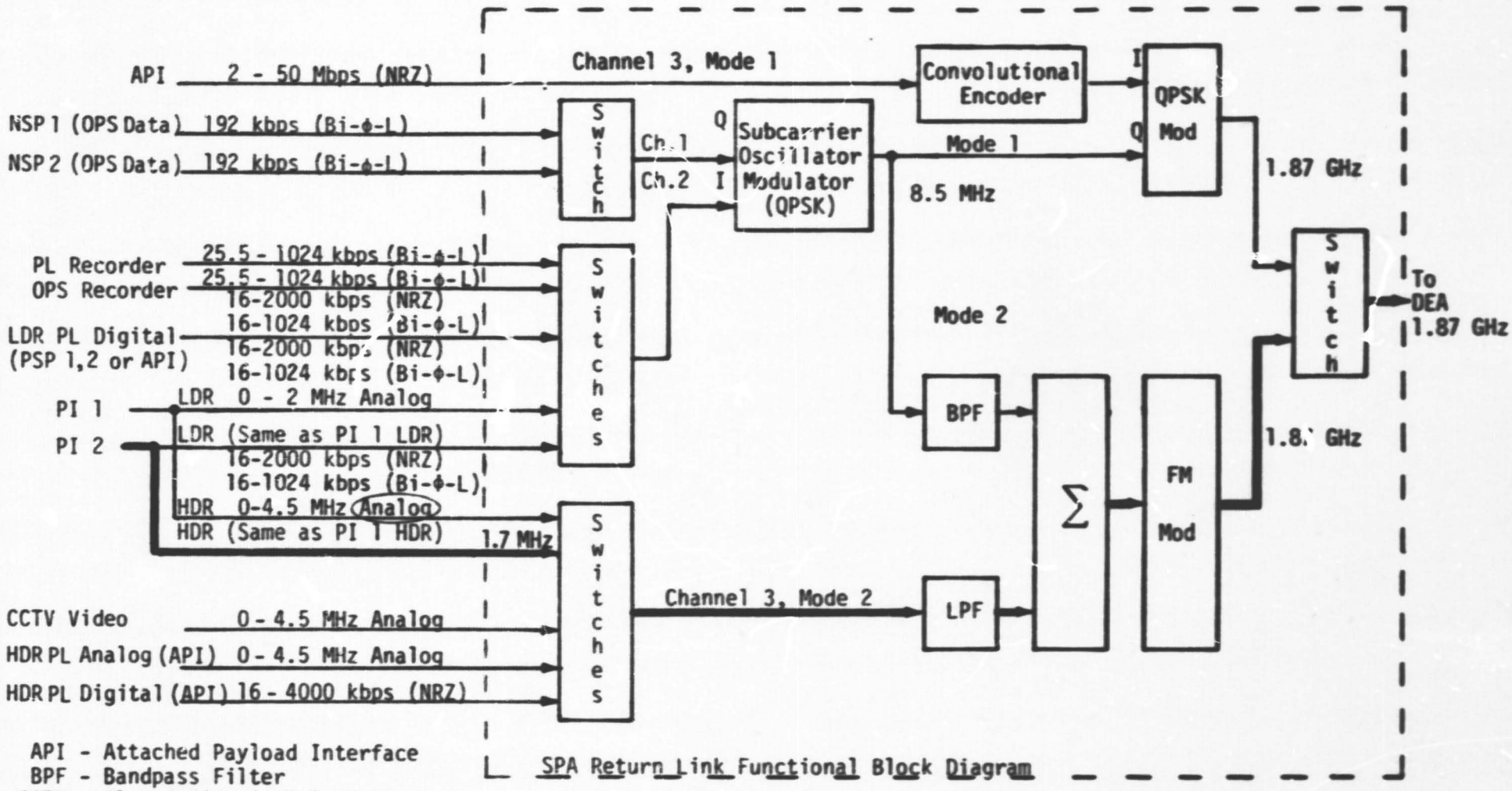

SPA Return Link Functional Block Diagram

API - Attached Payload Interface
BPF - Bandpass Filter
CCTV - Closed-Circuit Television
HDR - High Data Rate
LDR - Low Data Rate
LPF - Lowpass Filter
NSP - Network Signal Processor
OPS - Operations
PI - Payload Interrogator
PL - Payload
PSP - Payload Signal Processor

Test 031

Purpose: Same as Test 030

Results: Passed

Figure 72.

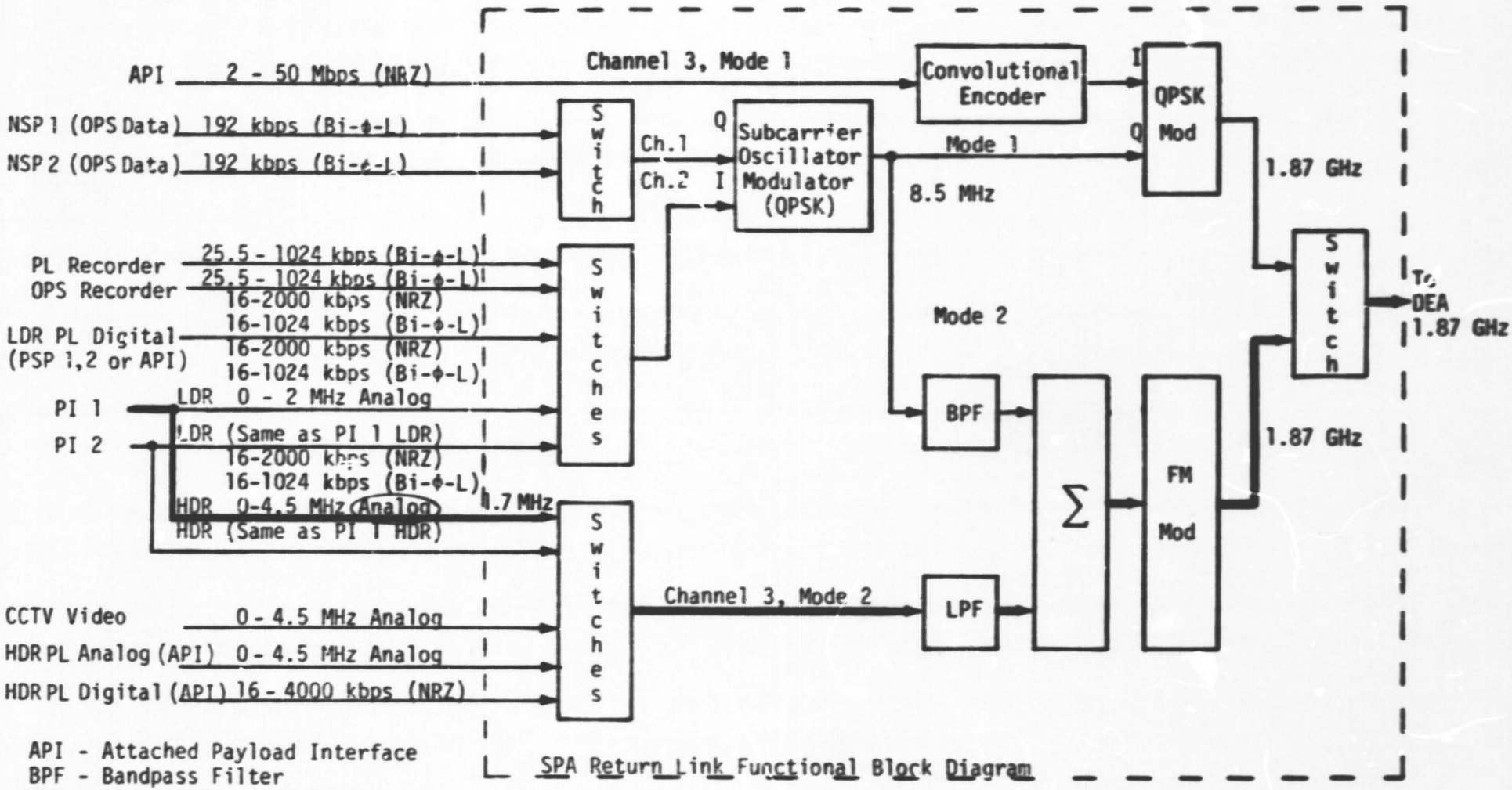

SPA Return Link Functional Block Diagram

API - Attached Payload Interface
BPF - Bandpass Filter
CCTV - Closed-Circuit Television
HDR - High Data Rate
LDR - Low Data Rate
LPF - Lowpass Filter
NSP - Network Signal Processor
OPS - Operations
PI - Payload Interrogator
PL - Payload
PSP - Payload Signal Processor

Test 032

Purpose: Same as Test 030

Results: Passed

Figure 73.

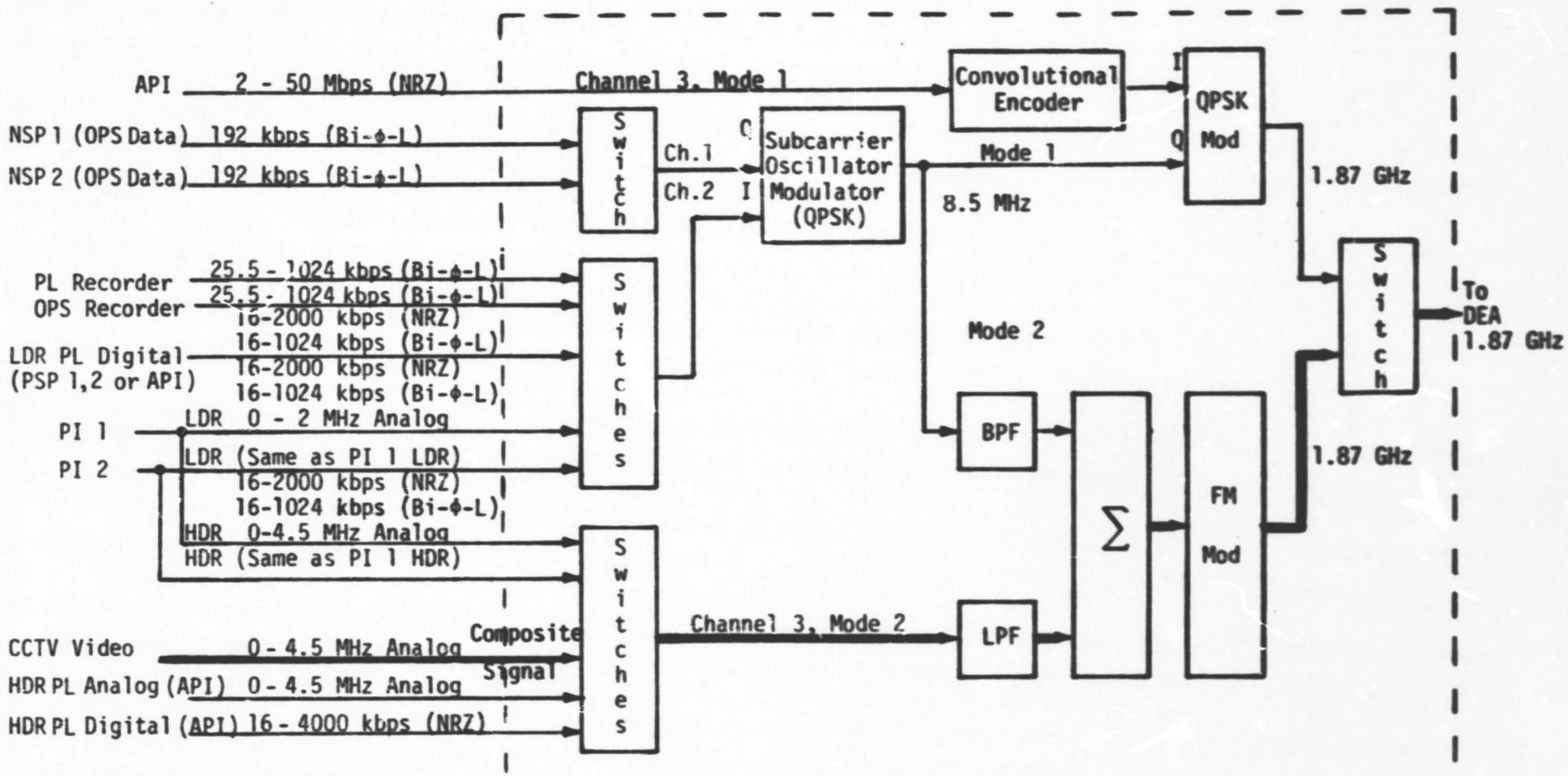

SPA Return Link Functional Block Diagram

API - Attached Payload Interface
BPF - Bandpass Filter
CCTV - Closed-Circuit Television
HDR - High Data Rate
LDR - Low Data Rate
LPF - Lowpass Filter
NSP - Network Signal Processor
OPS - Operations
PI - Payload Interrogator
PL - Payload
PSP - Payload Signal Processor

Test 033

Purpose: (1) Evaluate the FM baseband generator and FM modulator overall performance using a composite video waveform.
(2) Measure differential phase and gain distortion using a composite video waveform.
(3) Measure linearity distortion in mode 2 using a $\sin^2$ pulse and bar as a source.

Results: Failed; differential gain, differential phase and DC offset are out of specification.

Figure 74.

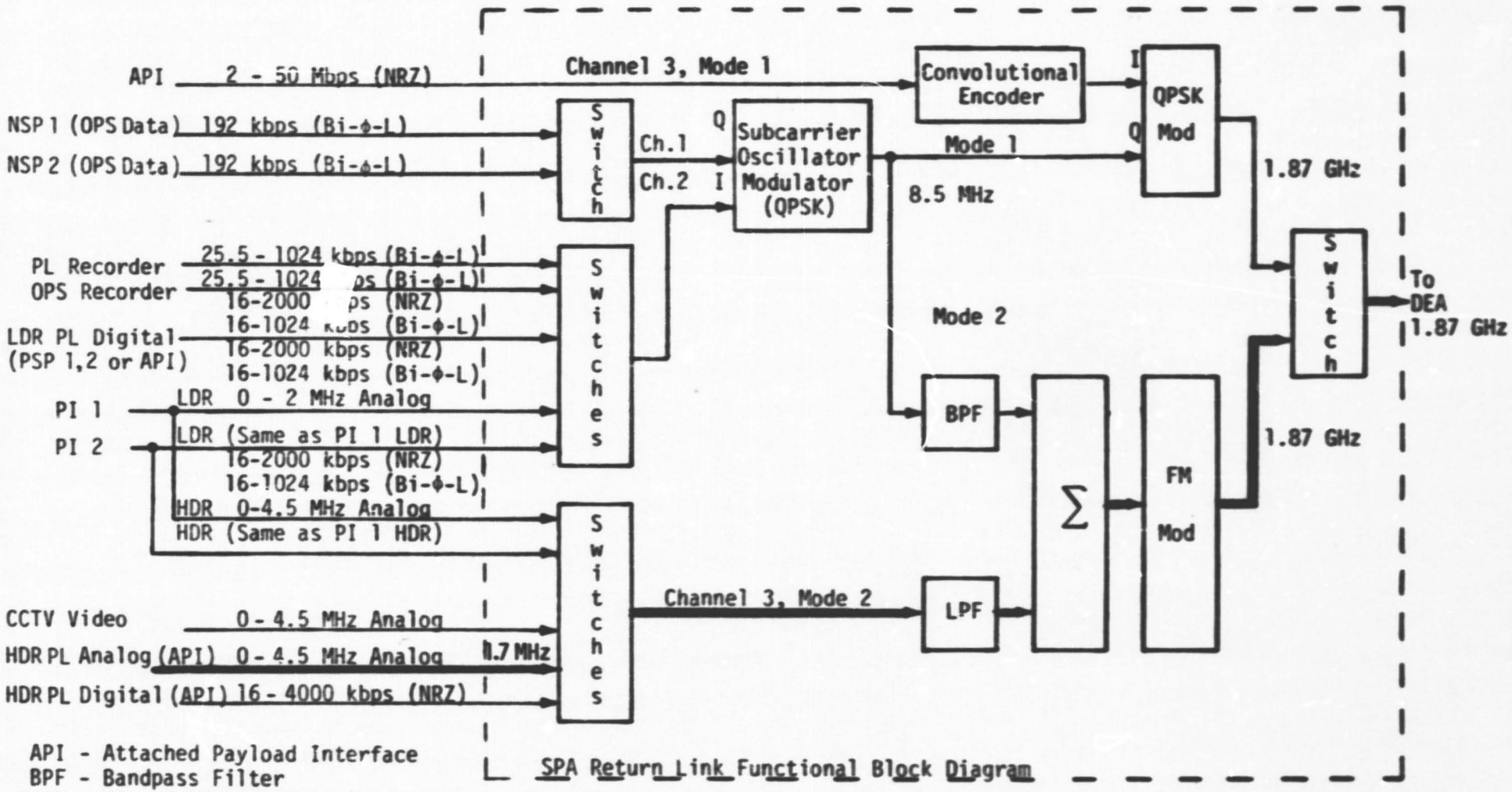

SPA Return Link Functional Block Diagram

Test 034

Purpose: Verify mode 2 is off when "HDR OFF" is selected.

Results: Passed

API - Attached Payload Interface
BPF - Bandpass Filter
CCTV - Closed-Circuit Television
HDR - High Data Rate
LDR - Low Data Rate
LPF - Lowpass Filter
NSP - Network Signal Processor
OPS - Operations
PI - Payload Interrogator
PL - Payload
PSP - Payload Signal Processor

Figure 75.

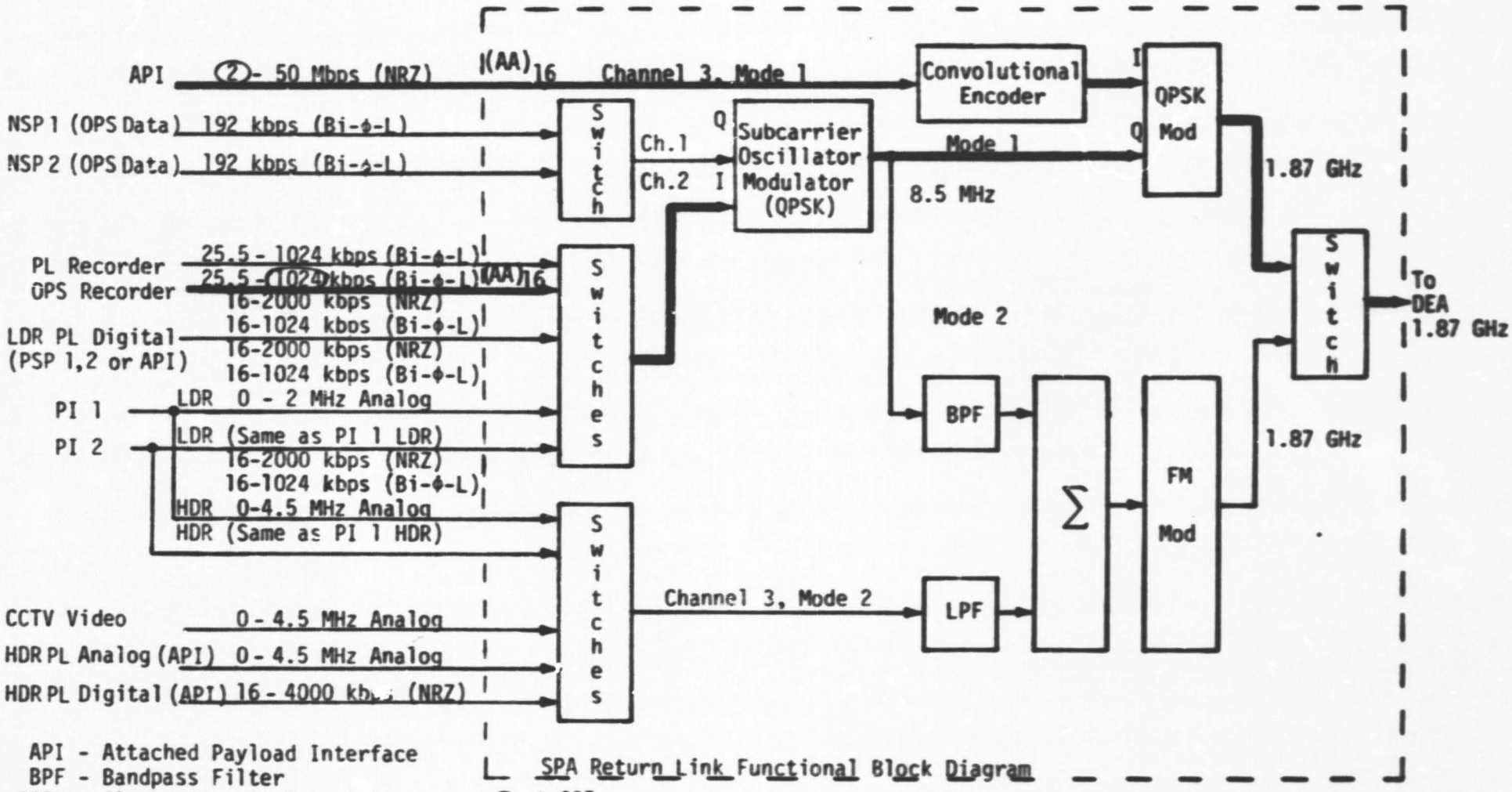

SPA Return Link Functional Block Diagram

API - Attached Payload Interface
BPF - Bandpass Filter
CCTV - Closed-Circuit Television
HDR - High Data Rate
LDR - Low Data Rate
LPF - Lowpass Filter
NSP - Network Signal Processor
OPS - Operations
PI - Payload Interrogator
PL - Payload
PSP - Payload Signal Processor

Test 035

Purpose: (1) Evaluate the FM baseband generator and QPSK modulator performance by comparing the demodulated data with the input data.
(2) Evaluate the effect of crosstalk

Results: Passed

Figure 76.

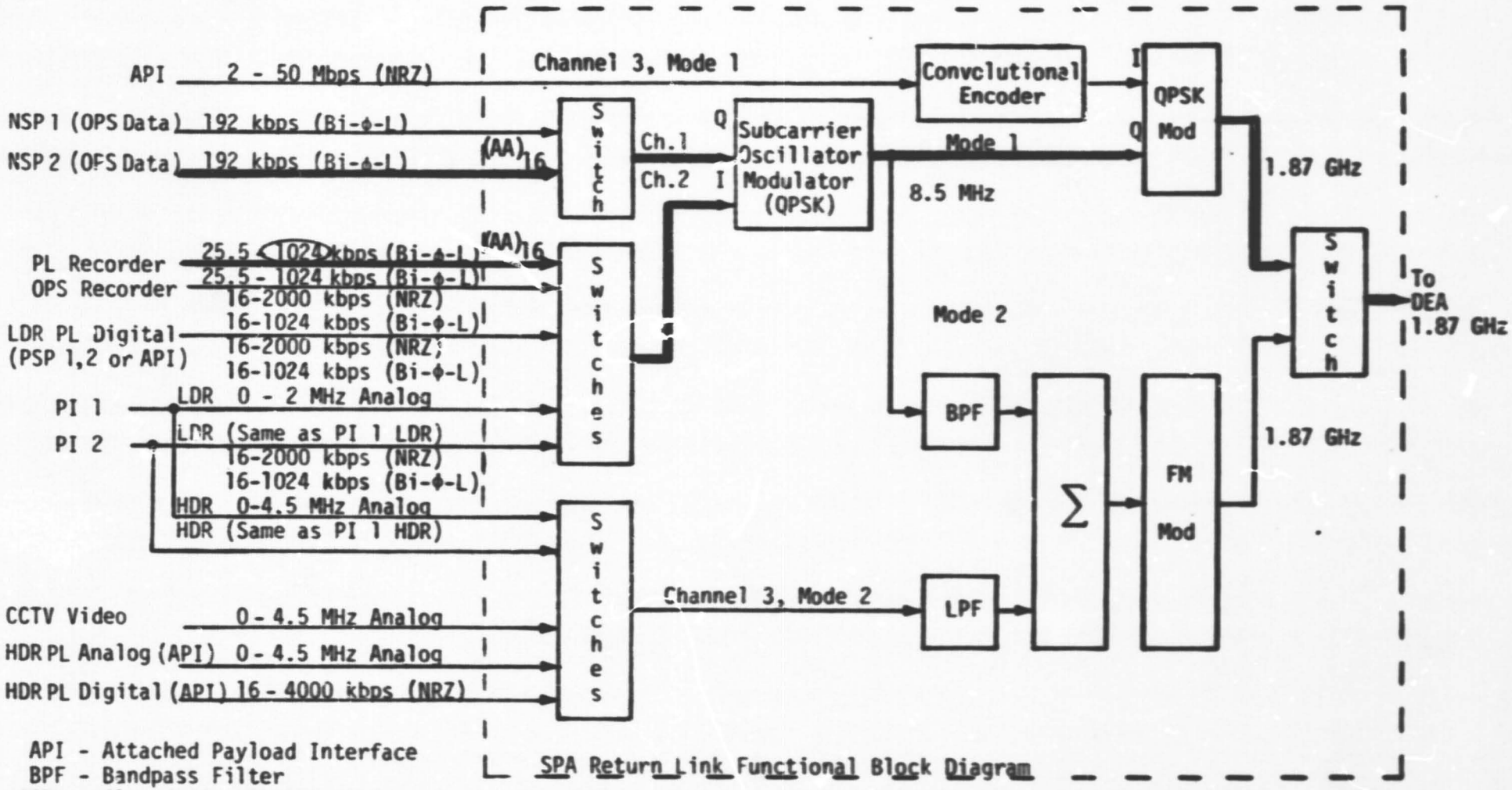

API - Attached Payload Interface
BPF - Bandpass Filter
CCTV - Closed-Circuit Television
HDR - High Data Rate
LDR - Low Data Rate
LPF - Lowpass Filter
NSP - Network Signal Processor
OPS - Operations
PI - Payload Interrogator
PL - Payload
PSP - Payload Signal Processor

SPA Return Link Functional Block Diagram

Test 036

Purpose: Same as Test 035

Results: Passed

Figure 77.

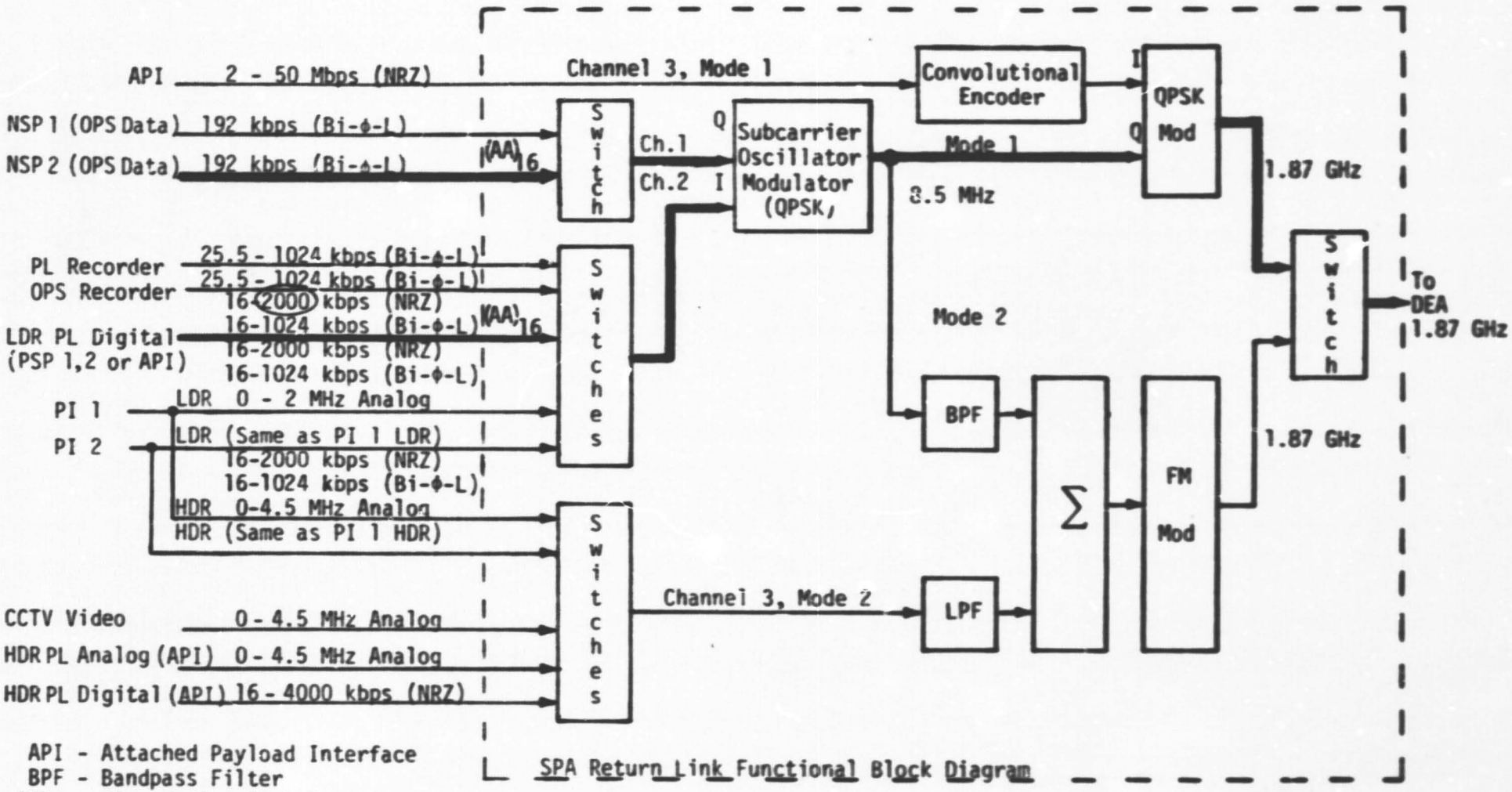

SPA Return Link Functional Block Diagram

API - Attached Payload Interface
BPF - Bandpass Filter
CCTV - Closed-Circuit Television
HDR - High Data Rate
LDR - Low Data Rate
LPF - Lowpass Filter
NSP - Network Signal Processor
OPS - Operations
PI - Payload Interrogator
PL - Payload
PSP - Payload Signal Processor

Test 037

Purpose: Same as Test 035

Results: Passed

Figure 78.

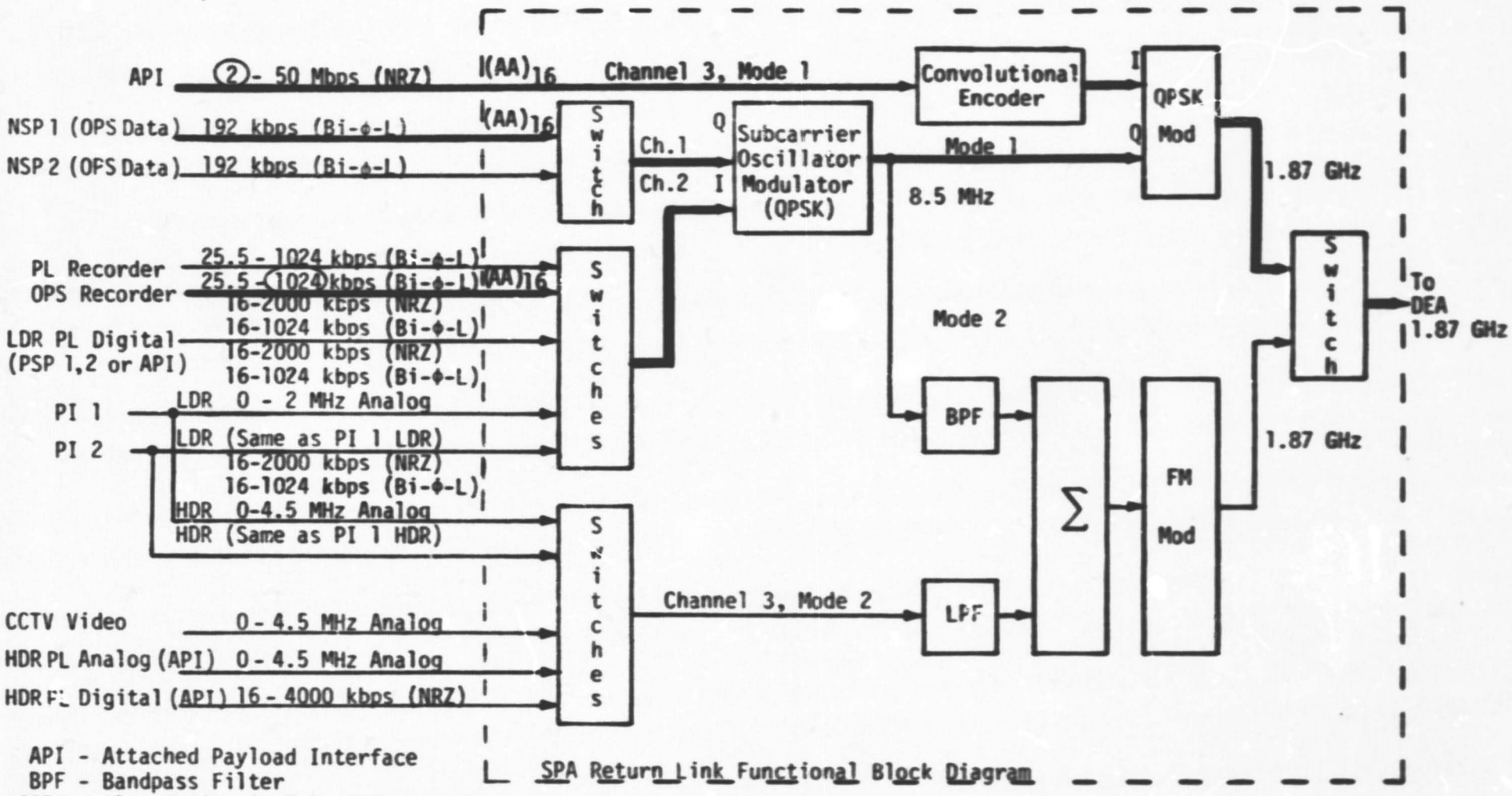

SPA Return Link Functional Block Diagram

API - Attached Payload Interface
BPF - Bandpass Filter
CCTV - Closed-Circuit Television
HDR - High Data Rate
LDR - Low Data Rate
LPF - Lowpass Filter
NSP - Network Signal Processor
OPS - Operations
PI - Payload Interrogator
PL - Payload
PSP - Payload Signal Processor

Note: There was no test 038 or 039

Test 040

Purpose: Same as Test 035

Results: Hughes states that unit failed, but test data indicates that unit passed.

Figure 79.

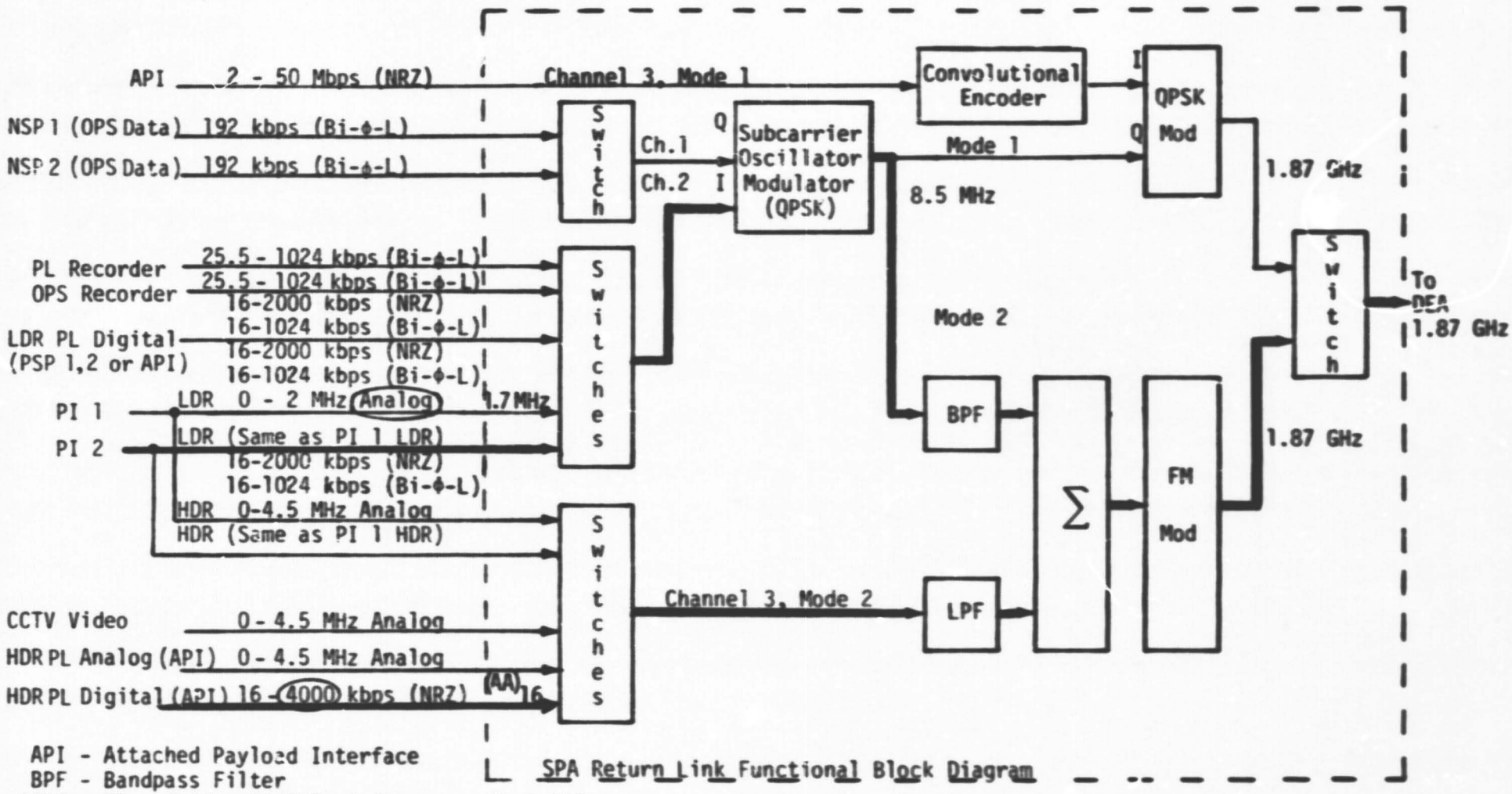

SPA Return Link Functional Block Diagram

API - Attached Payload Interface
BPF - Bandpass Filter
CCTV - Closed-Circuit Television
HDR - High Data Rate
LDR - Low Data Rate
LPF - Lowpass Filter
NSP - Network Signal Processor
OPS - Operations
PI - Payload Interrogator
PL - Payload
PSP - Payload Signal Processor

Test 041

Purpose: (1) Evaluate the FM baseband generator and FM modulator overall performance by comparing demodulated data with input data
(2) Evaluate the effect of crosstalk.

Results: Failed; output voltage amplitudes < 1.8V p-p.

Figure 80.

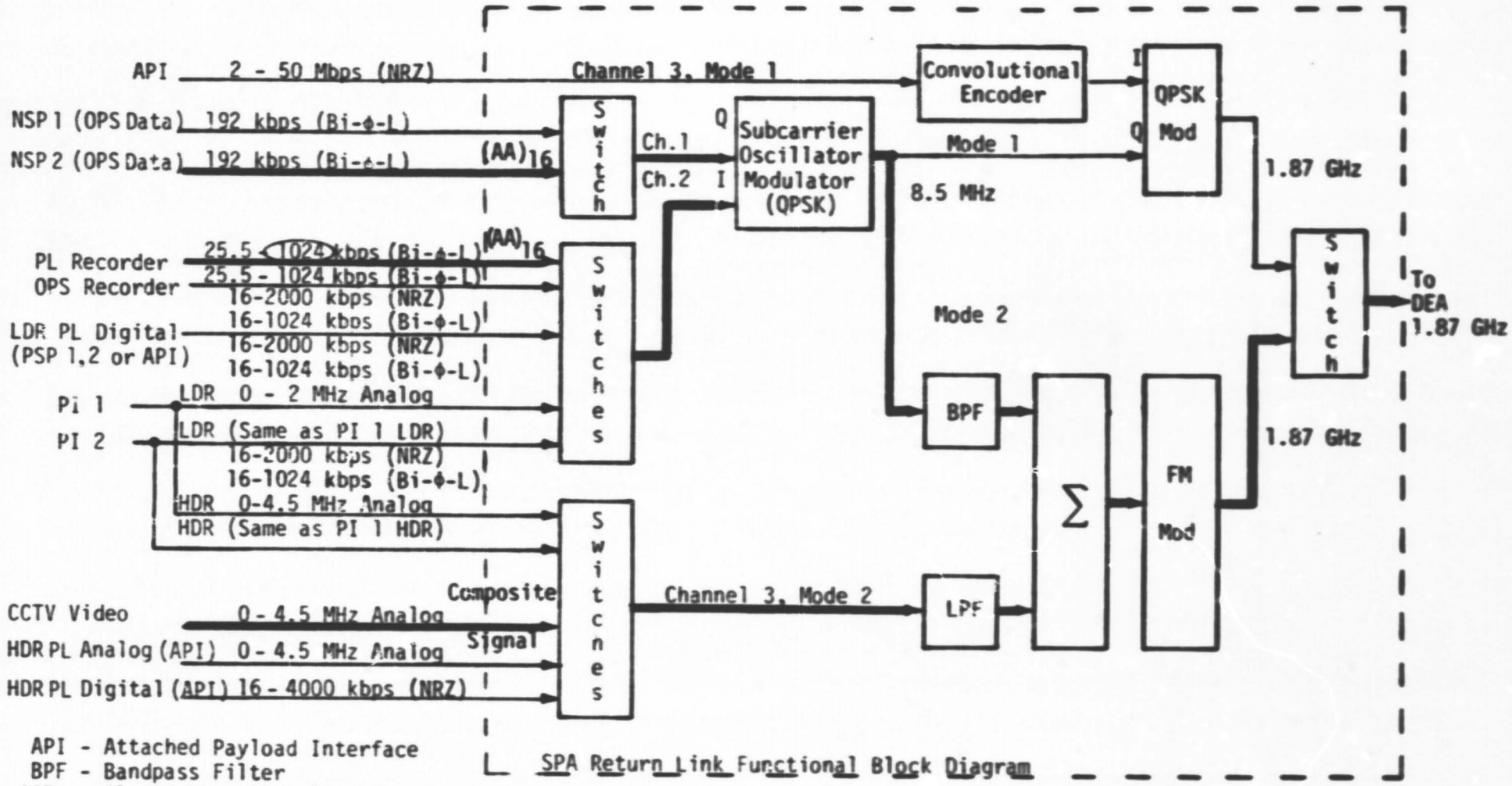

SPA Return Link Functional Block Diagram

API - Attached Payload Interface
BPF - Bandpass Filter
CCTV - Closed-Circuit Television
HDR - High Data Rate
LDR - Low Data Rate
LPF - Lowpass Filter
NSP - Network Signal Processor
OPS - Operations
PI - Payload Interrogator
PL - Payload
PSP - Payload Signal Processor

Test 042

Purpose: Same as Test 041

Results: Failed; (1) Channel 3 distortion and output voltages out of specification
(2) Channels 1 and 2 DC offsets 2-5 VDC, but should be 0.8 to 2.4 V.

Figure 81.

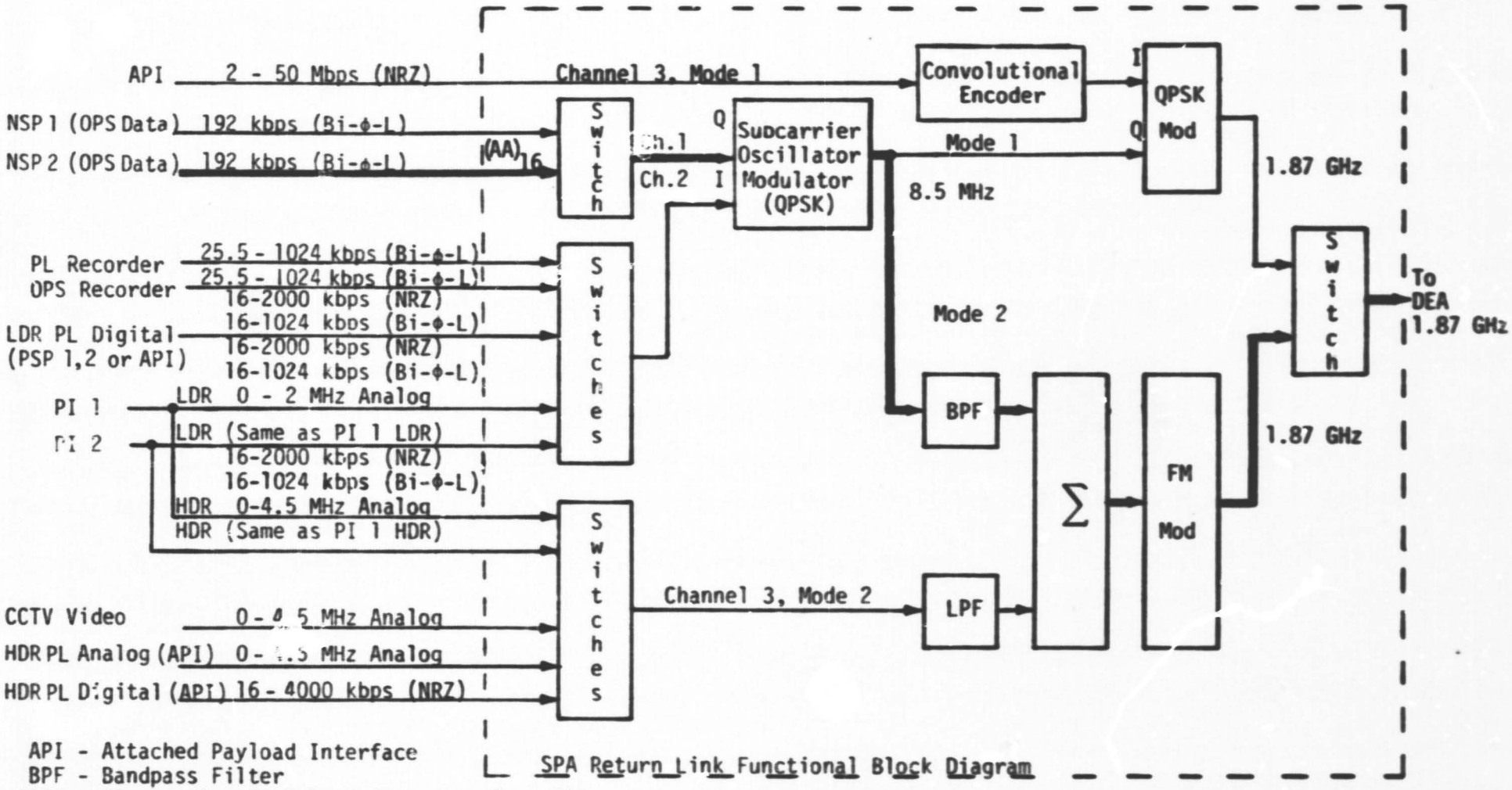

SPA Return Link Functional Block Diagram

API - Attached Payload Interface
BPF - Bandpass Filter
CCTV - Closed-Circuit Television
HDR - High Data Rate
LDR - Low Data Rate
LPF - Lowpass Filter
NSP - Network Signal Processor
OPS - Operations
PI - Payload Interrogator
PL - Payload
PSP - Payload Signal Processor

Test 043

Purpose: Same as Test 015. CDR test results package indicates that test purpose is the same as Test 013, but this is incorrect.

Results: Passed

Figure 82.

Table 24. SPA ADL LRU Return Link Test Failure Summary

Hughes Test Number	Test Purpose	Failure
007,010, 011,012 Reference Figure 4	1. Statically measure the QPSK spectral power density output to verify proper 80/20 power ratio. 2. Perform transmission and reflection measurements so that various network parameters such as gain, attenuation, insertion loss, SNR, return loss and impedance may be calculated from the data.	Phase state and VSWR out of specification. Failure is believed due primarily to level incompatibility between the FM baseband generator mode 1 output and the QPSK mode 1 input. The problem is under investigation.
014	1. Evaluate the FM baseband generator and QPSK modulator overall performance by comparing the demodulated data to the input data. 2. Verify proper switching and interfacing by management/handover.	Hughes states that the SPA passed this test. The test data indicates that the unit failed since the measured fall time was 900 ms, but should have been < 600 ms.
027	1. Evaluate the FM baseband generator and the FM modulator overall performance by comparing the demodulated data to the input data. 2. Verify proper switching and interfacing by management/handover.	Voltage output 1.3V p-p, but should be > 1.8V p-p.
030	1. Measure incidental FM and AM of the baseband generator and the FM modulator. 2. Take a mode 2 frequency response 3. Measure FM deviation 4. Measure static linearity of the FM VCO.	1. Incidental AM out of specification. 2. Mode 2 frequency response is not flat; output is between 3.4V p-p and 3.6V p-p from 40 Hz to 4 MHz but there is a 5.5V p-p peak at 550 kHz.

Table 24. SPA ADL LRU Return Link Test Failure Summary (Cont'd)

Hughes Test Number	Test Purpose	Failure
033	1. Evaluate the FM baseband generator and the FM modulator overall performance using a composite video input waveform. 2. Measure the differential phase and gain distortion using a composite video input waveform. 3. Measure linearity distortion in mode 2 using a $\sin^2$ and bar as a source.	Differential gain, differential phase and DC offset out of specification.
040	1. Evaluate the FM baseband generator and the QPSK modulator overall performance using the demodulated data with the input data. 2. Evaluate the effect of crosstalk between the channels.	Hughes states that the unit failed but the test data indicates that the unit passed.
041	1. Evaluate the FM baseband generator and the FM modulator overall performance by comparing the demodulated data to the input data. 2. Evaluate the effect of crosstalk between the channels.	Output voltage amplitudes < 1.8V p-p.
042	Same as test 041.	1. Channel 3 distortion and output voltage level out of specification. 2. Channels 1 and 2 DC offsets are 2.5 VDC but should be 0.8-2.4 VDC.

In addition to the 10 test failures, there were a number of input parameters which were not varied during the testing. For example, all data input signals are characterized in the Rockwell Rev. B specification in such terms as rise and fall times, amplitude and common mode voltage levels, etc. However, none of these parameters were varied during testing and, therefore, it is still unknown if the SPA will meet specification when the signal input tolerances are taken into account. Table 25 summarizes those return link input signal parameters which were not varied over their respective tolerance ranges.

Also, a number of output parameters were not measured. For example, the primary SPA output signal is 1.87 GHz to the DEA, but that signal was not measured during the ADL tests in terms of frequency offset, incidental AM, FM and PM, spurious products and frequency offset. Unfortunately, the Rockwell specification lists "TBS" for many of the parameters. Reference Table 26 for a summary of the nonmeasured return link output parameters.

10.1.2.2 SPA ADL LRU Forward Link Data

Figures 83 through 98 illustrate the signal paths used to verify forward link performance and also briefly describe each test. In addition, each figure indicates the data rate utilized for that test, along with the data rate ranges which each input is required to process.

Hughes tested all the various signal combinations. Of the 16 forward link tests, the SPA passed all but one test. Table 27 lists the one forward link test failure.

Hughes measured and characterized the output signals in terms of amplitude, rise and fall times, phase jitter and duty cycle. The output data met all the requirements listed in the Rockwell Rev. B specification.

As with the return link tests, there were a number of input parameters in the forward link tests which were not varied during testing and, therefore, it is still unknown if the SPA will meet specification when the signal input tolerances are taken into account. Again, some tolerances are unknown because some parameters are listed as "TBS" in the Rockwell document. Table 28 summarizes those forward link input signal parameters which were not varied over their respective tolerance ranges.

Table 25. SPA Input Signal Parameters Not Varied Over Their Respective Tolerance Ranges to Determine the Effect on Return Link Performance

I. HIGH DATA RATE PAYLOAD MAXIMUM DIGITAL DATA AND CLOCK INPUT TO SPA

1. Data and clock "1" and "0" voltage ranges*
2. Data and clock SNR
3. Data rise and fall times
4. Clock phase jitter
5. Data and clock frequency jitter
6. Data-to-clock phase offset
7. Asymmetry

II. SPA PAYLOAD DATA INPUT FROM PAYLOAD INTERROGATORS 1 AND 2

1. Differential signal levels
2. Offset voltage
3. Common mode voltage

III. SPA RETURN LINK OPERATIONAL DATA INPUT FROM NSP's 1 AND 2

1. Signal amplitude
2. Rise and fall times
3. Input data jitter
4. Common mode voltage

IV. PAYLOAD RECORDER DIGITAL DATA INPUT TO SPA

1. Signal level
2. Rise and fall times
3. Bit-to-bit jitter
4. Bit jitter and data asymmetry
5. Common mode voltage

*Future tests to verify the convolutional encoder bit detector redesign performance will vary the input signal voltage levels

Table 25. (Cont'd)

V. OPERATIONAL RECORDER DIGITAL DATA INPUT TO SPA

1. Signal level
2. Rise and fall times
3. Bit-to-bit jitter
4. Jitter and asymmetry
5. Common mode voltage

VI. SPA ORBITER CLOSED-CIRCUIT TELEVISION (CCTV) INPUT FROM VIDEO SWITCHING UNIT

1. Ability of SPA to handle standard video signal has not been demonstrated.

VII. LOW DATA RATE PAYLOAD DATA INPUT TO SPA

1. Signal level
2. RMS SNR
3. Rise and fall times
4. Frequency jitter
5. Common mode voltage

VIII. LOW DATA RATE PAYLOAD DATA INPUT TO SPA

1. Signal level
2. RMS SNR
3. Rise and fall times
4. Frequency jitter
5. Common mode voltage

IX. HIGH DATA RATE PAYLOAD ANALOG DATA INPUT TO SPA

1. Bandwidth
2. Signal level
3. SNR
4. Phase jitter
5. Common mode voltage

Table 26. SPA Return Link Output Signal Parameters Not Measured

I. SPA IF CARRIER OUTPUT TO DEPLOYED ASSEMBLY

1. Center frequency
*2. Maximum Frequency Offset
*3. Frequency stability (short-term/long-term)
*4. Level (unmodulated)
*5. Modulation bandwidth
*6. Incidental phase modulation--mode 1
*7. Incidental FM modulation--mode 2
*8. Incidental amplitude modulation--mode 1/mode 2
*9. Spurious products:
    In-band—mode 1/mode 2
    Out-of-band—mode 1/mode 2

II. SPA SERIAL DIGITAL STATUS DATA OUTPUT TO EA-1A AND EA-1B

1. Most parameters are listed as "TBS" in Rockwell specification
2. Rise and fall times

III. REFERENCE FREQUENCY INPUT TO SPA FROM EA-1A AND EA-1B

1. Most parameters are listed as "TBS" in Rockwell specification

*Parameters listed in the Rockwell requirements as "TBS"

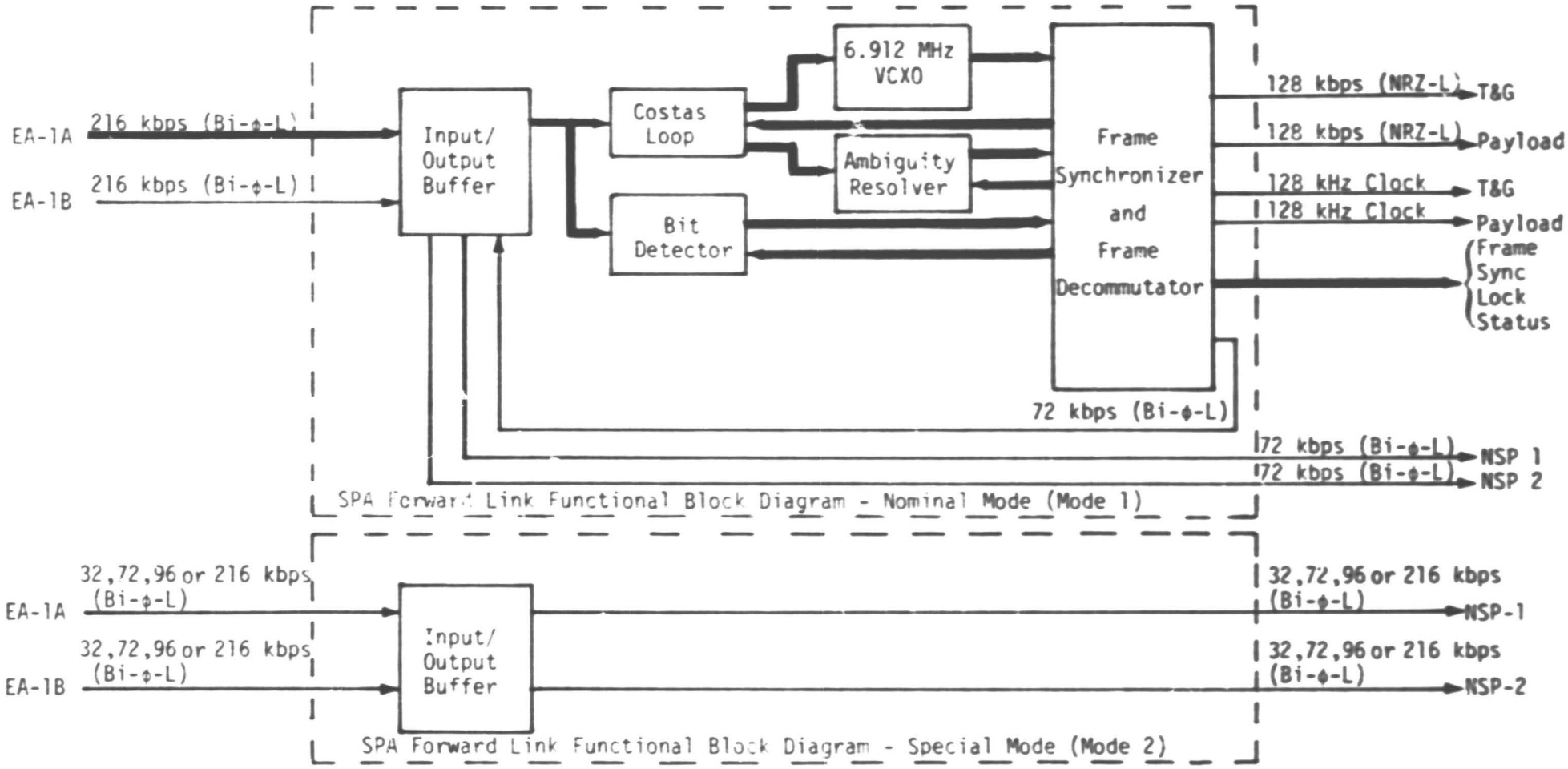

Test 044

Purpose: Verify all the various frame synchronization pattern combinations

Results: Failed to synchronize, with one error occurring in any of the last four bits

Figure 83.

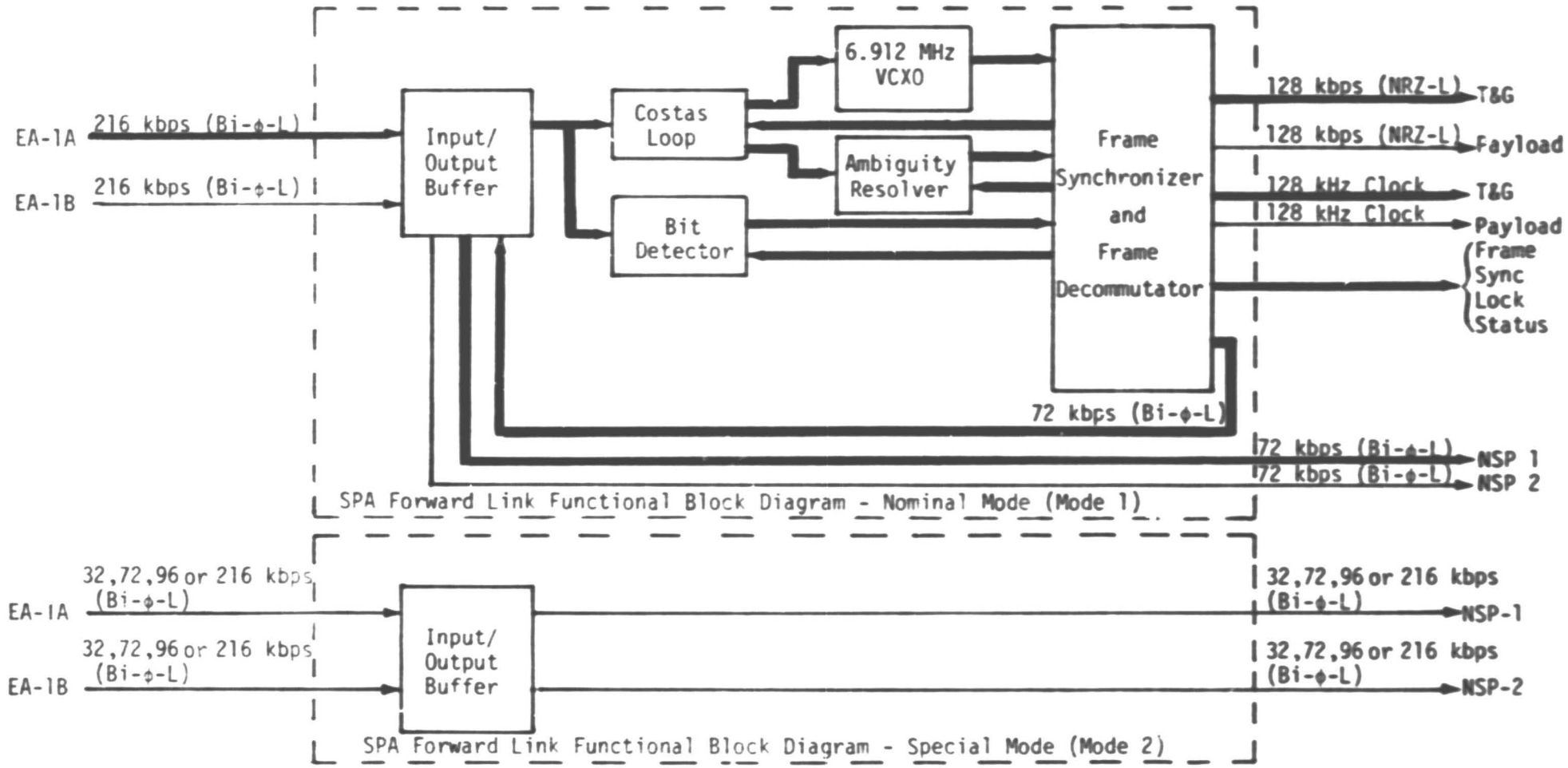

Test 045

Purpose: Verify frame synchronization lock-up to verify correct data type and measure output signals of the FL 72 kbps, FL 128 kbps and FL 128 kHz clocks.

Input Data: Valid frame synchronization (B7EB8CEC), OPS hex data (F502), SC hex data (FEAA002E).

Results: Passed

Figure 84.

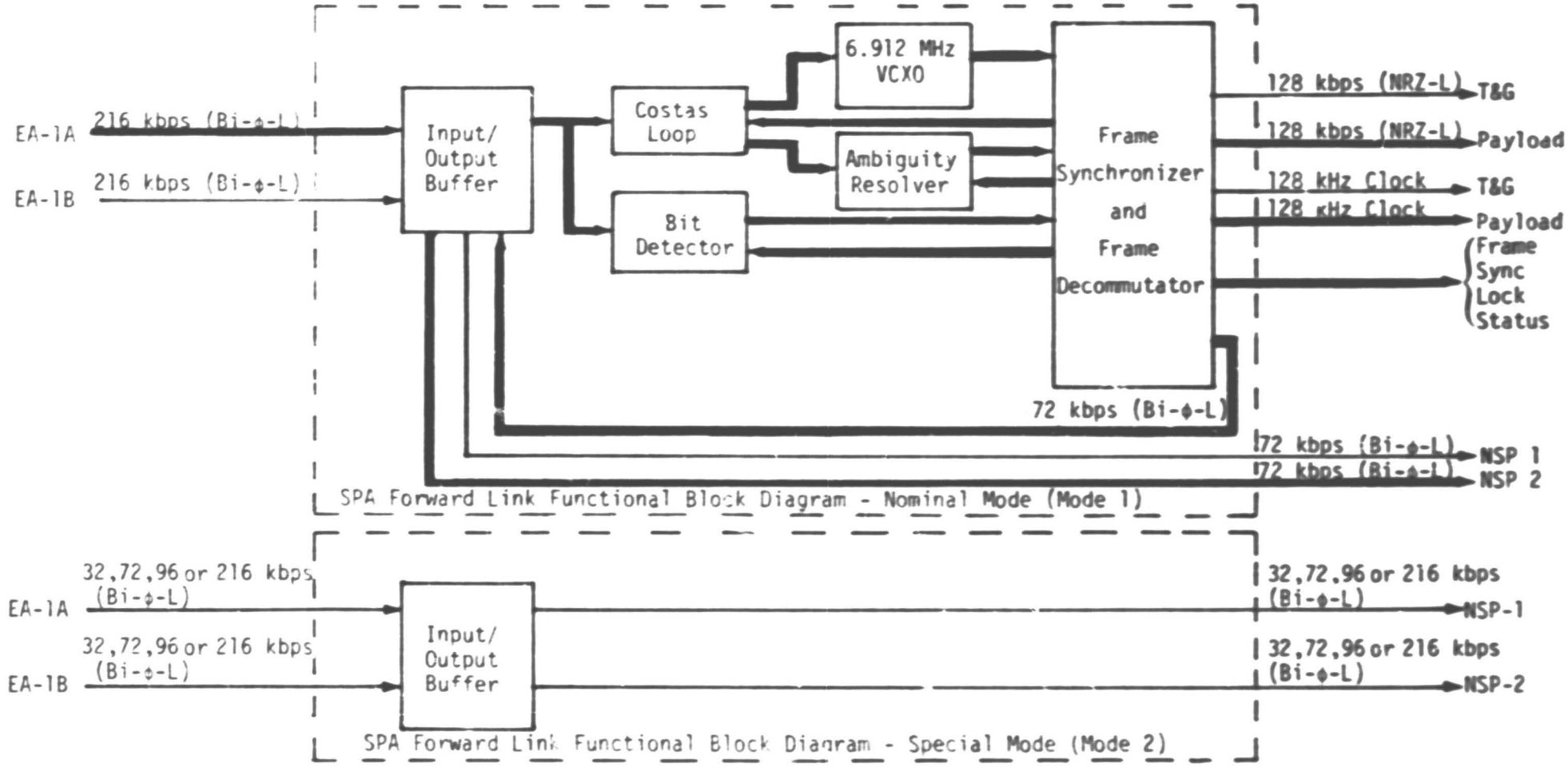

Test 046

Purpose: Same as Test 045

Input Data: Same as Test 045

Results: Passed

Figure 85.

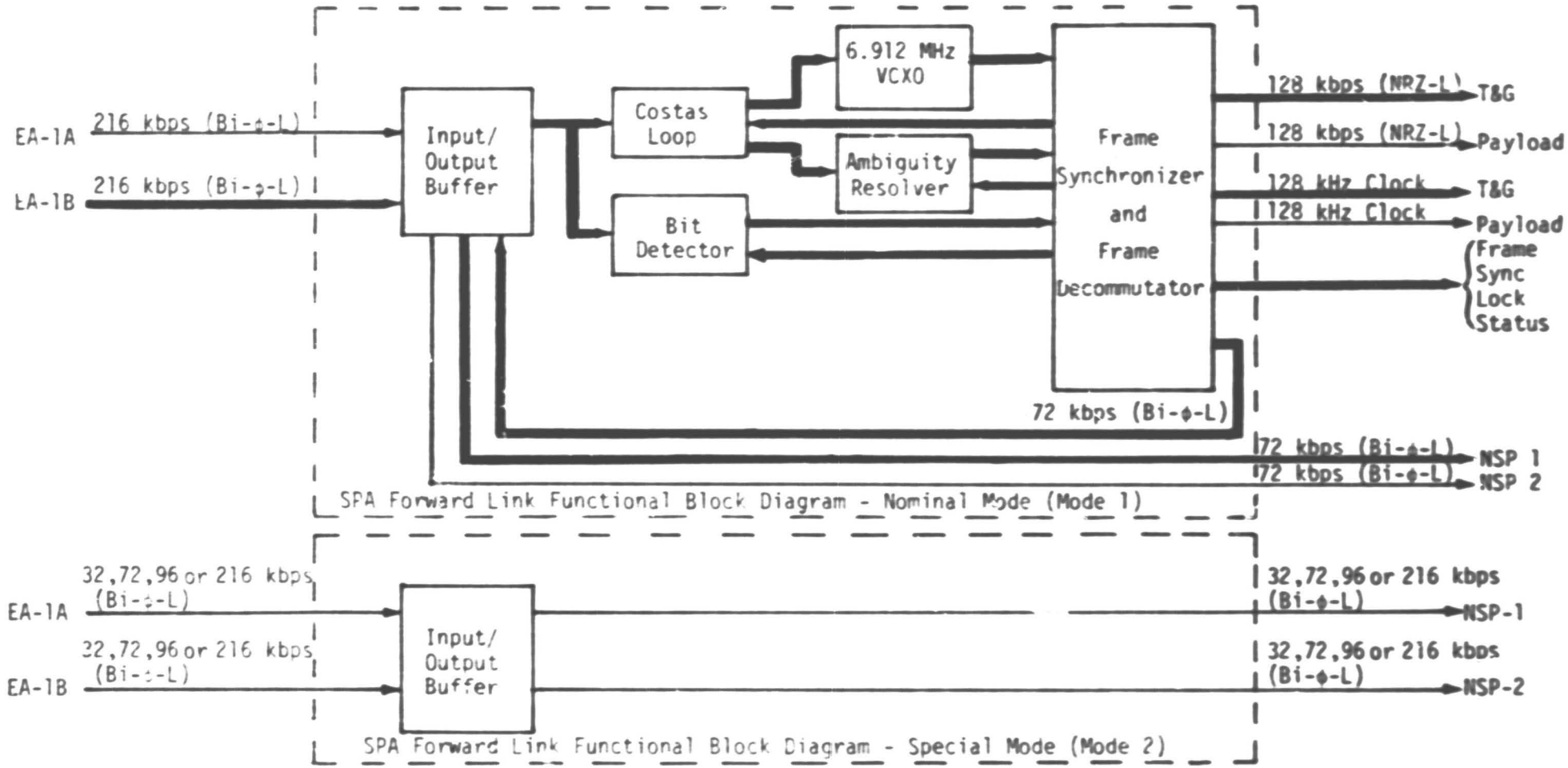

Test 047

Purpose: Same as Test 045

Input Data: Same as Test 045

Results: Passed (some data missing)

Figure 86.

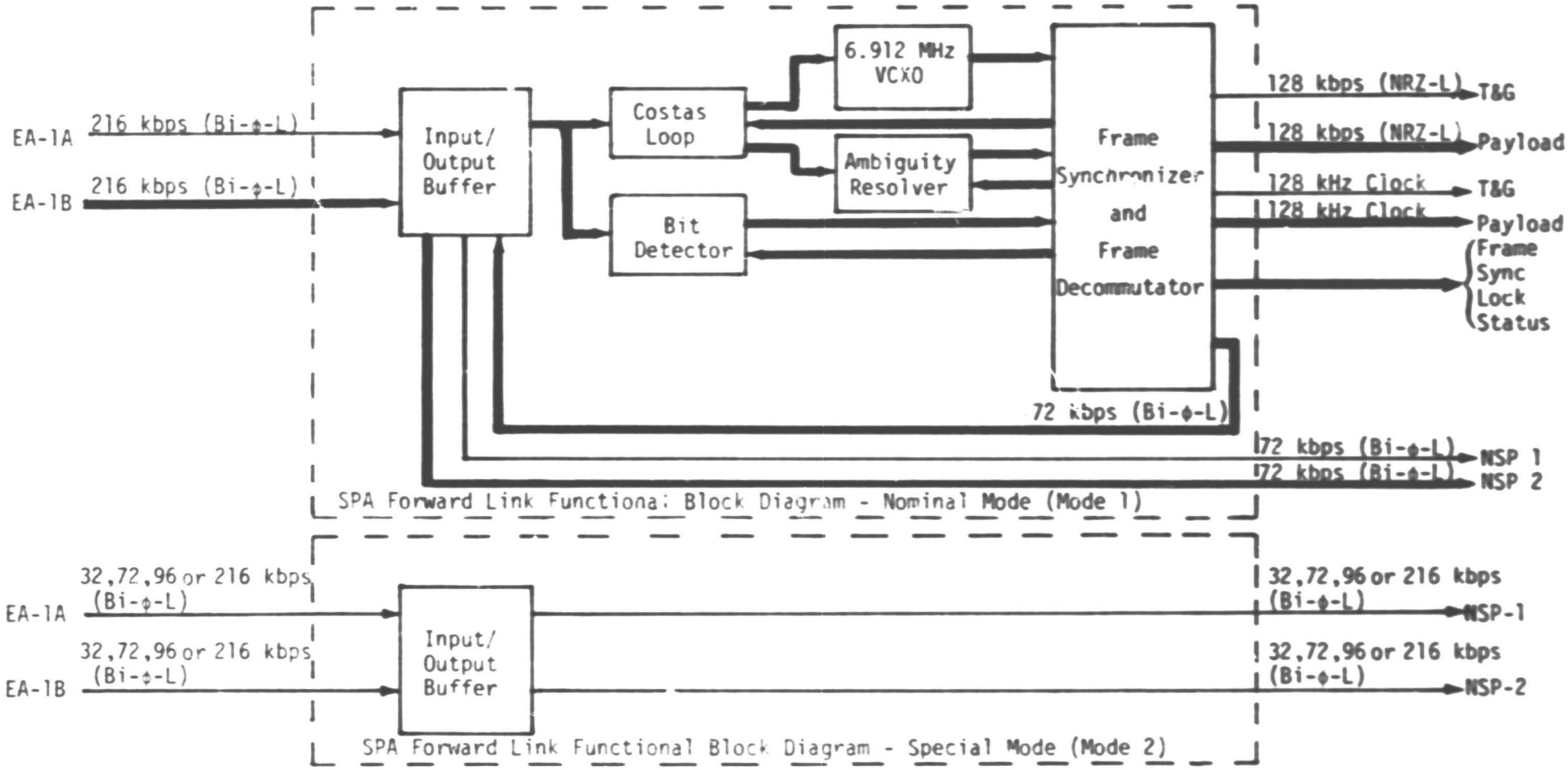

Note: There was no test 048 or 049

Test 050

Purpose: Same as Test 045

Input Data: Same as Test 045

Results: Passed (some data missing)

Figure 87.

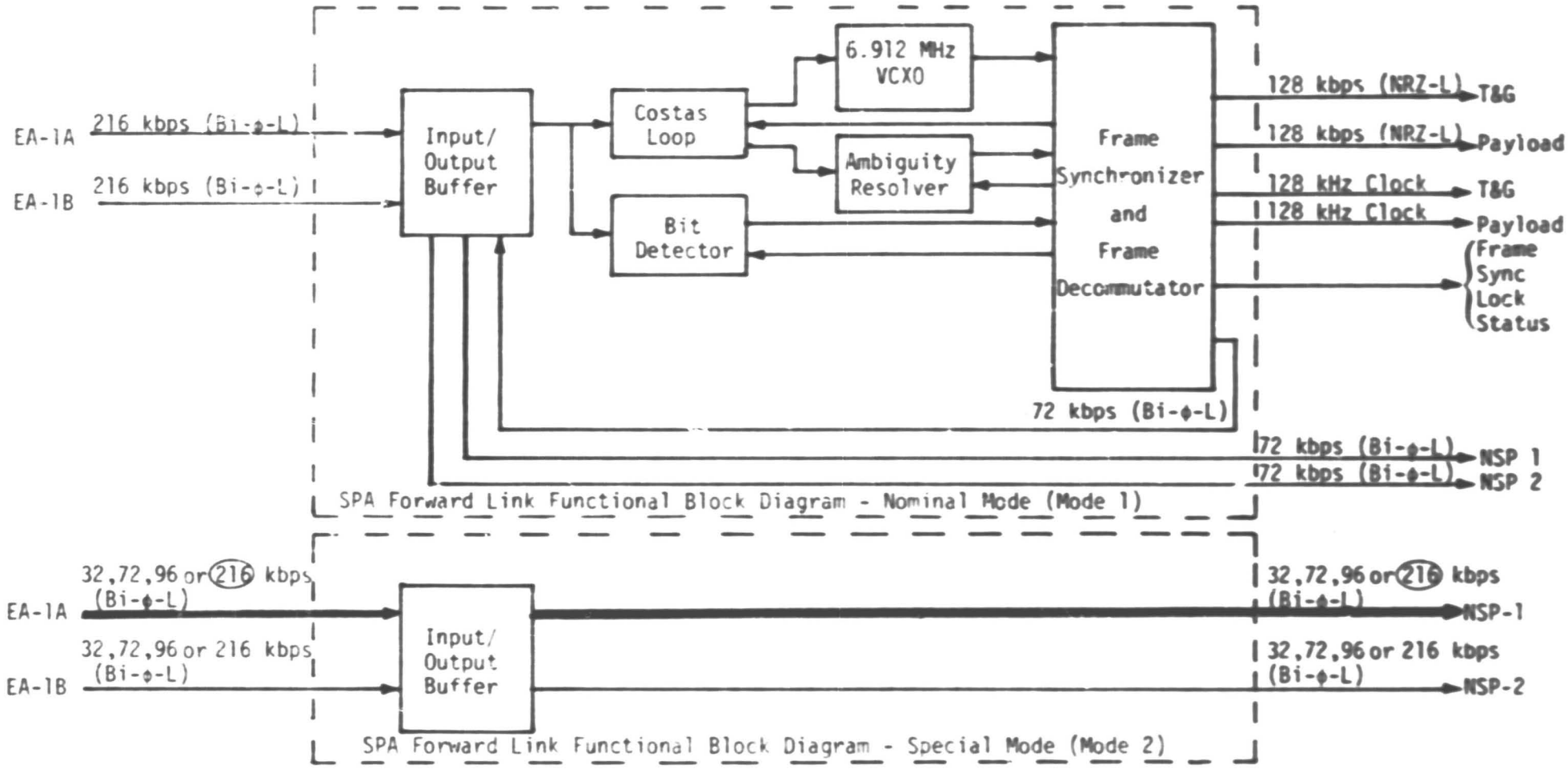

Test 051

Purpose: To test mode 2

Input Data: 1/0 pattern

Results: Passed

Figure 88.

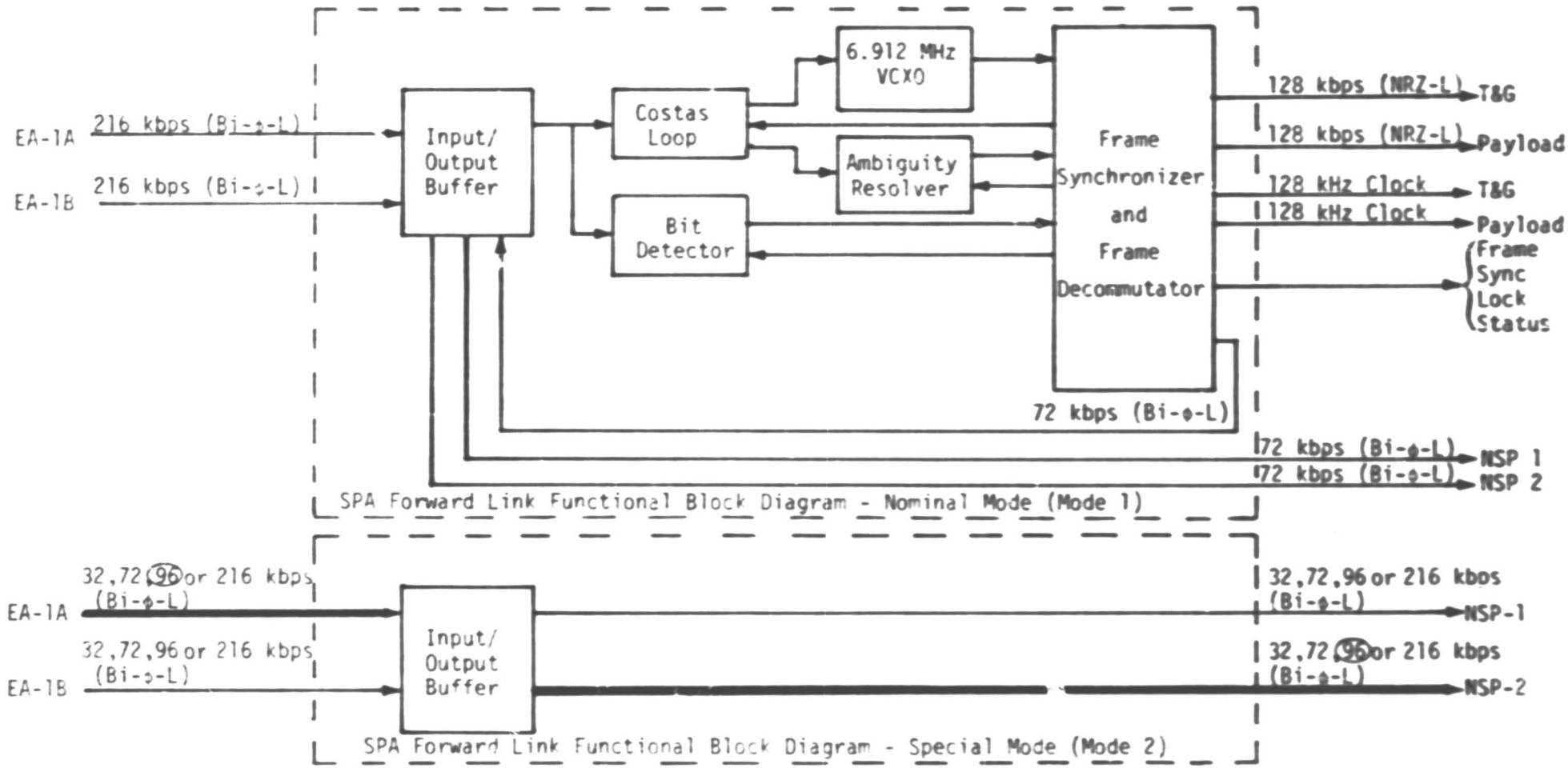

Test 052

Purpose: Same as Test 051

Input Data: 1/0 pattern

Results: Passed

Figure 89.

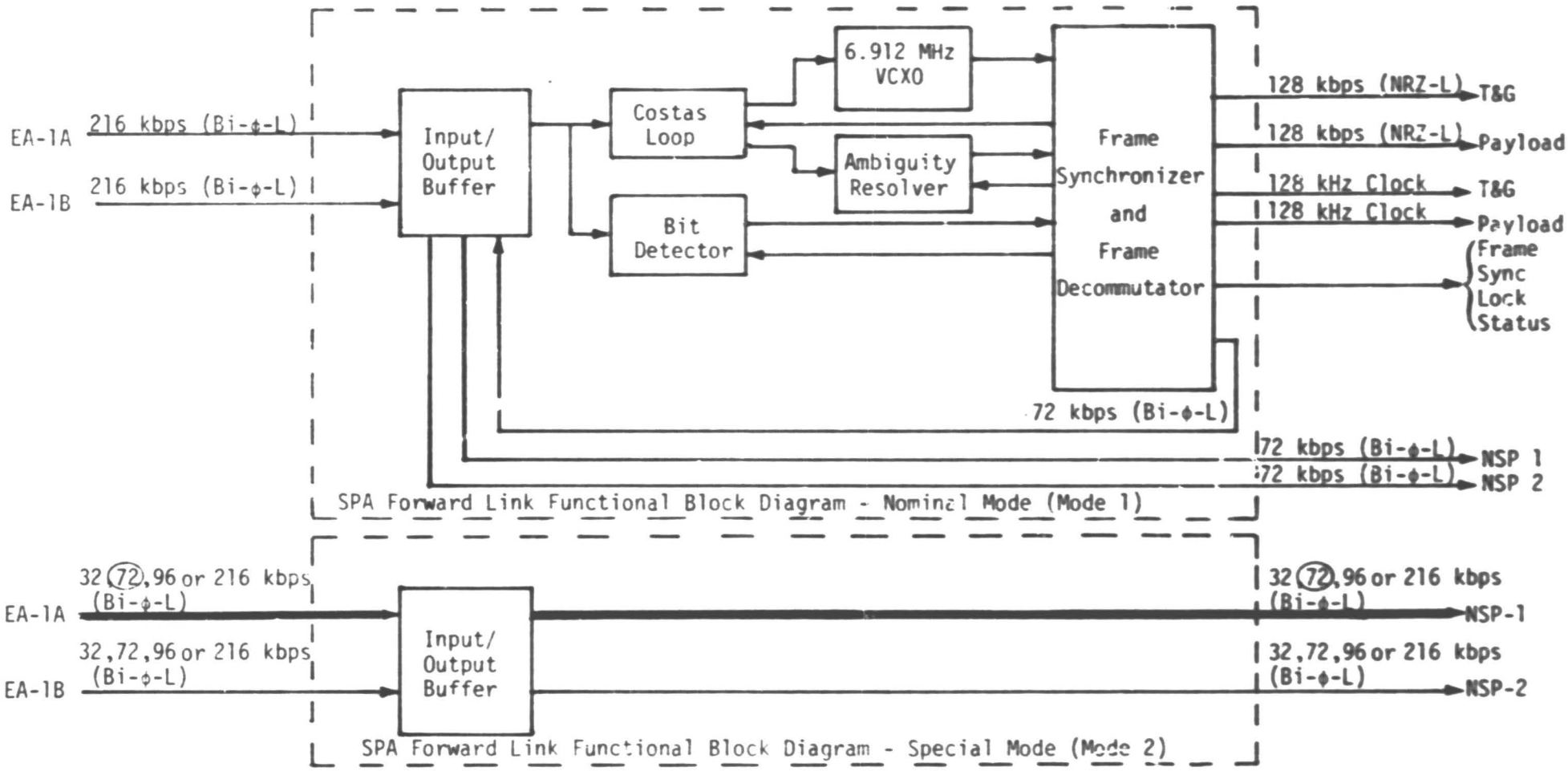

Test 053

Purpose: Same as Test 051

Input Data: 1/0 pattern

Results: Passed

Figure 90.

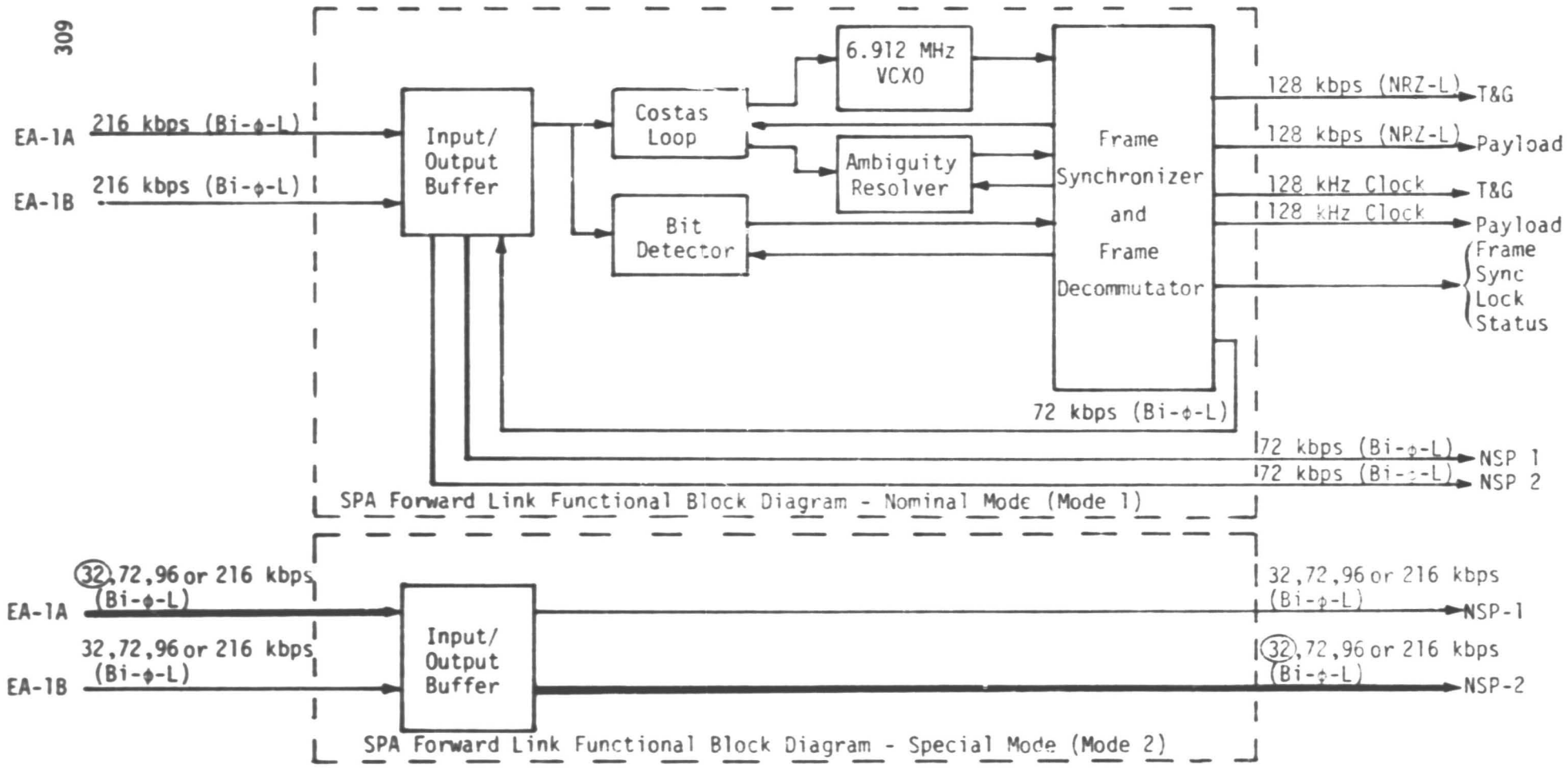

Test 054

Purpose: Same as Test 051

Input Data: 1/0 pattern

Results: Passed

Figure 91.

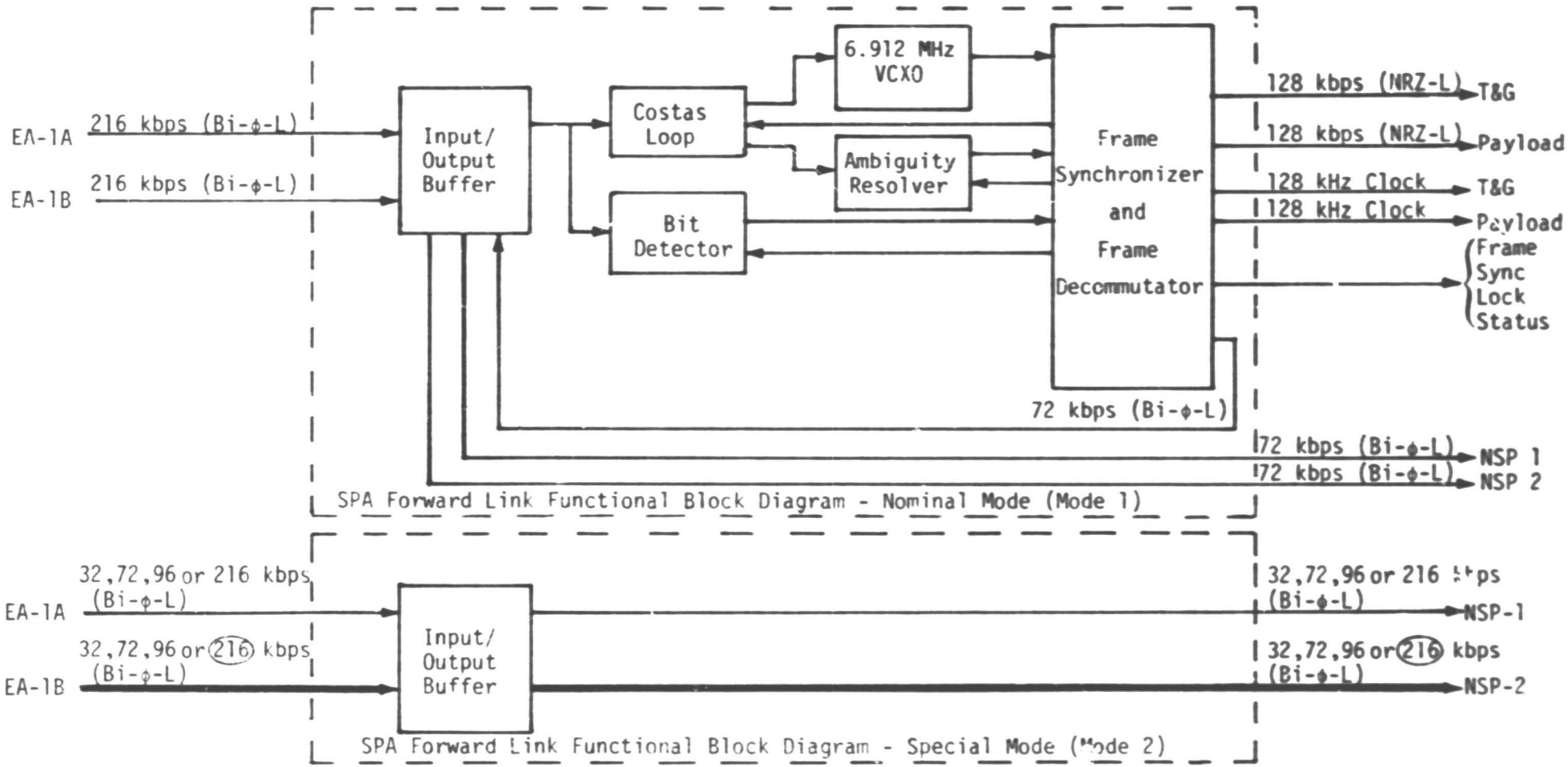

Test 055

Purpose: To test mode 2

Input Data: Valid frame synchronization (B7EB8CEC), OPS hex data (F502), SC hex data (FEAA002E)

Results: Passed

Figure 92.

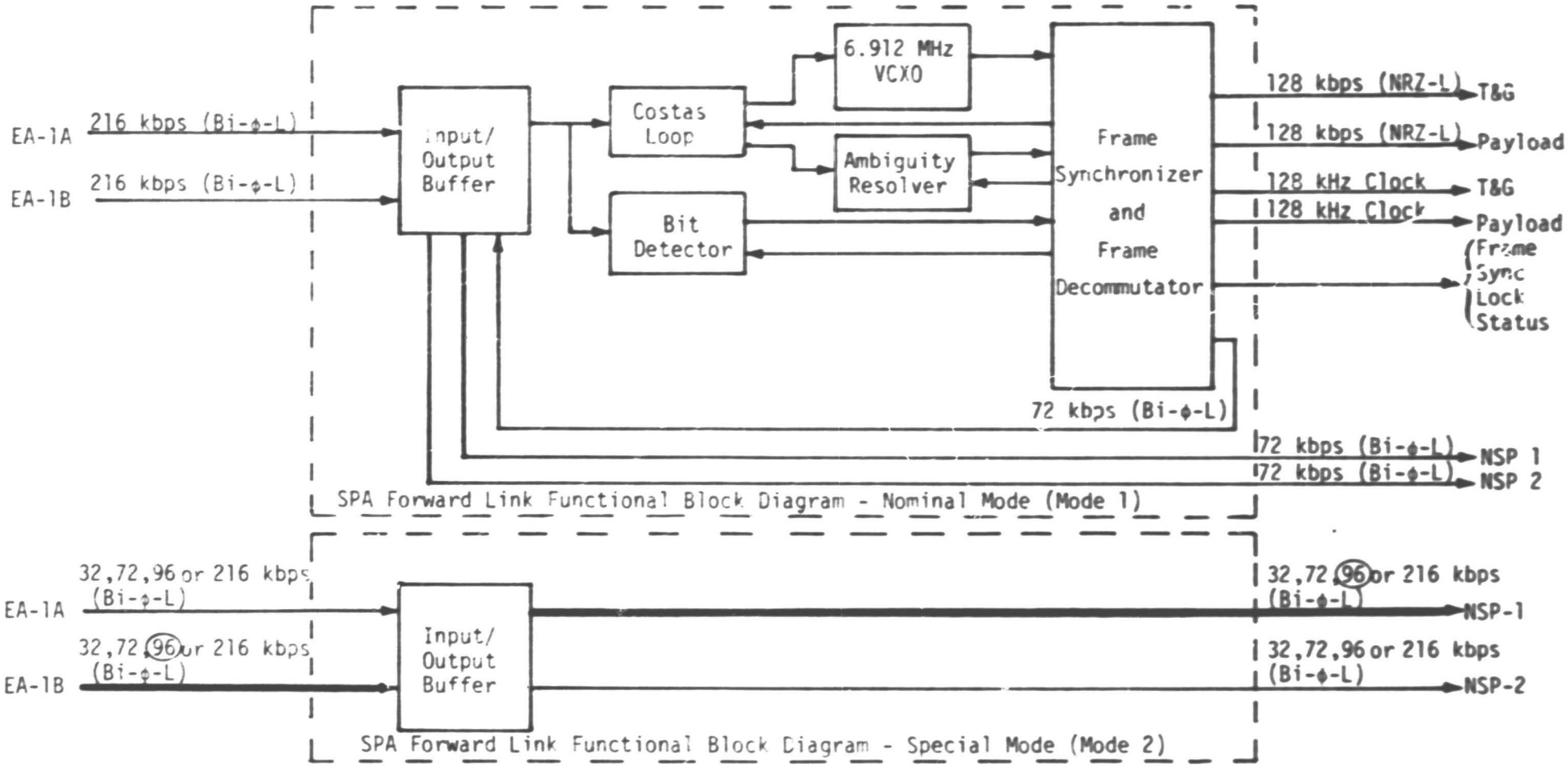

Test 056

Purpose: Same as Test 055

Input Data: Same as Test 055

Results: Passed

Figure 93.

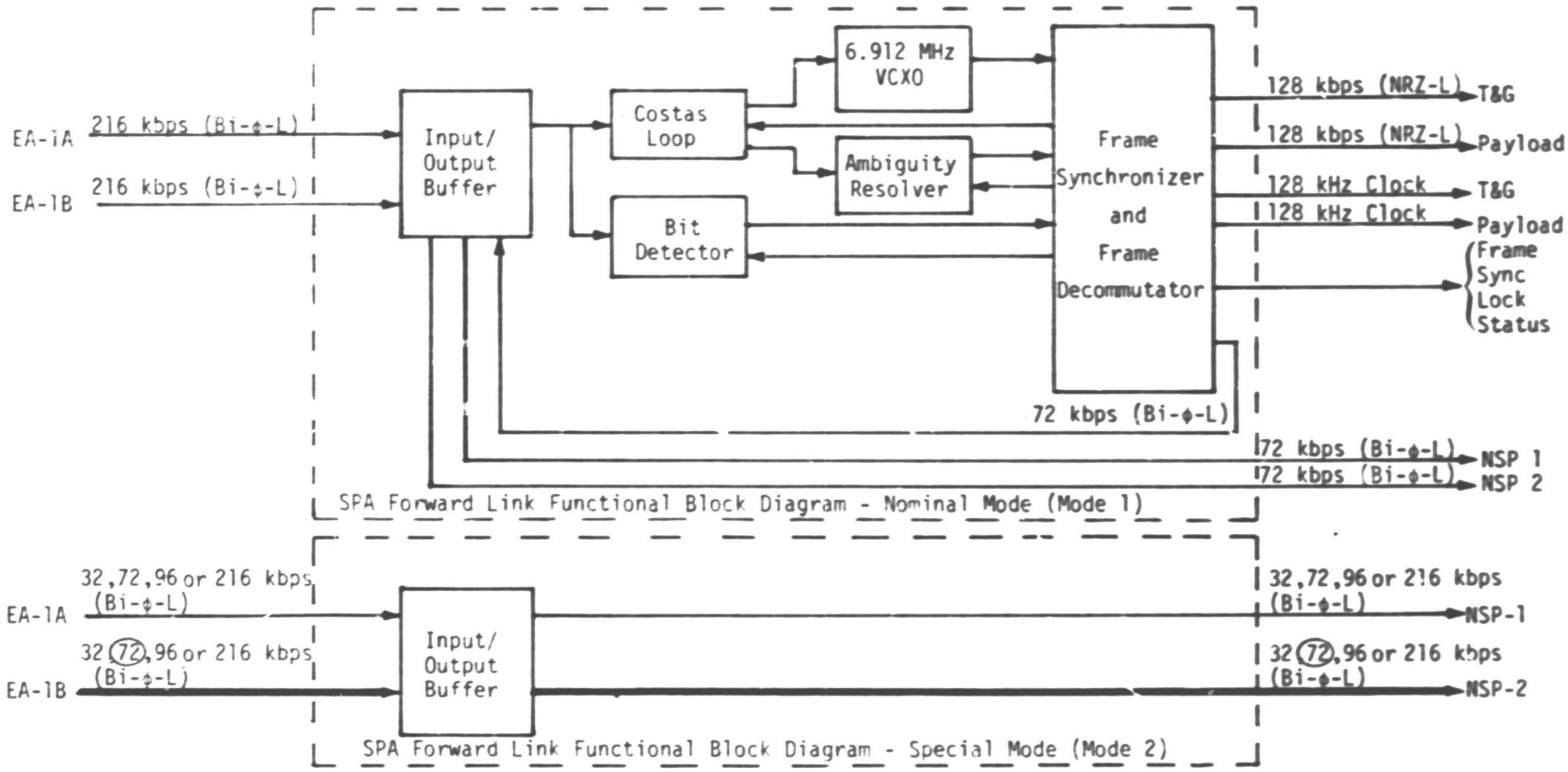

Test 057

Purpose: Same as Test 055

Input Data: Same as Test 055

Results: Passed

Figure 94.

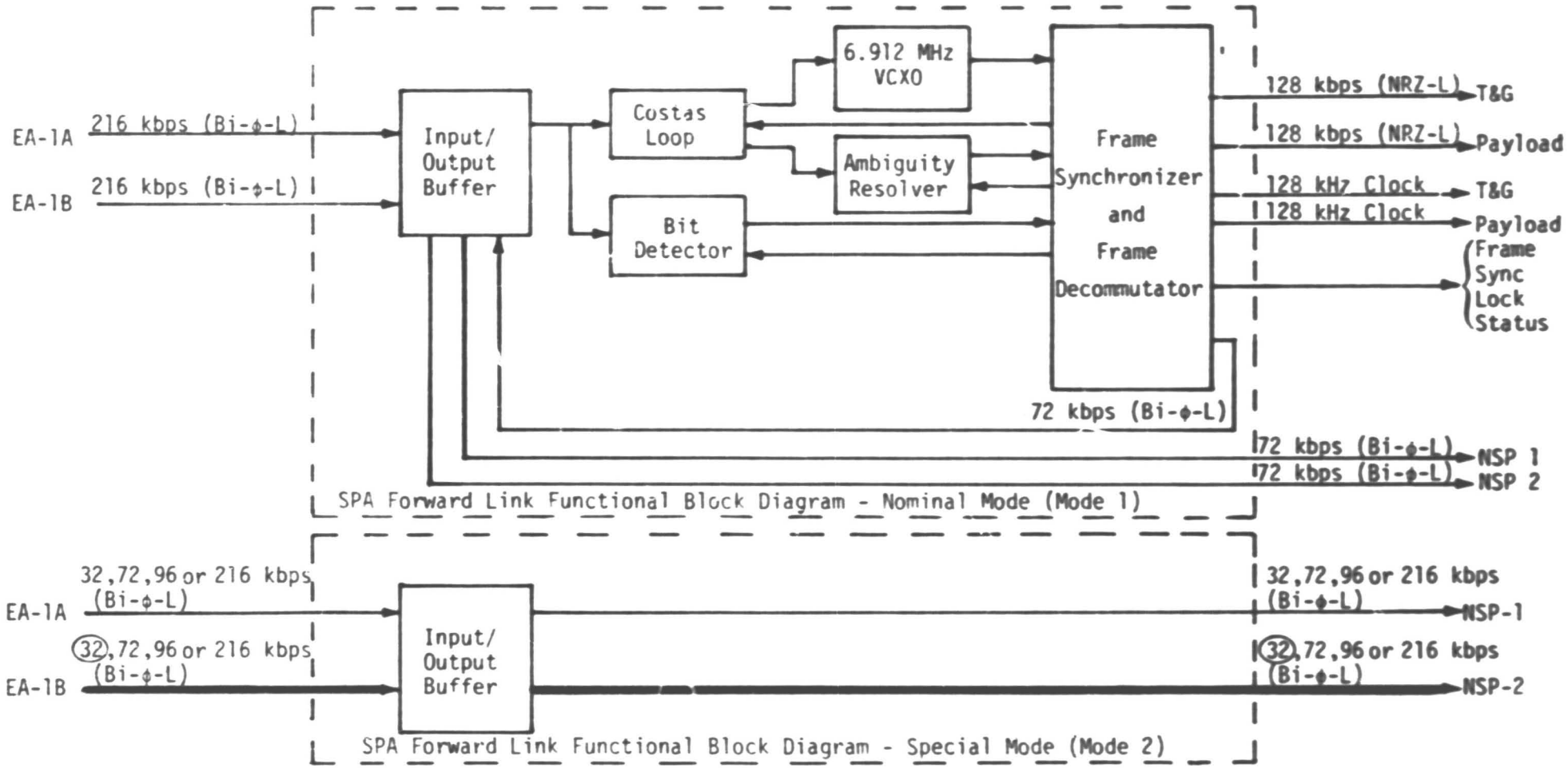

Note: There was no test 058 or 059

Test 060

Purpose: Same as Test 055

Input Data: Same as Test 055

Results: Passed

Figure 95.

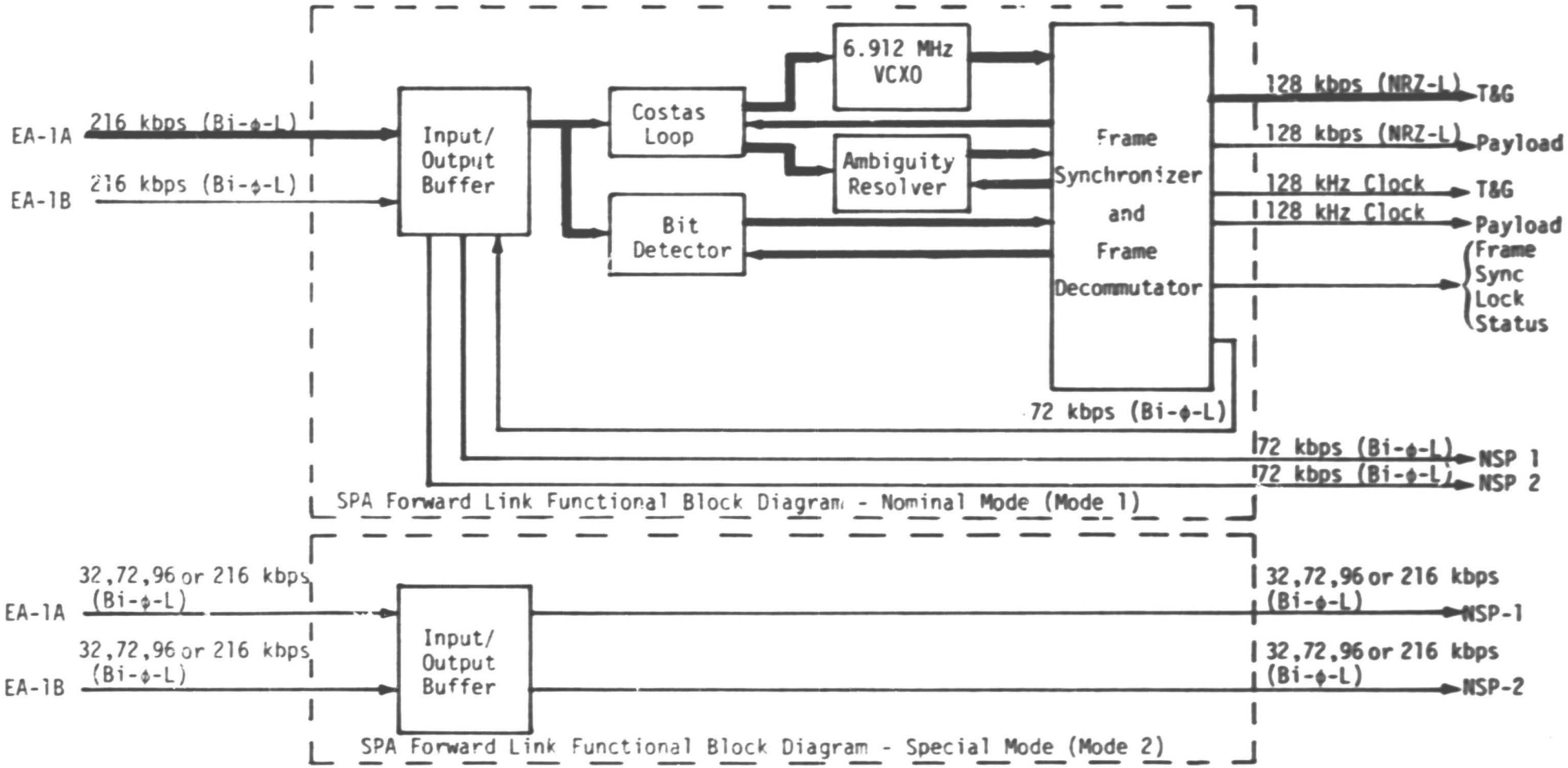

Test 061

Purpose: Verify mode 1 BER

Input Data: Valid frame synchronization (B7EB8CEC) and 1/0 data pattern

Figure 96.

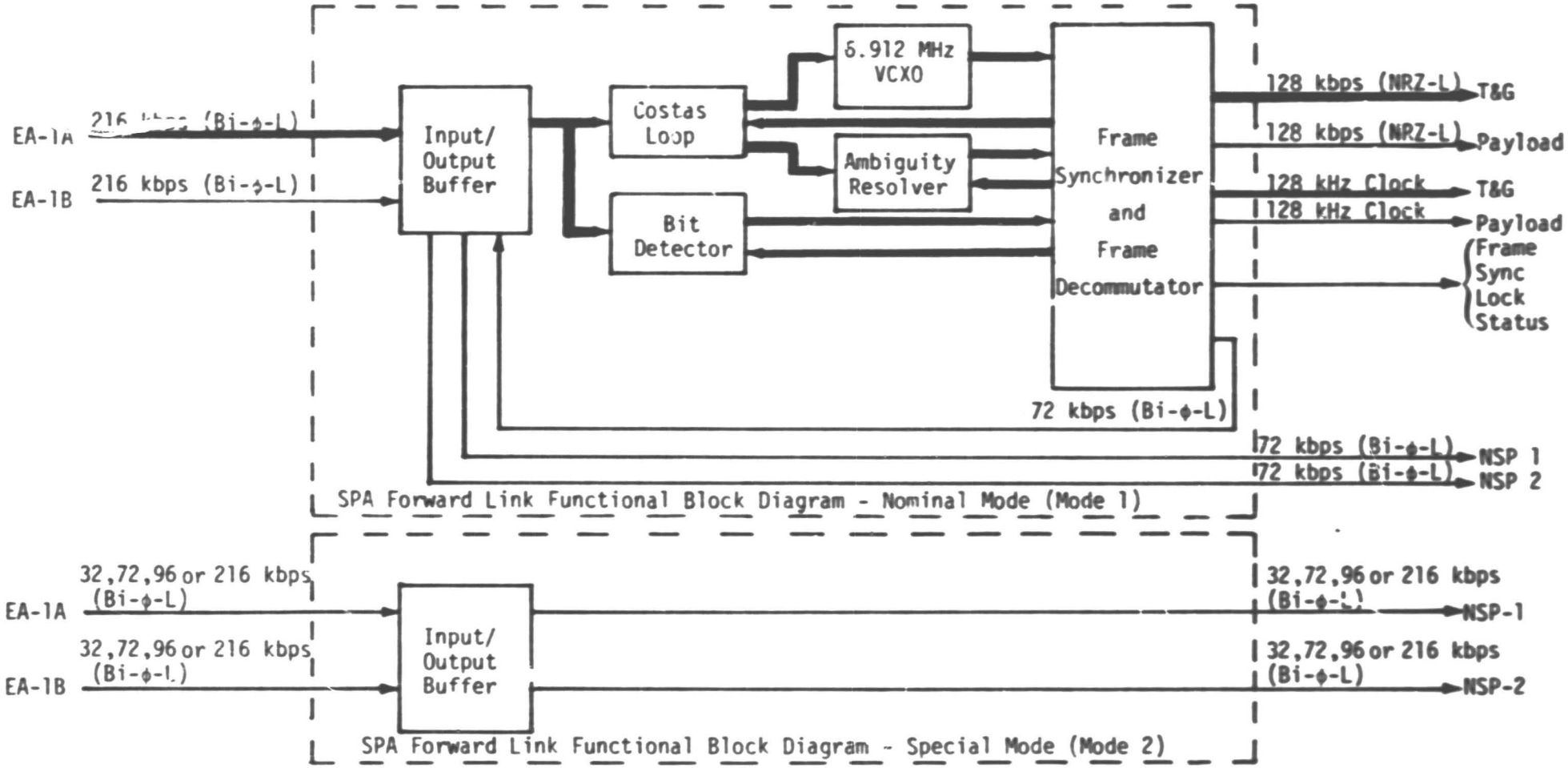

Test 062

Purpose: Same as Test 061

Input Data: Same as Test 061

Results: Passed

Figure 97.

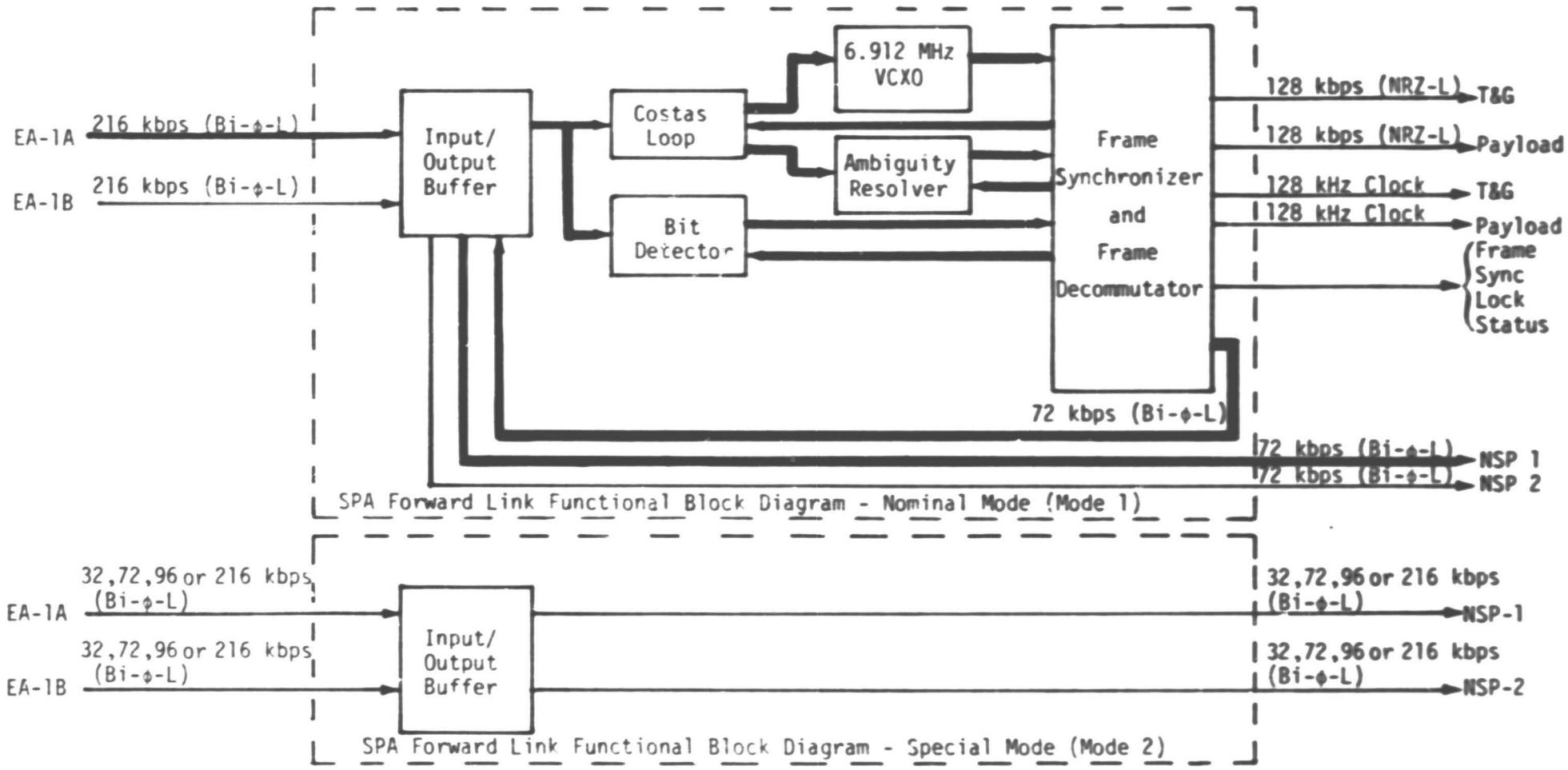

Test 063

Purpose: Same as Test 061

Input Data: Valid frame synchronization (B7EB8CEC) and all one data pattern

Results: Passed

Figure 98.

Table 27. SPA ADL LRU Forward Link Test Failure Summary

Hughes Test Number	Test Purpose	Failure
044	Verify all the various combinations of the frame synchronization pattern.	Failed synchronization, with one error occurring in any of the last four bits.

Table 28. SPA Input Signal Parameters Not Varied Over Their Respective Tolerance Ranges to Determine the Effect on Forward Link Performance

I. FORWARD LINK COMMUNICATIONS DIGITAL DATA INPUT FROM EA-1A AND EA-1B

1. Signal level
2. Rise and fall times
3. Jitter
4. Zero offset

II. SPA DATA TRANSFER CLOCK INPUT FROM EA-1A AND EA-1B

1. Rise and fall times
2. Phase jitter (TBS in RI Spec)
3. Phase offset (TBS in RI Spec)

III. SPA CONTROL DATA COVER PULSE INPUT FROM EA-1A AND EA-1B

1. Most parameters are listed as "TBS" in RI specification
2. Rise and fall times

IV. SPA STATUS COVER PULSE INPUT FROM EA-1A AND EA-1B

1. Most parameters are listed as "TBS" in Rockwell specification
2. Rise and fall times

10.1.3 Conclusions/Recommendations

In general, the SPA ADL LRU tests were fairly thorough. All the possible input signal combinations and the minimum and maximum data rates (except for one case) were tested and verified. The forward link digital output signal parameters were measured and found to meet the Rockwell requirements.

After evaluating the test data, Axiomatix has four concerns, listed as follows:

1. Most of the return link failures are very serious in nature and must be resolved as rapidly as possible. Axiomatix recommends that Hughes respond to each of the failures listed in Tables 24 and 27, indicating the corrective action and submitting additional test data.

2. The return link output signals (reference Table 26) have not been adequately measured. Axiomatix recommends that Rockwell update the Ku-band specification to eliminate all TBS's and that Hughes supply additional test data.

3. The effects of input signal tolerance variations on return link and forward link performance are unknown. It is possible for tolerance variations to have a very serious impact on system performance. Axiomatix recommends that additional data be supplied, either in the form of previous SRU data or new test data, to verify the effects of signal variations (reference Tables 25 and 28).

4. The minimum mode 2 return link data rate, 16 kbps, was not tested. Axiomatix recommends that future tests include 16 kbps for mode 2 return link.

10.2 EA-1 LRU CDR Test Data Evaluation

10.2.1 Introduction

The purpose of this section is to evaluate and assess the EA-1 LRU CDR test data presented by Hughes Aircraft Company (HAC) on August 25, 1980. Figure 99 illustrates the various EA-1 input and output signals. The CDR test data evaluation task involved ensuring that each signal path was adequately tested.

The CDR test data was gathered from both the ADL EA-1 LRU and the ESTL EA-1 LRU, with Hughes utilizing three categories of tests. These three test categories are as follows:

(1) Automated tests
(2) Manual tests
(3) RF module carry-forward data tests.

The majority of EA-1 tests were conducted using computer-controlled test equipment consisting of 20 individual tests. Table 29 gives a brief summary of each of the 20 automated tests. Hughes also employed four manual tests as summaried in Table 30. Finally, three carry-forward data tests, as summarized in Table 31, were used to measure a number of characteristics of the RF assembly SRU.

10.2.2 EA-1 Test Data

The EA-1 test data consisted of data from the automated, manual and RF module carry-forward data tests gathered from the ADL EA-1 LRU and automated and RF module carry-forward data tests gathered from the ESTL EA-1 LRU. The manual tests were not conducted on the ESTL EA-1 LRU.

Before reviewing the test data, it was necessary to determine which EA-1 parameters were verified by each test. As part of the CDR data package, HAC supplied a verification matrix indicating which tests satisfied the respective paragraphs of the Hughes EA-1 LRU development specification DS 32012-020, Rev. A. Since the baseline EA-1 performance document is the Rockwell specification MC 409-0025, Rev. B, not the Hughes LRU specification DS 32012-020, Rev. A, the first task was to establish a correlation between the Hughes LRU document and the Rockwell requirements.

The verification matrices, as shown in Appendix A, provide the correlation by listing the HAC LRU specification paragraph and title, the HAC verification method and test, and the corresponding Rockwell paragraph(s).

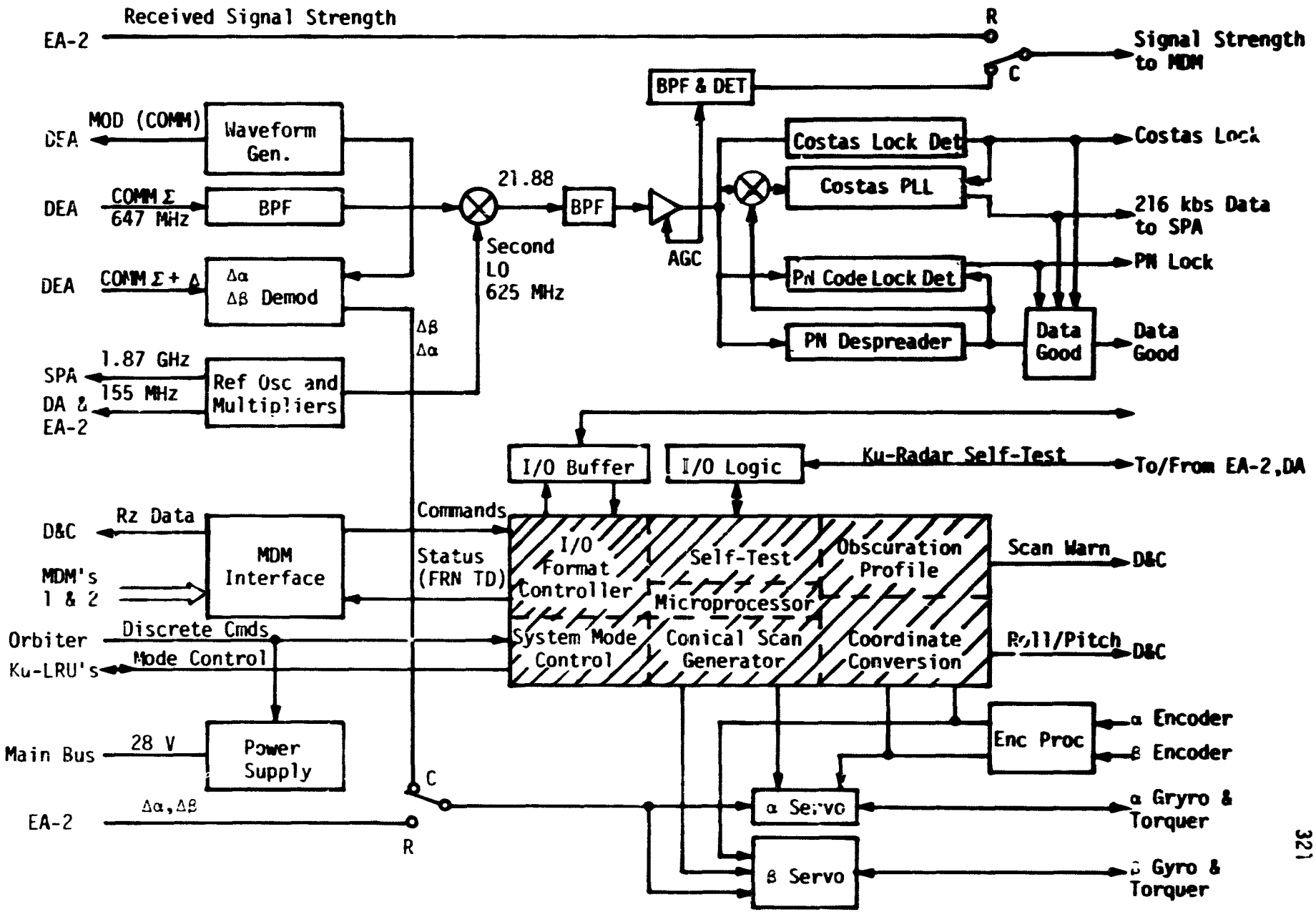

Figure 99. EA-1 Block Diagram

Table 29. Acceptance Test Procedure Summary (Automated Tests)

Test Number	Title	Purpose
1	Power Supply Test	Selected LRU power supply outputs are monitored and the following responses verified: • Operation from 24 to 32 VDC input voltage range • Nonoperation at undervoltage (18 VDC) • Operation of turn-on signal in response to COMM STBY, RADAR STBY, RADAR ON, COMM ON.
2	MDM Input Data Verification	Verifies that correct data occurs in serial digital data to MDM's 1 and 2. Also measures impedance, line noise, rise and fall times, signal rejection and common mode rejection.
3	Communication	Not implemented for ADL tests.
4	Self-Test	Not implemented for ADL tests.
5	Discrete Commands Test	Verifies discrete inputs and outputs not implicitly tested by combined other tests, which are as follows: • Radar Active/Passive • Linear Polarization • Radar Power Low • Radar Power Medium • Transmit Enable • Comm Stby/On • Radar Stby/On • Radar Alpha/Beta Lobing • Radar Alpha/Beta Lobing Phase • Widebeam Transmit Select • Widebeam Select • Delta Channel Select • Comm Alpha/Beta Lobing • Comm Alpha/Beta Lobing Phase
6	Encoder Input Tests	Checks the alpha and beta encoder processors.
7	Motor Drive Test	Verifies the following analog inputs to the antenna gimbal assembly: • Gyro primary excitation • Gyro spin motor drive (one and two) • Alpha gimbal motor drive (one and two) • Beta gimbal motor drive (one and two)

Table 29. Acceptance Test Procedure Summary
(Automated Tests)
(Continued)

Test Number	Title	Purpose
8	Servo Loop Characteristics and Pointing Loop Performance Test	Measures the servo loop characteristics and verifies the pointing loop performance.
9	GPC Acquisition Mode Test	Verifies pointing, tracking and searching in the GPC ACQUISITION mode for both radar and communications.
10	Autotrack and Manual Mode Test	Verifies that initial turn-on conditions are body stabilized, responds properly to slew commands and gimbals are stowed when commanded.
11	Radar/Communication Track Test	Measures alpha and beta fine and coarse gyro outputs.
12	GPC Designate Mode Test	Checks for proper operation when GPC DESIGNATE steering mode is commanded.
13	Break-Track Test	Verifies correct processing when a break-track condition occurs.
14	Scan Test	Not implemented for ADL tests.
15	Antenna Slew Rate Test	Verifies the slew rates in response to manual steering commands and the analog rate meter outputs for radar angle tracking.
16	Scan Warning Test	When the antenna LOS enters the obscuration zone, this test verifies that the scan warning discrete signal and the MDM serial scan warning bit are raised.
17	Coordinate Conversion Test	Verifies that the coordinate conversion error remains within tolerance within the 60° cone operating zone centered at 0.0 (-Z axis).
18	Boom Stow Tests	The stowing procedure is verified
19	Handover Tests	Verifies that EA-1 breaks track and goes to the latest designate when the TDRS EAST/WEST bits are toggled. Also, the test verifies that track is reestablished if COMM detect is high or that, if COMM detect is low, inertial hold is maintained.
20	Gimbal Constraints Test	The gimbal constraints are verified.

Table 30. EA-1 Manual Tests

Test Number	Title	Purpose
1	BER Tests	Measures forward link BER as a function of C/N_0
2	Signal Strength	Measures MDM 3 and D&C signal levels as functions of C/N_0 for four conditions, as follows: • Carrier • Carrier + PN code • Carrier + data • Carrier + PN code + data
3	Acquisition Time	Measures lock-up time for the signal condition indicators of Costas lock, PN code lock and data-present for four conditions, as follows: • Carrier • Carrier + PN code • Carrier + data • Carrier + PN code + data
4	RF Reference Outputs	Measures frequency and output power levels for the following signals: • 1876 MHz reference (SPA) • 156 MHz reference (EA-2) • 156 MHz reference (DA)

Table 31 . EA-1 RF Module Carry-Forward Data Tests

Test Number	Title	Purpose
1	Reference Generation Test	Measures the power output of the two RF assembly SRU 156 MHz reference signal outputs and of the RF assembly SRU 1875 MHz reference signal output.
2	Track IF Test	Measures the RF assembly SRU track IF output peak-to-peak voltage with -30 dBm input and -19 dBm input.
3	Data IF Test	Measures the RF assembly SRU data IF output to determine the LO leakage with respect to the carrier and measures parameters to calculate the gain and bandwidth.

After an extensive examination of both documents, the conclusion is that the Hughes LRU specification accurately reflects the Rockwell specification; therefore, the HAC verification tests should adequately test the EA-1 performance parameters with respect to the Rockwell requirements.

By studying the verification matrices shown in section 10.2.4 and the CDR test data, it becomes apparent that a number of tests were not performed on the ADL and ESTL EA-1 LRU's such as verifying self-test, communications mode tracking, and the analog MDM interfaces. Also, both LRU's experienced a number of failures, such as the out-of-specification gyro spin motor voltages, wrong RF switch logic for the widebeam transmit select, widebeam select, delta channel select, radar lobing and communication lobing, inadequate 1.875 MHz reference signal level output for the ADL LRU and reading invalid data from the MDMI SRU.

10.2.3 Conclusions/Recommendations

In reviewing the EA-1 CDR test data, a number of test omissions and failures were apparent. Since the Axiomatix evaluation revealed nothing that is not known to NASA, Rockwell or HAC, or has not been documented, Axiomatix feels it unnecessary to restate the omissions, failures and corrective action plans.

It is the opinion of Axiomatix that the Hughes tests were well documented and adequately tested the EA-1 performance. Finally, one benefit resulting from this CDR test data review by Axiomatix is that a document now exists in section 10.2.4 which, for the first time, relates the HAC EA-1 LRU specification to the Rockwell requirements.

10.2.4 Verification Matrices

In the following verification matrices, the paragraph numbers in the left-hand column refer to the Hughes LRU development specification DS 32012-020, Rev. A, and the paragraph numbers in the right-hand column refer to the Rockwell Ku-band specification MC 409-0025, Rev. B.

A TXX number refers to the automated test numbered XX, as listed in Table 29. "Manual test" refers either to the manually performed acceptance tests, as listed in Table 30, or the RF module carry-forward data tests, as listed in Table 31.

"DT" refers to verifications performed only by development tests. Items labeled "tester" are verified by the tester hardware interfaces during automated tests.

Hughes Specification DS 32012-020 Paragraph Ref.	Hughes Title	Hughes Verification Method								Hughes Verification Test	Rockwell Specification MC 409-0025, Rev. B Paragraph Ref.
		N/A	1	2		3			4		
				a	b	a	b	c			
3.	Requirements	X									N/A
3.1	Item Definition	X									N/A
3.1.1	Reserved	X									N/A
3.1.2	Interface Definition	X									N/A
3.1.2.1	Electrical Power Bus Voltage Limits									TBS	20.3.1.2.1
	Transient Surge Operation									TBS	
	Broadband Ripple MF0004 and MF0004-020									TBS	
3.1.2.2	Mechanical	X									N/A
3.1.2.2.1	Mounting			X							20.3.1.2.2.1
3.1.2.2.2	Connectors			X							20.3.1.2.2.2
3.1.2.3	Cooling and Heating									TBS	20.3.1.2.3
3.1.2.4	Signal Interface Definition	X									N/A
3.1.2.4.1	Digital MDM									T2	20.3.1.2.4.2, Ref. Appendix XII
	Pin Numbers				X	X	X	X			
	Time Tolerances									TBS	
3.1.2.4.1.1	Control Discrete Characteristics										20.3.1.2.4.2, Ref. Appendix XII
	(a) Receiver Type				X						
	(b) Logic Level				X						

NOTE: All input signals with tolerance variation characteristics will be certified by test set calibration.

N/A = Not Applicable
1 = Analysis
a = Inspection
b = Review of Design

3 = Test
a = Development
b = Qualification
c = Acceptance

4 = Carry-Forward Test(s)

Hughes Specification DS 32012-020 Paragraph Ref.	Hughes Title	Hughes Verification Method								Hughes Verification Test	Rockwell Specification MC 409-0025, Rev. B Paragraph Ref.
		N/A	1	2		3			4		
				a	b	a	b	c			
3.1.2.4.1.1 (Continued)	(c) Rise/Fall Times									TBS	
	(d) Signal Source Impedance	X									
	(e) Load Impedance				X						
	(f) Damage Threshold				X						
3.1.2.4.1.2	Serial Data to MDM										20.3.1.2.4.2, Ref. Appendix XII
	(a) Signal Type				X						
	(b) Logic Levels									TBS	
	(d) Driver Output Recovery									TBS	
	(e) Noise					X	X	X		T2	
	(f) Rise and Fall Times					X	X	X		T2	
	(g) Source Impedance					X	X	X		T2	
	(h) Pulse Width Variation Isolation Resistance					X	X	X		T2	
	(i) Common Mode Voltage				X	X	X	X		±20 T2	
	(j) Common Mode Damage Threshold									TBS	
3.1.2.4.1.3	Serial Data from MDM										20.3.1.2.4.2, Ref. Appendix XII
3.1.2.4.2	Ku-Band Serial										N/A
	Pins				X	X	X	X	X	T2, T9	
	Timing				X						
3.1.2.4.2.1	Data Transfer Clock										20.3.1.2.4.7.5.2 (EA-2) 20.3.1.2.4.1.4.2 (SPA)
	Signal				X	X	X	X			
	Clock Rate				X						
	Level				X	X				D.T.	

NOTE: All input signals with tolerance variation characteristics will be certified by test set calibration.

N/A = Not Applicable
1 = Analysis
a = Inspection
b = Review of Design

3 = Test
a = Development
b = Qualification
c = Acceptance

4 = Carry-Forward Test(s)

Hughes Specification DS 32012-020 Paragraph Ref.	Hughes Title	Hughes Verification Method								Hughes Verification Test	Rockwell Specification MC 409-0025, Rev. B Paragraph Ref.
		N/A	1	2		3			4		
				a	b	a	b	c			
3.1.2.4.2.1 (Continued)	Load Impedance				X	X				D.T.	
	Source Coupling				X	X				D.T.	
	Load Coupling	X								D.T.	
	Rise and Fall Times				X	X				D.T.	
3.1.2.4.2.2	Data and Status Cover Pulse										20.3.1.2.4.7.5.3 (EA-2 Data) 20.3.1.2.4.7.5.4 (EA-2 Status) 20.3.1.2.4.1.4.3 (SPA Data) 20.3.1.2.4.1.4.5 (SPA Status)
	Signal				X	X	X	X			
	Level				X	X				D.T.	
	Load Impedance				X	X	X	X		Tester	
	Source Coupling				X	X				D.T.	
	Load Coupling	X				X				D.T.	
	Rise and Fall Times				X	X				D.T.	
3.1.2.4.2.3	Data Output										20.3.1.2.4.7.5 (To EA-2) 20.3.1.2.4.1.4.1 (To SPA)
	Signal Digital Data				X	X	X	X			
	Data Rate				X						
	Data Type				X	X	X	X			
	Level				X	X				D.T.	
	Load Impedance				X	X				D.T.	
	Source Coupling				X	X				D.T.	
	Load Coupling	X								D.T.	
	Rise and Fall Times				X	X				D.T.	
	Jitter				X						

NOTE: All input signals with tolerance variation characteristics will be certified by test set calibration.

N/A = Not Applicable
1 = Analysis
a = Inspection
b = Review of Design

3 = Test
a = Development
b = Qualification
c = Acceptance

D.T. = Development Test
4 = Carry-Forward Test(s)

330

Hughes Specification DS 32012-020 Paragraph Ref.	Hughes Title	Hughes Verification Method								Hughes Verification Test	Rockwell Specification MC 409-0025, Rev. B Paragraph Ref.
		N/A	1	2		3			4		
				a	b	a	b	c			
3.1.2.4.2.4	Status Input										20.3.1.2.4.7.5.4 (From EA-2) 20.3.1.2.4.1.4.4 (From SPA)
3.1.2.4.3	Discrete Control Signals	X									N/A
3.1.2.4.3.1	Inputs				X	X	X	X		T1, T5, T9, T10, T12	20.3.1.2.4.5.1 (From ADA) 20.3.1.2.4.3.2 (From GCILU) 20.3.1.2.4.3.1 (From OCC) 20.3.1.2.4.6.2.2 (From DA)
3.1.2.4.3.2	Input Characteristics										20.3.1.2.4.3.2 (GCILU) 20.3.1.2.4.3.1 (OCC) 20.3.1.2.4.5.1 (ADA) 20.3.1.2.4.6.2 (DA)
	Data Rate				X						
	Waveform				X						
	Level				X						
	Source Current				X						
	Termination				X						
	Rise and Fall Times				X						
3.1.2.4.3.3	Outputs				X	X	X	X		T1, T4, T5 T18	20.3.1.2.4.5.2.1-2 (ADA) 20.3.1.2.4.4.1 (Displays) 20.3.1.2.4.7.1.1 (EA 2) 20.3.1.2.4.6.1.1-6 (DA) 20.3.1.2.4.1.1.1-2 (SPA)

NOTE: All input signals with tolerance variation characteristics will be certified by test set calibration.

N/A = Not Applicable
1 = Analysis
a = Inspection
b = Review of Design

3 = Test
a = Development
b = Qualification
c = Acceptance

4 = Carry-Forward Test(s)

Hughes Specification DS 32012-020 Paragraph Ref.	Hughes Title	Hughes Verification Method								Hughes Verification Test	Rockwell Specification MC 409-0025, Rev. B Paragraph Ref.
		N/A	1	2		3			4		
				a	b	a	b	c			
3.1.2.4.3.4	Output Characteristics										20.3.1.2.4.5.2.1-2 (ADA) 20.3.1.2.4.4.1 (Displays) 20.3.1.2.4.7.1 (EA-2 20.3.1.2.4.6.1 (DA) 20.3.1.2.4.1.1 (SPA)
	Data Rate				X	X	X	X		T5	
	Waveform				X						
	Level				X	X	X	X		T5	
	Source Current				X	X	X	X		T5	
	Short-Circuit Current				X	X	X	X		T5	
	Termination				X						
	Rise and Fall Times				X						
3.1.2.4.4	Differential Control Signals	X									N/A
3.1.2.4.4.1	Inputs				X	X	X	X		T5	20.3.1.2.4.7.2.1-4 (EA-2)
3.1.2.4.4.2	Input Characteristics										20.3.1.2.4.7.2 (EA-2)
	Signal				X						
	Level				X						
	Source Impedance				X						
	Source Coupling	X									
	Load Coupling				X						
	Rise and Fall Times				X						
3.1.2.4.4.3	Outputs and Characteristics										N/A
	Signal Title Lobing Phase 0/180				X						20.3.1.2.4.6.3.13
	Pins				X	X	X	X		T5	

NOTE: All input signals with tolerance variation characteristics will be certified by test set calibration.

N/A = Not Applicable
1 = Analysis
a = Inspection
b = Review of Design

3 = Test
a = Development
b = Qualification
c = Acceptance

4 = Carry-Forward Test(s)

Hughes Specification DS 32012-020 Paragraph Ref.	Hughes Title	Hughes Verification Method								Hughes Verification Test	Rockwell Specification MC 409-0025, Rev. B Paragraph Ref.
		N/A	1	2		3			4		
				a	b	a	b	c			
3.1.2.4.4.3 (Continued)	Signal				X						
	Frequency				X	X	X	X		T5	
	Level				X						
	Load Impedance				X						
	Source Coupling				X						
	Load Coupling	X									
	Rise and Fall Times				X						
	Signal Title Lobing Alpha-Beta										20.3.1.2.4.6.3.12
	Pins				X	X	X	X		T5	
	Signal				X						
	Frequency				X	X	X	X		T5	
	Level				X						
	Load Impedance				X	X	X	X		T5	
	Source Coupling				X						
	Load Coupling	X									
	Rise and Fall Times				X						
3.1.2.4.5	Antenna Control	X									N/A
3.1.2.4.5.1	Servo Motor Drive Outputs				X						N/A
	(1) Signal Title Alpha Motor Drive				X						20.3.1.2.4.6.3.1 (To DA)
	Pins				X	X	X	X		T7	
	Signal				X	X	X	X		T7	
	Frequency				X	X	X	X		T7	
	Level				X						
	Load Characteristics				X	X	X	X		T7	
	Source Coupling				X						

NOTE: All input signals with tolerance variation characteristics will be certified by test set calibration.

N/A = Not Applicable
1 = Analysis
a = Inspection
b = Review of Design

3 = Test
a = Development
b = Qualification
c = Acceptance

4 = Carry-Forward Test(s)

Hughes Specification DS 32012-020 Paragraph Ref.	Hughes Title	Hughes Verification Method								Hughes Verification Test	Rockwell Specification MC 409-0025, Rev. B Paragraph Ref.
		N/A	1	2		3			4		
				a	b	a	b	c			
3.1.2.4.5.1 (Continued)	Load Coupling	X									
	Rise and Fall Times				X						
	(2) Signal Title Beta Motor Drive				X						20.3.1.2.4.6.3.1 (To DA)
	Pins				X	X	X	X		T7	
	Signal				X	X	X	X		T7	
	Frequency				X	X	X	X		T7	
	Level				X						
	Load Characteristics				X	X	X	X		T7	
	Source Coupling				X						
	Load Coupling	X									
	Rise and Fall Times				X						
3.1.2.4.5.2	Gimbal Lock Drive Output										20.3.1.2.4.6.3.11 (To DA)
	Signal Title Antenna Gimbal Lock Drive				X						
	Pins				X	X	X	X		T18	
	Signal				X	X	X	X		T18	
	Current				X	X	X	X		T18	
	Load Impedance				X						
	Source Coupling				X						
	Load Coupling	X									
3.1.2.4.5.3	Encoder Drive										20.3.1.2.4.6.3.3 (To DA)
	Signal Title Encoder Input				X						
	Pins				X	X	X	X		T1	
	Signal				X						

NOTE: All input signals with tolerance variation characteristics will be certified by test set calibration.

N/A = Not Applicable
1 = Analysis
a = Inspection
b = Review of Design

3 = Test
a = Development
b = Qualification
c = Acceptance

4 = Carry-Forward Test(s)

Hughes Specification DS 32012-020 Paragraph Ref.	Hughes Title	Hughes Verification Method								Hughes Verification Test	Rockwell Specification MC 409-0025, Rev. B Paragraph Ref.
		N/A	1	2		3			4		
				a	b	a	b	c			
3.1.2.4.5.3 (Continued)	Level				X	X	X	X		T1	
	Source Current				X						
	Source Coupling				X						
	Load Coupling	X									
3.1.2.4.5.4	Gyro Drive										N/A
	(1) Signal Title Gyro				X						
	Primary Excitation										20.3.1.2.4.6.3.4 (To DA)
	Pins				X	X	X	X		T7	
	Signal				X						
	Frequency				X	X	X	X		T7	
	Level				X	X	X	X		T7	
	Source Current				X						
	Source Couping				X						
	Load Coupling	X									
	(2) Signal Title Gryo Spin				X						
	Motor Excitation				X						20.3.1.2.4.6.3.2 (To DA)
	Pins				X	X	X	X		T7	
	Quadrature Square Waves				X	X	X	X		T7	
	Frequency				X	X	X	X		T7	
	Level				X	X	X	X		T7	
	Source Current				X	X	X	X		Tester	
	Source Coupling				X						
	Load Coupling	X									

NOTE: All input signals with tolerance variation characteristics will be certified by test set calibration.

N/A = Not Applicable
1 = Analysis
a = Inspection
b = Review of Design

3 = Test
a = Development
b = Qualification
c = Acceptance

4 = Carry-Forward Test(s)

Hughes Specification DS 32012-020 Paragraph Ref.	Hughes Title	Hughes Verification Method								Hughes Verification Test	Rockwell Specification MC 409-0025, Rev. B Paragraph Ref.
		N/A	1	2		3			4		
				a	b	a	b	c			
3.1.2.4.5.5	RSA Inputs										N/A
	(1) Signal Title Alpha Axis High				X						20.3.1.2.4.6.4.5.1 (From DA)
	Pins				X	X	X	X		Tester	
	Signal				X	X	X	X		Tester	
	Frequency	X									
	Level				X						
	Scale Factor				X						
	Offset of Source	X									
	Source Impedance				X						
	Source Coupling	X									
	Load Coupling				X	X	X	X		Tester	
	(2) Signal Title Alpha Low				X						20.3.1.2.4.6.4.5.1 (From DA)
	Pins				X	X	X	X		Tester	
	Signal				X	X	X	X		Tester	
	Frequency	X									
	Level				X						
	Scale Factor				X						
	Scale Factor Accuracy of Source	X									
	Source Impedance				X						
	Source Coupling	X									
	Load Coupling				X	X	X	X		Tester	
	Offset of Source	X									

NOTE: All input signals with tolerance variation characteristics will be certified by test set calibration.

N/A = Not Applicable
1 = Analysis
a = Inspection
b = Review of Design

3 = Test
a = Development
b = Qualification
c = Acceptance

4 = Carry-Forward Test(s)

Hughes Specification DS 32012-020 Paragraph Ref.	Hughes Title	Hughes Verification Method								Hughes Verification Test	Rockwell Specification MC 409-0025, Rev. B Paragraph Ref.
		N/A	1	2		3			4		
				a	b	a	b	c			
3.1.2.4.5.5 (Continued)	(3) Signal Title Beta Axis High				X						20.3.1.2.4.6.4.5.1 (From DA)
	Pins				X	X	X	X		Tester	
	Signal				X	X	X	X		Tester	
	Frequency	X									
	Level				X						
	Scale Factor				X						
	Scale Factor Accuracy of Source	X									
	Source Impedance				X						
	Source Coupling	X									
	Load Coupling				X	X	X	X		Tester	
	Offset of Source	X									
	(4) Signal Title Beta Axis Low				X						20.3.1.2.4.6.4.5.1 (From DA)
	Pins				X	X	X	X		Tester	
	Signal				X	X	X	X		Tester	
	Frequency	X									
	Level				X						
	Scale Factor				X						
	Scale Factor Accuracy of Source	X									
	Source Impedance				X						
	Source Coupling	X									
	Load Coupling				X	X	X	X		Tester	
	Offset of Source	X									

NOTE: All input signals with tolerance variation characteristics will be certified by test set calibration.

N/A = Not Applicable
1 = Analysis
a = Inspection
b = Review of Design

3 = Test
a = Development
b = Qualification
c = Acceptance

4 = Carry-Forward Test(s)

Hughes Specification DS 32012-020 Paragraph Ref.	Hughes Title	Hughes Verification Method								Hughes Verification Test	Rockwell Specification MC 409-0025, Rev. B Paragraph Ref.
		N/A	1	2		3			4		
				a	b	a	b	c			
3.1.2.4.5.6	Encoder Inputs										N/A
	(1) Signal Title Alpha Encoder										
	Index				X						20.3.1.2.4.6.4.4.1 (From DA)
	Pins				X	X	X	X		Tester	
	Frequency				X						
	Level				X						
	Source Impedance				X						
	Source Coupling	X									
	Load Coupling				X	X	X	X		Tester	
	Rise and Fall Times	X									
	(2) & (3) Signal Title Alpha Encoder				X						
	Output & Encoder Quad Output										20.3.1.2.4.6.4.4.1 (From DA)
	Pins				X	X	X	X		Tester	
	Pulse Rate				X	X	X	X		T6, 750 Hz max.	
	Level				X						
	Source Impedance				X						
	Source Coupling	X									
	Load Coupling				X	X	X	X		Tester	
	Rise and Fall Times	X									
	(4) Signal Title Beta Encoder										
	Index				X						20.3.1.2.4.6.4.4.1 (From DA)
	Pins				X	X	X	X		Tester	
	Frequency				X						
	Level				X						

NOTE: All input signals with tolerance variation characteristics will be certified by test set calibration.

N/A = Not Applicable
1 = Analysis
a = Inspection
b = Review of Design

3 = Test
a = Development
b = Qualification
c = Acceptance

4 = Carry-Forward Test(s)

Hughes Specification DS 32012-020 Paragraph Ref.	Hughes Title	Hughes Verification Method								Hughes Verification Test	Rockwell Specification MC 409-0025, Rev. B Paragraph Ref.
		N/A	1	2		3			4		
				a	b	a	b	c			
3.1.2.4.5.6 (Continued)	Source Impedance				X						
	Source Coupling	X									
	Load Coupling				X	X	X	X		Tester	
	Rise and Fall Times	X									
	(5) Signal Title Beta Encoder Output				X						20.3.1.2.4.6.4.4.1 (From DA)
	Pins				X	X	X	X		Tester	
	Pulse Rate				X	X	X	X		T6, 750 Hz maximum	
	Level				X						
	Source Impedance				X						
	Source Coupling	X									
	Load Coupling				X	X	X	X		Tester	
	Rise and Fall Times	X									
	(6) Signal Title Beta Encoder Quad Output				X						20.3.1.2.4.6.4.4.1 (From DA)
	Pins				X	X	X	X		Tester	
	Pulse Rate				X	X	X	X		T6, 750 Hz maximum	
	Level				X						
	Source Impedance				X						
	Source Coupling	X									
	Load Coupling				X	X	X	X		Tester	
	Rise and Fall Times	X									

NOTE: All input signals with tolerance variation characteristics will be certified by test set calibration.

N/A = Not Applicable
1 = Analysis
a = Inspection
b = Review of Design

3 = Test
a = Development
b = Qualification
c = Acceptance

4 = Carry-Forward Test(s)

Hughes Specification DS 32012-020 Paragraph Ref.	Hughes Title	Hughes Verification Method								Hughes Verification Test	Rockwell Specification MC 409-0025, Rev. B Paragraph Ref.
		N/A	1	2		3			4		
				a	b	a	b	c			
3.1.2.4.5.7	Radar Track Inputs										N/A
	(1) Signal Title Alpha Error				X						20.3.1.2.4.7.4.2 (From EA-2)
	Pins				X	X	X	X		Tester	
	Signal				X	X	X	X		T11	
	Level				X	X	X	X		T11	
	Source Impedance	X									
	Source Coupling	X									
	Load Coupling				X						
	(2) Signal Title Beta Encoder				X						20.3.1.2.4.7.4.2 (From EA-2)
	Pins				X	X	X	X		Tester	
	Signal				X	X	X	X		T11	
	Level				X	X	X	X		T11	
	Source Impedance	X									
	Source Coupling	X									
	Load Coupling				X						
3.1.2.4.5.8	Power Supply Inputs	X									20.3.1.2.4.6.4.7
	(1) & (2) Pins				X	X	X	X		Tester	
	Signal				X	X	X	X		Tester	
	Level				X	X	X	X		Tester	
	Source Current				X						
	Source Coupling				X						
	Load Coupling				X						
3.1.2.4.5.9	Deleted										

NOTE: All input signals with tolerance variation characteristics will be certified by test set calibration.

N/A = Not Applicable
1 = Analysis
a = Inspection
b = Review of Design

3 = Test
a = Development
b = Qualification
c = Acceptance

4 = Carry-Forward Test(s)

Hughes Specification DS 32012-020 Paragraph Ref.	Hughes Title	Hughes Verification Method								Hughes Verification Test	Rockwell Specification MC 409-0025, Rev. B Paragraph Ref.
		N/A	1	2		3			4		
				a	b	a	b	c			
3.1.2.4.5.10	Widebeam Select/Delta Channel Control										20.3.1.2.4.6.1.7 (Wideband to DA) 20.3.1.2.4.6.1.8 (Delta to DA)
	(1) Signal Title Widebeam Select/Delta Channel Select				X						
	Pins				X	X	X	X		T5	
	Signal				X	X	X	X		T5	
	Level Execute				X						
	Load Impedance				X	X	X	X		Tester	
	Source Coupling				X						
	Load Coupling	X									
3.1.2.4.6	Forward Link	X									N/A
3.1.2.4.6.1	IF Inputs										N/A
	(1) Signal Title Data IF				X						20.3.1.2.4.6.4.1 (From DA)
	Connector				X	X	X	X		Tester	
	Signal				X	X	X	X		Tester	
	Frequency				X	X	X	X		Tester	
	Level				X	X	X	X		Manual Test	
	Source Impedance				X	X	X	X		Tester	
	Load Impedance				X						
	VSWR				X						
	(2) Signal Title Track IF				X						20.3.1.2.4.6.4.3 (From DA)
	Connector				X	X	X	X		Tester	
	Signal				X	X	X	X		Tester	
	Frequency				X	X	X	X		Tester	

NOTE: All input signals with tolerance variation characteristics will be certified by test set calibration.

N/A = Not Applicable
1 = Analysis
a = Inspection
b = Review of Design

3 = Test
a = Development
b = Qualification
c = Acceptance

4 = Carry-Forward Test(s)

Hughes Specification DS 32012-020 Paragraph Ref.	Hughes Title	Hughes Verification Method								Hughes Verification Test	Rockwell Specification MC 409-0025, Rev. B Paragraph Ref.
		N/A	1	2		3			4		
				a	b	a	b	c			
3.1.2.4.6.1 (Continued)	Level				X	X	X	X		Tester	
	Source Impedance				X	X	X	X		Tester	
	Load Impedance				X						
	VSWR				X						
3.1.2.4.6.2	Data Output										20.3.1.2.4.1.2.1 (To SPA) 20.3.1.2.4.1.2.1.1 20.3.1.2.4.1.2.1.2
	Signal Title 216 kbps Data				X						
	Pins				X	X	X	X		Manual Test	
	Signal				X	X	X	X		Manual Test	
	Data Rate				X	X	X	X		Manual Test	
	Level				X	X	X	X		Manual Test	
	Common Mode Voltage				X						
	Load Impedance				X						
	Source Coupling				X						
	Load Coupling	X									
3.1.2.4.7	Measurements and Reference Frequencies	X									N/A
3.1.2.4.7.1	Analog Measurements										N/A
	(1) Signal Title Radar Signal Strength				X						20.3.1.2.4.7.4.1 (From EA-2)
	Signal Level				X	X	X	X		T3	
	Source Impedance				X	X	X	X		Tester	
	Load Impedance				X						
	Source Coupling	X									
	Load Coupling				X						

NOTE: All input signals with tolerance variation characteristics will be certified by test set calibration.

N/A = Not Applicable
1 = Analysis
a = Inspection
b = Review of Design

3 = Test
a = Development
b = Qualification
c = Acceptance

4 = Carry-Forward Test(s)

Hughes Specification DS 32012-020 Paragraph Ref.	Hughes Title	Hughes Verification Method								Hughes Verification Test	Rockwell Specification MC 409-0025, Rev. B Paragraph Ref.
		N/A	1	2		3			4		
				a	b	a	b	c			
3.1.2.4.7.1 (Continued)	(2) Signal Title Transmit RF Power				X						20.3.1.2.4.6.4.2 (From DA)
	Pins				X	X	X	X		T3	
	Signal Level				X	X	X	X		T3	
	Source Impedance				X	X	X	X		Tester	
	Load Impedance				X						
	Source Coupling	X									
	Load Coupling				X						
	(3) Signal Title Transmit RF Power				X						20.3.1.2.4.2.3 (To MDM)
	Pins				X	X	X	X		T3	
	Signal				X	X	X	X		T3	
	Level				X	X	X	X		T3	
	Source Impedance				X						
	Source Coupling				X						
	Load Coupling	X									
	(4) Signal Title Signal Strength (MDM)				X						20.3.1.2.4.2.3 (To MDM)
	Pins				X	X	X	X		T3	
	Signal				X	X	X	X		T3	
	Level				X	X	X	X		T3	
	Source Impedance				X						
	Source Coupling				X						
	Load Coupling	X									

NOTE: All input signals with tolerance variation characteristics will be certified by test set calibration.

N/A = Not Applicable
1 = Analysis
a = Inspection
b = Review of Design

3 = Test
a = Development
b = Qualification
c = Acceptance

4 = Carry-Forward Test(s)

Hughes Specification DS 32012-020 Paragraph Ref.	Hughes Title	Hughes Verification Method								Hughes Verification Test	Rockwell Specification MC 409-0025, Rev. B Paragraph Ref.
		N/A	1	2		3			4		
				a	b	a	b	c			
3.1.2.4.7.1 (Continued)	(5) Signal Title Signal Strength (D&C)				X						20.3.1.2.4.4.2.2 (To D&C)
	Pins				X	X	X	X		T3	
	Signal				X	X	X	X		T3	
	Level				X	X	X	X		T3	
	Source Impedance				X						
	Source Coupling				X						
	Load Coupling	X									
	(6) Signal Title Antenna Pitch Rate				X						20.3.1.2.4.4.2.1 (To Displays)
	Pins				X	X	X	X		T15	
	Signal				X	X	X	X		T15	
	Level				X	X	X	X		T15	
	Source Impedance				X						
	Load Impedance				X						
	(7) Signal Title Antenna Roll Rate			X							20.3.1.2.4.4.2.1 (To Displays)
	Pins				X	X	X	X		T15	
	Signal				X	X	X	X		T15	
	Level				X	X	X	X		T15	
	Scale Factor				X	X	X	X		T15	
	Source Impedance				X						
	Load Impedance				X						
	Source Coupling				X						
	Load Coupling	X									

NOTE: All input signals with tolerance variation characteristics will be certified by test set calibration.

N/A = Not Applicable
1 = Analysis
a = Inspection
b = Review of Design

3 = Test
a = Development
b = Qualification
c = Acceptance

4 = Carry-Forward Test(s)

Hughes Specification DS 32012-020 Paragraph Ref.	Hughes Title	Hughes Verification Method								Hughes Verification Test	Rockwell Specification MC 409-0025, Rev. B Paragraph Ref.
		N/A	1	2		3			4		
				a	b	a	b	c			
3.1.2.4.7.2	Digital Displays										20.3.1.2.4.4.3 (To Displays)
	Signal Title Digital Dedicated Display Data				X						
	Pins				X	X	X	X		Tester	
	Signal				X	X	X	X		T9	
	Data Rate				X						
	Level				X						
	Rise and Fall Times				X						
	Load Impedance				X						
	Source Coupling				X						
	Load Coupling	X									
3.1.2.4.7.3	RF Reference										N/A
	(1) Signal Title 1876 MHz Ref				X						20.3.1.2.4.1.3.1 (To SPA)
	Connector				X	X	X	X		Tester	
	Level				X	X	X	X		Manual Test	
	Source Impedance				X						
	Load Impedance				X						
	(2) Signal Title 156 MHz Ref (EA-2)				X						20.3.1.2.4.7.3.1 (To EA-2)
	Connector				X	X	X	X		Tester	
	Signal				X	X	X	X		Manual Test	
	Level				X	X	X	X		Manual Test	
	Source Impedance				X						
	Load Impedance				X						

NOTE: All input signals with tolerance variation characteristics will be certified by test set calibration.

N/A = Not Applicable
1 = Analysis
a = Inspection
b = Review of Design

3 = Test
a = Development
b = Qualification
c = Acceptance

4 = Carry-Forward Test(s)

Hughes Specification DS 32012-020 Paragraph Ref.	Hughes Title	Hughes Verification Method								Hughes Verification Test	Rockwell Specification MC 409-0025, Rev. B Paragraph Ref.
		N/A	1	2		3			4		
				a	b	a	b	c			
3.1.2.4.7.3 (Continued)	(3) Signal Title 156 MHz										
	Ref (DA)				X						20.3.1.2.4.6.3.8 (To DA)
	Connector				X	X	X	X		Tester	
	Signal				X	X	X	X		Manual Test	
	Level				X	X	X	X		Manual Test	
	Source Impedance				X						
	Load Impedance				X						
3.1.2.4.8	DC Power	X									
3.1.2.4.8.1	VBUS										20.3.1.2.1
	Signal Title				X						
	Pins				X	X	X	X		T1	
	Signal				X	X	X	X		T1	
	Level				X	X	X	X		T1	
	Source Current				X	X	X	X		T1	
	Source Coupling				X	X	X	X		T1	
	Load Coupling				X	X	X	X		T1	
3.1.2.4.8.2	Panel Power										N/A
	Signal Title 28 VDC Control										
	Panel Power In				X						20.3.1.2.1
	Pins				X	X	X	X		T1	
	Signal				X	X	X	X		T1	
	Level				X	X	X	X		T1	
	Source Current				X						
	Source Coupling				X	X	X	X		T1	
	Load Coupling				X	X	X	X		T1	

NOTE: All input signals with tolerance variation characteristics will be certified by test set calibration.

N/A = Not Applicable
1 = Analysis
a = Inspection
b = Review of Design

3 = Test
a = Development
b = Qualification
c = Acceptance

4 = Carry-Forward Test(s)

Hughes Specification DS 32012-020 Paragraph Ref.	Hughes Title	Hughes Verification Method								Hughes Verification Test	Rockwell Specification MC 409-0025, Rev. B Paragraph Ref.
		N/A	1	2		3			4		
				a	b	a	b	c			
3.1.2.4.8.2	Signal Title 28 VDC Control Panel Power Out				X						20.3.1.2.4.3.3
	Pins				X	X	X	X		T1	
	Signal				X	X	X	X		T1	
	Level				X	X	X	X		T1	
	Source Current				X						
	Source Coupling				X	X	X	X		T1	
	Load Coupling	X									
3.1.2.4.9	Test and Measurements	X									N/A
3.1.2.4.9.1	Test Connector Access				X						N/A
3.1.2.4.10	Deleted										
3.1.2.4.11	Common Mode Protection				X						Requirements spread throughout RI Specification
3.1.3	Item Identification			X							N/A
3.2	Characteristics	X									N/A
3.2.1	Performance	X									N/A
3.2.1.1	Life Requirements				X						20.3.2.1.1
3.2.1.1.1	Operating Life									TBS	20.3.2.1.1.1
3.2.1.1.2	Useful Life									TBS	20.3.2.1.1.2
3.2.1.1.3	Shelf Life									TBS	20.3.2.1.1.3

NOTE: All input signals with tolerance variation characteristics will be certified by test set calibration.

N/A = Not Applicable
1 = Analysis
a = Inspection
b = Review of Design

3 = Test
a = Development
b = Qualification
c = Acceptance

4 = Carry-Forward Test(s)

Hughes Specification DS 32012-020 Paragraph Ref.	Hughes Title	Hughes Verification Method								Hughes Verification Test	Rockwell Specification MC 409-0025, Rev. B Paragraph Ref.
		N/A	1	2		3			4		
				a	b	a	b	c			
3.2.1.2	Forward Link	X									
3.2.1.2.1	Forward Link Input Signals	X									N/A
3.2.1.2.1.1	Data IF Signal				X					D.T.	20.3.2.1.2.1.1.5.1 20.3.2.1.2.1.1.6
3.2.1.2.1.2	Track IF Signal				X					D.T.	20.3.2.1.2.1.1.5.2
3.2.1.2.2	Forward Link Output Signals	X									N/A
3.2.1.2.2.1	Signal Strength Indication				X	X	X	X		T3	20.3.2.1.2.1.2.9w 20.3.2.1.2.1.3.6.1.1a
3.2.1.2.2.2	Comm Detect Flag				X	X	X	X		T3	20.3.2.1.2.1.3.6.1.2m
	0.99 Prob in 350 ms		X		X	X	X	X		T3	
	10^{-6} Prob for C/N_0 56.9 dB-Hz		X								
	Functional				X	X	X	X		T3	
2.3.1.2.2.3	Data-Present Flag										20.3.2.1.2.1.3.6.1.2w
	Logical Condition for Output				X	X	X	X		T3	
	0.99 Prob in 2.5 sec w/o PN		X		X	X	X			Manual Test	
	0.98 Prob in 12.5 sec w/PN		X		X	X	X			Manual Test	
3.2.1.2.2.4	Baseband Data Output				X	X	X	X		T3	20.3.2.1.2.1.1.6 (Portions only)
3.2.1.2.3	Bit Error Rate Degradation				X	X	X	X		Manual Test	Table 3-IV
3.2.1.2.4	Angle Track Processing Functional				X	X	X	X		T11	Requirements spread throughout RI Specification
	Scale Factor				X				X		

NOTE: All input signals with tolerance variation characteristics will be certified by test set calibration.

N/A = Not Applicable
1 = Analysis
a = Inspection
b = Review of Design

3 = Test
a = Development
b = Qualification
c = Acceptance

4 = Carry-Forward Test(s)

Hughes Specification DS 32012-020 Paragraph Ref.	Hughes Title	Hughes Verification Method								Hughes Verification Test	Rockwell Specification MC 409-0025, Rev. B Paragraph Ref.
		N/A	1	2		3			4		
				a	b	a	b	c			
3.2.1.3	Antenna Servo	X									N/A
3.2.1.3.1	Point Mode				X	X	X	X		T9, T12, T17	Requirements spread throughout RI Specification
3.2.1.3.1.1	Body Stabilization										
	Servo Response Ramp				X						
	Functional				X	X	X	X		T12	
	Pointing Accuracy				X	X	X	X		T12	
3.2.1.3.1.2	Inertial Stabilization				X						
3.2.1.3.2	Tracking										
	Gain Accuracy				X						
	Radar and Comm				X						
	Functional Tests				X	X	X	X		T11	
3.2.1.3.3	Slewing										
	Function and Accuracy				X	X	X	X		T10, T15	
	Implementation				X						
3.2.1.3.4	Position Reference Initialization				X	X	X	X		T18	Requirements spread throughout RI Specification
3.2.1.3.5	Rate Loop Characteristics	X									N/A

NOTE: All input signals with tolerance variation characteristics will be certified by test set calibration.

N/A = Not Applicable
1 = Analysis
a = Inspection
b = Review of Design

3 = Test
a = Development
b = Qualification
c = Acceptance

4 = Carry-Forward Test(s)

Hughes Specification DS 32012-020 Paragraph Ref.	Hughes Title	Hughes Verification Method								Hughes Verification Test	Rockwell Specification MC 409-0025, Rev. B Paragraph Ref.
		N/A	1	2		3			4		
				a	b	a	b	c			
3.2.1.3.5.1	Analog Shaping				X	X	X	X	X	T8	Hughes internal requirement
3.2.1.3.5.2	Digital Input	X									" " "
3.2.1.3.5.3	DC Offsets	X									" " "
3.2.1.3.5.3.1	Radar Track	X									" " "
3.2.1.3.5.3.2	Comm Track	X									" " "
3.2.1.3.5.3.3	Fine Inertial Hold	X									" " "
3.2.1.3.5.3.4	Coarse Inertial Hold	X									" " "
3.2.1.3.5.4	Motor Driver	X									N/A
3.2.1.3.5.4.1	Limits				X	X	X	X		T7	Hughes internal requirement
3.2.1.3.5.4.2	Transfer Function				X	X	X	X	X	Manual Test	" " "
3.2.1.3.5.5	Tachometer Shutdown				X	X	X	X		T6	" " "
3.2.1.3.5.6	DAC Stability and Linearity				X						" " "
3.2.1.3.6	Scan Mode										" " "
	Moding				X	X	X	X		T14	" " "
	Scans versus Range				X						" " "
3.2.1.4	Antenna Control	X									" " "
3.2.1.4.1	Angle Transforms				X	X	X	X		T6, T17	" " "
3.2.1.4.2	LOS Angle Rate Transformations				X	X	X	X		T15	" " "

NOTE: All input signals with tolerance variation characteristics will be certified by test set calibration.

N/A = Not Applicable
1 = Analysis
a = Inspection
b = Review of Design

3 = Test
a = Development
b = Qualification
c = Acceptance

4 = Carry-Forward Test(s)

Hughes Specification DS 32012-020 Paragraph Ref.	Hughes Title	Hughes Verification Method								Hughes Verification Test	Rockwell Specification MC 409-0025, Rev. B Paragraph Ref.
		N/A	1	2		3			4		
				a	b	a	b	c			
3.2.1.4.3	Obscuration Calculation (Selected Angles Tested)				X	X	X	X		T16	Hughes internal requirement
3.2.1.4.4	Stow				X	X	X	X		T18	" " "
3.2.1.4.5	Unstow				X	X	X	X		T16	" " "
3.2.1.4.6	Wiggle Test				X	X	X	X			" " "
3.2.1.4.7	Motor Protection - Deleted	X									" " "
3.2.1.4.8	Zero Rate Command				X						" " "
3.2.1.4.9	Deleted	X									N/A
3.2.1.5	Mode Control	X									N/A
3.2.1.5.1	Forward Link Functions				X	X	X	X		T3, T11 Manual Test	Requirements spread throughout RI Specification
3.2.1.5.2	Servo Modes				X	X	X	X		T11, T12 T14, T15	Hughes internal requirement
3.2.1.5.3	Antenna Steering Control Functions				X	X	X	X		T11, T12 T14, T15	Requirements spread throughout RI Specification
3.2.1.5.4	System Control				X	X	X	X		T11, T12 T14, T15	
3.2.1.5.4.1	Initialization Procedure				X	X	X	X		All automatic except T1	Requirements spread throughout RI Specification

NOTE: All input signals with tolerance variation characteristics will be certified by test set calibration.

N/A = Not Applicable
1 = Analysis
a = Inspection
b = Review of Design

3 = Test
a = Development
b = Qualification
c = Acceptance

4 = Carry-Forward Test(s)

Hughes Specification DS 32012-020 Paragraph Ref.	Hughes Title	Hughes Verification Method								Hughes Verification Test	Rockwell Specification MC 409-0025, Rev. B Paragraph Ref.
		N/A	1	2		3			4		
				a	b	a	b	c			
3.2.1.5.4.2	Acquisition Procedure--TBS									TBS	
3.2.1.5.5	Self-Test									TBS	20.3.2.1.2.1.2.13
3.2.1.5.6	Displays & Controls Functions				X	X	X	X		T9	Requirements spread throughout RI Specification
3.2.1.5.7	System Reference Signals				X	X	X	X		T1, T3 T5, T7	
3.2.1.5.8	Priorities				X						Requirements spread throughout RI Specification
3.2.1.5.9	Control & Output Status Signals	X									N/A
3.2.1.5.9.1	Orbiter Serial Outputs				X	X	X	X		All automatic except T1	20.3.2.1.2.1.3.6.1.2
3.2.1.5.9.2	Orbiter Discrete Otuputs				X	X	X	X		T1, T9, T10 T16, T18	20.3.2.1.2.1.3.6.4.[illegible] (ADA) 20.3.2.1.2.1.3.6.[illegible] (D&C)
3.2.1.5.9.3	Ku Serial Outputs				X	X	X	X		T9	20.3.2.1.2.1.2.14.1.5 (EA-2 20.3.2.1.2.1.1.13.1.4.1 (SPA)
3.2.1.5.9.4	Ku Discrete Outputs				X	X	X	X		T4, T5	20.3.2.1.2.1.1.13.1.1 (SPA) 20.3.2.1.2.1.2.14.1.1 (EA-2) 20.3.2.1.2.1.3.6.5.1 (DA)
3.2.1.5.10	Control & Status Input Signals	X									N/A
3.2.1.5.10.1	Orbiter System Input Signals	X									20.3.2.1.2.1.3.6.1.3 (MDM) 20.3.2.1.2.1.3.6.2.1 (OCC) 20.3.2.1.2.1.3.6.4.1 (ADA) 20.3.2.1.2.1.3.6.2.2 (GCILU)

NOTE: All input signals with tolerance variation characteristics will be certified by test set calibration.

N/A = Not Applicable

1 = Analysis
- a = Inspection
- b = Review of Design

3 = Test
- a = Development
- b = Qualification
- c = Acceptance

4 = Carry-Forward Test(s)

Hughes Specification DS 32012-020 Paragraph Ref.	Hughes Title	Hughes Verification Method								Hughes Verification Test	Rockwell Specification MC 409-0025, Rev. B Paragraph Ref.
		N/A	1	2		3			4		
				a	b	a	b	c			
3.2.1.5.10.2	Ku Input Signal										20.3.2.1.2.1.3.6.5.2 (DA) 20.3.2.1.2.1.2.14.1.2 (EA-2) 20.3.2.1.2.1.2.14.1.6a-i (EA-2) 20.3.2.1.2.1.1.13.1.4.2 (SPA)
3.2.1.5.10.3	Internal Status Discretes	X									Hughes internal requirement
3.2.1.6	System Control	X									N/A
3.2.1.6.1	Data Control	X									N/A
3.2.1.6.1.1	Format				X	X	X	X		All automatic except T1	
3.2.1.6.1.2	Protocols				X	X	X	X		All automatic except T1	20.3.2.1.2.1.1.13.1.4 (SPA) 20.3.2.1.2.1.1.13.1.4.2 (SPA) 20.3.2.1.2.4.7.5.1 (EA-2) 20.3.2.1.2.4.7.5.4 (EA-2)
3.2.1.6.1.3	Timing				X						
3.2.1.7	Self-Test	X									20.3.2.1.2.1.2.13
3.2.1.7.1	Enable and Disable				X	X	X	X		T4	Hughes internal requirement
3.2.1.7.2	Sequence									TBS	" " "
3.2.1.7.3	Signals and Data	X									" " "
3.2.1.7.3.1	Output Signals									TBS	" " "
3.2.1.7.3.2	Input Signals									TBS	" " "
3.2.1.7.3.3	MDM Data									TBS	" " "
3.2.1.7.3.4	D&C Data									TBS	" " "

NOTE: All input signals with tolerance variation characteristics will be certified by test set calibration.

N/A = Not Applicable
1 = Analysis
a = Inspection
b = Review of Design

3 = Test
a = Development
b = Qualification
c = Acceptance

4 = Carry-Forward Test(s)

Hughes Specification DS 32012-020 Paragraph Ref.	Hughes Title	Hughes Verification Method								Hughes Verification Test	Rockwell Specification MC 409-0025, Rev. B Paragraph Ref.
		N/A	1	2		3			4		
				a	b	a	b	c			
3.2.1.7.3.5	Correlation									TBS	Hughes internal requirements
3.2.1.7.4	Time to Perform Self-Test									TBS	" " "
3.2.1.8	Displays and Controls	X									N/A
3.2.1.8.1	Discrete Command and Status Interface	X									N/A
3.2.1.8.2	Orbiter Status and Displays Interface	X									N/A
3.2.1.8.2.1	Digital Displays				X	X	X	X		T9	20.3.2.1.2.1.2.14.16 20.3.1.2.4.4.3 20.3.2.1.2.12.14.2.2
	Frequency and Update				X						
3.2.1.8.2.2	Analog Displays										20.3.1.2.4.2.3 (Comm) 20.3.2.1.2.1.2.14.2.1.1 (Radar)
	3.2.1.8.4.1 Requirements	X									
	All other provisions				X	X	X	X		T15	
3.2.1.8.3	Digital MDM Interface	X									20.3.1.2.4.2.1 20.3.1.2.4.2.2 20.3.2.1.2.1.3.6.1.2 20.3.2.1.2.1.3.6.1.3
3.2.1.8.3.1	Operating Modes										
	Functional Table 3.2.1.8-3				X						
	100 μs Separation				X						
	Malfunction Operation				X						

NOTE: All input signals with tolerance variation characteristics will be certified by test set calibration.

N/A = Not Applicable
1 = Analysis
a = Inspection
b = Review of Design

3 = Test
a = Development
b = Qualification
c = Acceptance

4 = Carry-Forward Test(s)

Hughes Specification DS 32012-020 Paragraph Ref.	Hughes Title	Hughes Verification Method								Hughes Verification Test	Rockwell Specification MC 409-0025, Rev. B Paragraph Ref.
		N/A	1	2		3			4		
				a	b	a	b	c			
3.2.1.8.3.2	Performance				X	X	X	X	X	Singer Data	
3.2.1.8.3.3	Data Format				X	X	X	X		All automatic except T1	
3.2.1.8.3.4	Transmission Format				X	X	X	X		All automatic except T1	
3.2.1.8.3.5	Transmission Protocols										
	Functional				X	X	X	X		T2	
	3.1.2.4.1	X									
3.2.1.8.3.6	Data Validation				X	X	X	X		T2	
3.2.1.8.4	Analog MDM Interface	X									20.3.1.2.4.2.3 20.3.2.1.2.1.2.14.1.4(a)
3.2.1.8.4.1	Signal Strength										
	Pins				X	X	X	X		Tester	
	Output Level				X	X	X	X			
	Bandwidth				X	X	X	X			
	Gain				X	X	X	X			
	Idle Channel Noise--TBS									TBS	
	DC Offset--TBS									TBS	
3.2.1.8.4.2	Transmit RF Power										
	Pins				X	X	X	X			
	Output Level				X	X	X	X			
	Bandwidth				X	X	X	X			
	Gain				X	X	X	X			

NOTE: All input signals with tolerance variation characteristics will be certified by test set calibration.

N/A = Not Applicable
1 = Analysis
a = Inspection
b = Review of Design

3 = Test
a = Development
b = Qualification
c = Acceptance

4 = Carry-Forward Test(s)

Hughes Specification DS 32012-020 Paragraph Ref.	Hughes Title	Hughes Verification Method								Hughes Verification Test	Rockwell Specification MC 409-0025, Rev. B Paragraph Ref.
		N/A	1	2		3			4		
				a	b	a	b	c			
3.2.1.8.4.2 (Continued)	Idle Channel Noise--TBS									TBS	
	DC Offset--TBS									TBS	
3.2.1.9	System Reference Signals	X									
3.2.1.9.1	Reference Frequency Generation										
	156 MHz Reference Frequency								X		20.3.1.2.4.6.3.8
											20.3.2.1.2.1.2.14.1.3
	Frequency					X	X	X	X	Manual Test	
	Temperature Stability					X			X	D.T.	
	Long-Term Stability								X	TBS	
	Level					X	X	X	X	Manual Test, D.T.	
	Amplitude Stability								X	TBS	
	Phase Stability					X	X	X	X	D.T.	
	Incidental FM								X	TBS	
	Spurious Outputs					X	X	X	X	D.T.	
	Jitter								X	TBS	
	1.876 GHz Reference Frequency										20.3.1.2.4.1.3.1
	Frequency					X	X	X	X	TBS	
	Temperature Stability								X	TBS	
	Long-Term Stability								X	TBS	
	Level					X	X	X	X		
	Phase Stability								X	TBS	
	Incidental FM								X	TBS	
	Spurious Outputs								X	TBS	
	Jitter								X	TBS	

NOTE: All input signals with tolerance variation characteristics will be certified by test set calibration.

N/A = Not Applicable
1 = Analysis
a = Inspection
b = Review of Design

3 = Test
a = Development
b = Qualification
c = Acceptance

D.T. = Development Test
4 = Carry-Forward Test(s)

Hughes Specification DS 32012-020 Paragraph Ref.	Hughes Title	Hughes Verification Method								Hughes Verification Test	Rockwell Specification MC 409-0025, Rev. B Paragraph Ref.
		N/A	1	2		3			4		
				a	b	a	b	c			
3.2.1.9.2	Encoder Drive										20.3.1.2.4.6.3.3
	Waveform				X	X	X	X		T1	
	Voltage				X	X	X	X		T1	
	Ripple				X						
	Max Current				X						
3.2.1.9.3	Antenna Lobing										20.3.1.2.4.6.3.12 20.3.1.2.4.6.3.13 20.3.2.1.2.1.2.14.1.2c,d
	Functional				X	X	X	X		T5	
	Transitions				X						
	Asymmetry				X						
3.2.1.9.4	Gyro Excitation										20.3.1.2.4.6.3.2 20.3.1.2.4.6.3.4
	Excitation										
	Waveform				X						
	Voltage		X		X	X	X	X		T7	
	Frequency				X	X	X	X		T7	
	Current				X						
	Spin Motor										
	Waveform				X						
	Voltage				X	X	X	X		T7	
	Frequency				X	X	X	X		T7	
	Max Current				X	X	X	X		Tester	

NOTE: All input signals with tolerance variation characteristics will be certified by test set calibration.

N/A = Not Applicable
1 = Analysis
a = Inspection
b = Review of Design

3 = Test
a = Development
b = Qualification
c = Acceptance

4 = Carry-Forward Test(s)

REFERENCES

1. John Ruze, "Feed Support Blockage Loss in Parabolic Antennas," The Microwave Journal, Vol. 11, No. 12, December 1968, pp. 76-80.

2. Alan F. Kay, "Electrical Design of Metal Space Frame Randomes," IEEE Trans. on Antennas and Propagation, AP-13, No. 2, March 1965, pp. 188-202.

3. H. Jasik, Antenna Engineering Handbook, McGraw-Hill, 1961, pp.17-18, 17-19.

4. "Microwave Coax Connectors," Omni Spectra Catalog #2/79-30-M-56-SUL.

5. Thad Dreher, "Cabling Fast Pulses" Don't Trip On The Steps." The Electronic Engineer, August 1969.

6. Bob Botos, "Nanosecond Pulse Handling Techniques, In I/C Interconnections," Motorola Applications Note #AN-270.

7. P. H. Conway, "Ku-Band Proposed Data Sampler With and Without Bit Synchronizer," Hughes Aircraft Company

8. R. K. Kimura, "Logic Description of the Motorola MSI Digital Phase Detectors," TRW IOC 7333.11-21, October 31, 1974.

9. Motorola MC4344-MC4044 Phase Frequency Detector Specifications and Operating Characteristics, Issue A, 1972.

10. Motorola MC12040 Phase Frequency Detector Specifications Contained in Motorola Semiconductor Library, Vol. IV, MECL Integrated Circuits, Series A, 1974.

11. J. K. Holmes, "Critique of a Hughes Shuttle Ku-Band Data Sampler/Bit Synchronizer," Axiomatix Report No. R8003-1, March 14, 1980.

12. "Mid-Bit Corrector," Hughes Aircraft Company (Culver City) Note, dated about March 1980.

13. R. K. Kimura, "Logic Description of the Motorola MSI Digital Phase Detectors," TRW IOC 7333.11-21, October 31, 1974.

14. C. L. Weber and W. K. Alem, "Study to Investigate and Evaluate Means of Optimizing the Ku-Band Combined Radar/Communication Functions for the Space Shuttle," Axiomatix Report No. R7710-5, October 28, 1977.

15. D. K. Shingledecker and H. G. Magnusson, "Results of Computer Analysis of Ku-Band Radar Search Mode Detection Probability," Hughes Aircraft Company IDC #2705.00/109.

REFERENCES (Cont'd)

16. W. B. Davenport, Jr. and W. L. Root, Random Signals and Noise, McGraw-Hill, 1958, Chapter 8, page 163.

17. W. Magnus and F. Oberhettinger, Special Functions of Mathematical Physics, Chelsea, NY, 1949, Chapter III.

18. D. Middleton, Introduction to Statistical Communication Theory, McGraw-Hill, 1960, Appendix C.

19. "Handbook of Mathematical Functions with Formulas, Graphs and Mathematical Tables," U.S. Department of Commerce, National Bureau of Standards, Chapter 17.

20. Gaylord K. Huth and Sergei Udalov, "Spiral Scan Analysis," Axiomatix Report No. R7606-4, July 31, 1976.

21. "Ku-Band EA-1 Flight Software, Release IV (Listing), Hughes Aircraft Company, August 17, 1979.

22. "EA-1 Software Description Document," Release IV, Hughes Aircraft Company, August 17, 1979.

23. "EA-1 Preliminary Design Review," Hughes Aircraft Company Document No. HS237-1531, Vol. II, Part 1, March 20, 1978.

24. "EA-2 Preliminary Design Review," Volume III, Hughes Aircraft Company Document #HS237-1531-3, March 14-24, 1978.